

# **CHARACTERIZATION OF SWELLING STRESS AND SOIL MOISTURE DEFICIENCY RELATIONSHIP FOR EXPANSIVE UNSATURATED SOILS**

by

**ARMAND AUGUSTIN FONDJO TAKOUKAM**

A dissertation submitted in fulfilment of the requirements for the degree

*Master of Engineering in Civil Engineering*

in the

Department of Civil Engineering

of the

Faculty of Engineering, Built Environment and Information Technology

of the

Central University of Technology, Free State, South Africa

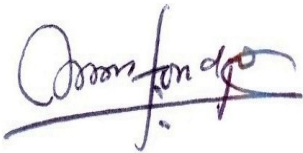
Supervisor: Prof, E. Theron

June 2018

## DECLARATION

I, the undersigned, declare that the dissertation hereby submitted by me for the degree *Master of Engineering in Civil Engineering* at the Central University of Technology, Free State, is my own independent work and has not been submitted by me to another University and/or Faculty in order to obtain a degree. I further cede copyright of this dissertation in favour of the Central University of Technology, Free State.

Armand Augustin Fondjo Takoukam



Signature:

Date: June 2018

Bloemfontein, South Africa

## ABSTRACT

Expansive soils vary in volume, in relation to water content. Volume changes when wetting (swelling) and drying (shrinkage). Lightweight structures in construction are the most vulnerable structures experiencing severe defects when built on these soils. In South Africa, expansive soils are the most problematic which impose challenges to civil engineers. The prediction of the swelling stress has been a concern to the construction industry for a long time. The swelling stress is generally ignored in engineering practice. Nonetheless, the swelling stress can develop significant uplift forces detrimental to the stability of foundations. Considering the swelling stress in foundation design in expansive soils enhance the durability, the service life, and reduce the cost of assessment and repair works to be undertaken in the future. Mathematical models are offered as an alternative to direct oedometer testing. Mathematical models are a useful tool to assess swelling stress.

The aim of this study was to characterize the relationship between the swelling stress, the soil suction, and other soil parameters. Moreover, develop mathematical models to predict the swelling stress of field compacted expansive soils. Laboratory tests have been performed such as particle size distribution, Atterberg limits, linear shrinkage, specific gravity, free swell ratio, X-ray diffraction, soil suction measurement, modified Proctor compaction test, and zero-swell test (ZST). Multiple regression analysis was performed using software NCSS11 to analyze the data obtained from the experiments. The relationships between the swelling stress and other soil parameters were established. It was observed that, at the optimum moisture content (OMC), the swelling stress values are within the range of 48.88 kPa to 261.81 kPa, and the matric suction values are within the range of 222.843 kPa to 1,778.27 kPa. The swelling stress values on the dry side of the OMC are higher than values on the wet side. In addition, compaction at the OMC can reduce the swelling stress by 15%. Furthermore, the geotechnical index properties, the swelling parameters, affect the swelling stress of compacted expansive soils. Nevertheless, there is a key impact of the type of clay mineral on swelling stress.

Six predictive mathematical models were developed. These models were validated using soil samples collected from various areas across the province of Free State (Petrusburg, Bloemfontein, Winburg, Welkom, and Bethlehem).

Lastly, good correlations between predicted values and values obtained from experimental works confirm the reliability of the multiple regression analysis. The data points are very close to the line 1:1. Furthermore, the graphical analysis shows that the correlation of the values obtained from the models developed in this study are more precise than the values obtained from other models. Therefore, the predictive models developed in this research work are capable to estimate the swelling stress with acceptable accuracy.

**Keywords:** Compaction, expansive soils, filter paper, soil parameters, smectite, soil suction, swelling stress.



## RESUME

Les sols expansifs sont ces sols qui changent de volume en fonction de leur teneur en eau. Leur volume augmente suite à l'augmentation de la teneur en eau, et diminue avec la réduction de la teneur en eau, suivi de la dessiccation lorsqu'ils sont asséchés. Les constructions légères sont plus exposées aux dégâts engendrés par les sols expansifs. En Afrique du Sud, les sols expansifs sont considérés comme les plus problématiques. La problématique des sols expansifs est un défi à relever par les ingénieurs du génie civil. La prédiction de la pression de gonflement a longtemps été une préoccupation importante dans l'industrie de la construction. La pression de gonflement est généralement ignorée dans la pratique. Cependant, cette pression est capable de développer des forces de soulèvement destructrices pour les fondations. La considération de la pression de gonflement dans le calcul des fondations améliore la durée de vie des ouvrages, réduit les coûts onéreux d'évaluations et de réparations. Les modèles développés dans cette étude sont une alternative à l'essai œdométrique direct, et peuvent être utilisés pour évaluer la pression de gonflement des sols expansifs.

Le but de cette recherche était de caractériser la relation entre la pression de gonflement, la succion du sol, et les autres paramètres de sol. Ensuite, proposer des modèles pour prédire la pression de gonflement des sols. Plusieurs tests de laboratoire ont été réalisés, notamment l'analyse granulométrique, limites d'Atterberg, limite au retrait, gravité spécifique, l'Indice de gonflement libre, ratio du gonflement libre, l'analyse minéralogique par diffraction au rayon X, la mesure de la succion de sol, l'essai de compactage, et la mesure de la pression de gonflement à volume constant. L'analyse des données expérimentales obtenues des essais de laboratoire ont été conduites par l'analyse par régression multiple avec l'outil logiciel NCSS11. Plusieurs corrélations entre la pression de gonflement, la succion de sol, et les autres paramètres de sol ont été établies. A la teneur en eau optimale, la pression de gonflement varie de 48.88kPa à 261.81 kPa, et la succion matricielle de 222.843 kPa à 1778.27kPa. Les valeurs de la pression de gonflement du côté sec de la teneur en eau optimale sont supérieures à celle obtenues du côté humide. Par ailleurs, le compactage des sols expansifs à la teneur en eau optimale réduit la pression de gonflement d'environ 15%. En

dehors de la succion matricielle, plusieurs autres paramètres de sol influencent la pression de gonflement. Cependant, le type de minéral argileux a une influence importante sur la pression de gonflement.

Six modèles pour prédire la pression de gonflement ont été proposés. Ces modèles ont été validés sur des sols prélevés dans cinq villes de la province de Free State à savoir : Petrusburg, Bloemfontein, Winburg, Welkom, et Bethlehem. De très bonnes corrélations ont été établies entre les données expérimentales et celle obtenues des modèles proposés. Les données graphiques de ces corrélations sont très proches de la ligne 1:1. Aussi, la comparaison des valeurs obtenues des modèles développés dans cette étude avec les valeurs obtenues des autres modèles existants montre que les modèles proposés dans cette étude donnent une meilleure corrélation. En conclusion, les modèles développés dans cette étude sont capables de prédire la pression de gonflement avec une précision acceptable.

**Mots clés:** Compactage, sol expansifs, papier filtre, paramètres de sol, montmorillonite, succion de sol, pression de gonflement.

## ACKNOWLEDGEMENTS

A number of special acknowledgements deserve specific mention:

- (a) The Rectorate and relevant functionaries from the Central University of Technology, Free State, for the opportunity of completing this research;
- (b) The various agencies for funding and in particular the Central University of Technology, Free State;
- (c) Pr. E, Theron my supervisor, for guidance and support given;
- (d) My family and colleagues, for their patience and understanding throughout this research; and
- (e) My wife and our children for their love and support.

Acknowledgement above all to my Heavenly Father for setting my feet on a rock and making my steps secure (Ps. 40).

## TABLE OF CONTENTS

	Page
Declaration .....	ii
Abstract .....	iii
Résumé .....	v
Acknowledgements .....	vii
Table of Contents .....	viii
List of Tables .....	xiv
List of Figures .....	xv
List of Appendices .....	xxi
List of Abbreviations .....	xxiii
Notations and Symbols .....	xxiv
<b>CHAPTER 1 : INTRODUCTION .....</b>	<b>1</b>
1.1 Background .....	1
1.2 Problem statement .....	2
1.3 Research objective .....	3
1.4 Research scope .....	4
1.5 Dissertation layout .....	4
<b>CHAPTER 2 : LITERATURE REVIEW .....</b>	<b>5</b>
<b>PART 1: EXPANSIVE SOILS .....</b>	<b>5</b>
2.1 Definition .....	5
2.2 Origin .....	5
2.3 Climate .....	6
2.4 Topography .....	6
2.5 Time .....	6
2.6 Mineralogical composition of clays .....	7
2.6.1 Kaolinite .....	7
2.6.2 Illite .....	7
2.6.3 Montmorillonite .....	7
2.7 Assessment and classification of expansive soils .....	9
2.7.1 Laboratory testing .....	10
2.7.2 Particle size distribution .....	10

2.7.3 Atterberg limit.....	10
2.7.4 Mineralogical testing .....	12
2.8 Swell potential testing (indirect measurement).....	12
2.8.1 Expansive capacity classification based on plasticity table .....	12
2.8.2 Swelling capacity classification based on advanced physical properties of soils.....	12
2.8.3 Casagrade's chart plasticity for swelling potential classification.....	14
2.9 Swell potential testing (Direct measurement).....	14
2.9.1 Free swell test.....	14
2.10 Site investigation .....	15
2.11 In situ testing.....	16
2.12 Classification of expansive soils.....	16
2.13 Mechanism of swelling .....	17
2.14 Factor affecting swell/ shrink behaviour of soil.....	18
<b>PART 2: UNSATURATED SOIL MECHANICS .....</b>	<b>20</b>
2.15 Introduction.....	20
2.16 Unsaturated soil mechanics domains application.....	22
2.17 Phase of unsaturated soils .....	22
2.17.1 Contractile skin ( Air water interface) .....	23
2.17.2 Water phase.....	24
2.17.3 Air phase.....	24
2.17.4 Solid phase .....	24
2.18 Surface tension .....	25
2.19 Capillary phenomenon.....	27
2.20 Capillary Height .....	28
2.21 Capillary pressure .....	29
2.22 Theory of soil suction.....	31
2.23 Components of soil suction .....	32
2.24 Unsaturated soil stress state variables.....	34
2.24.1 Equilibrium analysis .....	34
2.24.2 Stress state variables.....	36
2.24.3 Other combination of stress state variables .....	37

2.25 Soil water characteristic curve .....	37
--	----

### **CHAPTER 3 : PREVIOUS STUDIES ON PREDICTION OF THE SWELL**

<b>STRESS</b> .....	41
3.1 Introduction.....	41
3.2 Swelling stress .....	41
3.2.1 Definition .....	41
3.3 Swelling stress prediction based on oedometer tests .....	41
3.3.1 Technique 1 .....	42
3.3.2 Technique 2 .....	42
3.3.3 Technique 3 .....	43
3.4 Proposed models to predict the swelling stress .....	44
3.5 Conclusion.....	49

### **CHAPTER 4: EXPERIMENTAL STUDY**.....

4.1 Introduction.....	50
4.2 Sample location.....	50
4.3 Laboratory tests.....	52
4.3.1 Particle size distribution .....	52
4.3.2 Sieve analysis .....	53
4.3.3 Hydrometer analysis .....	53
4.3.4 Atterberg limits .....	54
4.3.5 Liquid limit.....	55
4.3.6 Plastic limit.....	57
4.3.7 Plasticity index .....	58
4.3.8 Linear shrinkage test.....	58
4.3.9 Specific gravity .....	60
4.3.10 Free swell index .....	61
4.3.11 Free swell ratio.....	63
4.4 X-ray diffraction (XRD) .....	64
4.4.1 introduction .....	64
4.4.2 Procedure .....	64
4.5 Modified proctor compaction test.....	66
4.5.1 Compaction test procedure .....	66

4.5.2	Calculation of compaction test parameters .....	70
4.5.3	Plotting of compaction curve .....	71
4.6	Swelling stress test, experimental procedure and equipment.....	72
4.7	Soil suction measurement .....	75
4.7.1	Filter paper calibration process .....	76
4.7.2	Indirect measurement of suction using filter paper .....	80
4.8	Multiple regression analysis .....	91
4.8.1	Introduction .....	91
4.8.2	Regression analysis process .....	91
4.8.3	Statement of problem.....	91
4.8.4	Selection of relevant variables .....	91
4.8.5	Data collection .....	92
4.8.6	Model specification .....	93
4.8.7	Model fitting.....	94
4.8.8	Model validation .....	94
<b>CHAPTER 5</b>	<b>: ADVANCED TESTING AND ANALYSIS.....</b>	<b>96</b>
5.1	Introduction.....	96
5.2	Soil characteristic properties .....	96
5.2.1	Grain size classification analysis.....	96
5.2.2	Unified soil classification system.....	98
5.2.3	Linear shrinkage .....	99
5.2.4	Specific gravity.....	100
5.2.5	Activity of clay .....	101
5.2.6	Free swell index results analysis.....	101
5.2.7	Free swell ratio results analysis .....	102
5.2.8	Comparison free swell ratio and free swell index test results.....	103
5.3	X- Ray diffraction results analysis .....	103
5.3.1	Comparison of the results obtained from X-ray diffraction and Free swell ratio.....	106
5.4	Proctor compaction test results .....	106
5.4.1	Compaction curves .....	106
5.5	Soil suction test results.....	111
5.5.1	Soil suction calibrated curves.....	112

5.5.2 Analysis and discussion of the relationship between soil suction and water content .....	114
5.6 Soil water characteristic curve (SWCC).....	118
5.6.1 Introduction .....	118
5.6.2 Modelling of SWCC.....	118
5.6.3 Analysis and discussion of SWCC .....	119
5.6.4 Soil water characteristic curve fit results .....	120
5.6.5 Soil water characteristic curve fitting parameters and equations .....	123
5.7 Swelling stress results analysis .....	123
5.8 Summary of laboratory results.....	125
5.9 Analysis and discussion of the correlation between swelling stress and soil parameters .....	125
5.9.1 Analysis and discussion of the correlation between swelling stress and soil suctions.....	125
5.9.2 Analysis and discussion of the correlation between swelling stress and initial dry density.....	127
5.9.3 Analysis and discussion of the correlation between swelling stress and initial water content.....	128
5.9.4 Analysis and discussion of the correlation between swelling stress and plasticity index .....	130
5.9.5 Analysis and discussion of the correlation between swelling stress and liquid limit.....	130
5.9.6 Analysis and discussion of the correlation between swelling stress and linear shrinkage .....	131
5.9.7 Analysis and discussion of the correlation between swelling stress and activity of clay .....	132
5.9.8 Analysis and discussion of the correlation between swelling stress and free swell index.....	133
5.9.9 Analysis and discussion of the correlation between swelling stress and free swell ratio .....	133
5.9.10 Analysis and discussion of the correlation between swelling stress and clay fraction .....	134



5.9.11 Conclusion for analysis and discussion of the correlation between swelling stress and soil properties .....	135
5.10 Constitutive models to predict the swelling stress .....	136
5.10.1 Determination of the constitutive models, multi-regression analysis coefficients, intercepts, and regression statistics .....	136
5.11 Validation of the models .....	138
5.11.1 Model validation by comparing predicted swelling stress values to the values obtained from experimental works.....	138
5.11.2 Model validation by comparing the predicted values of swelling stress to the results obtained from other existing models .....	141
<b>CHAPTER 6 : CONCLUSION AND PERSPECTIVES.....</b>	<b>145</b>
6.2 Summary .....	145
6.2 Conclusions.....	145
6.3 Perspectives.....	146
<b>REFERENCES.....</b>	<b>147</b>

## LIST OF TABLES

	Page
<b>Table 2.1:</b> Residual soils prone to expansiveness, department of local government, housing and works (1990).....	6
<b>Table 2.2:</b> Some of clay mineral characteristics (Mitchell, 1993) .....	8
<b>Table 2.3:</b> Classification for shrink-swell clay soils (BRE, 1990).....	11
<b>Table 2.4:</b> Potential swell based on plasticity (Hollz & Gribbs, 1956) .....	12
<b>Table 2.5:</b> Specific gravity of several minerals (Lambe & Whitman, 1979) .....	25
<b>Table 2.6:</b> Surface tension of contractile skin at several temperatures (Kaye and Laby, 1973).....	26
<b>Table 2.7:</b> Possible combination of stress state variables for unsaturated soil (Fredlund & Hasan, 1979) .....	37
<b>Table 3.1:</b> Models to predict the swelling stress .....	44
<b>Table 3.2:</b> Models to predict the swelling stress .....	44
<b>Table 4.1:</b> Summary of test standards .....	52
<b>Table 4.2:</b> Classification of soils base on FSR (Sridharan & Prakash, 2000) ...	63
<b>Table 4.3:</b> Relative density of water according to temperature .....	67
<b>Table 4.4:</b> Summary of suction measurement methods.....	75
<b>Table 4.5:</b> Total suction of Nacl at 20°C (Lang, 1967) .....	76
<b>Table 4.6:</b> Equilibration times for filter paper method (Leong, 2002) .....	84
<b>Table 4.7:</b> Regression analysis data.....	92
<b>Table 4.8:</b> List of variable statistical models and their regression equations....	94

## LIST OF FIGURES

	Page
<b>Figure 1.1:</b> Regional distribution map of clay in South Africa (Diop,2011) .....	1
<b>Figure 1.2:</b> Structural defects caused by expansive soil in Free State .....	2
<b>Figure 2.1:</b> Diagram of the structure of (a) kaolinite; (b) illite; (c) montmorillonite.....	8
<b>Figure 2.2:</b> Clay mineral layers (Odom, 1984) .....	9
<b>Figure 2.3:</b> Tetrahedral and octahedral sheets (Odom, 1984) .....	9
<b>Figure 2.4:</b> Grain size distribution for dry and wet sieve analysis.....	10
<b>Figure 2.5:</b> Relationship in Atterberg limits.....	11
<b>Figure 2.6:</b> Chart for evaluation of potential expansiveness (Seed et al.,1975).....	13
<b>Figure 2.7:</b> Classification chart for swelling potential by carter and Bentley (1991).....	13
<b>Figure 2.8:</b> Plot of clay mineral on casangrande's chart (Chleboard et al., 2005).....	14
<b>Figure 2.9:</b> Phase diagrams of free swell.....	15
<b>Figure 2.10:</b> Expansive soil, polygonal making of shrinkage fissures on the surface of the soil.....	16
<b>Figure 2.11:</b> Presentation of diffuse double layer and force of attraction.. ..	17
<b>Figure 2.12:</b> Swell/shrink mechanism .....	19
<b>Figure 2.13:</b> Categories of soil mechanics (Fredlund & Rahardjo, 1933).....	21
<b>Figure 2.14:</b> Excessively arid and semi-arid regions of the world.(Meigs, 1953; Dregne, 1976; Fredlund & Rahardjo, 1993) .....	21
<b>Figure 2.15:</b> Stress distribution of dessication (Fredlund and Rahardjo, 1993).....	22
<b>Figure 2.16:</b> A component of unsaturated soil with a continuous air phase (Fredlund and Rahardjo, 1993).....	23
<b>Figure 2.17:</b> Rigorous fourth-phase unstaured soil system (Fredlund and Rahardjo, 1993) .....	24
<b>Figure 2.18:</b> Density distribution over air-water interface (Kyklima, 2000) .....	24

<b>Figure 2.19:</b> Surface tension phenomenon on contractile skin. (a) intermolecular forces at air-water interface and water. (b) Pressures and surface tension acting on a curved two dimensional surface ( Fredlund, 1993).....	26
<b>Figure 2.20:</b> Surface tension on three-dimension warped membrane (Fredlund and Rahardjo, 1993).....	27
<b>Figure 2.21:</b> Physical model and phenomenon related to capillarity (After Fredlund, 1993).....	29
<b>Figure 2.22:</b> Relationship of the suction matric to pore size for various soils.....	30
<b>Figure 2.23:</b> Forces acting on capillary tube (Fredlund, 1993).....	31
<b>Figure 2.24:</b> Thermodynamic equilibrium between relative humidity and total suction.....	32
<b>Figure 2.25:</b> Total suction and its components: matric and osmotic suction (After Fredlund, 1993).....	33
<b>Figure 2.26:</b> Normal and shear stresses on a cubical soil element of infinitesimal dimensions .....	35
<b>Figure 2.27:</b> The stress state variables for unsaturated soil.....	36
<b>Figure 2.28:</b> Typical SWCC for different soil types (Fredlund and Xing, 1994).....	38
<b>Figure 2.29:</b> Definition of variables associated with the SWCC .....	38
<b>Figure 3.1:</b> Deformation versus vertical stress, single point test technique 1 (ASTM-D4546).....	42
<b>Figure 3.2:</b> Deformation versus vertical stress, technique 2 (ASTM-D4546).....	43
<b>Figure 3.3:</b> Deformation versus vertical stress, loading after wetting test technique 3 (ASTM-D4546) .....	43
<b>Figure 3.4:</b> Relation between suction and swelling stress (Thakur et al., 2005).....	46
<b>Figure 4.1:</b> Map showing the location of sampling points .....	51
<b>Figure 4.2:</b> Collection of the samples from field sites .....	51
<b>Figure 4.3:</b> (a) Sieve analysis, (b) Agitation of sedimentation cylinder, (c) Hydrometer analysis .....	54
<b>Figure 4.4:</b> Apparatus used for Atterberg limits test.....	55

<b>Figure 4.5a:</b> Casagrande liquid limit test.....	56
<b>Figure 4.5b:</b> Casagrande liquid limit test results. ....	56
<b>Figure 4.6:</b> Soil crumbles during the plastic limit test.....	57
<b>Figure 4.7:</b> Apparatus used for linear shrinkage test .....	58
<b>Figure 4.8:</b> Linear shrinkage test .....	59
<b>Figure 4.9:</b> Dried trough with the material .....	59
<b>Figure 4.10:</b> A view for soil specific gravity test .....	61
<b>Figure 4.11:</b> Free swelling test: (a) BTS: Bethlehem soil, (b) WKS: Welkom soil, (c) PTS: Petrusberg soil, (d) BLS: Bloemfontein soil, (e) WBS: Winburg soil. ....	62
<b>Figure 4.12:</b> Sample preparation by front loading for XRD test.....	65
<b>Figure 4.13:</b> Multi-purpose diffractometer (MPD) used for XRD test.....	65
<b>Figure 4.14:</b> Philips automated powder diffractometer.....	65
<b>Figure 4.15:</b> Proctor compaction test. ....	69
<b>Figure 4.16:</b> Maximum dry density and optimum moisture content determination through Proctor test.....	71
<b>Figure 4.17:</b> (a) consolidation cell, (b) saturation of porous stone, (c) assembled consolidation cell, (d) setup of oedometer for swelling stress measurement.....	73
<b>Figure 4.18:</b> (a) compacted specimens wrapped in airtight plastic bag, (b) specimens kept in a constant temperature bath, (c) compacted sample inserts inside a consolidation ring using a jack. ....	74
<b>Figure 4.19:</b> A view of a conventional consolidometer setup .....	74
<b>Figure 4.20:</b> Total suction calibration test sketch .....	77
<b>Figure 4.21:</b> Filter papers calibration curves (reproduced from ASTM D5298).....	78
<b>Figure 4.22:</b> (a) Glass jar, salt solution, plastic support, filter paper and tweezers. (b) Glass jar filled with salt solution .....	79
<b>Figure 4.23:</b> (a) Plastic support hold filter papers; (b) glass jar close tightly .....	79
<b>Figure 4.24:</b> Non-contact and contact filter paper technique for measuring the total and matric suction (1 <sup>st</sup> Step).....	81
<b>Figure 4.25:</b> Non-contact and contact filter paper technique for measuring the total and matric suction (2 <sup>nd</sup> Step).....	81

<b>Figure 4.26:</b> (a) Preparation of compacted soil sample for suction measurement.....	85
<b>Figure 4.27:</b> Three filter papers placed for matric suction measurement. ....	86
<b>Figure 4.28:</b> Edges of the sample sealed with electrical tape. ....	86
<b>Figure 4.29:</b> (a) plastic ring put on soil specimen, (b) Filter paper carried using tweezers, (c) Filter paper placed over the ring support for total suction measurement; (d) sealed glass jar.....	87
<b>Figure 4.30:</b> Temperature regulatory apparatus.....	88
<b>Figure 4.31:</b> Moisture tin is weighed before filter paper were taken out from the jar.....	88
<b>Figure 4.32:</b> Filter papers are put into labeled moisture tines for suction measurement.....	89
<b>Figure 4.33:</b> (a) oven dried moisture tin, (b) moisture tin put on the metal block to cool it down quickly.....	90
<b>Figure 5.1:</b> Grain size distribution curve.....	97
<b>Figure 5.2a:</b> Chart-grain size distribution. ....	97
<b>Figure 5.2b:</b> Chart-grain size distribution. ....	98
<b>Figure 5.3:</b> Liquid limit versus soil designation.....	98
<b>Figure 5.4:</b> Plasticity index versus soil designation.....	99
<b>Figure 5.10:</b> Casagrande plasticity chart.....	99
<b>Figure 5.11:</b> Linear shrinkage of soil designation.....	100
<b>Figure 5.12:</b> Specific gravity of soil designation. ....	101
<b>Figure 5.13:</b> Activity of soil designation.....	101
<b>Figure 5.14:</b> Free swell index test results.....	102
<b>Figure 5.15:</b> Free swell ratio test results. ....	103
<b>Figure 5.16:</b> X-ray diffraction pattern (WKS). ....	104
<b>Figure 5.17:</b> X-ray diffraction pattern (BLS).....	104
<b>Figure 5.18:</b> X-ray diffraction pattern (PTS). ....	105
<b>Figure 5.19:</b> X-ray diffraction pattern (WBS). ....	105
<b>Figure 5.20:</b> X-ray diffraction pattern (BTS). ....	106
<b>Figure 5.21:</b> Compaction curve graph.....	108
<b>Figure 5.22:</b> Compaction curve graph (BTS).....	108
<b>Figure 5.23:</b> Compaction curve graph (PTS).....	109
<b>Figure 5.24:</b> Compaction curve graph (BLS).....	109

<b>Figure 5.25:</b> Compaction curve graph (WBS) .....	110
<b>Figure 5.26:</b> Compaction curve graph (WKS) .....	111
<b>Figure 5.27:</b> Calibrated curve using Whatman No 42 filter paper.....	112
<b>Figure 5.28:</b> Calibrated curve and adopted curve graph .....	113
<b>Figure 5.29:</b> Measured vs predicted values of suction from calibration curve .....	113
<b>Figure 5.30:</b> Total suction for soil designation at OMC .....	115
<b>Figure 5.31:</b> Matric suction for soil designation at OMC.....	115
<b>Figure 5.32:</b> Osmotic suction for soil designation at OMC .....	115
<b>Figure 5.33:</b> Suction versus water content (WKS) .....	116
<b>Figure 5.34:</b> Suction versus water content (WBS) .....	116
<b>Figure 5.35:</b> Suction versus water content (BLS).....	116
<b>Figure 5.36:</b> Suction versus water content (PTS).....	117
<b>Figure 5.37:</b> Suction versus water content (BTS).....	117
<b>Figure 5.38:</b> Total suction versus water content .....	117
<b>Figure 5.39:</b> Matric suction versus water content .....	118
<b>Figure 5.40:</b> Volumetric water content at Air entry value (AEV) .....	120
<b>Figure 5.41:</b> Matric suction at Air entry value (AEV) .....	120
<b>Figure 5.42:</b> Soil water characteristic curve for WKS as compacted .....	121
<b>Figure 5.43:</b> Soil water characteristic curve for WBS as compacted .....	121
<b>Figure 5.44:</b> Soil water characteristic curve for BLS as compacted .....	122
<b>Figure 5.45:</b> Soil water characteristic curve for PTS as compacted .....	122
<b>Figure 5.46:</b> Soil water characteristic curve for BTS as compacted .....	123
<b>Figure 5.47:</b> Swelling stress for soil designation at OMC .....	124
<b>Figure 5.48:</b> Maximum swelling stress for soil designation .....	124
<b>Figure 5.49:</b> Swelling stress versus total suction .....	126
<b>Figure 5.50:</b> Swelling stress versus matric suction .....	126
<b>Figure 5.51:</b> Swelling stress versus osmotic suction .....	126
<b>Figure 5.52:</b> Swelling stress versus initial dry density .....	127
<b>Figure 5.53:</b> Swelling stress versus initial dry density at OMC .....	128
<b>Figure 5.54:</b> Swelling stress versus initial water content .....	129
<b>Figure 5.55:</b> Swelling stress versus optimum water content .....	129
<b>Figure 5.56:</b> Swelling stress versus plasticity index at OMC .....	130
<b>Figure 5.57:</b> Swelling stress versus liquid limit at OMC .....	131

<b>Figure 5.58:</b> Swelling stress versus linear shrinkage at OMC .....	132
<b>Figure 5.59:</b> Swelling stress versus activity of clay at OMC .....	132
<b>Figure 5.60:</b> Swelling stress versus free swell index at OMC .....	133
<b>Figure 5.61:</b> Swelling stress versus free swell ratio at OMC .....	134
<b>Figure 5.62:</b> Swelling stress versus clay fraction at OMC .....	135
<b>Figure 5.63:</b> Comparison between experimental and predicted values of swelling stress (model 6) .....	139
<b>Figure 5.64:</b> Comparison between experimental and predicted values of swelling stress (model 5) .....	139
<b>Figure 5.65:</b> Comparison between experimental and predicted values of swelling stress (model 4) .....	140
<b>Figure 5.66:</b> Comparison between experimental and predicted values of swelling stress (model 3) .....	140
<b>Figure 5.67:</b> Comparison between experimental and predicted values of swelling stress (model 2) .....	141
<b>Figure 5.68:</b> Comparison between experimental and predicted values of swelling stress (model 1) .....	141
<b>Figure 5.69:</b> Comparison of predicted values of swelling stress from proposed models, and predictive model by Forouzan (2016) .....	143
<b>Figure 5.70:</b> Comparison of predicted values of swelling stress from proposed models, and predictive model by Yusuf and Ohran (2007) .....	143
<b>Figure 5.71:</b> Comparison of predicted values of swelling stress from proposed models, and predictive model by Tu and Vanapalli (2016) .....	144



## LIST OF APPENDICES

### APPENDIX A:

<b>Table 5.1:</b> Grain size classification.....	157
<b>Table 5.2:</b> Unified soil classification system (USCS).....	157
<b>Figure 5.5:</b> Casagrande liquid limit test (BLS).....	157

### APPENDIX B:

<b>Figure 5.6:</b> Casagrande liquid limit test (BTS).....	158
<b>Figure 5.7:</b> Casagrande liquid limit test (WBS).....	158
<b>Figure 5.8:</b> Casagrande liquid limit test (PTS).....	158

### APPENDIX C:

<b>Figure 5.9:</b> Casagrande liquid limit test (WKS).....	159
<b>Table 5.3:</b> Linear shrinkage test results .....	159
<b>Table 5.4:</b> Specific gravity test results.....	159

### APPENDIX D:

<b>Table 5.5:</b> Free swell index test results.....	160
<b>Table 5.6:</b> Classification of soil base on FSI.....	160
<b>Table 5.7:</b> Free swell ratio test results .....	160
<b>Table 5.8:</b> Classification of soils based on FSR.....	160

### APPENDIX E

<b>Table 5.9:</b> Summary of X-Ray diffraction results.....	161
<b>Table 5.10:</b> Compaction test results.....	161
<b>Table 5.11:</b> Calibrated curves .....	161

### APPENDIX F:

<b>Table 5.12:</b> Suction test results.....	162
--	-----

### APPENDIX G:

<b>Table 5.13:</b> Soil water characteristic curve data (WKS).....	163
<b>Table 5.14:</b> Soil water characteristic curve data (WBS).....	163
<b>Table 5.15:</b> Soil water characteristic curve data (BLS).....	163

### APPENDIX H:

<b>Table 5.16:</b> Soil water characteristic curve data (PTS) .....	164
<b>Table 5.17:</b> Soil water characteristic curve data (BTS).....	164

<b>Table 5.18:</b> Summary of SWCC results .....	164
<b>APPENDIX I:</b>	
<b>Table 5.19:</b> SWCC fitting parameters and equations for soils WKS & WBS .....	165
<b>APPENDIX J:</b>	
<b>Table 5.20:</b> SWCC fitting parameters and equations for soils BLS & PTS.....	166
<b>APPENDIX K:</b>	
<b>Table 5.21:</b> SWCC fitting parameters and equations for soils BTS .....	167
<b>APPENDIX L:</b>	
<b>Table 5.22:</b> Zero swelling test results.....	168
<b>APPENDIX M:</b>	
<b>Table 5.23:</b> Summary of laboratory test results @OMC .....	169
<b>Table 5.24:</b> Summary of laboratory test results .....	169
<b>Table 5.25:</b> Summary of laboratory test results .....	169
<b>APPENDIX N:</b>	
<b>Table 5.26:</b> Correlation Matrix A.....	170
<b>APPENDIX O:</b>	
<b>Table 5.27:</b> Correlation Matrix B.....	171
<b>Table 5.28:</b> Intercepts, coefficients for regression analysis models .....	171
<b>Table 5.29:</b> Intercepts, coefficient for regression analysis models .....	171
<b>APPENDIX P:</b>	
<b>Table 5.30:</b> Compaction test data sheet.....	172
<b>APPENDIX Q:</b>	
<b>Table 5.31:</b> Measurement of soil suction using filter paper data sheet.....	173

## LIST OF ABBREVIATIONS

AIC	Akaike Information Criterion
AEV	Air Entry Value
ASTM	American Society for Testing and Material
BLS	Bloemfontein Soil
BTS	Bethlehem Soil
CST	Consolidation Swelling Test
CH	High Plastic Clay
CL	Medium Plastic Clay
DOT	Double Oedometer Test
FSI	Free Swell Index
FSR	Free Swell Ratio
FPM	Filter Paper Method
GSD	Grain size distribution
IS	Indian Standards
MFSI	Modified Free Swell Index
MPD	Multi-Purpose Diffractometer
MSR	Mean Square Error
OMC	Optimum moisture content
PTS	Petrusburg Soil
RSS	Residual Sum of Squares
RSD	Relative Standard Deviation
SWCC	Soil Water Characteristic Curve
TMH	Technical Method for Highways
USCS	Unified Soil Classification System
VCP	Volume Change Potential
XRD	X-ray diffraction
WBS	Winburg Soil
WKS	Welkom Soil
ZST	Zero Swelling Test

## NOTATIONS AND SYMBOLS

### Roman letters

$a_f$	Soil parameter related to the air entry of the soil
$A_c$	Activity of clay
$br$	Beam ratio
$C$	Correction factor
$e_c$	Unit electron charge
$e$	Natural constant 2.718
$f^*$	Interaction function between the equilibrium of the soil structure and the equilibrium of the contractile skin
$F_{sy}^w$	Interaction force between water phase and the soil particle in direction (y)
$F_{sy}^a$	Interaction force between the air phase and the soil particle in direction (y)
$g$	Gram
$G_s$	Specific gravity
$h_c$	Capillary height
$I_{ss}$	Swell-shrink index
$K$	Boltzmann's constant
$K_o$	Number of estimated parameter
$LL$	Liquid limit
$LS$	Linear shrinkage
$m$	Number of relevant soil parameter
$m_1$	Mass of wet filter paper + cold tare
$m_2$	Mass of wet filter paper + hot tare mass
$m_f$	Soil parameter related to the residual water content condition
$M$	Total mass
$M_1$	Empty mass of volumetric flask
$M_2$	Mass of pycnometer + oven dry soil
$M_3$	Mass of pycnometer + oven dry soil + filled water
$M_4$	Mass of pycnometer + filled with water only
$M_a$	Mass of air

$M_w$	Mass of water
$M_s$	Mass of solids
$M_c$	Mass of the contractile skin
$M_f$	Mass of the dry filter paper
$M_i$	Unit mass of surcharge
$M_m$	Mass of the mould and base plate
$M_{soil}$	Mass of the dry soil
$M_t$	Mass of the mould, base plate, and wet soil
$M_w$	Mass of water to be added
$M_v$	Mass of water in the filter paper
$N$	Number of blows
$n$	Number of surcharges
$n_f$	Soil parameter related to the rate of desaturation
$n_w$	Porosity relative to the water phase
$n_c$	Porosity relative to the contractile skin
$n_s$	Porosity relative to the soil particles
$PI$	Plasticity index
$P_s$	Swelling stress
$PL$	Plastic limit
$P_{so}$	Intercept on the $P_s$ axis at zero suction value
$Q(x)$	Complementary cumulative normal distribution function
$R$	Radius of the capillary tube
$R^2$	Correlation coefficient
$R_T$	Universal gas constant
$R_d$	Relative density of water according to temperature
$R_s$	Sheath radius of curvature/ Radius of curvature of the meniscus
$R_1, R_2$	Radius of curvature of warped membrane
$S$	Degree of saturation
$S_e$	Effective saturation
$t$	Two layers thicknesses
$T$	Temperature
$T_c$	Cold tare mass
$T_h$	Hot tare mass

$T_s$	Tension surface
$T_k$	Absolute temperature
$T_{zy}$	Shear stress on the z-plan in y direction
$U_a$	Pore air pressure
$U_w$	Pore water pressure
$\bar{u}_v$	Partial pressure of pore
$\bar{u}_{v0}$	Saturation pressure of water steam over a flat surface of pure water at the same temperature
$V$	Total volume
$V_a$	Volume of air
$V_c$	Volume of contractile skin
$V_d$	Volume of the soil specimen read from the graduated cylinder containing distilled water.
$V_f$	Final volume of the specimen
$V_i$	Initial volume of the specimen
$V_k$	Volume of the soil specimen read from the graduated cylinder containing Kerosene
$V_s$	Volume of solids
$V_m$	Volume of the mould
$V_w$	Volume of water
$W$	Moisture content
$W_1$	Mass of container + wet soil
$W_2$	Mass of container + wet soil
$W_c$	Mass of container
$W_f$	Water content of the filter paper
$W_i$	Initial water content
$W_{opt}$	Optimum moisture content
$W_t$	Targeted moisture content
$X_{ij}$	Independent variables
$Y$	Dependent variable

## Greek letters

$\alpha_1$	Angle of contact
$\beta$	Angle between the tension surface and horizontal
$\varepsilon_c$	Dielectric constant medium
$\varepsilon$	Random error representing the discrepancies in the approximation
$\eta$	Electrolyte concentration
$\nu$	Cation valence
$\rho_w$	Density of water
$\rho_s$	Soil particle density
$\psi_t$	Total soil suction
$\psi_m$	Matric suction
$\psi_o$	Osmotic suction
$\tau_{xy}$	Shear stress on the plan (y,z), perpendicular to direction (y)
$\tau_{zy}$	Shear stress on the plan (x,y), perpendicular to direction (x)
$\sigma_y$	Total normal stress parallel to direction (y)
$\theta_s$	Volumetric water at saturation
$\theta_r$	Residual volumetric water content
$\theta_w$	Volumetric water content
$\gamma_d$	Dry density
$\gamma_{dmax}$	Maximum dry density
$\lambda_o, \eta_o, \xi_o, \zeta_o, \beta_o, \mu_o$	Intercepts
$\lambda_i, \eta_i, \xi_i, \zeta_i, \beta_i, \mu_i$	Multi-regression analysis coefficient
$\frac{\delta(\gamma_d)}{\delta w}$	Differential function
$\phi(x)$	Normalized form of the cumulative normal distribution function
$\phi$	Internal diameter of the consolidation ring
$\Delta U$	Difference in stress on a two - dimension curved arc
$\Delta V$	Initial change in volume of a specimen

## CHAPTER 1: INTRODUCTION

### 1.1 Background

Defects on constructions caused by heaving soils were first reported in South Africa in 1950, particularly in Goldfield Mine Free State. Lightweight structures such as subsidy houses failed to fulfil their service life and were demolished prematurely. Lightweight constructions are the most vulnerable to heaving soils because these structures are less capable to overcome the differential movement. Figure 1.1 shows the distribution of expansive soils across South Africa, and Figure 1.2 shows defects caused by expansive soils on some structures in Free State. In South Africa, expansive soils are considered the most problematic (Williams; Pidgeon and Day, 1985). The repairs cost of damages caused by heaving soils inside South Africa has been estimated at R100 million annually (Williams et al., 1985). The cost of similar problems in the United Kingdom is estimated at £400 million per year (Crilly and Driscoll, 2000). The American Society of Civil Engineers estimated that 25 % of houses have some damages caused by heaving soils (Jones and Jefferson, 2012). Expansive soils cause a higher annual financial loss than hurricane, flood, earthquake, and tornadoes combined (Nelson and Miller, 1992).

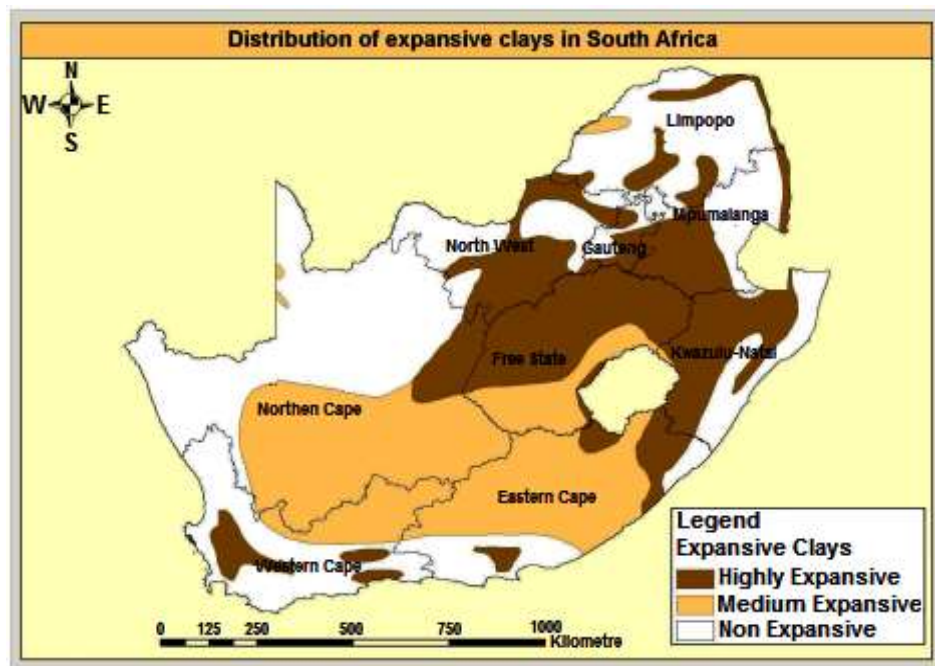


**Figure 1.1:** Map showing the distribution of expansive soils in South Africa (Diop et al., 2011).



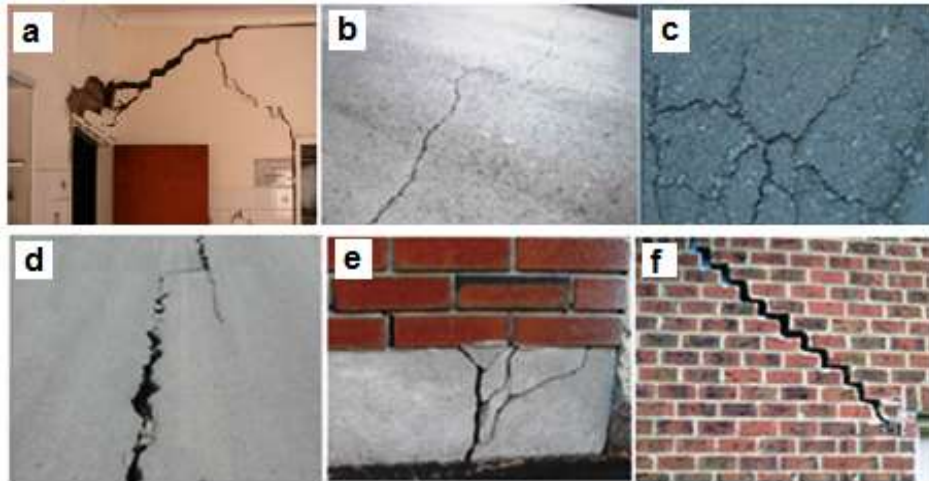


**Figure 1.2:** Structural defects caused by heaving soils in Free State.

a) Structural damage in a house cause by end lift in Bloemfontein. b) Transverse crack on pavement caused by swell/shrink in Bethlehem. c) Map cracks caused by excessive swelling stress on pavement support in Welkom. d) Longitudinal cracks on pavement at Petrusburg. e) Buckled foundation defect at Kroonstad. f) Crack at the corner of a wall opening due to foundation differential settlement at Winburg.

A good understanding of the physical and hydromechanical properties of compacted expansive soils it is very important to enhance engineering design. Expansive soils present significant structural and geotechnical engineering challenges worldwide. Abeb and Vermeer (2009) investigated the numerical simulation of heaving soils behaviour. As a result, the analysis of the behaviour of heaving soils can be achieved efficiently using unsaturated soil mechanics.

## 1.2 Problem Statement

The consideration of the swelling stress in foundation design for expansive soils enhance durability, service life, and reduce the cost of assessments and repairs works to be undertaken in the future. Swelling stress is generally ignored in engineering practice. This stress can develop significant uplift forces detrimental to the foundation stability.

The prediction of swelling stress has been a concern in construction industry for many years. Furthermore, models proposed to predict the swelling stress are generally developed using artificial test specimens. Nonetheless, a model developed using artificial samples must be verified using soils from the field.

Models developed using field compacted samples could predict more precisely the swelling stress.

The oedometer swelling test is a commonly used technique to measure the swelling stress. The oedometer swelling test in engineering practice is cumbersome and time-consuming, making the test unattractive and not cost-effective for the low-cost housing project. It becomes important to propose models to predict the swelling stress to alleviate the need for conducting this test. Laboratory tests used to measure the soil parameters such as soil suctions, Atterberg limits, dry density, water content, and free swell ratio, have been well established with standard guidelines. A correlation between the swelling stress and these soils parameters can be used to indirectly approximate the swelling stress for a field compacted expansive soils.

Field conditions are often different from those considered in classical soil mechanics, and particularly when heaving soils are present. Classical soil mechanics consider the pore pressures to be negligible. However, for unsaturated conditions, the true nature of pore pressures is more complex. For expansive soils, unsaturated conditions may prevail, often creating substantial negative pore pressures, which work to maintain low void ratios and very little expansion. Nonetheless, as more moisture is introduced into the soil matrix, the soil expands significantly with a large magnitude of forces. Adopting the classical approach as described above fails to consider the true nature of the soil. Therefore, a more appropriate way to consider such soils is through the application of unsaturated soil mechanics. By doing so, one may better quantify the swelling stress and its dependence on soil moisture. This leads to a more realistic approach to foundation design in expansive soils.

### **1.3 Research objective**

The main objective of this study is to characterize the relationship between the swelling stress and the soil moisture deficiency for compacted expansive soil. However, the objectives of this research will further focus on the relationship between the swelling stress and other soil parameters such as geotechnical index properties, expansive soil parameters.

1. Undertake a comprehensive review of previous research concerned with the prediction of swelling stress in expansive soils.
2. Perform laboratory experiments to determine the physical and hydro-mechanical properties of soil specimens as well as the soil water characteristic curve.
3. Analyze data obtained from laboratory tests, quantitatively by multiple regression analysis using software NCSS11. Develop a mathematical model to predict the swelling stress of compacted expansive soils.
4. Validate the models by comparing predicted values obtained from models proposed in this study to the values obtained from other models.

#### **1.4 Research scope**

The results of this study can be applied to foundation design in heaving soils for lightweight structure. Other problematic soils encountered in South Africa such as dolomite, collapsible soils, and soft clay are beyond the scope of this study. The variability of soil parameters, the difference between field and laboratory measurements due to scale effect, and the degree of accuracy of laboratory tests performed make this study a contribution.

#### **1.5 Dissertation layout**

The research work is organized into six chapters: Chapter 1 covers the general background, problem statement, aim, and scope of the research. Chapter 2 presents the expansive soils and the unsaturated soil mechanics. Chapter 3 covers previous research works on the prediction of swelling stress. Chapter 4 describes the experimental study. Chapter 5 focus on advanced testing and analysis. Chapter 6 presents the conclusion and perspectives.

---

## CHAPTER 2: LITERATURE REVIEW

### PART 1: EXPANSIVE SOILS

#### 2.1 Definition

Heaving soils vary in volume in relation to water content. This term is commonly used to characterize rock or soil material with an important swell/shrink potential. These soils contained clay minerals that swell as the moisture content increases and shrink when the moisture content decreases.

#### 2.2 Origin

Heaving soils originate from a combination of processes and conditions. Specific clay minerals formed with a mineralogical and chemical configuration that attracts and holds a noteworthy volume of water. The parent rock composition and the intensity of chemical and physical weathering that the materials are exposed determine the clay mineralogy and likelihood of heave. Parent materials related to heaving soils are classified into two categories (Grim, 1968). The first category is formed by basic igneous rock that is composed of a significant metallic base such as olivine, amphibole, biotite, and pyroxene. Such rock contains volcanic glass and basalts. The second category comprises the sedimentary rock that contains smectite. Shale and clay stones constituents are formed with a varying quantity of glass and volcanic ash that are weathered to form montmorillonite.

Heaving soils may be either residual or transported materials. In residual soil, heaving soils originates from in-situ chemical weathering of rock. For transported soil, heaving soils is removed from its in-situ location by wind, water, gravity or ice and deposited in a different location (William *et al.*, 1985). Transported soils are as follows: Alluvium (stream or river), Lacustrine deposits (Originating from a stream then deposited in lake or still water), Gully wash (from local catchment and which contain a variety of heaving soils), Hill wash (from lower velocity sheet wash, usually with less expansive material). Residual soils are the main source of expansive soils and are summarized in Table 2.1.

**Table 2.1:** Residual soils prone to expansiveness  
Department of local government, housing and works (1990).

Geology	Residual Soil
Basic Igneous Rocks	Norite of the bushveld igneous complex- often referred to as "black turf"
	Dolerite of the Karoo super group.
	Andesite or dolerite in the Pretoria group, Transvaal super group.
	Lavas (andesitic) of the ventersdorp super group.
Argillaceous Rocks	Shale, mudrock, tillite and varvites of the Dwyka formation, Karoo Supergroup.
	Shale and mudrock of the Ecca and Beaufort group, Karoo Supergroup.
	Cretaceous marine formation (Port Elizabeth and Uitenhage).

### 2.3 Climate

Climate is a relevant factor that governs the type and the rate of soil formation. Climate affects the rate of chemical, mineralogical, biological and physical processes involved in soil formation through the actions of precipitation and temperature. Temperature is often represented by mean annual temperature while rainfall is quantified by annual rainfall and length of the dry season. In semi-arid climate, evaporation exceeds precipitation and alternate wet and dry seasons may lead to the formation of smectite.

### 2.4 Topography

Topography influences soils formation through deposition, erosion, and the residence time of water that may infiltrate into the soil horizon. Infiltration has a major influence on soil mineralogy since chemical weathering processes require water. Steep slopes does not allow infiltration, but erosion will expose parent igneous rock to further chemical weathering and lead to the formation of smectite.

### 2.5 Time

Time affects soil formation in two ways: the value of a soil-forming factor is time dependent and the extent of pedogenetic reaction depends on its duration. The influence of climate on the development of soil from parent material takes time. It is a critical factor because the process of soil formation is an equilibrium reaction requiring a significant amount of time to accomplish a full evolution from rock to soil.

## 2.6 Mineralogical composition of clays

The structure of the soil is a combination of the effects of the fabrics and interparticle forces. Holtz et al.,(1981) stated that a soil fabric refers only to the geometrical arrangement of particles. Clay mineral refer to hydrous aluminum phyllosilicates minerals that are fine - grained ( $< 0.002$  mm) with a sheet layer structure and very high surface area (Cameron et al., 1992). Clay minerals are built up with silicon oxygen tetrahedral  $(\text{Si}_4\text{O}_{16})_2$  layers and aluminum  $\text{Al}_2(\text{OH})_6$  or magnesium  $\text{Mg}_3(\text{OH})_6$ , gibbsite or brucite sheet in octahedral layers (Wu, 1978) as shown in Figures 2.2 and 2.3. Kaolinite group, Illite group, and smectite group are common clay mineral.

**2.6.1 Kaolinite:**  $[\text{Si}_2\text{Al}_2\text{O}_5(\text{OH})_4]$  is formed with a sequence layer of elemental silica gibbsite sheets in 1:1 lattice, as shown in Figure 2.1a. Each layer is about  $7.2 \text{ \AA}$  thick. Hydrogen bonding holds layers together. The specific surface of Kaolinite particle is around  $15\text{m}^2/\text{g}$ . Kaolinite is a non - heaving clay mineral, it will not crack during drying, instead produces high soil strength.

**2.6.2 Illite:**  $[(\text{K},\text{H}_3\text{O})(\text{Al},\text{Mg},\text{Fe})_2(\text{Si},\text{Al})_4\text{O}_{10}((\text{OH})_2,(\text{H}_2\text{O}))]$  is a clay mineral of 2:1 type mica mineral formed by gibbsite layer bounded to silica layers-one at the bottom and another at the top as shown in Figure 2.1b. Illite sheets are bonded by potassium ions. The potassium ions are balanced by negative charge. Potassium ion comes from the substitution of aluminum for some silicon in tetrahedral sheets. Illite is not expansive even it is nearly identical to 2:1 phyllosilicate (smectite).

**2.6.3 Montmorillonite:**  $[(\text{NaCa})(\text{AlMg})_2(\text{Si}_4\text{O}_{10})(\text{OH})_2.n\text{H}_2\text{O}]$  is the most common smectite, it is located in arid to the semi - arid climate in which evapotranspiration exceeds rainfall during the significant period of the year. This is partly explained by the theory that absence of leaching in moisture deficiency zones helps the development of montmorillonite (Mitchell, 1993). Montmorillonite structure looks like that of illite: a gibbsite sheet sandwiched between two silica layers Figure 2.1c. Montmorillonite contains an isomorphous substitution of magnesium and iron for aluminum in octahedral layers. Montmorillonite particles have lateral dimensions of 1000 to 5000  $\text{Å}$  and thicknesses of 10 to 50  $\text{Å}$ . The specific surface is about  $800\text{m}^2/\text{g}$ . A molecule of water and exchangeable cations such as magnesium,

calcium are located between layer spaces to balance charge deficiencies (Murray, 2007).

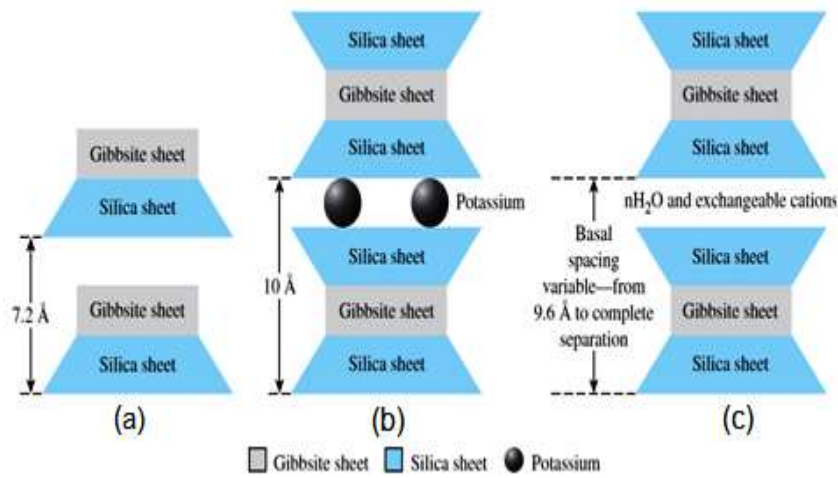


**Figure 2.1:** Diagram of structures (a) kaolinite; (b) illite; (c) montmorillonite

The basal spacing value (in Angstroms) determined by X-ray diffraction, and the specific area surface and cation exchange capacity (CEC) for different clay mineral groups are given in Table 2.2.

**Table 2.2:** Some of clay mineral characteristics (Mitchell, 1993).

Minerals	Interlayer bond	Basal spacing	Specific surface area (m <sup>2</sup> /gm)	Cation exchange capacity (meq/100g)
Kaolinite	Hydrogen; Strong	7.2 Å	10 - 20	3 - 15
Montmorillonite	Oxygen - Oxygen Very weak	9.6 Å	700 - 840	80 - 150
Illite	K ions; Strong	10 Å	65 - 100	10 - 40
Vermiculite	Weak	10.5 - 14 Å	870	100-150
Chlorite	Strong	14 Å	80	10 - 40



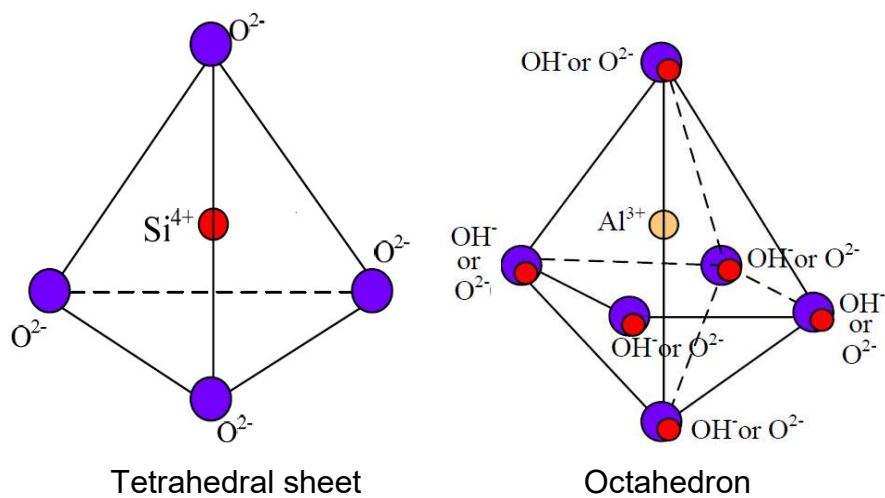
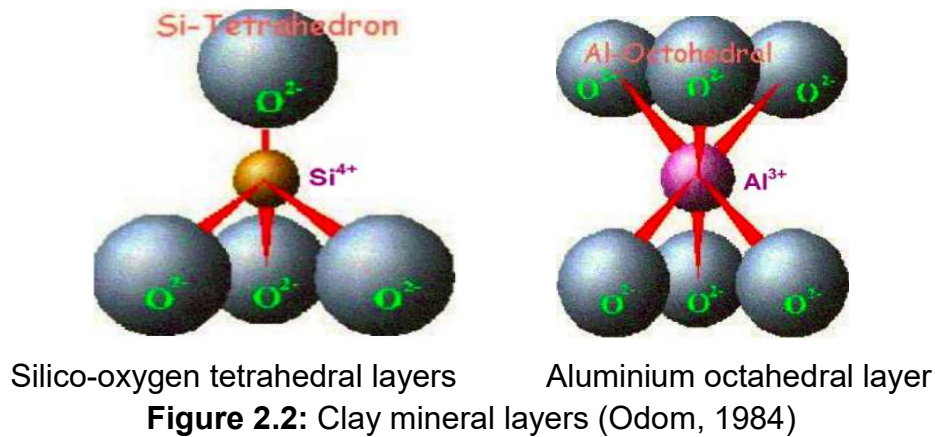


**Figure 2.3:** Tetrahedral and octahedral sheets (Odom, 1984)

### 2.7 Assessment and classification of expansive soils

Swell potential and shrinkage are important parameters to be considered for effective design methods for construction (Van der Merwe, 1964). When dealing with heaving soils, it is very important to have a good understanding of potential issues at the early stage to make sure that cost - effective design approach is adopted to avoid costly assessments and repairs works to be undertaken later. The method of measuring swell potential is the key factor for heaving soils classification. Because of the lack of standard definition of swell potential, there is no universal technique to assess clay swell potential (Nelson and Miller, 1992). Several geotechnical methods are used to measure the swell potential of heaving soils, each of these methods has their own merit. The swell potential of clay can be measured directly or indirectly using correlations with other test data. Few data are available based on direct measurement of parameters of heaving soils



because these data are required for a few engineering applications. Nonetheless, these procedures give a good indicator of expansive potential when the soil is subjected to laboratory test conditions. Therefore, reliance must be placed on estimation base on index parameters such as plasticity index, dry density (Reeve et al., 1980; Holtz and Kovacs, 1981; Oloo et al., 1987).

### 2.7.1 Laboratory testing

Generally, three different methods are used to assess heaving soils in the laboratory: index tests, mineralogy test, and swelling-shrinkage test.

### 2.7.2 Particle size distribution

Particle size distribution is the cumulative percentage of soil that is smaller than a given diameter, starting at 100 % (large diameter) and ending near 0% (small diameter). The sedimentation process is used to measure the sized of particles smaller than 0.002 mm, and the distribution of sized particle larger than 0.002 mm is determined by dry sieving as illustrated in Figure 2.4. Expansive capacity is directly linked to the quantity of sized particles (diameter < 0.002 mm).

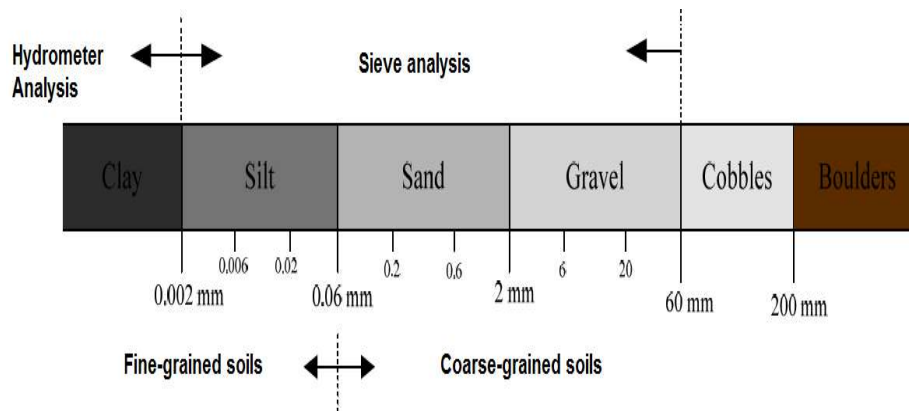


**Figure 2.4:** Grain size distribution for dry and wet sieve analysis.

### 2.7.3 Atterberg limit

Around 1908, Albert Mauritz Atterberg (1846-1916), a Swedish soil scientist and chemist, defined a clay - size fraction as the percentage by weight of particle smaller than 0.002 mm in size. He recognized the significant role of clay particles in soil and its plastic behaviour. In 1911, he defined the consistency of cohesive

soils by describing liquid, plastic, and shrinkage limits as shown in Figure 2.5. He also established the plasticity index (PI) as the difference between liquid limit and plastic limit (Atterberg, 1911).

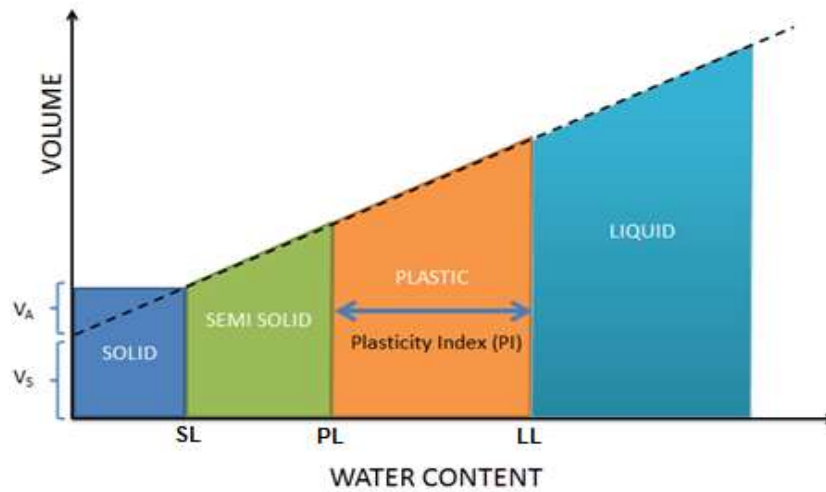


**Figure 2.5:** Relationship in Atterberg limits

Atterberg limits are the most common procedures for collecting information on swelling behavior and mechanical properties of heaving soils (Williams, 1958). The most useful classification data for assessing the relative expansive potential are liquid limit (LL) and plasticity index (PI). However, the most widely used parameter for measuring the expansive capacity and the shrinkage is the plasticity index (PI). The Plasticity Index is based on remolded samples. Nonetheless, the test is undertaken according to established procedures and performed under reproducible conditions according to worldwide standards (Jones, 1999). A modified plasticity index (PI') is presented in the Building Research Establishment Digest 240 (BRE, 1993), and it is used when the data of particle size, precisely the portion passing a 425µm sieve, is available or is assumed to be 100% passing as shown in Table 2.3.

**Table 2.3:-** Classification for shrink-swell clay soils (BRE, 1993)

PI' (%)	Volume Change Potential (VCP)
> 60	Very high
40-60	high
20-40	medium
< 20	low

Where:  $PI' = PI \times (\% < 425\mu m) / 100\%$

Modified plasticity index (PI') is considered for the total specimen and not only the fine fraction. It gives a better indication of the true plasticity value of soil as foundation support and reduces significantly the discrepancies due to the particle size

### 2.7.4 Mineralogical testing

Energy disperse X-ray (EDX) is used to determine the nature of particles inside the clay such as the component minerals shape of clay particles, deficiency of the charge, the activity of the clay surface, feature of crystal dimensions, surface area, etc. These properties control the expansive behaviour of soil. In addition to the traditional parameters used to identify the mineralogy of weathered clays, other parameters related to the swelling of consolidated or compacted clays and shale's have been used to assess the mineralogy: disjoining pressure (Derjagin et al., 1987) dielectric dispersion (Basu and Arulanandan, 1974).

## 2.8 Swell potential testing (indirect measurement)

### 2.8.1 Expansive capacity classification based on plasticity table

The Atterberg limits of soil specimen are used to indicate the swelling potential as shown in Table 2.4. For example, a soil specimen with liquid limit greater than 70% and index of plasticity exceeding 35% and shrinkage limit less than 11% is considered to have a very high swelling capacity.

**Table 2.4:** Potential swell based on plasticity (Holtz, 1954)

Classification of Potential swell	Liquid limit (LL),%	Plasticity Index (PI),%	Shrinkage Limit (SL),%
Low	20-35	< 18	>15
Medium	35-50	15-28	10-15
High	50-70	28-41	7-12
Very high	>70	>35	<11

### 2.8.2 Swelling capacity classification based on advanced physical properties of soil.

Researchers such as Van der Merwe (1964)., Skempton (1953) and Seed et al.,(1960) have established correlations between the expansive capacity and physical properties of soils such as clay content, plasticity index, soil activity, etc. Preliminary classification based on clay content fraction (soil particle < 0.002 mm

in diameter) and the plasticity index can be used to categorize probable severity as presented in Figure 2.6.

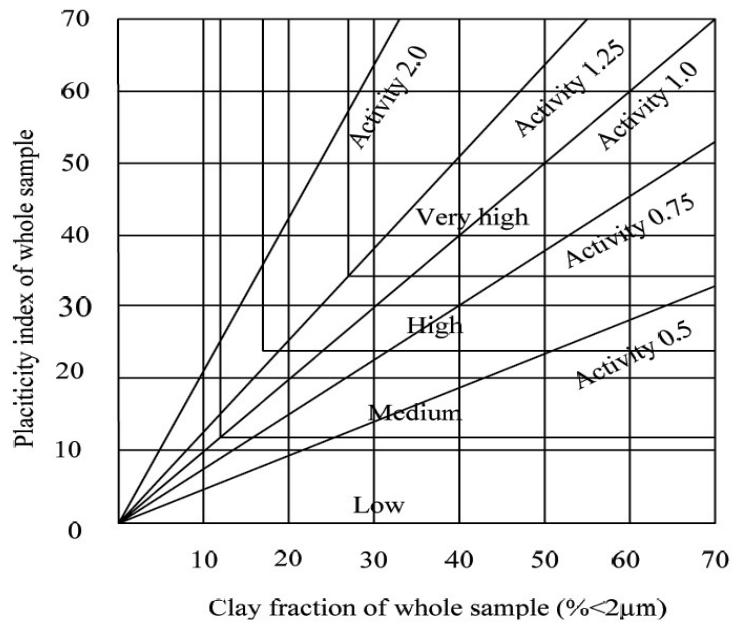


**Figure 2.6:** Chart for evaluation of potential expansiveness (Seed et al, 1960)

Another method for investigating heaving soils is the use of activity method presented by Carter and Bentley (1991). The proposed classification chart is shown in Figure 2.7.

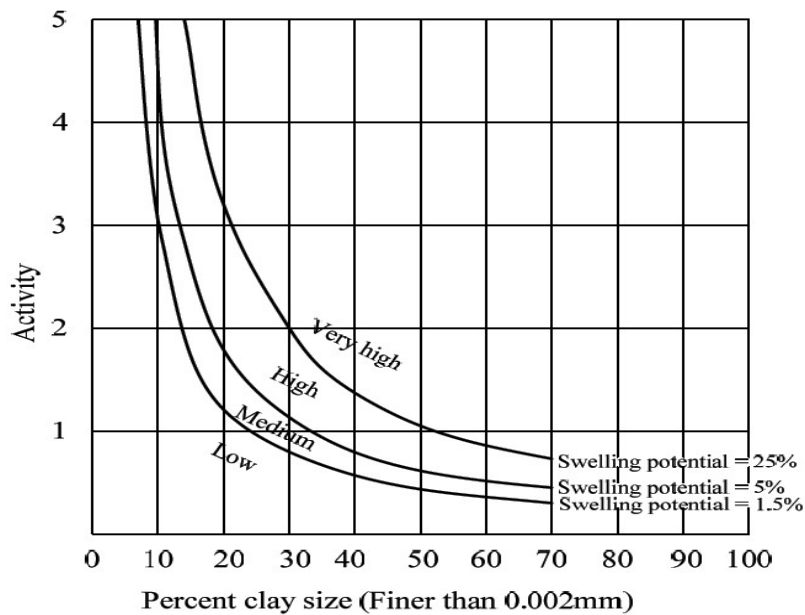


**Figure 2.7:** Classification chart for swelling potential by Carter and Bentley (1991)

### 2.8.3 Casagrande's chart plasticity for swelling potential classification

The Casagrande plasticity chart in Figure 2.8 is used to plot the plasticity index against liquid limit. For example, a soil specimen with a plasticity index (PI) 30% and a liquid limit (LL) 45% plot in the area typical for montmorillonite showing that is a high potential for swelling.

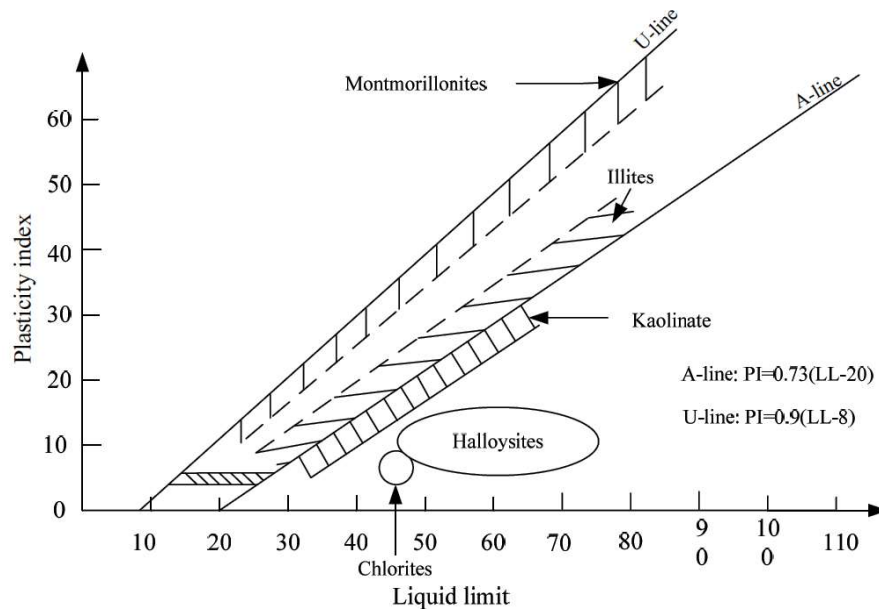


**Figure 2.8:** Casagrande chart (Chleboard et al., 2005)

Soils that are plotted beyond A-line are plastic clays. Those plotted below the A-line are organic soils, clay, and silt containing a high amount of rock flour (BS 5930, 1981). The U-line shows the upper bound for soils, therefore no soil should be plotted beyond U-line.

## 2.9 Swell potential testing (Direct measurement)

### 2.9.1 Free swell index test

This test is a very simple procedure run to indicate the basic swell properties of soil. It is carried out by pouring 10cm<sup>3</sup> of dry soil passing the 0.425mm sieve into graduated cylinder filled with distilled water (Holtz, 1954). The free expansion is defined as the ratio of increase in the volume of soil from a loose dry powder to the equilibrium volume of sediment when water is poured into it. Determined as a percentage of initial volume as shown in Figure 2.9.

$$\text{Free swell index} = \frac{\Delta V}{V_i} \times 100 \quad (2.1)$$

Where:

$\Delta V = V_S - V_i$  initial change in volume (V) of a specimen,

$V_i$  = initial volume ( $10\text{mm}^3$ ) of the specimen, and

$V_S$  = final volume of the specimen.

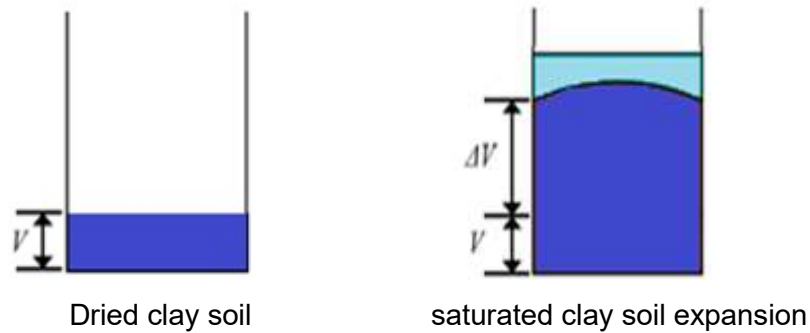


**Figure 2.9:** Phase diagrams of free swell.

Soil with free swell greater than 50% could exhibit expansion problems whereas soil with free swell less than 50% are not expected to display a swelling behavior. In addition, values around or greater than 100% are associated with high swelling capacity.

### 2.10 Site investigation

The main difficulty of heaving soils is that they sometimes show important changes from one location to another (i.e. spatial variability). The essence of investigating heaving soils is to have a sound knowledge of local geology using maps to provide a guideline for locations and extent of swelling soils. For any site investigation, reconnaissance and a field survey can provide useful data about the likelihood and characteristics of heaving soils and their associated issues. Indicators that should be used as a guide that heaving soils might be present include fissures in the ground surface as shown in Figure 2.10.



**Figure 2.10:** Expansive soils, polygonal marking of shrinkage fissures on the surface of the soil

During the dry season, heaving soils exhibit typical shrinkage crack patterns. The features of heaving soils are as follows: deep shrinkage fissures, dry strength is high, wet strength is low, high soil plasticity and shear areas have glazed surface.

### 2.11 In situ testing

Electrical resistivity is a promising method to measure the swelling and shrinkage pressure of heaving soils (Zha et al., 2006). Electrical resistivity was found to increase as both shrinkage and swell pressure increases. The depth of the active zone can be established by measuring the water content profile over many wet and dry periods (Nelson et al., 2001).

### 2.12 Classification of expansive soils

Parameters obtained from heaving soils index tests have been combined in several classification schemes. However, before using any soil classification system, the engineer should understand the database from which it was derived and establish its limitations. Otherwise, poor reliability and lack of certainty may result in the system. Classification systems used for heaving soils are based on the indirect or direct prediction of swell capacity or a combination of both. Several researchers have attempted to use classification of shrinking and swelling in order to characterize expansive soils. Some have even tried to establish a unified swelling potential index using common index properties (Sridharan and Prakash, 2000; Kariuki et al., 2004).



### 2.13 Mechanism of swelling

When water interacts with particles of clay, cations concentrate around the negatively charged clay particle surface. The polarity of water molecules will align them near the clay surface and interact with adsorbed cations as well as separate into hydrogen and hydroxyl under certain conditions (Oweis and Khera, 1998). As a result, electrostatic forces are created between exchangeable cations and negative surface (Das, 2008). The interparticle electrical force field depends on the magnitude of negative surface charge, Van Der Waals forces, electrochemistry of surrounding water, and adsorptive forces between clay surfaces and molecules of water. The interparticle force field will find equilibrium because there is no pressure applied externally to balance change, space between particles will change. This modification in particle spacing is a result of disturbance of internal pressure equilibrium is known as shrink/swell (Nelson and Miller, 1992). The area of negative charges on the surface of clay and the balancing cations in solution around the surface of the clay is called diffuse double layer (Das, 2008). Figure 2.11 depicts layers of a molecule of water where attraction force layers of a molecule of water can be split into two parts: double layer and adsorbed water.

Adsorbed water is strongly held by the particle as a very small layer all over it, which is marked as "b" in Figure 2.11. Liquid water from the double layer is less attracted and control clay plasticity (Al-Rawas and Goosen, 2006). In Figure 2.11 region "c" is termed as diffuse since it is farther from the surface and forces of attraction are no longer bind it to the clay. The attraction decreases by the inverse square of the distance as shown in Figure 2.11.

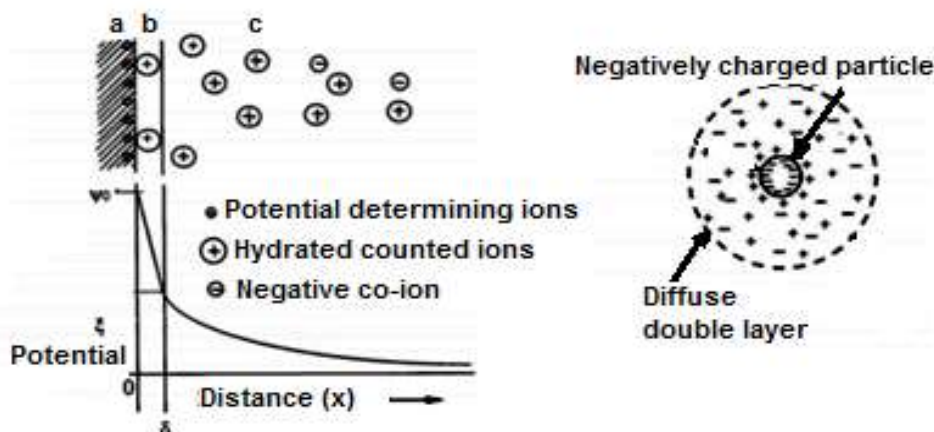


**Figure 2.11:** Presentation of diffuse double layer and force of attraction



A theoretical expression is proposed by Gouy - Chapman in Equation 2.2 for diffuse double layer thickness: ( $t$ ) which can be assumed as radius in Figure 2.11.

$$t = \sqrt{\frac{\epsilon_c \times k \times T}{8 \times \pi \times \eta \times e_c^2 \times v^2}} \quad (2.2)$$

The diffuse double layer thickness depends on dielectric constant medium ( $\epsilon_c$ ), Boltzmann's constant ( $k$ ), absolute temperature ( $T$ ), electrolyte concentration ( $\eta$ ), unit electronic charge ( $e_c$ ) and cation valence ( $v$ ). Diffuse double layer thickness is critical for the evaluation of the expansive capability and the permeability of the soil. The interparticle spacing increases while the thickness diminishes. Therefore, water can easily penetrate and result in an expansion of interparticle spacing.

Patel et al., (2007) stated that clays expand in two manners: hydration of surface and osmotic expansion. Hydration of surface occurs where water molecules layer is adsorbed on the crystal surface by hydrogen bonding. Water molecules in successive layers increase spacing with a quasi-crystalline alignment. However, when osmotic water moves between unit layers in clay mineral from the higher cation concentration to lower concentrations, bulk volume increases. This process is called osmotic expansion. The increase of volume triggered by osmotic expansion is greater than that is generated by hydration of surface. Some clay mineral like sodium montmorillonite undergoes osmotic expansion whereas hydration of surface happens in all categories of clays.

### 2.14 Factors affecting the swell/ shrink behaviour of soil

The shrink-swell capacity of heaving soils is controlled by its initial amount of water; void proportion; vertical pressure; internal structure, the type and amount clay minerals in the soil. These minerals determine the normal expansion of the soil and include smectite, montmorillonite, nontronite, vermiculite, illite, and chlorite. For the most part, the larger the quantity of these minerals present in the soil, the more the expansive capacity. Nonetheless, these swelling impacts may reduce due to the presence of certain non-swelling minerals, for example, carbonate and quartz.

Swelling stress can cause heaving, or lifting, of structures while shrinkage can cause differential settlement. Defect results when the volume changes are

unevenly distributed underneath the construction support. Swelling and shrinkage are not completely reversible processes. The process of shrinkage causes cracks, which on rewetting, don't close up correctly and consequently cause the soil to bulk-out slightly, and furthermore improved the access to water for the swelling process.

In geological time scales shrinkage, cracks may become in-filled up with the residue, in this way giving heterogeneity of the soil. At the point when material falls into cracks the soil is unfit to move back, subsequently improved swelling stress (Jones, 2012).

A simple shrink and swell mechanism is depicted in Figure 2.12 where shrinking and swelling occurs when soil moisture content reduces and increases respectively. The mechanism takes place near the surface of heaving soils.

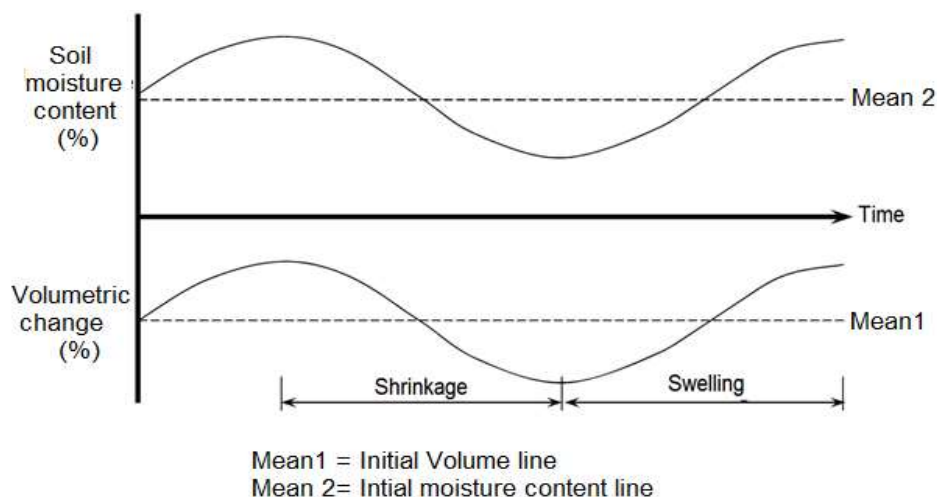


**Figure 2.12: Swell / Shrink Mechanism**

Factors affecting the shrink-swell potential of a soil can be broadly classified in three categories:

- The state of stress,
- The environmental parameters that affect the variation that may take place into the internal system of stress,
- The soil features that affect the basic nature of the internal stress of the field. The conditions of the stress caused by the stress history, loading, soil profile (Kassif and Baker, 1971) and the in-situ conditions.

The environmental conditions that influence shrink-swell potential are as follows: initial moisture conditions (Nelson and Miller, 1992), moisture variation caused by climate, groundwater drainage, man-made water sources, vegetation, permeability and temperature (Johnson, 1973). Soil parameters that affect shrink-swell capacity are clay mineralogy and clay content (Grim, 1968; Mitchell, 1976 and Mitchell, 1979), soil water chemistry (Johnson and Snethen, 1978), soil moisture deficiency, plasticity index (Nelson and Miller, 1992), soil structure and fabric (Johnson and Snethen, 1978), dry density (Chen, 1973). Water fluctuation, current stress, and clay content are three main factors that control the swelling and shrinkage process of heaving soils. An assessment of the effect of clay fraction ( $< 0.002\text{mm}$ ) showed that an increase in clay fraction increased the amplitude and ratio of swelling (Sorochan, 1991). Many researchers (Katti et al., 1969) characterize this correlation as linear.

## **PART 2: UNSATURATED SOIL MECHANICS**

### **2.15 Introduction**

There are many soils used in construction practice that require the application of unsaturated soil mechanics in order to comprehend their behaviour. The study of soil mechanics can be divided into two categories (Fredlund and Rahardjo, 1993): the first is related to saturated soil mechanics and the second related to unsaturated soil mechanics as shown in Figure 2.13. The difference between saturated and unsaturated soil mechanics are essentially due to the interaction of pore water and fine fraction (silt, clay). Interparticle water in fine soils can produce negative pore stress through matric suction, sorption, and double layer attraction. This leads to a more complex state of stress inside the soil matrix and has a significant effect on stress-strain and the volume change behaviour. Soils used in construction are commonly located above ground - water table and may experience negative pore pressure. Natural saturation of soils may experience negative pore pressure. Natural saturation of soil may likewise reduce when evapotranspiration exceeds infiltration.

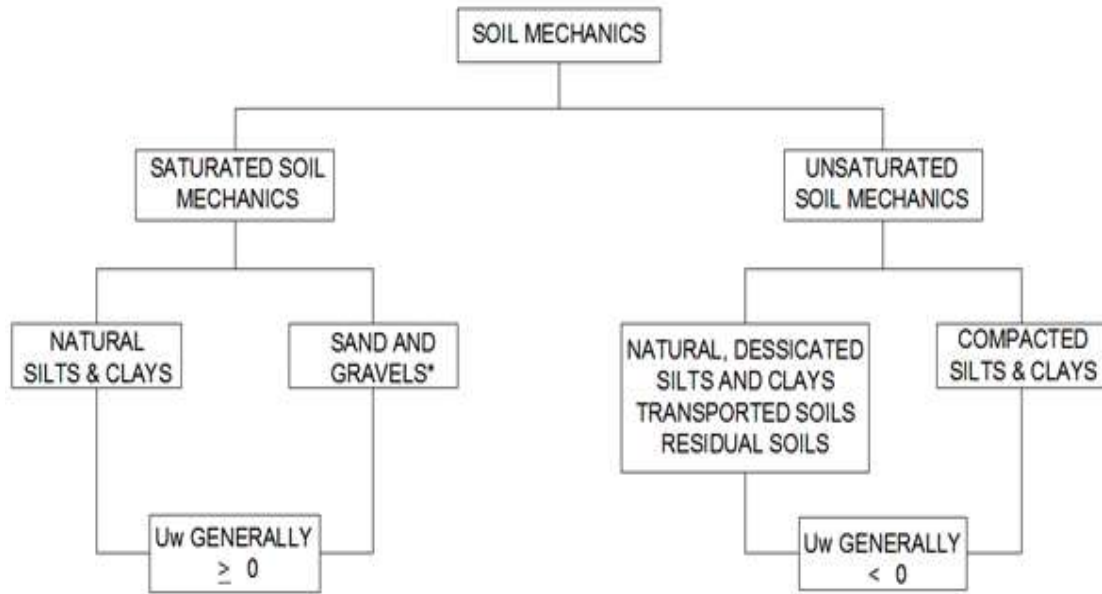


**Figure 2.13:** Categories of soil mechanics (Fredlund & Rahardjo, 1993)

Figure 2.14 shows the climatic categorization of excessively arid and semi-arid spaces in the world. Around 33% of the earth’s area is recognized to be unsaturated (Dregne, 1976).

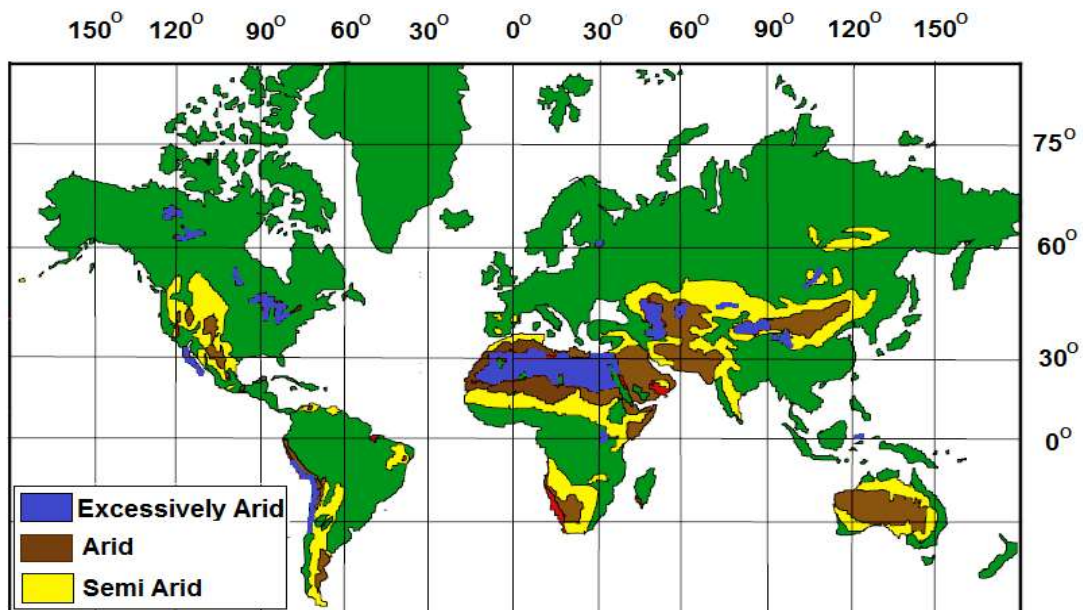


**Figure 2.14:** Excessively arid, and semi-arid regions of the world. (Meigs, 1953; Dregne, 1976; Fredlund & Rahardjo, 1993)

Fredlund and Morgenstern (1997) called air–water interface or contractile skin on fluid menisci, the fourth phase. This fourth phase renders unsaturated soil different from saturated soil with respect to essential engineering properties. Both saturated and unsaturated zones are influenced by climatic factors such as precipitation,

transpiration, and evaporation. The principal feature of the soil in an unsaturated zone is the soil moisture deficiency. Negative pore-stress is available at some depth. Close to the ground surface, soil material is commonly exposed to negative pore-water stress and potential of desaturation as shown in Figure 2.15.

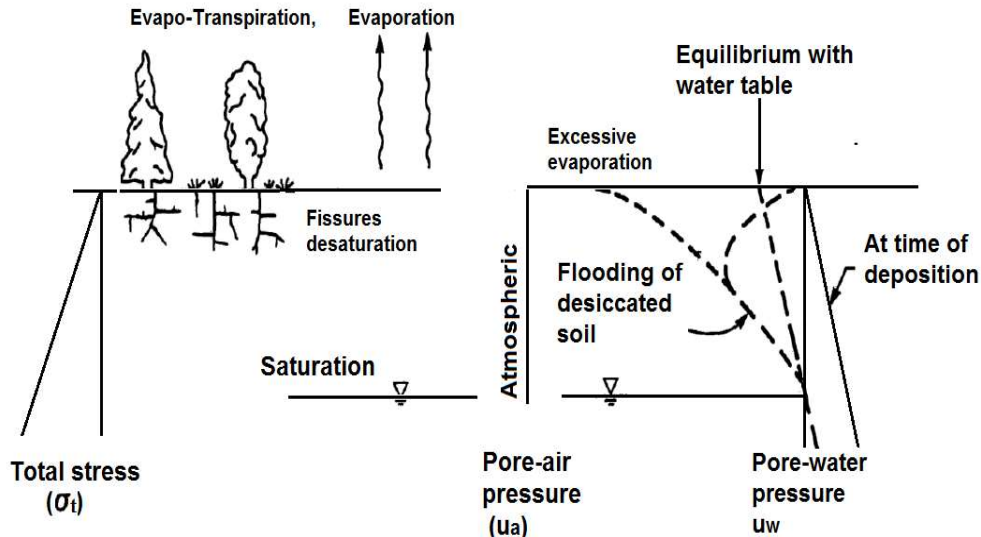


**Figure 2.15:** Stress distribution to desiccation (Fredlund and Rahardjo, 1993)

### 2.16 Unsaturated soil mechanics domains of application

Soil suction is an essential characteristic of unsaturated soils. The class of unsaturated soil issues involving negative pore - water stress that has received the most attention from geotechnical engineers is that of heaving soils. Fredlund et al.,(2012) Stated that unsaturated soil mechanics can be applied to other unsaturated soil issues such as bearing limit of foundations, pavement design, the stability of vertical excavations, mounding underneath waste retention ponds, slope stability, construction of a dam, etc.

### 2.17 Phases of unsaturated soil

Unsaturated soils are commonly considered as having three phases: air, water, and solids. However, it is worthy to recognize that the fourth phase is known as the contractile skin or air-water interface (Fredlund and Morgenstern, 1997). Thus, unsaturated soils can be considered as a four-phase system because of the fundamental role of contractile skin on soil behaviour. Air-water interface is a thin layer interlaced between and within voids of soils, developing a fixed partition between water and air phases. The change of water content, shear stress and

volume can be impacted by the variation of the stress of contractile skin. Figure 2.16 shows a component of unsaturated soil with continuous air phase.

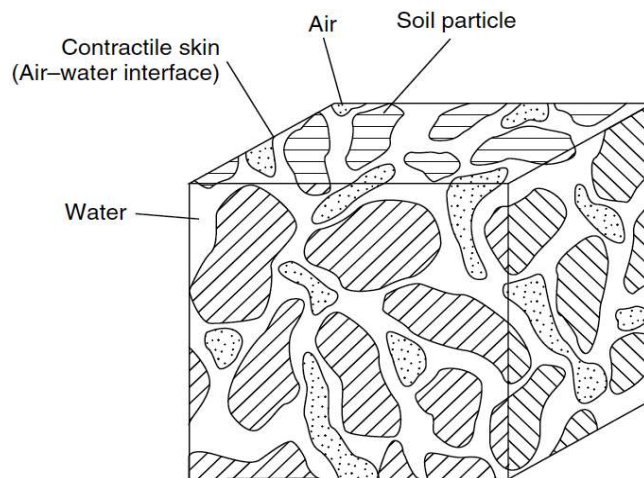


**Figure 2.16:** Component of unsaturated soil with a continuous air phase (Fredlund and Rahardjo, 1993).

A phase diagram as shown in Figure 2.17 can depict the volume and mass of each phase.

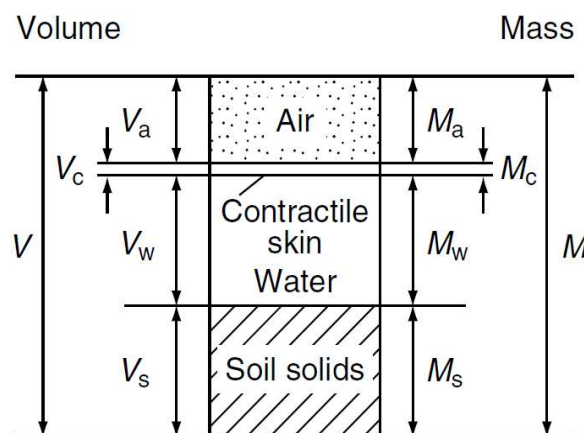


**Figure 2.17:** Rigorous fourth-phase unsaturated soil system (Fredlund and Rahardjo, 1993).

### 2.17.1 Contractile Skin (air-water interface)

The fundamental property of air-water interface is its ability to exert a tensile action. It acts as if it is a flexible sheet joined between the whole structures of the solid soil matrix. Most of the contractile skin features appear to be different from that of continuous water phases (Davies and Rideal, 1963). Acknowledging the uniqueness of air-water interface (fourth phase) helps to understand the state of



stress variable for an unsaturated soils (Fredlund and Morgenstern, 1997). Many studies have been conducted on the nature of air-water interface point toward its essential and independent role on unsaturated soils (Wang and Fredlund, 2003). Recent research recommends that the thickness of contractile skin range of 1.5 to 2 molecules of water in diameter (i.e., 5Å) (Israelachvili, 1991). The distribution of water molecules over contractile skin appears as a hyperbolic tangent function as presented in Figure 2.18. (Kykilema, 2000).

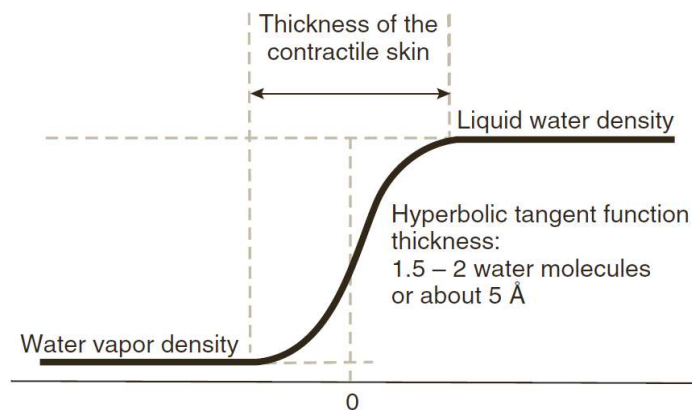


**Figure 2.18:** Density distribution over air-water interface (Kykilema, 2000)

### 2.17.2 Water Phase

Water plays an important role in the mechanical and physical properties of soil. Physical properties that are especially interesting when dealing with soil are as follows: water density, thermal property, dissolved salts or contaminants, viscosity, and cavitation.

### 2.17.3 Air Phase

Physical properties of air phase that change significantly with pressure and temperature are density, thermal properties, relative humidity, saturated vapour pressure, etc.

### 2.17.4 Solid Phase

Regardless of the clay – water electrolyte behaviour examined previously, a few essential properties of the solid phase can be defined. However, density, specific volume, and thermal properties (specific heat capacity, thermal conductivity) is fundamental. Table 2.5 shows the specific gravity of a few minerals.

**Table 2.5:** Specific gravity of several minerals (Lambe and Whitman, 1979).

Mineral	Specific Gravity, Gs
Quartz	2.65
K feldspars	2.54 – 2.57
Na – Ca feldspars	2.62 – 2.76
Calcite	2.72
Dolomite	2.85
Muscovite	2.7- 3.1
Biotite	2.8 -3.2
Chlorite	2.6-2.9
Pyrophyllite	2.84
Serpentine	2.2 – 2.7
Kaolinite	2.61 <sup>a</sup> ; 2.64 ± 0.02
Halloysite (2H <sub>2</sub> O)	2.55
Illite	2.84 <sup>a</sup> ; 2.60-2.86
Montmorillonite	2.74 <sup>a</sup> ; 2.75 - 2.78
Attapulgit	2.30

<sup>a</sup> Calculated from crystal structure

### 2.18 Surface tension

Surface tension is a property resulting from contractile skin (air-water interface). The occurrence of surface tension arises from intermolecular forces acting on molecules in the water-air interface. These actions are not the same as those that act on molecules inside the water (Figure 2.19a). The tension on the surface causes water-air interface to act as a flexible membrane. Air-water interface behaves like an inflated balloon with greater pressure inside than outside.

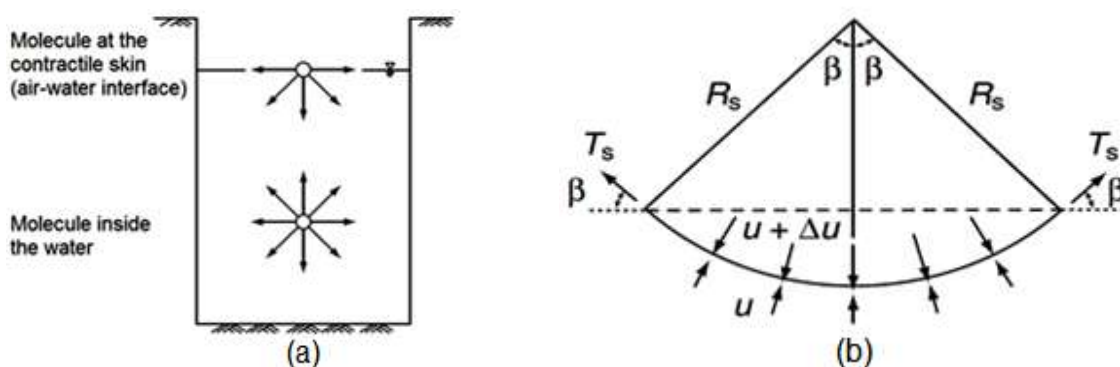


**Figure 2.19:** Surface tension phenomenon on contractile skin. (a) Intermolecular forces at air-water interface and water. (b) Pressures and surface tension acting on a curved two-dimension surface (Fredlund et al., 1993).



The difference in pressure over the surface of the curve can be correlated to the curved membrane radius and the tension at the surface Figure 2.19b.  $U + \Delta U$  Are the stresses acting on the membrane.  $R_S$  is the membrane radius of curvature, and  $T_S$  is the surface tension. Equation 2.3 gives the equilibrium in the vertical direction.

$$2 T_S \sin\beta = 2 \Delta U R_S \sin \beta \tag{2.3}$$

Where:

$2 \Delta U R_S \sin \beta =$  Length of the membrane projected onto a plane surface

Rearranging of Equation 2.3

$$\Delta U = \frac{T_S}{R_S} \tag{2.4}$$

Equation 2.3 gives the difference in stress on a two-dimension curved area with surface tension  $T_S$  and a radius  $R_S$ .

**Table 2.6:** Surface tension of contractile skin at several temperatures  
(Kaye and Laby, 1973)

Temperature (°C)	Surface Tension, $T_s$ (mN/m)
0	75.7
10	74.2
20	72.75
30	71.2
40	69.6
60	66.2
80	62.6
100	58.8

For a warped three-dimensional membrane, Equation 2.5 used for a two-dimensional membrane can be extended using the Laplace transformation equation.

$$\Delta U = T_S \left( \frac{1}{R_1} + \frac{1}{R_2} \right) \tag{2.5}$$

Where:

$R_1, R_2$  = Radii of curvature of a warped membrane according to the orthogonal principal planes

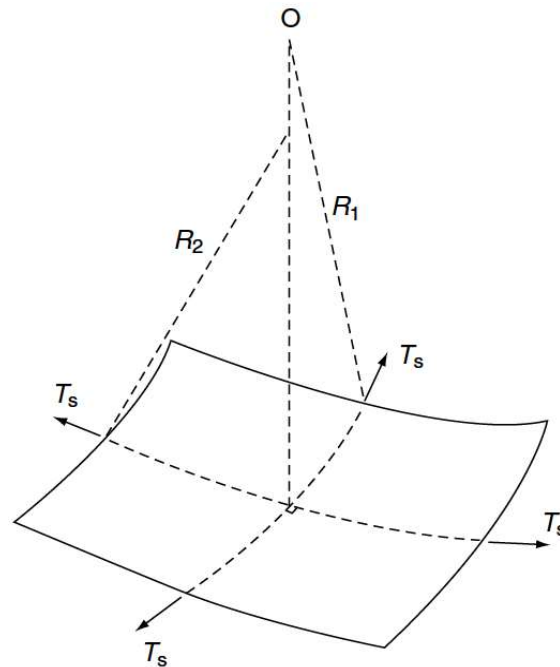


**Figure 2.20:** Surface tension on the three-dimension warped membrane (Fredlund and Rahardjo, 1993)

In unsaturated soil, air-water interface is governed by pore water pressure  $u_w$  smaller than pore air pressure  $u_a$ . The stress difference ( $u_a - u_w$ ) is referred to as matric suction. Equation 2.6 gives the difference in stress created by the contractile layer to bend to a curvature. Equation 2.6 is referred to as Kelvin's capillary model equation.

$$U_a - U_w = \frac{2T_s}{R_s} \tag{2.6}$$

### 2.19 Capillary phenomenon

Matric suction component of the total suction drives capillary transport. The level of water rise inside a capillary tube and the radius of curvature of meniscus directly affects the matric suction. The curvature of the meniscus is related to water content since various portions of particle-matrix hold the menisci as saturation changes. Generally, at lower saturation, the menisci are smaller (higher tension) and higher saturations have larger menisci (lower tension). This relationship is

non-linear, yet might be evaluated in the laboratory by a few different methods to obtain the soil water characteristic curve (SWCC). For sands and silts, the pore spaces inside the soil matrix remain steady, and the SWCC is more easily defined. For clays, the procedure is complicated by higher suction values and changes in pore volume within the solid matrix.

### 2.20 Capillary Height

Consider the vertical equilibrium force of capillary water in a tube shown in Figure 2.21. The vertical component of the surface force (i. e;  $2\pi r T_s \cos\alpha_1$ ) supports the weight of the water column, which has an elevation  $h_c$  (i. e;  $\pi r^2 h_c \rho_w g$ ).

$$\pi r^2 h_c \rho_w g = 2\pi r T_s \cos\alpha_1 \quad (2.7)$$

Where:

$\alpha_1$  = angle of contact, °C,

$r$  = radius of the capillary tube, mm,

$T_s$  = water surface tension, N. m<sup>-1</sup>,

$h_c$  = capillary height, cm,

$g$  = gravitational acceleration, 9.8 m. S<sup>-2</sup>, and

$\rho_w$  = density of water, 1000 kg. m<sup>-3</sup>

Equation 2.8 can be transposed as to give the ultimate level of liquid in the capillary tube,  $h_c$  :

$$h_c = \frac{2 T_s}{\rho_w g R_s} \quad (2.8)$$

Where:

$R_s$  = radius of curvature of the meniscus (i. e.  $\frac{r}{\cos\alpha_1}$ )

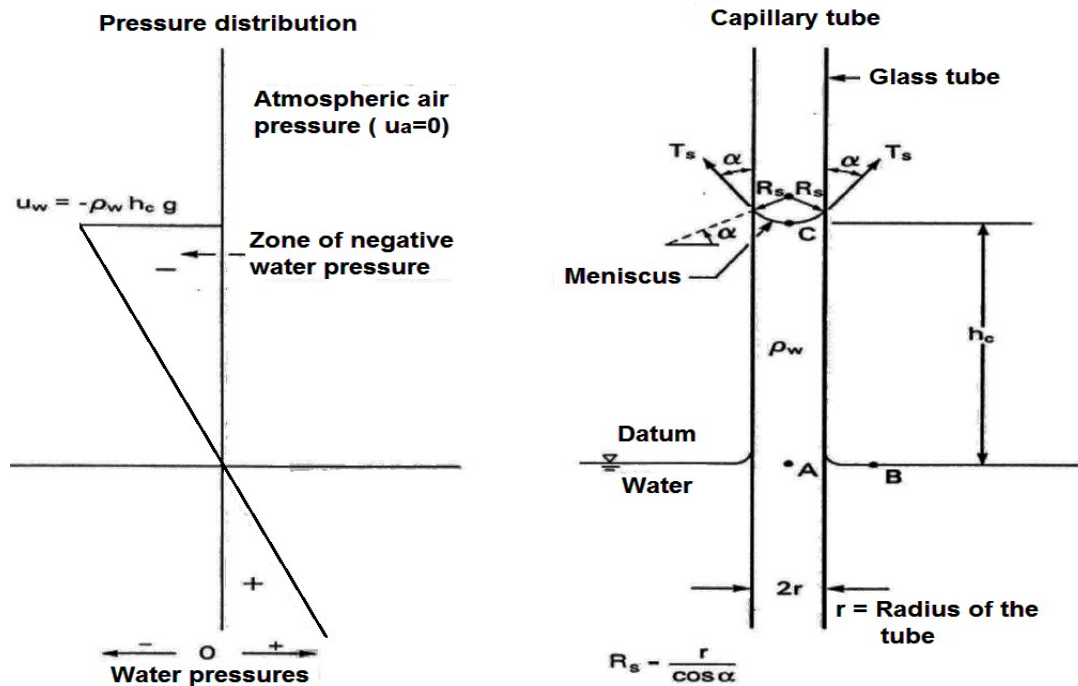


**Figure 2.21:** Physical model and phenomenon related to capillarity (Fredlund et al., 1993).

### 2.21 Capillary pressure

Points C, B, and A in the capillary system illustrated in Figure 2.21 are in hydrostatic equilibrium. The atmospheric water pressure occurs at points B and A. The height of points A and B above the water surface depends on the datum or reference elevation of the system (zero elevation). Hence, the hydraulic head at point B and A are equivalent to zero. Point C is a distance  $h_c$  above reference. Hydrostatic equilibrium among points C, B, and A is fulfilled only when the hydraulic head of the three points is the same. This implies the pressure head at point C is equal to the negative value of the elevation head at point C. Equation 2.9 gives water pressure at C.

$$u_w = - \rho_w g h_c \tag{2.9}$$

Where

$u_w$  = water pore pressure, kPa

$h_c$  = capillary height, cm,

$g$  = gravitational acceleration,  $9.8 \text{ m} \cdot \text{s}^{-2}$ , and,

$\rho_w$  = density of water,  $1000 \text{ kg/m}^3$ .

The pressures of water above point A in the capillary tube is negative, as shown in Figure 2.21. In the capillary tube, water is subjected to tension. Nonetheless, water pressure below point A is positive due to the conditions of hydrostatic pressure. At point C, air pressure is atmospheric (i.e;  $u_a = 0$ ) and water pressure is negative (i.e  $u_w = -\rho_w g h_c$ ). Matric suction ( $u_a - u_w$ ) at point C can be expressed as follows:

$$u_a - u_w = \rho_w g h_c \tag{2.10}$$

The substitution of Equation 2.8 in Equation 2.10 gives another expression for the magnitude of the matric suction:

$$u_a - u_w = \rho_w g \times \frac{2 T_s}{\rho_w g R_s} = \frac{2 T_s}{R_s} \tag{2.11}$$

As the pore radius ( $R_s$ ) gets smaller, the soil matric suction becomes larger, as shown in Figure 2.22.

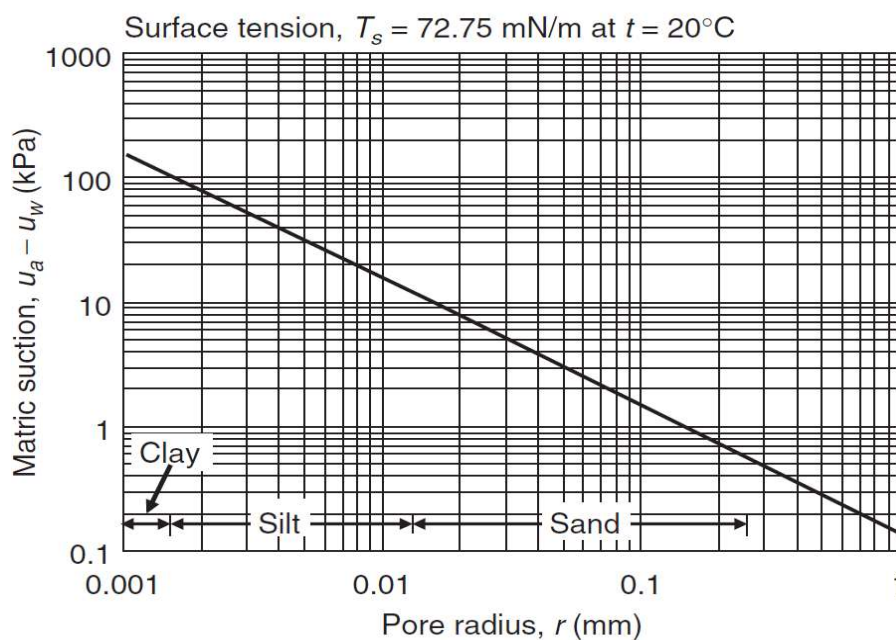


**Figure 2.22:** Relationship of matric suction to pore size for various soil

The surface strain can support a water column,  $h_c$ , in a capillary tube where tension area combined with water- air interface creates a reaction as depicted in Figure 2.23. The reaction force vertical component produces compressive stresses hangs on the wall of the tube. In other words, the weight of the water column is

transferred to the tube through the air-water interface. When the soil has a capillary zone, the water-air interface results in an augmentation of the compression of the solid matrix. Therefore, matric suction in unsaturated soils causes a volume reduction, and generally an increase of shear stress of soil.

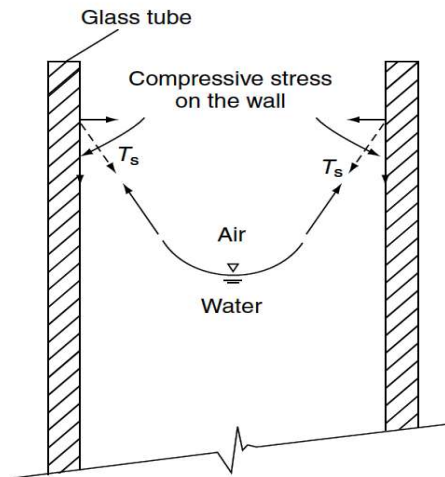


**Figure 2.23:** Forces acting on capillary tube (Fredlund et al., 1993).

## 2.22 Theory of soil suction

Soil suction is a free energy state of water inside the soil. This free energy of water in the soil can be estimated utilizing partial vapour pressure of soil water. Equation 2.12 gives the thermodynamic correlation between soil moisture deficiency and fractional pressure of pore water vapour.

$$\psi_t = -\frac{R T_K}{u_{w0} \omega_u} \ln \left( \frac{\bar{u}_u}{\bar{u}_{u0}} \right) \quad (2.12)$$

Where:

$\psi_t$  = total soil suction, kPa,

$R$  = universal (molar) gas constant [ i. e; 8.31432 j/(mol K)],

$T_K$  = absolute temperature [ i. e;  $T_K = 273.15 + T(^{\circ}C)$  ],

$u_{w0}$  = specific volume of water or the inverse of the density of water  $\left( \frac{1}{\rho_w} \right) \frac{m^3}{kg}$ ,

$\omega_u$  = molecular mass of water vapour [ i. e; 18.016 kg/kmol],

$\bar{u}_u$  = partial presure of pore – water vapor, kPa, and

$\bar{u}_{u0}$  = saturation pressure of water steam over a flat surface of pure water at the same temperature, kPa.

The relative water vapour in the air immediately beside to water,  $\frac{\bar{u}_u}{\bar{u}_{u0}}$ , is called relative humidity ( $h_r$  or RH, %), if we choose a reference temperature of 20°C, the constant in equation (2.13) can now be written as a relationship between the total soil moisture deficiency in kilopascals and the relative vapour pressure:

$$\psi_t = -135,022 \ln \left( \frac{\bar{u}_u}{\bar{u}_{u0}} \right) \quad (2.13)$$

Figure 2.24 is the graph of Equation 2.13 for three temperatures types. Relative humidity less than 100 % in soil will generate negative pore pressure in the soil. The soil moisture deficiency of most common interest in geotechnical engineering is similar to high values of relative humidity.

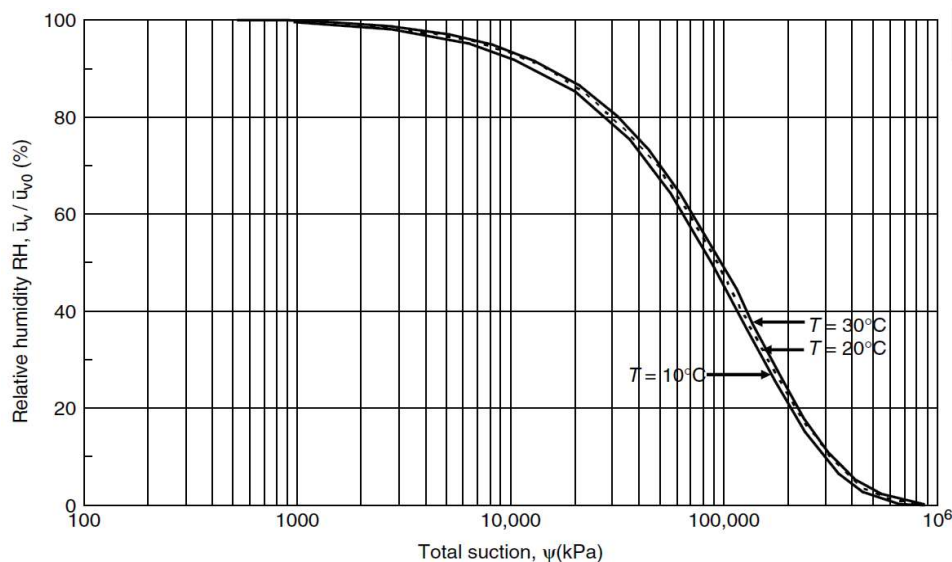


**Figure 2.24:** Thermodynamic equilibrium between relative humidity and total suction

### 2.23 Components of soil suction

The total suction  $\psi_t$  can be estimated in terms of the relative humidity next to the water surface. There are two primary components to soil suction namely suction matric ( $u_a - u_w$ ) and the osmotic suction  $\psi_0$ . Therefore, the total suction corresponds to the soil water: the matric and the osmotic suction are the constituent elements of the free energy. Equation 2.14 gives the constitutive algebraic relation between the constituent's elements of soil suction.

$$\psi_t = \psi_m + \psi_o \tag{2.14}$$

Where:

$\psi_t$  = total soil suction, kPa,

$\psi_m = u_a - u_w$  = matric suction, kPa,

$u_a$  = pore air pressure, kPa,

$u_w$  = pore water pressure, kPa, and

$\psi_o$  = osmotic suction, kPa.

Figure 2.25 represents the general notion of total suction and its constituent's elements as related to the free energy of the soil water.

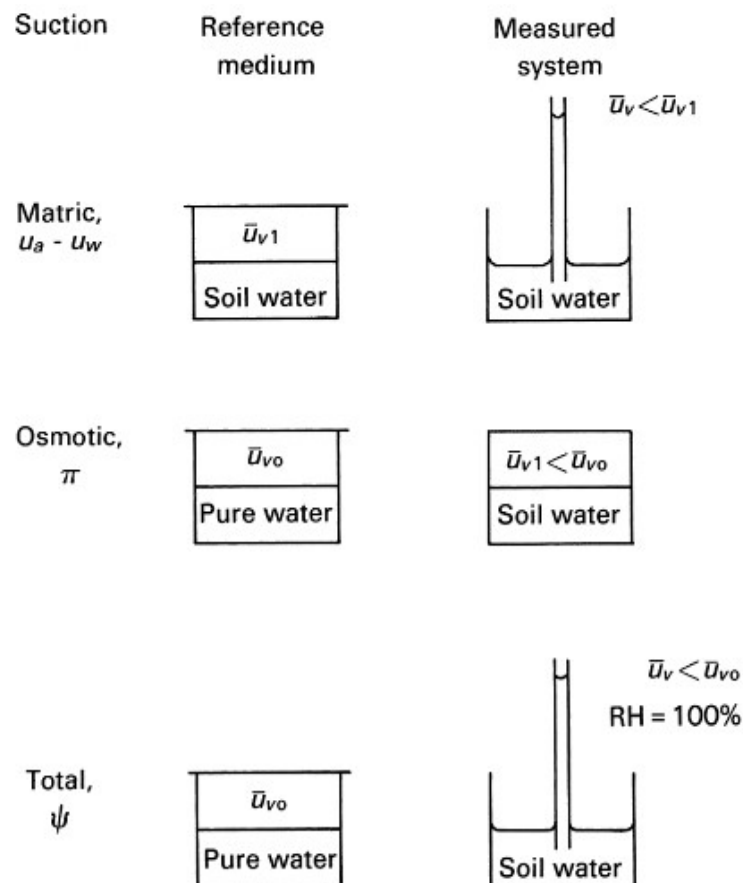


**Figure 2.25:** Total suction and its components: matric and osmotic suction (Fredlund et al., 1993).

Consider a tube of glass filled with soil water. The area of water in the tube of glass is curved and is called meniscus. However, similar soil water will have a flat surface when put in a large container. The partial pressure of water vapour above the curved surface of soil water ( $\bar{u}_v$ ) is less than the partial pressure of water



vapour above a plane surface of identical soil water ( $\bar{u}_{v1}$ ). In other words, RH in the soil will diminish because of the curved water surfaces produced by the capillary phenomenon. The water vapour pressure or RH diminishes as the radius of curvature of the water surface decreases. Accordingly, the radius of curvature is inversely proportional to the difference between the air and water pressures across the surface (i.e;  $u_a - u_w$ ) and is called matric suction. Consequently, one component of the total suction is matric suction, and it contributes to a reduction in the relative humidity.

## 2.24 Unsaturated soil stress state variables

As indicated by soil mechanics, the behaviour of soil relies on the stress variables that control the equilibrium of soil material. Along these lines, the stress variable necessary to describe the equilibrium of the soil structure can be considered as the stress state variables for the soil. The stress variables must be quantifiable, for example, the total stress,  $\sigma$ , the air-water pressure,  $u_a$ , and water pore pressure,  $u_w$ . Stress equilibrium can be assessed on unsaturated soil, by considering the state of stress at a point in the soil.

### 2.24.1 Equilibrium analysis

Body forces and surface forces can both act on an element of soil. The stress component perpendicular to a plane is the normal stress,  $\sigma$ , while the parallel component is identified as shear stress,  $\tau$ . A cubical element that is completely enclosed by imaginary, boundaries yields a free body for stress equilibrium analysis. Figure 2.26 shows a soil element with dimensions of  $d_x$ ,  $d_y$  and  $d_z$  in Cartesian coordinates. The shear and normal stress on each plane of the element are shown in Figure 2.26.

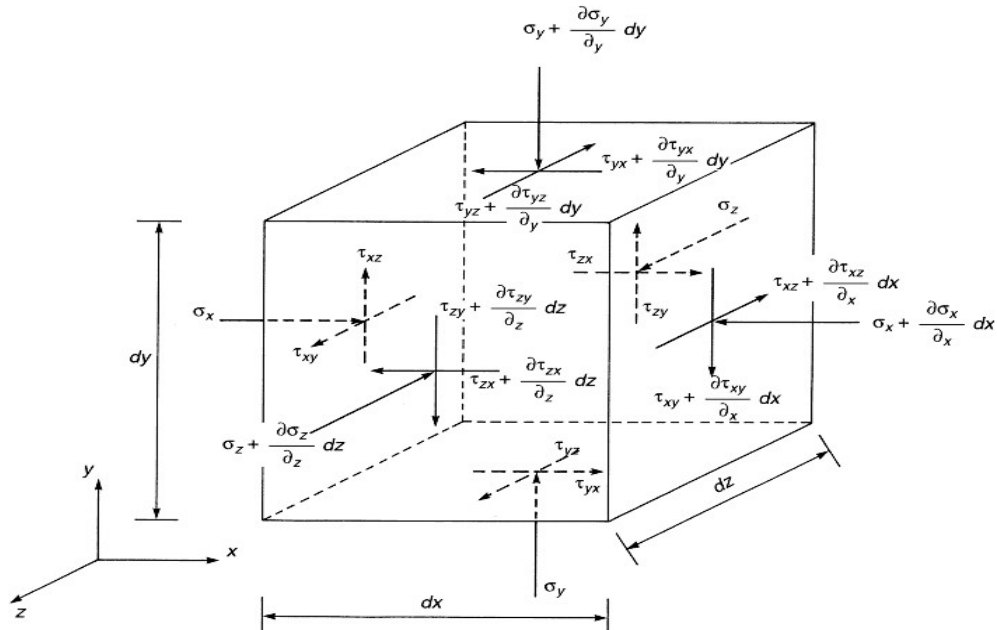


**Figure 2.26:** Normal and shear stresses on a cubical soil element of infinitesimal dimensions.

The equation of equilibrium for the air phase, water phase, and contractile skin, together with the total equilibrium equation for the soil element are utilized to define the equation of equilibrium of soil. In y-direction, (equation 2.15) gives the equilibrium state.

$$\frac{\partial \tau_{xy}}{\partial x} + \frac{\partial (\sigma_y - u_a)}{\partial y} + (n_w + n_c f^*) \frac{\partial (u_a - u_w)}{\partial y} + \frac{\partial \tau_{zy}}{\partial z} + (n_c + n_s) \frac{\partial u_a}{\partial y} + n_s \rho_s g - F_{sy}^w - F_{sy}^a + n_c (u_a - u_w) \frac{\partial f^*}{\partial y} = 0 \quad (2.15)$$

Where:

$\tau_{xy}$  = shear stress on plane (y, z) perpendicular to direction (y), kPa,

$\sigma_y$  = total normal stress parallel to direction (y), kPa,

$u_a$  = pore air pressure, kPa,

$f^*$  = intreaction function between the equilibrium of soil structure and equilibrium of contractile skin,

$(\sigma_y - u_a)$  = net normal stress parallel to direction (y), kPa,

$n_w$  = porosity relative to water phase, % ,

$n_c$  = porosity relative to contractile skin, % ,

$u_w$  = pore – water pressure, kPa,

$u_a - u_w$  = matric suction, kPa

$\tau_{zy}$  = shear stress on plane (x,y)perpendicular to direction (z), kPa,

$n_s$  = porosity relative to soil particles, %,

$g$  = gravitational acceleration,  $9.8\text{m. s}^{-2}$

$\rho_s$  = soil particle density,  $\text{kN. m}^{-3}$ ,

$F_{sy}^w$  = Interaction force (i. e. body force)between the water phase and the soil particles parallel to the direction (y),  $[\text{M}][\text{L}][\text{T}]^{-2}$ , and

$F_{sy}^a$  = Interaction force (i. e. body force)between the air phase and the soil particles parallel to the direction (y),  $[\text{M}][\text{L}][\text{T}]^{-2}$ .

### 2.24.2 Stress state variables

The independent sets of normal stresses from the equation of equilibrium for soil in Figure 2.27 are:  $(\sigma_y - u_a)$ ,  $(u_a - u_w)$  and  $(u_a)$ , which control the equilibrium of contractile skin and soil structure.  $(\sigma_y - u_a)$  and  $(u_a - u_w)$  are considered as the stress state variables for unsaturated soils. Therefore, independent tensors of stress can be used to represent the complete form of stress state. Figure 2.27 shows two independent tensors acting on a component in unsaturated soils.

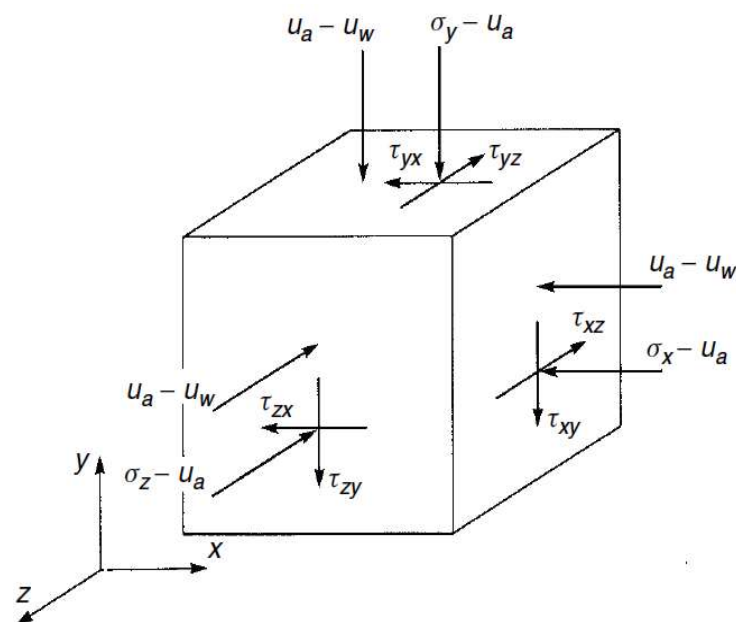


**Figure 2.27:** Stress state variables for unsaturated soil.

$$\begin{bmatrix} (\sigma_x - u_a) & \tau_{yx} & \tau_{zx} \\ \tau_{xy} & (\sigma_y - u_a) & \tau_{zy} \\ \tau_{xz} & \tau_{yz} & (\sigma_z - u_a) \end{bmatrix} \quad (2.16)$$

$$\begin{bmatrix} (u_a - u_w) & 0 & 0 \\ 0 & (u_a - u_w) & 0 \\ 0 & 0 & (u_a - u_w) \end{bmatrix} \quad (2.17)$$

### 2.24.3 Other combination of stress state variables.

The three stresses state variables combinations shown in Table 2.7 are obtained from equations of equilibrium of the soil which are derived from three references stresses (i. e.  $\sigma$ ,  $u_a$  and  $u_w$ ). Nonetheless,  $(\sigma - u_a)$  and  $(u_a - u_w)$  combination is more suitable for engineering practice (Fredlund, 1979; Fredlund and Rahardjo, 1987).

**Table 2.7:** Possible combination of stress state variables for unsaturated soil (Fredlund and Hasan, 1979)

Reference Pressure	Stress State Variables
Air pressure, $u_a$	$(\sigma - u_a)$ and $(u_a - u_w)$
Water pressure, $u_w$	$(\sigma - u_w)$ and $(u_a - u_w)$
Total stress, $\sigma$	$(\sigma - u_a)$ and $(\sigma - u_w)$

### 2.25 Soil water characteristic curve

Soil water characteristic curve (SWCC) describes the relationship between the matric suction and either the gravimetric water content,  $\omega$ , volumetric water content,  $\theta_s$ , or degree of saturation,  $S$ . As soil changes from saturated condition to unsaturated state, the distribution of water (and menisci) and air phase's change. As water content diminishes, larger pores (low contractile skin tension) empty, leaving water in smaller pore spaces with higher contractile tension. Pore pressures become more negative as water content drops. At some point, the water network covering the solid matrix becomes disconnected, leaving isolated islands of moisture within the solid matrix. While matric water continues to exert tension on the soil matrix, as the soil dries further due to vapour migration, its distribution

turns out to be increasingly inadequate. For clay soils, this leads to very high suction stress and shrinkage. For silts and sands, the impact on volume change is not as drastic. Typical SWCC's for different soils are shown in Figure 2.28.

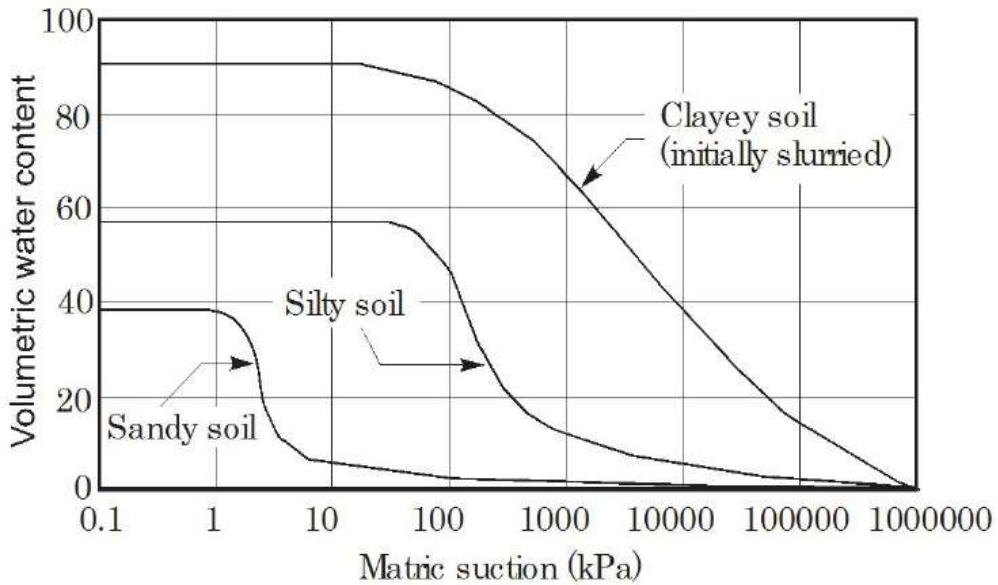


Figure 2.28: Typical SWCC for different soil types (Fredlund and Xing, 1994)

SWCC has three stages that describe the drying process (i.e. for increasing suction) of soil as shown in Figure 2.29. These are outlined below starting with fully saturated conditions in the soil.

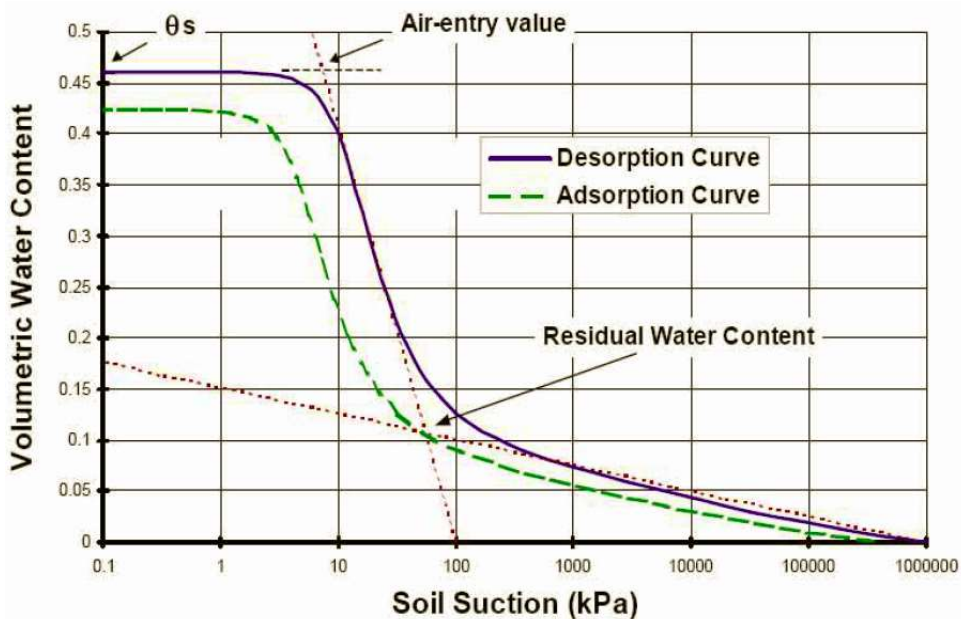


Figure 2.29: Definition of variables associated with the SWCC.

- 1- The capillary saturation zone where pore-water is in tension but the soil remains saturated. This stage stops when air entry occurs (AEV), where suction overcomes the largest pores in the soil.
- 2- The desaturation zone where water is drawn in from the soil matrix by evaporation on the boundary or other removal mechanisms. This stage stops at residual water content,  $\theta_r$ , where pore-water becomes discontinuous. At this point, hydraulic conductivity is decreased by several orders of magnitude and is controlled by vapour transport as much as fluid transport.
- 3- The Residual saturation zone where water is tightly adsorbed onto soil particles and flows occurs only by vapour transport. This stage is done at a moisture level equivalent to oven dryness. When the soil is heated to 105°C, the soil is characterized to have zero water content and soil moisture deficiency is approximately 1.10<sup>6</sup> kPa (Fredlund and Rahardjo, 1993).

A few equations have been proposed to represent SWCC. A detailed comparison between commonly utilized curve-fitting equations for soil water characteristic curve utilizing a database of in excess of 200 soils has been conducted by Sillers et al.,(2001). It discovered that (Fredlund and Xing, 1994) equation was the best curve fitting equation in the sense that it provided a close fit to point it data. Equation suggested by Fredlund and Xing (1994) to the empirical best - fit the SWCC is as follows:

$$\theta_w = C(\Psi) \left[ \frac{1}{\ln \left[ e + \left( \frac{\Psi}{a_f} \right)^{n_f} \right]} \right]^{m_f} \quad (2.18)$$

Where:

$\theta_w$  = volumetric water content, % ,

$e$  = natural constant , 2.718,

$\Psi_t$  = total soil suction, kPa ,

$a_f$  = soil parameter related to the air entry of the soil,

$n_f$  = soil parameter related to the rate of desaturation,

$m_f$  = soil parameter related to the residual water content conditions, and

$C(\Psi)$  = correction factor to ensure that the function goes  $10^6$  kpa ( $P^F = 7$ ),  
of suction zero water content ;  $kpa = 10^{P^F - 1}$ .

While it is very simple to quantify the SWCC in vivo, it is still generally costly. Thus, the assessment of the SWCC utilizing grain size analysis and volume-mass properties is advantageous. An empirical curve could be fitted based on grain size distribution (Fredlund, 2000).

---

## CHAPTER 3: PREVIOUS STUDIES TO PREDICT THE SWELLING STRESS

### 3.1 Introduction

This chapter presents the swelling stress prediction based on oedometer tests, and review the proposed models used to predict the swelling stress of expansive soils.

### 3.2 Swelling stress

#### 3.2.1 Definition

There are at least three general definitions of the swelling stress as follows:

- (a) Swelling stress is defined as that stress due to a surcharge load for which there will be neither compression nor expansion of the specimen upon saturation.
- (b) Swelling stress is defined as the stress to compress a fully swollen specimen back to its initial void ratio.
- (c) Swelling stress is also defined as the pressure required to maintain the initial volume when the specimen is subjected to an increment in moisture. Moreover, the swelling stress is the load at which the void ratio is the same as the initial void ratio.

In this research work, the swelling stress is in accordance with the definition (c)

#### 3.3 Swelling stress prediction based on oedometer test

During the natural swelling process, the expanding soil may be fully or partly constrained by the structure above the soil. The pressure exerted by the swelling soil can exceed the overburden stress as well as the structural loads, and lift both soil and structure. Many investigations have tried to determine the swelling stress of heaving soils. Numerous investigations have also attempted to identify the various parameters affecting the expansion and the stress produced by it. The oedometer was first used to estimate swelling stress of heaving soils (Holtz, 1954, Jennings and Knight, 1957). The pressure which must be exerted to the soil such that it prevents the heaving soil specimen from any further swelling by wetting is called swelling stress. This procedure is also designated as zero swell test (ZST) (Basma et al., 1995; Fattom and Barakat, 2000). Furthermore, the Consolidation Swell Test (CST) uses the opposite approach. The CST allows the specimen to



heave under a small-applied load within the oedometer, and then the load is gradually applied to recompress the specimen to its original volume. Therefore, the amount of the final applied pressure that brings the specimen back to its original volume is called the swelling stress. The double oedometer test (DOT) was proposed by Jennings and Knight (1957). The settlement rate or total heave can be predicted through this technique. The oedometer has the potential to indicate both volume change and the forces developed in expansive clay. Theoretically, it should give meaningful results. According to ASTM D4546 standard, there are three main techniques for swell stress prediction of expansive soils using one-dimensional oedometer test.

### 3.3.1 Technique 1

The specimen is submerged in water and allowed to undergo vertical volume change at the seating pressure, 1kPa, applied by the load on top of the porous stone and load plate. There is no loading until the initial swell is completed. Then the additional load is exerted until its original void ratio/height is obtained.

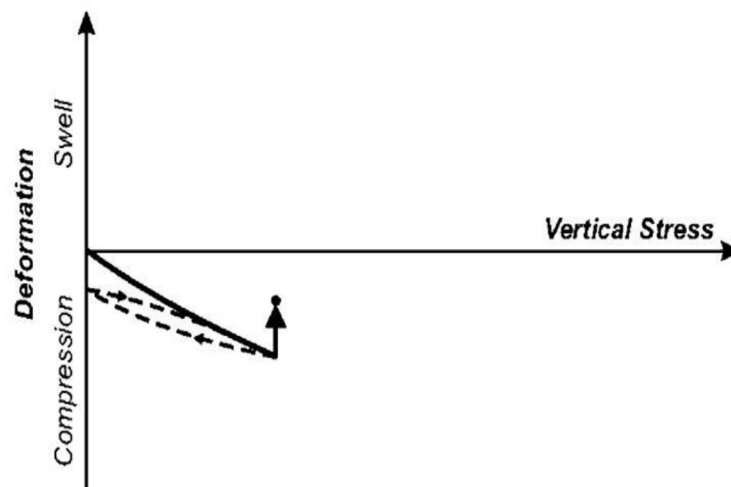


**Figure 3.1:** Deformation versus vertical stress, single-point test. Technique 1 (ASTM D4546).

### 3.3.2 Technique 2

A vertical pressure, generally comparable to the in-situ vertical overburden pressure, structural loading, or both are applied to the specimen before the specimen is given access to water. Later, the specimen is submerged. The quantity of expansion or settlement can be measured at the applied load after the

device reaches equilibrium, and additional movement versus time is negligible. The final applied load which retains the specimen at its initial height is called swelling stress.

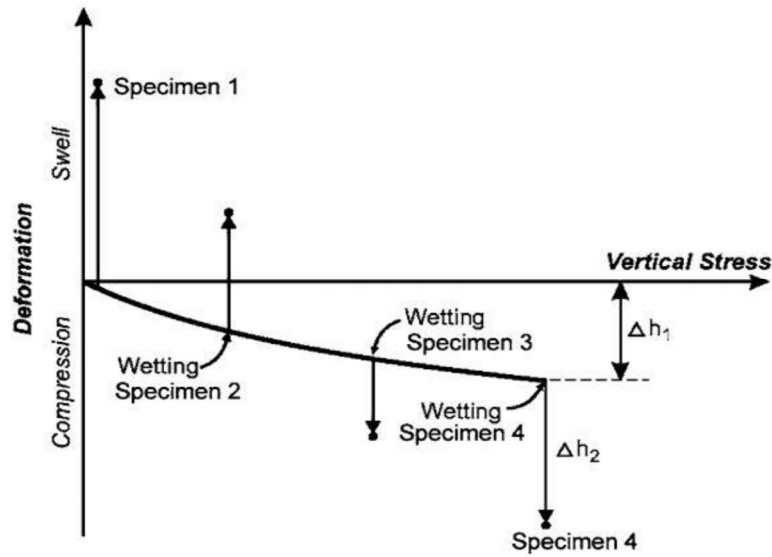


**Figure 3.2:** Deformation versus vertical stress, Technique 2 (ASTM D4546).

### 3.3.3 Technique 3

This procedure includes keeping the specimen at a constant height by adjustment in vertical load after the specimen is given access to free water. The stress that keeps the volume constant is interpreted as the swelling stress.

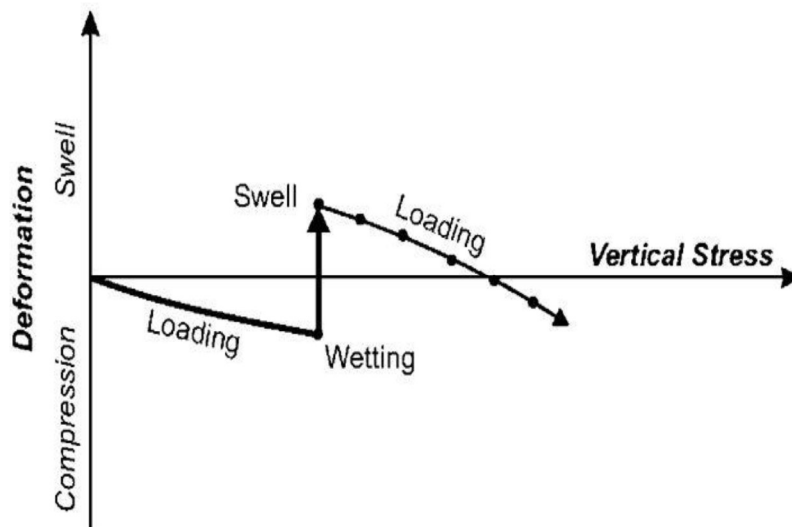


**Figure 3.3:** Deformation versus vertical stress, loading after wetting test. Technique 3 (ASTM D4546).

### 3.4 Proposed models to predict the swelling stress

**Table 3.1:** Models to predict the swelling stress

Source	Model	Legend / description
Komornik and David (1969)	$\log(P_s) = 2.132 + 0.0208LL + 0.000665 \gamma_d - 0.0269 W_i \quad (3.1)$	<p>LL = liquid limit, %,  <math>\gamma_d</math> = dry density, <math>\frac{kg}{m^3}</math>, and  <math>W_i</math> = initial moisture content, %.  <math>P_s</math> = swelling stress, kPa.</p>
Thakur et al., (2005)	<p><b>Montmorillonite</b></p> $P_s = 139 \Psi_m - 328 \quad (3.2)$ <p><b>Sodium montmorillonite</b></p> $P_s = 64 \Psi_m - 183 \quad (3.3)$	<p><math>P_s</math> = swelling stress, kPa, and  <math>\Psi_m</math> = matric suction, kPa</p>
Yusuf and Orhan (2007)	<p><math>0 &lt; P_s \leq 100kPa</math>;</p> $P_s = -3.72 + 0.0111 \times PI + 2.077\gamma_d + 0.244 \log \Psi_m \quad (3.4)$ <p><math>R^2 = 0.92</math></p> <p><math>100kPa &lt; P_s &lt; 350 kPa</math>;</p> $P_s = -16.31 + 0.0330 \times PI + 8.253\gamma_d + 0.829 \log \Psi_m \quad (3.5)$ <p><math>R^2 = 0.94</math></p>	<p><math>P_s</math> = swell stress, kPa,  PI = plasticity index, %,  <math>\gamma_d</math> = dry density, <math>\frac{kN}{m^3}</math>, and  <math>\Psi_m</math> = matric suction, kPa, and  <math>R^2</math> = coefficient coefficient.</p>
Elisha (2012)	$\log(P_s) = -5.423 + 0.0145 \times PI + 2.563\gamma_d - 0.0168w_i \quad (3.6)$ <p><math>R^2 = 0.95</math></p>	<p><math>P_s</math> = swelling stress, kPa,  <math>w_i</math> = initial moisture content, %,  <math>\gamma_d</math> = dry density, <math>\frac{kg}{m^3}</math>,  PI = plasticity index, %, and  <math>R^2</math> = correlation coefficient.</p>

**Table 3.2:** Models to predict the Swelling stress

Source	Model	Legend / description
Israr et., al (2014)	$P_s = 43.6 A_c + 68 W_i - 915 \quad (3.7)$ $R^2 = 0.958$	$P_s$ = swell stress , kPa, $w_i$ = natural moisture content , %, $A_c$ = activity of the clay, and $R^2$ = correlation coefficient.
Ya Tan (2016)	$\log(P_s) = -0.284 + 0.0686 I_{ss} - 0.185 \gamma_d - 0.031 W_i \quad (3.8)$ $R^2 = 0.94$	$P_s$ = Swelling stress, kPa, $W_i$ = initial moisture content, %, $\gamma_d$ = dry density, $\frac{kg}{m^3}$ $I_{ss}$ = shrink swell index, %, and $R^2$ = correlation coefficient.
Forouzan (2016)	$\log(P_s) = 14.155 + 0.021 A_c - 7.469 \gamma_d - 0.063 W_i \quad (3.9)$ $R^2 = 0.975$	$P_s$ = swelling pressure, kPa, $A_c$ = activity of clay, $\gamma_d$ = dry density, $\frac{gr}{cm^3}$ , $W_i$ = initial moisture content, %, $R^2$ = correlation coefficient.
Tu and Vanapalli, (2016)	$P_s = 55 + \beta_c \psi_m \left( \frac{S}{100} \right)^2 \quad (3.10)$ $\beta_c = \frac{0.25 \times e^{5.306 \times \gamma_{dmax}}}{1000} \quad (3.11)$	$P_s$ = swelling pressure of compacted expansive soils, kPa, $\beta_c$ = model parameter for compacted expansive soil, $\psi_m$ = matric suction, kPa, $\gamma_{dmax}$ = maximum dry density, $\frac{Mg}{m^3}$ , $S$ = degree of saturation, %.

Komornik and David (1969) carried out intensive laboratory tests on a number of undisturbed natural soil specimens to verify a predictive model in Equation 3.1 for swelling stress using statistical analysis of their data. Nevertheless, Equation 3.1 is not suitable to predict the swelling stress of compacted expansive soils. This model is designed only for undisturbed soil specimens. In addition, one of the most important parameters for unsaturated expansive soils, the matric suction is not used as an independent variable in this model.

Thakur et al.,(2005) studied the correlation between soil suction and the swelling stress in clay minerals. Sodium Montmorillonite and Montmorillonite were used. The suction was measured using Dew-point potentiometer (WP4). One dimensional expanding stress and free swelling test were conducted to develop the correlation between the soil suction and the swelling stress for sodium Montmorillonite and montmorillonite. Figure 3.4 shows the swelling stress and the suction relationship.

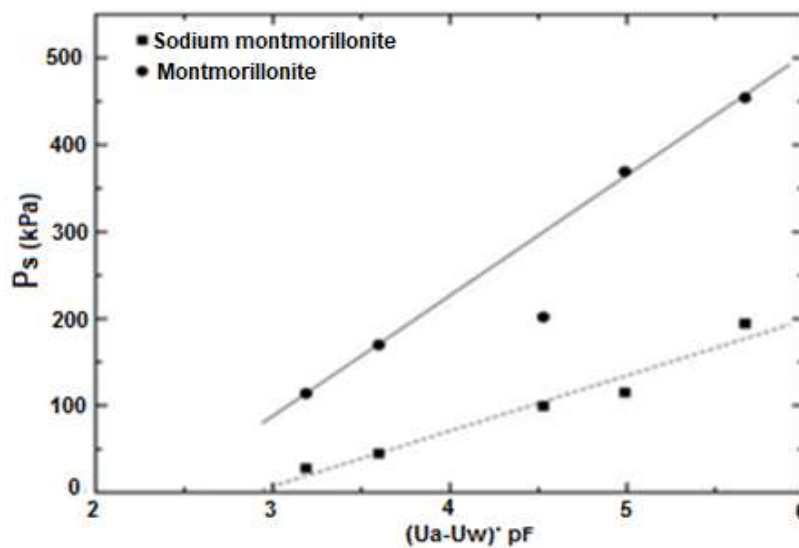


**Figure 3.4:** Relation between suction and swelling stress (Thakur et al., 2005)

Equation 3.2 and 3.3 shown in Table 3.1, proposed by Thakur et al., (2005) have been developed using the suction values obtained from the Dew-Point Potentiometer (WP4), which has a suction measurement within the range of 0 to 1500kPa. However, the filter paper technique can be used to measure all suction range. Likewise, these proposed models are developed using non-compacted specimens.

Yusuf and Orhan (2007) attempted to predict the swelling stress from soil suction measurements. Sodium bentonite was mixed with kaolinite in ratios of 5, 10, 15, 20 and 25% of dry kaolinite to have a material with plasticity indexes (i.e 30, 50, 68, 84, and 97%). The soil suction measurement was performed using thermocouple psychrometers technique on artificial compacted specimens. The soil suction was associated to specific surface areas, cation exchange capacity, dry density and plasticity index. A standard swell volume test was conducted on the specimens, and the results were used to develop a relationship between the

swelling stress and the logarithm of soil suction. The proposed equations 3.4 to 3.5 are shown in Table 3.1. The proposed models cannot predict a swelling stress beyond 350 kPa. In addition, the models were design using artificial compacted expansive soils made up by mixing sodium bentonite with Kaolinite. Hence, these models are not suitable to predict precisely the swelling stress of field compacted expansive soils.

Elisha (2012) performed one-dimensional swell tests on expansive clay mixed with different percentages of kaolinite and bentonite to yield a wide range of plasticity. Specimens were compacted at different initial water contents and dry densities. Model Equation 3.6 shown in Table 3.1 use to predict the swelling stress is based on three independent variables: plasticity index, water content and dry density, and it is developed using multiple regression analysis. Soil suction is an essential parameter for expansive soils. However, the model proposed by Elisha (2012) is built up without the soil suction. The matric suction should have been added as an independent variable in the model to enhance the prediction of the swelling stress. Furthermore, the impact of the soil suction on the prediction of the swelling stress was mentioned by Tu et al., (2016), they have developed a model to predict the swelling stress of expansive soils using the soil suction values obtained from the soil water characteristic curve (SWCC).

Israr et al., (2014) studied the correlations between the index properties and the swelling stress of expansive soils, and the model Equation 3.7 in Table 3.2 was developed to predict the swelling stress of expansive soils. The results given by the proposed model were obtained with an accuracy of + 5% with respect to tests values. The model proposed by Israr et al., (2014) is developed based on two independent variables, the activity of clay, and initial water content. Even though the predicted swelling stress was obtained with an accuracy of 5%, another research work by Sridharan and Prakash (2000) concluded that the index properties such as liquid limit, plasticity index, activity of the clay and related parameters could not accurately predict the soil swelling behaviour of expansive soils because they do not consider the effect of soil mineralogy. This model should have been enhanced by adding the soil suction as an independent variable.

Ya Tan (2016) conducted a series of oedometer test on expansive soils to determine the swelling stress developed within the soil specimens upon initial moisture content, dry density, and swell-shrink index. A multiple regression analysis was performed to analyze the data obtained from the experiment and develop model Equation 3.8 shown in Table 3.2 to predict the swelling stress. The Plasticity Index and the soil suction are not used as an independent variable in model Equation 3.8. Israr et al., (2014) pointed out that, the augmentation of the plasticity index increases significantly the swelling stress of expansive soils. Another research work conducted by Tu et al., (2016) revealed that the soil suction is an important parameter in the prediction of the swelling stress. Because of the variability of soil material, it would be beneficial to develop a model with many relevant independent parameters for more accuracy. However, according to the results of the study carried out by Sridharan and Prakash (1998) on expansive soil, the swell/shrink index is a not good predictor of the swelling behaviour of fine-grained soils because while the soil swelling stress is influenced by the presence of the clay mineral, the soil shrinkage is a result of packing phenomenon and controlled by the relative particle size distribution of fine-grained materials.

Forouzan (2016) developed mathematical model to predict the swelling stress of expansive soils based on artificial soils made by mixing kaolinite and bentonite in various proportions. Model Equation 3.9 is built with three independent variables: the activity of clay, dry density, and initial water content. Other relevant parameters to predict the swelling stress of expansive soil such as the soil suction had not been used as independent variables in this model.

Tu et al., (2016) proposed a mathematical Equation 3.10 for the prediction of the swelling stress of one - dimensional heave for expansive compacted soil with respect to matric suction using the soil water characteristic curve (SWCC). The matric suction can be used as a relevant independent variable to predict certain behaviour of expansive soils like the swelling stress. The soil water characteristic curve (SWCC) used to build up the model Equation 3.10 can be used to measure soil suction, degree of saturation, water content (gravimetric or volumetric) but not the maximum dry density as used in Equation 3.11 or other relevant soil parameters that influence the swelling stress.

Nevertheless, it is important to mention that the semi-empirical model proposed by Tu et al., (2016) did not use only the matric suction as the independent variable. The maximum dry density and the degree of saturation were used in Equation 3.10. Therefore, this model is not developed using only the matric suction, but by using three independent variables. According to the precedent proposed models, there are several other relevant soil parameters that influence significantly the swelling stress. Therefore, it would be good to use a maximum of relevant independent variables to develop an efficient predictive model.

### **3.5 Conclusion**

Several models have been developed over the years to predict the swelling stress of expansive soils, and the data used to develop the majority of these models were collected from artificial specimen made up by a mixture of bentonite/kaolinite with field soil. Soil compaction is widely used in construction to maximize the dry density and achieve a desired strength. Nonetheless, few models to predict the swelling stress were developed using field compacted expansive soils. Furthermore, because of the variability of soil material, previous authors' models were developed for a specific type of soil material. Some models to predict the swelling stress are summarized in Tables 3.1 and 3.2. These models were developed using different types and different numbers of soil parameters as independent variables, the number and the type of independent variables vary from one model to another. These independent variables are as follows: unsaturated soil characteristics (Matric suction, SWCC), geotechnical index properties (initial dry density, Initial water content, plasticity index, liquid limit, and activity of clay), expansive soil indexes (modified free swell index, swell/shrink index). The majority of these models are developed with a minimum of two, and a maximum of four independent variables. An increment of the number of independent variables would improve the accuracy of the predictive models. To enhance foundation design in expansive soils in Free State province, a correlation between the swelling stress and other soils parameters must be investigated. Furthermore, models used to predict the swelling stress of compacted expansive soils have to be developed.



---

## CHAPTER 4: EXPERIMENTAL STUDY

### 4.1 Introduction

This research is based on experiments conducted in the geotechnical laboratory of the department of the civil engineering at the Central University of Technology, Free State. Additionally, X-ray diffraction tests were performed at the analytical facility of the University of Johannesburg. In this chapter, the type test standard, and the processes of experimental works are described.

The laboratory tests conducted to assess the physical and hydromechanical properties of soils tested are as follows: Particle size distribution (sieve analysis, hydrometer analysis), Atterberg limits, linear shrinkage, specific gravity, free swell index, free swell ratio, X-ray diffraction, Proctor compaction test, swelling stress test, soil suction estimation by filter paper technique, and the soil water characteristic curve (SWCC).

The results obtained from laboratory tests are analyzed, discussed qualitatively and quantitatively. The correlations between the swelling stress, the soil suction, and other soil parameters are determined. Predictive models are developed by multiple regression analysis using software NCSS11 to predict the swelling stress of compacted expansive soils with respect to the soil suction, geotechnical index properties, expansive soil indexes, and mineralogy characteristic. The validation of the proposed models is achieved by comparing the predicted values to the values obtained from experimental works, and by comparing the predicted values obtained from the developed models to the values obtained from other existing models.

### 4.2 Sample locations

Soil samples were collected from various locations across the province of Free State (Petrusburg, Bloemfontein, Winburg, Welkom, and Bethlehem). The location of sampling points are shown in Figure 4.1, and the samples collection from the field is shown in Figure 4.2.

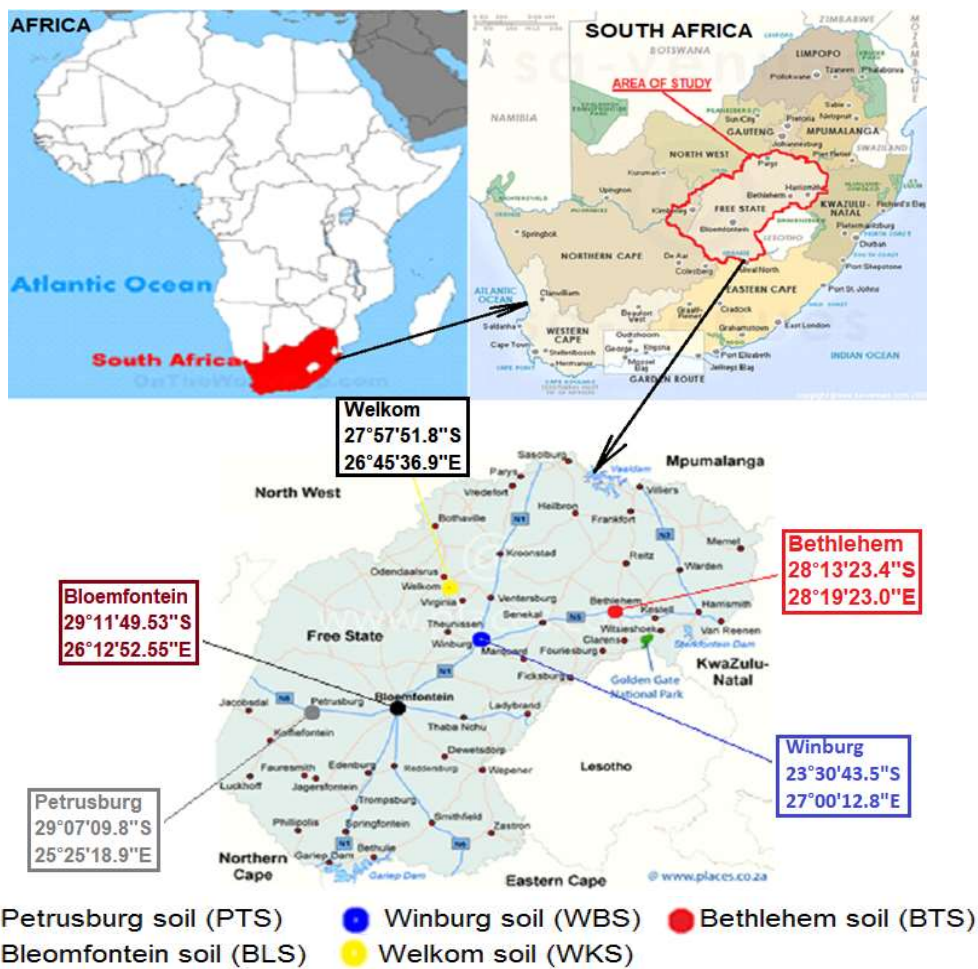


**Figure 4.1:** Map showing the location of sampling points



**Figure 4.2:** Collection of samples from field sites

### 4.3 Laboratory tests

The experimental standards used in this research work are summarized in Table 4.1.

**Table 4.1:** Summary of test standards

No	TEST		REFERENCE
01	Particle size distribution	Sieve analysis	ATSM D6913
		Hydrometer analysis	ATSM D7928
02	Atterberg Limits	Liquid limit	ASTM D4318
		Plastic limit	
03	Linear shrinkage Test		TMH-1 Method A4
04	Free swell index of soil		BIS, I. 1977
05	Identification of soil clay mineralogy by free swell ratio		Sridharan & Prakash ( 2000)
06	X-Ray Diffraction (XRD)		Brindley and Brown (1984)
07	Specific gravity test		ASTM D854
08	Modified Proctor compaction		TMH-1 Method A7
9	Swelling pressure test		ASTM, D4546
10	Soil suction measurement		ASTM D5298
11	Soil water characteristic curve (SWCC)		Seki (2007) Fredlund and Xing (1994) Van Genuchten (1980)

#### 4.3.1 Particle size distribution

Particle size distribution (PSD), known as soil gradation tests, were conducted on particulate materials within the range of clay to boulders. This fundamental experiment refers to discern the percentage of particles within a specified particle size range across all the sizes represented for the soil samples. The distribution of different grain sizes affects the engineering properties of soil, and it is required for soil classification. The particle size distribution was conducted in accordance with ASTM D6913 for sieve analysis, and ASTM D7928 for hydrometer analysis. The

PSD was performed in two steps. In the first step, particle sizes greater than 75  $\mu\text{m}$  (retained on the No. 200 sieve) were estimated by mechanical sieve analysis Figure 5.3a. In the second step, the distribution of particle sizes smaller than 75  $\mu\text{m}$  was estimated by sedimentation technique, using a hydrometer as shown in Figure 5.3c.

#### 4.3.2 Sieve Analysis

About 500g of oven dry soil sample was taken to perform sieve analysis. The mass of each sieve as well as the bottom pan was recorded. Then, all the sieves were cleaned and assembled in the ascending order of sieve number (# 4 sieve at the top and #200 sieve at the bottom). The measured oven-dried sample was poured into the top sieve, and covered with the lid. The sieve stack was placed on the mechanical shaker and agitated for 10 minutes Figure 4.3a. After, the stack was removed from the shaker, and carefully weighed to record the soil mass retained in each sieve. The weight of the bottom pan with its retained fine soil was measured. The soil mass retained on each sample was obtained by subtracting the mass of the empty sieve from the mass of the sieve plus retained soil, and the mass was recorded in a data sheet. The sum of the retained masses was approximately the same as the initial mass for soils PTS, BLS, WBS, WKS, and BTS used for the experiment. The percentage of the retained soil on each sieve was obtained by dividing the retained mass on each sieve by the original mass. The percentage of passing was obtained by starting with 100 percent and subtracting the percent retained on each sieve in a cumulative process. After, a semi-logarithmic graph of the grain size versus percent finer was plotted.

#### 4.3.3 Hydrometer Analysis

Finer soil, silt and clay fraction (smaller than 75  $\mu\text{m}$ ) cannot be assessed by sieve analysis. It is usually performed by sedimentation technique (hydrometer analysis). The soil retained on the pan after sieve analysis was dried and about 100 g of soil was taken for the hydrometer analysis. The specimen was mixed with 125 ml of 4%  $(\text{NaPO}_3)_6$  (Sodium hexametaphosphate) solution in a small evaporating dish and then, the dish was covered with a wet paper towel to reduce evaporation. The mixture was kept for 16 hours to soak. After soaking, the mixture was transferred to a dispersion cup, and water was added until the cup was around 2/3 full. After,



the mixture was transferred to the sedimentation cylinder and stirred for about 1 minute to achieve the uniformity of the mixture as shown in Figure 4.3b. After, the sedimentation cylinder was set up for the hydrometer analysis; the first reading was recorded at an elapsed time of 30 seconds. Simultaneously, the temperature of the water was recorded. At least 15 seconds before the taking reading, the hydrometer was placed on the cylinder so that it would stabilize.

The readings on the hydrometer and thermometer were continuously recorded at approximated elapsed times of 2,4,8,16, 30 and 60 minutes; after 2, 4, 8, 24, 48 and 72 hours.

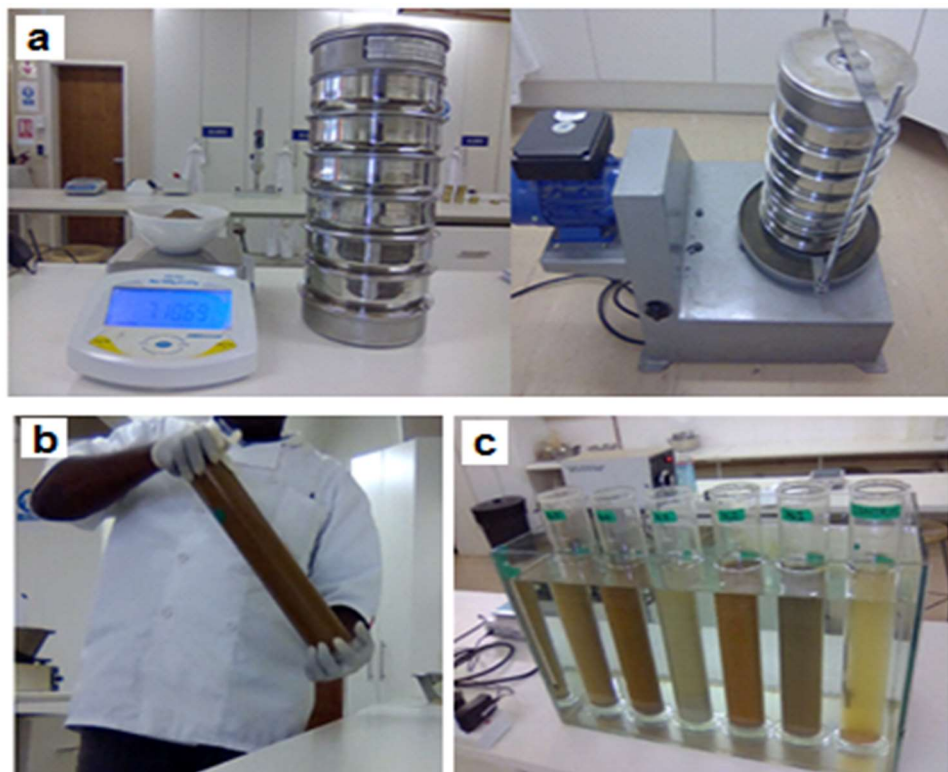


**Figure 4.3:** (a) Sieve analysis. (b) Agitation of sedimentation cylinder. (c) Hydrometer analysis.

#### 4.3.4 Atterberg limits

The term Atterberg limits are the physical state of soil pertaining to water content at that time. It can be also defined as the resistance to deformation due to mechanical strength or firmness of fine-grained soils at several water contents. Atterberg noticed that the consistency of fine-grained soils is tremendously affected by the water content within the soils. Thus, the water content at which the state of the soil changes from one state to another state is defined as Atterberg limits or consistency limits (Murthy, 2002). Fine-grained soil can display any of

these four states depending on the moisture content: solid state, a semi-solid state, plastic state, and liquid state. The water content at the boundaries of these states is known as shrinkage limit (SL), plastic limit (PL), and liquid limit (LL), respectively (Lambe and Whitman, 1969). LL is known as the water content at which the soil flows and PL is determined as the water content at which the soil starts crumbling when rolled into 3.175mm diameter thread. The numerical difference between LL and PL known as plasticity index (PI) characterizes the plastic nature of the soil. The consistency limits can be used to between different types of silts and clays.

### 4.3.5 Liquid limit

There are two common methods used to determine the liquid limit in laboratory: Casagrande liquid limit test, and fall cone test method. The Casagrande liquid limit has been chosen in this study and performed according to ASTM D4318. Figure 4.4 shows the apparatus used.



**Figure 4.4:** Apparatus used for Atterberg limit test

Casagrande liquid limit test according to the liquid limit test method is defined as the moisture content at which two sides of a groove come closer together for a distance of 12.7mm under the impact of 25 numbers of blows as shown in Figures 4.5a, and 4.5b. Given the fact that it is time-consuming and difficult to obtain a test with exactly 25 numbers of blows, the process is conducted several times with a range of water contents, and the results are interpolated.

The moisture content and the corresponding number of blows for the two liquid limits determination are used to calculate the liquid limit (LL) at 25 blows.

$$LL (\%) = \frac{W_1 - W_2}{W_2 - W_c} \times 100 \quad (4.1)$$

Where

$W_1$  = Mass of container + wet soil, g ,

$W_2$  = Mass of container + dry soil, g ,

$W_c$  = Mass of container, % , and

LL = Liquid Limit, %.



Figure 4.5a: Casagrande liquid limit test

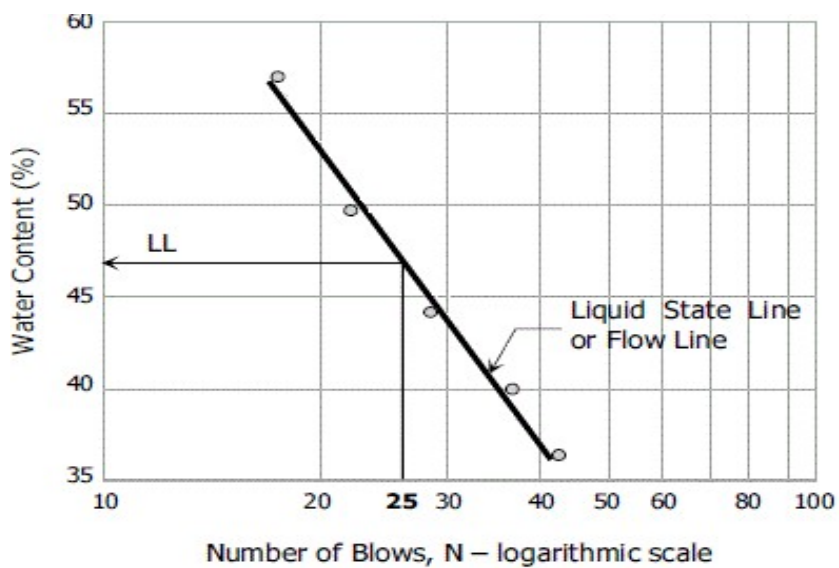


Figure 4.5b: Casagrande liquid limit test results

### 4.3.6 Plastic limit

The plastic limit is defined as the water content above which the soil-water mixture is in the state of plasticity. At this stage, the mixture undergoes deformations to any shape under any small stress. By the reduction of moisture content, the mixture passes to a semi-solid state. Any variation in moisture content on either side of the plastic limit induces volume variation of the soil. In this study, the method used to determine the plastic limit is based on ASTM D4318. The plastic limit is defined as the moisture content at which the soil begins to crumble when rolled up into a thread of 3.2 mm in diameter as shown in Figure 4.6.

$$PL (\%) = \frac{W_1 - W_2}{W_2 - W_c} \times 100 \quad (4.2)$$

Where

PL = plastic limit, % ,

$W_1$  = mass of container + wet soil, g ,

$W_2$  = mass of container + dry soil, g , and

$W_c$  = mass of container, g .

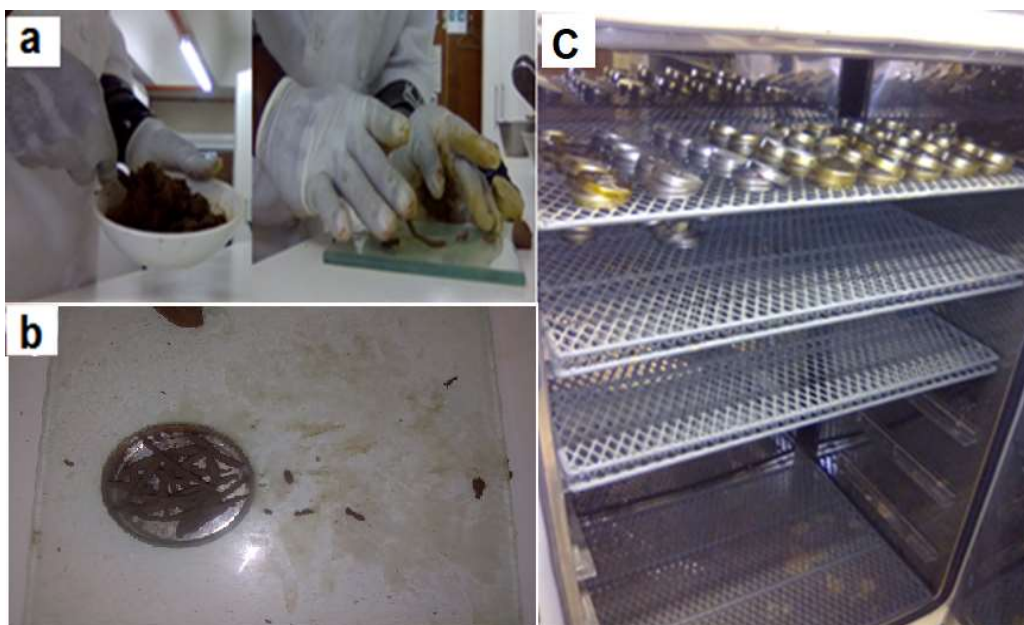


**Figure 4.6:** (a) Soil crumbles during the plastic limit test (b) Crumbled soils in moisture tin (c) Oven dried samples for moisture content determination



### 4.3.7 Plasticity index

The plasticity index is the difference between the liquid limit and the plastic limit of a soil. Plasticity index indicates the degree of plasticity of soil, i.e. the greater the difference between the liquid limit and the plastic limit, the greater the plasticity of the soil.

### 4.3.8 Linear shrinkage test

The linear shrinkage of soil for the water content equivalent to the liquid limit is the decrease in length, expressed as a percentage of the original length of the soil mass when the water content is reduced from the liquid limit to an oven-dried state. The test is conducted according to TMH1-Method A4. Figure 4.7 shows the apparatus used for the linear shrinkage test.



**Figure 4.7:** Apparatus used for linear shrinkage test

A dry shrinkage trough is warmed firstly to prevent the premature setting of the grease; the inside is then fully covered with a thin layer of molten grease applied by means of a small paintbrush. Any excess of molten grease is shaken out by tapping the trough lightly in an inverted position. The trough was inspected carefully, to make sure that there are no patches without any grease.

After a one-point liquid limit test has been completed, the moist material left over was used to fill the trough without further mixing. The number of blows required for groove closure for the final determination in the Liquid limit test was recorded. Half of the greased trough was filled with the wet soil by taking smaller part of soils on

the spatula, pressing the soil down against one end of the trough, and working along the trough until the whole side was filled so that the soil forms a diagonal surface from the top of one side to the bottom of the opposite side Figure 4.8a. The trough was then turned around, and the other part was filled in the same manner Figure 4.8b. The hollow along the top of the soil was filled so that the soil is raised above the sides of the trough Figure 4.8c. The excess material was removed by drawing the blade of the spatula once only from one end of the trough to the other. The index finger was pressed down on the blade so that the blade moves along the edges of the trough as depicted in Figure 4.8d.

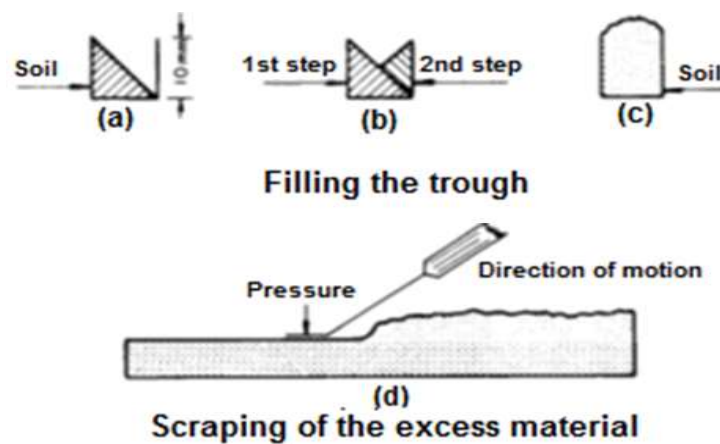


**Figure 4.8:** Linear shrinkage test

The trough is filled with moist material was placed in a drying oven and dried overnight at a temperature of 105°C until the shrinkage stopped. The trough with material was taken out and allowed to cool in the air Figure 4.9.

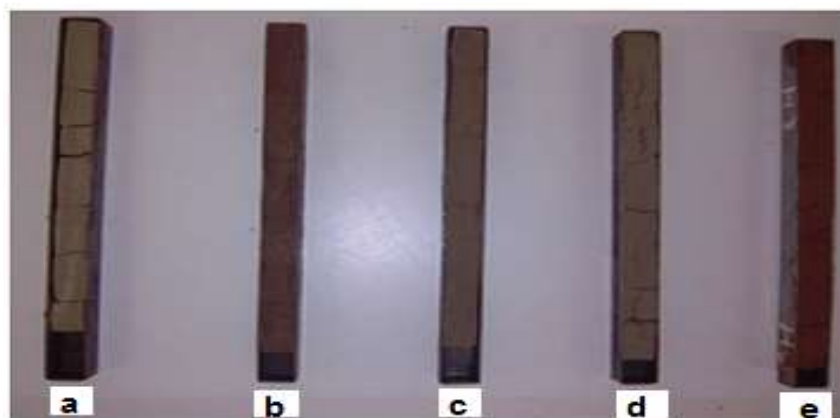


**Figure4.9:** dried trough with the material

(a) BTS: Bethlehem soil, (b) BLS: Bloemfontein soil, (c) PTS: Petrusburg soil,  
(d) WBS: Winburg soil, (e) WBS: Welkom soil

The linear shrinkage was calculated from the following formula:

$$LS (\%) = \text{shrinkage in mm as measured} \times \left( \frac{100}{150} \times \frac{0.8}{1 - 0.008N} \right) \quad (4.3)$$

Where:

LS = Linear shrinkage, % , and

N = number of blows in liquid limit test.

The Linear shrinkage is reported to the nearest 0.5%.

#### 4.3.9 Specific gravity

The specific gravity of a material is defined as the ratio of the mass of a unit volume of a material to the mass density of gas-free distilled water at a stated temperature. ASTM D854 suggests a method to determine fine grained-soil specific gravity. Samples were oven-dried at 105 for a period of 16 to 24 hours.

The test was performed by measuring the empty mass of a clean dry pycnometer. Then, approximately 50g of the oven dry was added to the pycnometer to obtain the mass of the pycnometer and the oven dry soil. After tap water was added to cover the soil and was soaked for 12 hours, the entrapped air was removed by boiling the specimen for 10 min. The pycnometer was agitated periodically to assist in driving out the air. The mass of the pycnometer, water, and soil was determined. The temperature of the soil and water was measured.

Then, the pycnometer was filled with the temperature stabilized water to 500ml. The mass of the pycnometer and water were measured. The apparatus used for specific gravity determination is shown in Figure 4.10. The Specific gravity of soil solids was calculated using the following equation.

$$G_s = \frac{M_2 - M_1}{[(M_4 - M_1) - (M_3 - M_2)]} \quad (4.4)$$

Where:

$G_s$  = specific gravity,

$M_1$  = empty mass of volumetric flask, g ,

$M_2$  = mass of pycnometer + oven dry soil, g ,

$M_3$  = mass of pycnometer + oven dry soil + filled water, g , and

$M_4$  = mass of pycnometer + filled with water only, g .

The specific gravity was computed by multiplying by a correction factor that accounts for differences in water density with temperature. The average of two tests was used to determine the specific gravity.

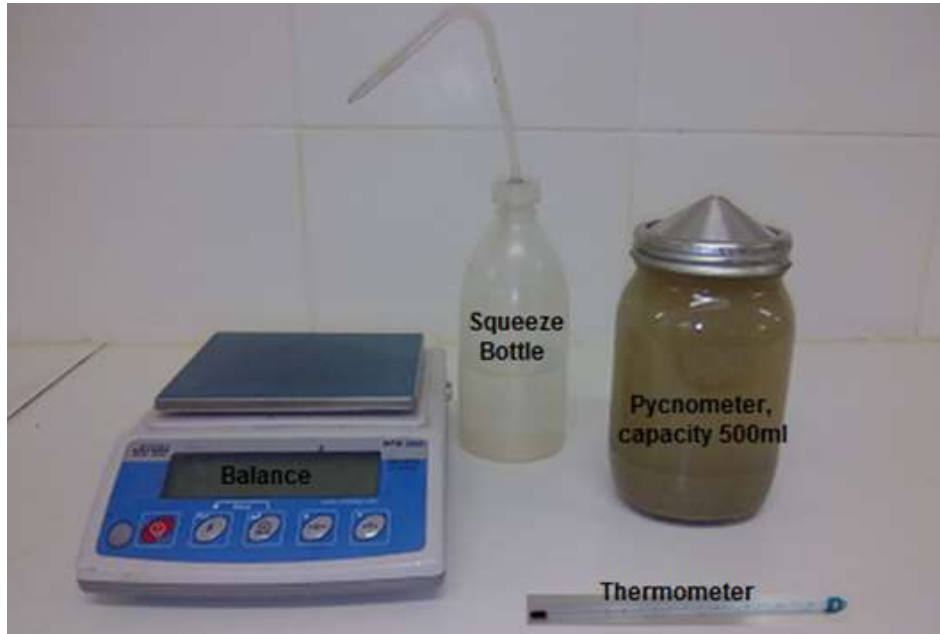


**Figure 4.10:** A view for soil specific gravity test

#### 4.3.10 Free swell index

The free swell index test is used for the determination of soil expansiveness potential. It is a quick test and so, it is preferred for preliminary site investigation. In order to get an idea about the expansiveness of soil, free swell index test was performed in compliance with the Indian Standard Method BIS, I. 1977. The free swell index is the increase in the volume of soil, without any external restraints, on submerging in water.

Two representative's ovens dried soil specimens of 10 grams were sieved through 425-micron sieve. Each soil sample was poured in two glasses graduated cylinder of 100ml capacity. One cylinder was filled up with kerosene, and another with distilled water up to 100ml mark as shown in Figure 4.11.

The entrapped air inside the cylinder was removed by shaking and stirring with a glass rod. 24 hours were allowed to the soil samples to attain the equilibrium state of volume without any further change in the volume of the soil, and the final volume of soil in each cylinder is recorded. The average of two tests was used to determine the free swell index.

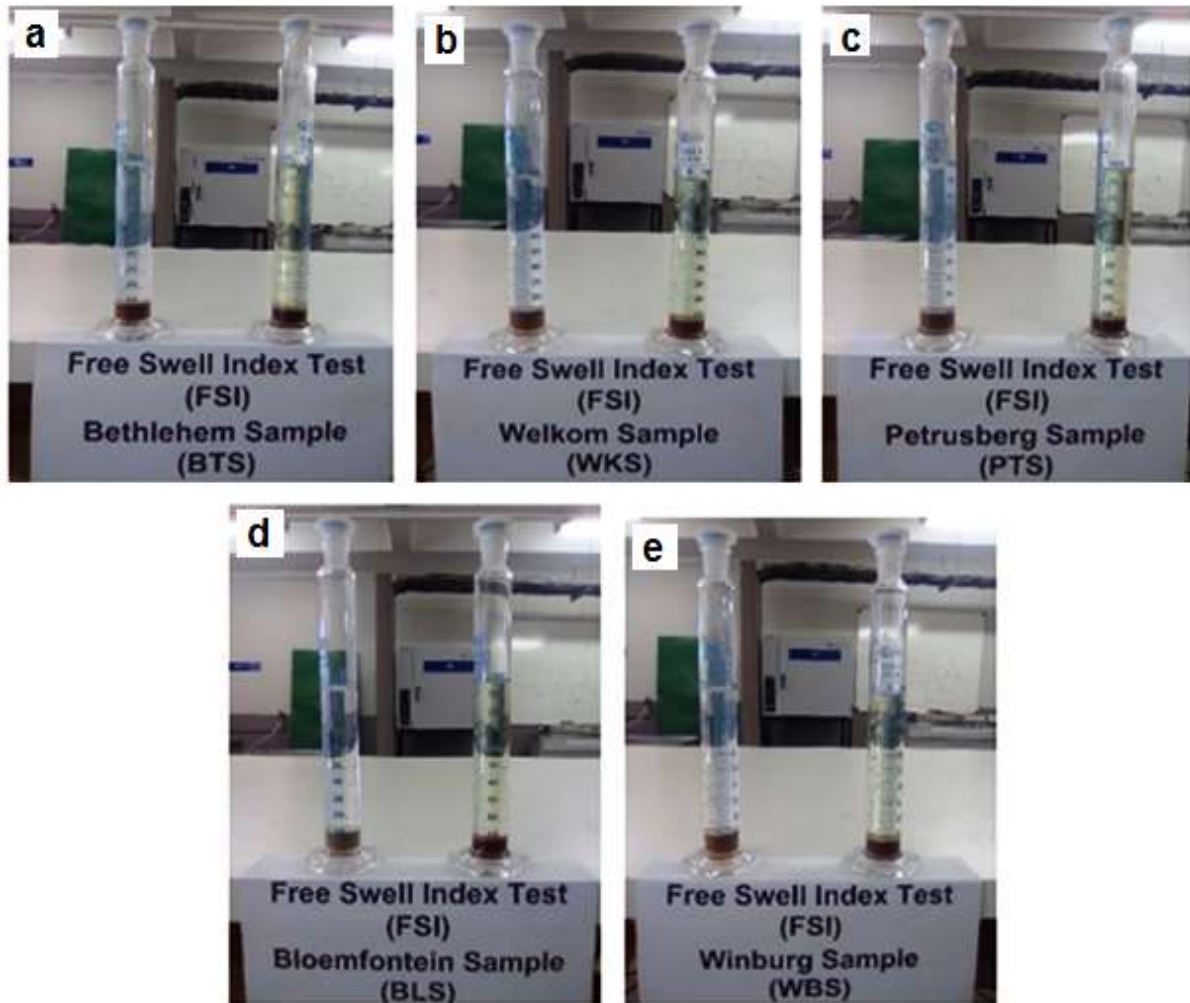


**Figure 4.11:** Free swelling test: (a) BTS: Bethlehem soil, (b) WKS: Welkom soil, (c) PTS: Petrusburg soil, (d) BLS: Bloemfontein soil; (e) WBS: Winburg soil

The free swell Index was calculated from the following equation.

$$FSI (\%) = \frac{V_d - V_K}{V_K} \times 100 \quad (4.5)$$

Where:

FSI = free swell index, % ,

$V_d$  = volume of the soil specimen read from the graduated cylinder containing distilled water, ml, and

$V_K$  = volume of the soil specimen read from the graduated cylinder containing kerosene, ml.

### 4.3.11 Free swell ratio and clay mineralogy

This test is used to assess the soil expansivity, and the type of dominant clay mineral. According to the study conducted by Sridharan and Prakash (2000), free swell ratio (FSR) method is a very competitive method that required a simple procedure to assess the swell potential of expansive soil and the clay mineralogy. The procedure is the same as the Free swell index test. The Free swell ratio was determined using the following equation.

$$FSR = \frac{V_d}{V_k} \tag{4.6}$$

Where:

FSR = free swell ratio,

$V_d$  = volume of soil specimen read from graduated cylinder containing distilled water, ml, and

$V_k$  = volume of soil specimen read from graduated cylinder containing kerosene, ml .

Table 4.2 was used to classify the degree of expansivity of the soil based on their FSR. On the other hand, Table 4.2 was also used to identify the dominant clay mineral.

**Table 4.2:** Classification of soil based on FSR (Sridharan & Prakash, 2000)

Free Swell Ratio	Clay Type	Soil Expansivity	Dominant clay Mineral Type
=1	Non - swelling	Negligible	Kaolinite
1.0 - 1.5	Mixture of swelling and non - swelling	Low	Mixture of Kaolinitic and Montmorillonitic
1.5 - 2.0	Swelling	Moderate	Montmorillonitic
2.0 - 4.0	Swelling	High	Montmorillonitic
> 4.0	Swelling	Very High	Montmorillonitic

The free swell ratio method has been shown to be a simple and user-friendly method that can be adopted in the field for characterizing the expansive soil, and for the identification of their mineralogical composition.

## 4.4 X-Ray Diffraction (XRD)

### 4.4.1 Introduction

Soil behaviour is partially due to the nature and the quantity of the mineral present in the soil. Therefore, the mineral composition of any soil influences the physical and mechanical properties. The X-ray diffraction test is used for examining the mineralogical composition via the crystallographic structure of the lattices of stacked clay mineral sheets as well as other components such as quartz, feldspar, etc. The results of this test could provide information about the mineral characteristic of the soil. In this study, X-ray diffraction test was conducted on soils WKS, BTS, PTS, WBS, and BLS.

### 4.4.2 Procedure

Samples were analyzed for their major mineral contents by mean of the X-ray diffraction technique (Brindley and Brown, 1984). The technique is based on assessing the pattern of basal peaks, their corresponding relative magnitude values occurring in the X-ray diffraction pattern (Sachan and Penumadu, 2007). A Philips automated powder diffractometer shown in Figure 4.14, was used for XRD analysis in this study. Soil samples were ground to maximize sample representativeness and minimize the orientation preference. Sample holders were front-loaded using larger well holder as shown in Figure 4.12. After that, the sample holder is kept at 45° with the horizontal to check if the loading is done in a proper manner; in this case, the sample inside the holder will not fall into small pieces. The loading sample process is conducted so that the plane of the sample is the same as the plane of the sample holder. After that, the tray containing the loaded sample holder is placed in the multi-purposes diffractometer as shown in Figure 4.13. Thereafter, the doors were closed for safety because of X-ray radiations. The process is computer-assisted, using the software package Diffrac plus XRD Commander. The procedure is continued until the end of the test. Prior to start the scan, the standard scan setting is selected as follows:

Start value:	10	2Theta
End value:	90	2Theta
Increment:	0.02	1Theta
Time:	1	Second.



The job was created as follows:

The samples identification is done using these abbreviations: BTS, PTS, BLS, WBS, WKS. The raw file is used to save all the samples data and colour assignments. The parameters file is created using XRD Wizard. Afterward, the scan is performed, and the results are saved automatically in the raw file. When the test is completed, samples are removed, and the openings are closed.



**Figure 4.12:** Sample preparation by front-loading for XRD test

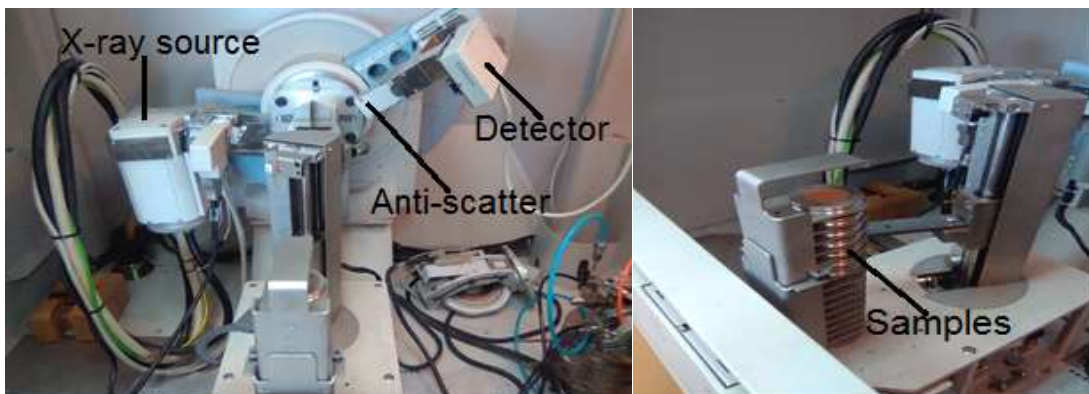


**Figure 4.13:** Multi-purpose diffractometer (MPD) used for XRD test equipped with a copper (Cu) anode and a goniometer with the cradle, allowing angular movements in 2 Theta, Omega, Psi, as well as linear positioning in x, y, and z.



**Figure 4.14:** Philips automated powder diffractometer.



## 4.5 Modified Proctor compaction test

Compaction at carefully controlled moisture content enhances soil strength and compressibility in the construction of a road, buildings, earth dams, and many other engineering structures. Compaction is defined as densification and rearrangement of soil particles by removing air void using mechanical equipment such as compaction machine. The dry unit weight of the soil is a reference parameter to determine the degree of compaction. Compaction increases the shearing resistance, enhance the bearing capacity and reduce the permeability of the soil. Moisture within the soil sample influences the degree of densification for a given compaction energy. Water added during the compaction process acts as a lubricating agent on the soil particle, and the dry unit weight increases simultaneously with additional water up to an optimal point. Beyond this point, the dry unit weight reduces upon water addition. The optimum water content is the water content at which the maximum dry unit weight is achieved under constant mechanical energy.

### 4.5.1 Compaction test procedure

Compaction tests were conducted in accordance with the standard test method for laboratory compaction characteristics of soil TMH-1 Method A7. Soils were compacted on several water content distributed on the dry side of optimum, on the optimum, and on the wet side of optimum moisture content.

The test was done with a mould that has a volume of 2355.74 ml a diameter of  $152.4 \pm 0.5$  mm, and  $152.4 \pm 1$ mm high with a detachable collar base plate and a  $25.4 \pm 1$  mm thick spacer plate with the proviso that the spacer plate inside the mould, the effective depth of the mould shall be of  $127 \pm 1$ mm. A  $4.536\text{kg} \pm 20$  gram tamper with a  $50.8 \pm 1$ mm diameter face and with a sheath to give a  $457 \pm 2$  mm drop. To determine the volume of the mould, both ends of the mould and the circumference of the spacer plates and the mould were greased, spacer and base plate assembled. Any excess grease was removed. The assembled mould plus the 180 mm square glass plate was weighed. Water was poured inside the mould and when filled up, the glass plate was gently slid over the top of the mould. Before the glass plate covers almost the mould, a final drop of water was added using a pipette.

The mould with water and glass plate were weighed, and the mass of water in the mould computed. The temperature of the water was measured, and the volume of the mould was computed as follows:

$$V_m = \frac{\text{Mass of water in gram}}{\text{RD of water at test temperature}} \quad (4.7)$$

Where:

$V_m$  = volume of the mould, ml, and

RD = relative density of water according to temperature.

**Table 4.3:** Relative density of water according to temperature

Temp.°C	RD of water	Temp.°C	RD of water
15	0.99913	23	0.99756
16	0.99897	24	0.99732
17	0.99880	25	0.99707
18	0.99862	26	0.99681
19	0.99843	27	0.99654
20	0.99823	28	0.99626
21	0.99802	29	0.99597
22	0.99780	30	0.99567

Samples were sieved through 425-micron sieve; approximately 35 kg of the sample was oven-dried at 105°C for a period of 16 to 24 hours and divided to obtain five basins of exactly similar material.

The specific mass of water to be added to the material in the basin was calculated using Equation 4.8. While adding water, the material was mixed continuously with a trowel.

$$M_w = \frac{M_{\text{soil}} (W_t - W_i)}{100} \quad (4.8)$$

Where

$M_w$  = mass of water to be added , g ,

$M_{\text{soil}}$  = mass of the dry soil , g ,

$W_t$  = targeted moisture content , % , and

$W_i$  = initial moisture content, % .

Water was added until the material can be readily pressed together by hand to form a lump that was not crumbled, this state denoted the material is at or near its plastic limit, which is normally slightly below. The mixed material was covered with a damp sack to prevent evaporation and allowed to soak overnight.

The dry mould was cleaned up, weighed to the nearest 5 g accuracy, and assembled on the base plate with the spacer plate. The internal surface of the mould was covered with a lubricant to make the demoulding of compacted soil more easily. Two 150 mm rounds of filter paper were placed on the spacer plate to prevent the material from sticking to the plate. The collar was then fitted to the mould.

After mixing again, about 1 kg of the material was weighed out and transferred to the mould. The surface of the soil was leveled by hand by pressing down and tamped 55 times with 4.536 kg tamper, which was dropped at 457, 2 mm. The blows were distributed over the whole layer in five cycles of 11 blows each. For each cycle, eight blows are applied to the outside circumference, and three blows around the centre. After tamping the first layer, the depth of the surface of the tamped material below the top of the mould, without the collar, was measured and kept within 96 to 99 mm. Four more layers of material were tamped in exactly the same manner. The depths from the top of the mould to the surfaces of the compacted layers were conducted according to the following limits:

- 1<sup>st</sup> layer: 96 to 99 mm
- 2<sup>nd</sup> layer: 68 to 71 mm
- 3<sup>rd</sup> layer: 43 to 46 mm
- 4<sup>th</sup> layer: 15 to 20 mm

After the compaction of the fifth layer, the surface of the material was kept between 5 and 15 mm above the top of the mould without the collar. The compaction test in the laboratory is shown in Figure 4.15.



**Figure 4.15:** Proctor compaction test

After compaction, a representative sample between 500 gram and 1000 gram was taken from the material in the basin and placed in a suitable container to determine the moisture content. The moist sample was weighed immediately, accurate to the nearest 0.1gram, and dried to constant mass in an oven at 105°C. The moisture content was determined to the nearest 0.1 percent and recorded on a lab form. Other additional points for the moisture-density relationship curve were determined by the same procedure for the other four basins of prepared material at various moisture contents. After the second compaction, the approximated dry density for the two compactions was calculated, using the assumed moisture content which is the percentage of water added plus the estimated moisture content of the air-dried sample. The approximate dry densities plotted against the assumed moisture contents, and the relative position of the two points will indicate the amount of water to be added for the third point. After plotting the third point, the shape of the curve will indicate the best moisture content for the remaining points. If possible, at least two points differing by about one percent in moisture content should be obtained on either side of the peak of the moisture density curve and the last point should be taken as near to the peak as possible unless one has already been obtained earlier near that point.

#### 4.5.2 Calculation of compaction test parameters

The moisture content of the material was calculated using the average of the water contents for each point to the nearest 0.1 % according to Equation 4.9

$$W(\%) = \frac{(W_1 - W_2)}{(W_2 - W_C)} \times 100 \quad (4.9)$$

Where:

$W_1$  = mass of container + wet soil , g ,

$W_2$  = mass of container + dry soil , g ,

$W_1 - W_2$  = mass of water , g ,

$W_2 - W_C$  = mass of the oven dry soil , g, and

$W$  = moisture content, %.

The total density in  $\text{kg}/\text{m}^3$  of the compacted soil sample were determined by dividing the wet mass by the volume of the mould used for each point corresponding to a specific moisture content using Equation 4.10.

$$\gamma_m = \frac{(M_t - M_m)}{V} \quad (4.10)$$

Where:

$M_t$  = mass of mold, base plate, and wet soil , (kg),

$M_m$  = mass of mold and base plate , (kg),

$V_m$  = volume of the mould , ( $\text{m}^3$ ), and

$\gamma_m$  = total density , ( $\text{kg} \cdot \text{m}^{-3}$ ).

The dry density of the material was determined for each point corresponding to a specific moisture content using Equation 4.11.

$$\gamma_d = \frac{\gamma_m}{1 + \frac{W}{100}} \quad (4.11)$$

Where:

$\gamma_m$  = total density, ( $\text{kg} \cdot \text{m}^{-3}$ ),

$\gamma_d$  = dry density , ( $\text{kg} \cdot \text{m}^{-3}$ ), and

$W$  = moisture content in , (%).

The compaction equation curve for the compacted saturated dry density of the soil material (zero air void line) was determined for each point corresponding to a specific moisture content using Equation 4.12. The modified Proctor compaction test data sheet is shown in Table 5.30 found in Appendix P.

$$\gamma_d = \frac{G_s \times \gamma_m}{1 + W \times G_s} \quad (4.12)$$

Where:

$\gamma_m$  = total density, (kg. m<sup>-3</sup>),

$\gamma_d$  = dry density, (kg. m<sup>-3</sup>),

$G_s$  = specific gravity, and

$W$  = moisture content in, (%).

#### 4.5.3 Plotting of compaction curve

The graph of the dry density values on the (y) axis and the moisture content on (x) axis was plotted in Figure 4.16.

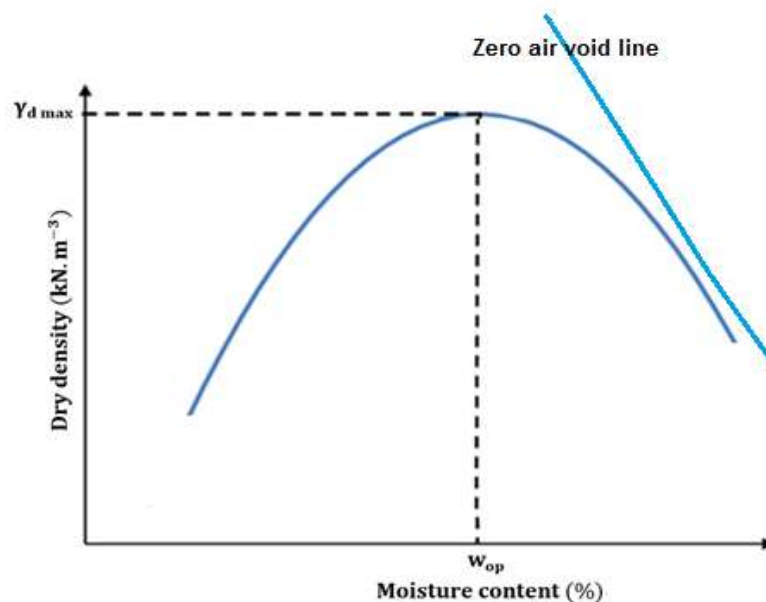


**Figure 4.16:** Maximum dry density and optimum moisture content determination through Proctor test

#### 4.6 Swelling stress test, experimental procedure, and equipment

The swelling stress is defined as the maximum external load that is required to prevent swelling soil from any further deformation while wetting. Usually, geotechnical engineers in the laboratory assess and determine the intensity of swelling stress produced by heaving soil using the conventional oedometer setup - dimensional wetting induced expansion. Figure 4.19 shows a conventional consolidometer setup for swelling stress measurement.

According to the studies conducted by Basma et al., (1995); Fattom and Barakat (2000) on swelling stress, the best-used method to determine the swelling stress is designated as zero swell test (ZST).

The standard used for this test is ASTM D 4546. The soil specimens were compacted according to modified Proctor compaction test TMH-1 Method A7, at various moisture content on the dry side, at the optimum moisture content, and on the wet side. After compaction, soil specimens were wrapped using a double airtight plastic bag and kept in a constant temperature bath to maintain the moisture content in the samples constant. After that, a jack was used to insert the compacted sample in the consolidation ring as shown in Figure 4.18c.

The consolidation ring with the compacted soil sample was then prepared for the zero-swell test. The porous stones were boiled for overnight and kept in a tight container for saturation as shown in Figure 4.17b. Thereafter, the ring with sample, porous stone and filter paper were embedded on the top, and bottom of the sample with the ring-shaped filter paper. The ring containing the compacted specimen was placed in a circular cylinder as shown in Figure 4.17c.

Before the submergence of the specimen in water, load applicator bar was adjusted, reset to zero in order to measure the vertical displacement of the compacted sample by addition of water as shown in Figure 4.17d. Finally, tap water was used to soak the specimen. By the start of the vertical deformation, a surcharge was added in small increments to prevent the specimen from swelling.

This process continues until the sample ceases to heave. When no further deformation (less than 0.05) was observed for several hours, the experiment was completed, and the total stress applied to prevent sample for swelling is called swelling stress.

$$P_s = \left( \frac{(\sum_{i=1}^n M_i) \times g \times b_r}{\frac{\pi \times \phi^2}{4}} \right) / 1000 \quad (4.13)$$

Where:

$P_s$  = swelling stress , (kPa),

$\sum_{i=1}^n M_i$  = total surcharge in , (kg),

$g$  = gravity in , ( 9.81 m/s<sup>2</sup>),

$b_r$  = beam ratio , (m),

$n$  = number of surcharge, and

$\phi$  = internal diameter of the consolidation ring , (m).

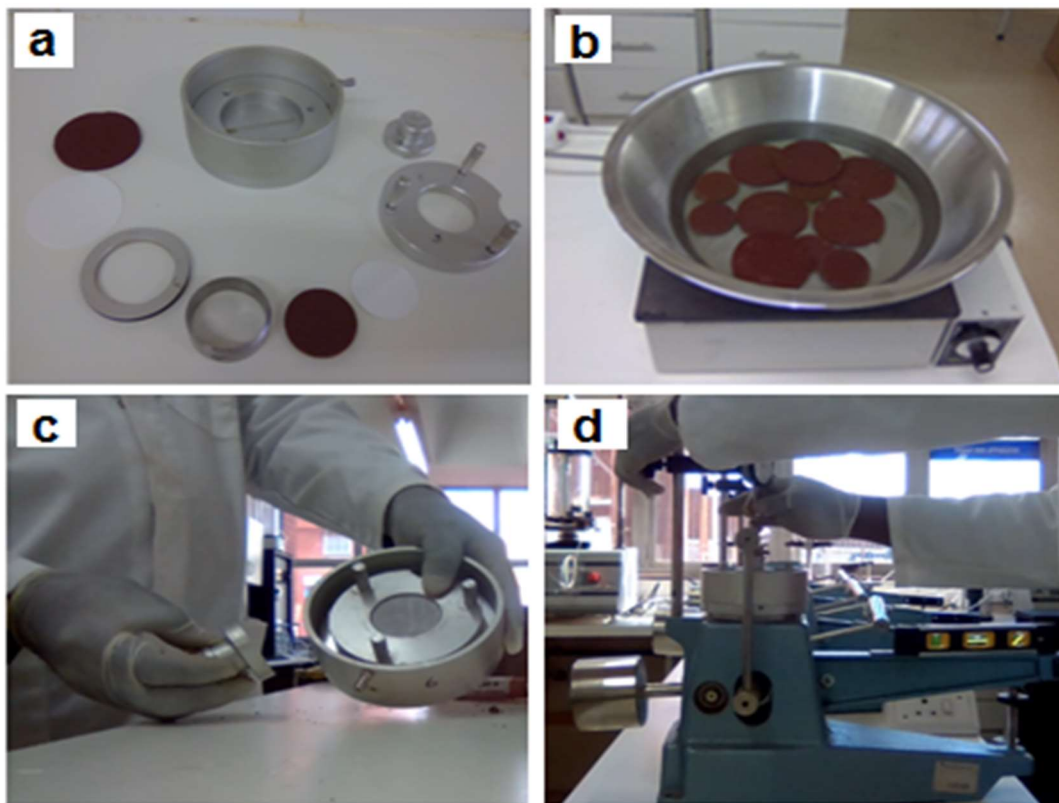


**Figure 4.17:** (a) consolidation cell, (b) saturation of porous stone, (c) assembled consolidation cell, (d) set up of oedometer for swelling stress measurement.



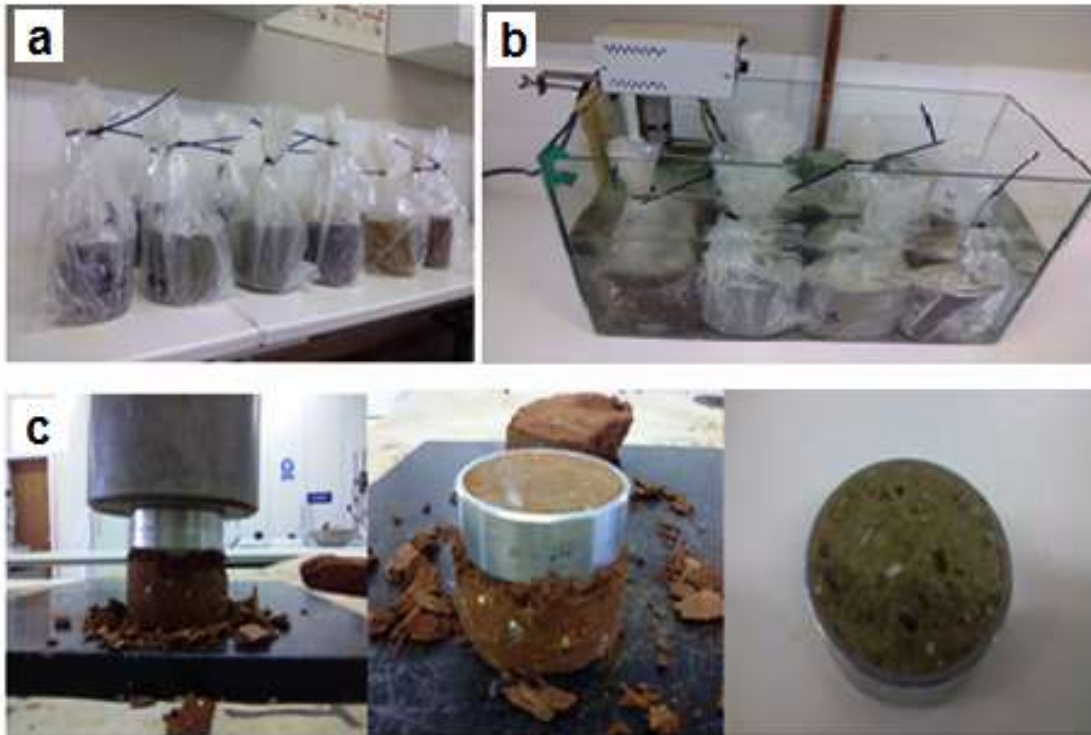


**Figure 4.18:** (a) compacted specimens wrapped in airtight plastic bag (b) specimens kept in constant temperature bath (c) compacted specimens inserts inside a consolidation ring using a jack.



**Figure 4.19:** A view of a conventional consolidometer setup

### 4.7 Soil suction measurement

Suction estimation is challenging both in the laboratory and in the field. Numerous instruments that can be utilized for this aim have been developed with recent technological advancements. Nonetheless, there are still limitations regarding reliability, cost, suction range, availability, the scope of activity and suitability for use within either field or laboratory settings. Suction estimation can be divided into two general categories, the direct and indirect techniques. Based on the above-mentioned, filter paper approach was chosen as the primary method to estimate soil suction. A summary of suction measurement methods is shown in Table 4.4.

**Table 4.4:** Summary of suction measurement methods

		Method / Technique	Suction Range (kPa)	Equilibrium time	Laboratory (L) or field application (F)	
Direct method	Matric suction	Tensiometer	0 - 1500	Minutes	L & F	
		Suction Probe				
Indirect Method	Matric suction	Electrical conductivity sensor	50 - 1500	6-50 hours	L & F	
		Thermal conductivity sensor	0 - 1500	Hours-day	L & F	
		In - contact filter paper	All	7-14 days	L & F	
		Time Domain Reflectometry (TDR)	0 - 1500	Hours	L & F	
	Total suction	Osmotic suction	Squeezing technique	0 - 1500	days	L
			Thermocouple Psychrometer	0 - 1500	1 Hours	L & F
			Transistor Psychrometer	100 - 8000	Hours-day	L
			Chilled - mirror hygrometer	150 - 30000	10 minutes	L
			Non - contact filter paper	All	7- 14 days	L & F

The filter paper method (FPM) is probably the simplest technique to determine the soil suction for the full range of interest for vapour transport, fluid and other geotechnical applications (Houston et al., 1994). The filter paper method is an indirect procedure to determine the soil suction by measuring the filter paper water content at equilibrium that is related to soil suction through a predetermined suction calibration curve. In this study, the suction measurement was performed using Whatman No 42 type filter paper (Ashless circles 70 mm diameter, Cat No1442-070).

#### 4.7.1 Filter paper calibration process

Two technicians perform the moisture content estimation for the filter paper in order to reduce the time of exposure of the filter paper in the laboratory environment and keep to a minimum the moisture gain/lost during measurement. All the items to be used are carefully cleaned. Tweezers and latex gloves are used to handle the materials during all the calibration steps. Filter papers and moisture tins are never touched with bared hands. The filter paper calibration curve is developed using a salt solution as an osmotic potential source for suction above 2.5 pF. The calibration procedure used in this research project is as follows:

- a) NaCl solutions are prepared from 0 to 2.7 molality. The molality is defined as the number of moles of NaCl in 1000ml of distilled water. For example, one mole of NaCl is 58.4428 g. Hence, 2 molality NaCl means 2 times 58.4428 g or 116.8856 g NaCl in 1000ml distilled water. Table 4.5 gives the NaCl weight at various suction values.

**Table 4.5:** Total suction of NaCl at 20°C (Lang, 1967)

NaCl	Suction		NaCl	Suction	
molality	(kPa)	pF*	molality	(kPa)	pF*
0.002	9.8	1.991	0.4	1791	4.253
0.005	24.2	2.384	0.5	2241	4.350
0.01	48	2.681	0.7	3151	4.498
0.02	95	2.978	0.9	4102	4.613
0.05	230	3.362	1.2	5507	4.741
0.1	454	3.657	1.7	8000	4.903
0.2	900	3.954	2.2	10695	5.029
0.3	1344	4.128	2.7	13641	5.134
*pF= 1+ Log(kPa)					

- b) A 300 ml glass jar is filled up with about 200 ml of a solution of known molality of NaCl and the glass jar is labeled with the solution molality used for the jar.
- c) Then, plastic support is put into the glass jar. The sketch of the setup is presented in Figure 4.20.
- d) Two filter papers are put on the top of plastic support in order to double check the accuracy in the scale readings. If one filter paper is accidentally dropped, the other filter is utilized. The lid of the glass jar must be airtight; if not plastic tape can be utilized to seal the glass jar.

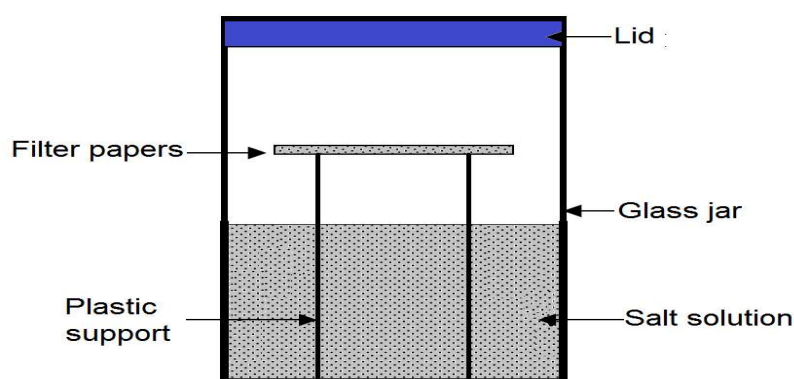


**Figure 4.20:** Total suction calibration test sketch

- e) Step b. and d. are repeated for each different NaCl concentration. The prepared containers are inserted into plastic bags for extra protection. Then, the glass jar is kept inside a controlled temperature apparatus. The equilibrium period was 4 weeks.

After the equilibrium is attained, the moisture content evaluation in the filter paper is conducted as follows:

- a) Prior to take the measurements, all the items related to the calibration procedure are cleaned, and the gloves are used throughout the procedure. Prior to take out the glass jar from the controlled temperature apparatus, all moisture tins to be used for moisture content estimation are weighed to the nearest 0.0001g accuracy and the filter paper water content is recorded on a data sheet.
- b) Then, all the measurements are performed by two technicians. During the time that one technician is opening the sealed glass jar, while the other

technician is inserting the filter paper into the moisture tin rapidly (commonly under 5 seconds) using the tweezers.

- c) After that, the mass of each moisture tin with the wet filter paper are recorded with the moisture tin labels and if it is the bottom or the top filter paper.
- d) Then, all moisture tins are placed into the oven and kept at a  $105 \pm 5 \text{ }^\circ\text{C}$  temperature for 24 hours with the lids half-close to allow evaporation.
- e) Moisture tins are closed with lids and allowed to equilibrate for 5 minutes in the oven, prior to weight measurements on the dried filter papers. The moisture tin is removed from the oven and put on a metal block used as a heat sink to cool them for about 20 seconds. Then, the moisture tin with the filter paper inside is weighed again quickly. The dry filter paper is taken from the tin, and the cold tin is weighed in a few seconds. All the values are recorded on the data sheet.
- f) Step (e) is for every moisture tin.

The calibration curve of moisture content versus the corresponding suction values of the filter paper is obtained from this calibration process. The calibration curve of the filter paper is obtained when the suction value in pF or Log (kPa) units are represented with the corresponding moisture content. The type of calibration curves shown in Figure 4.21 can also be adopted using Whatman No 42 type papers; Schleicher & Schuell No 589 White Ribbon as given by ASTM D 5298.

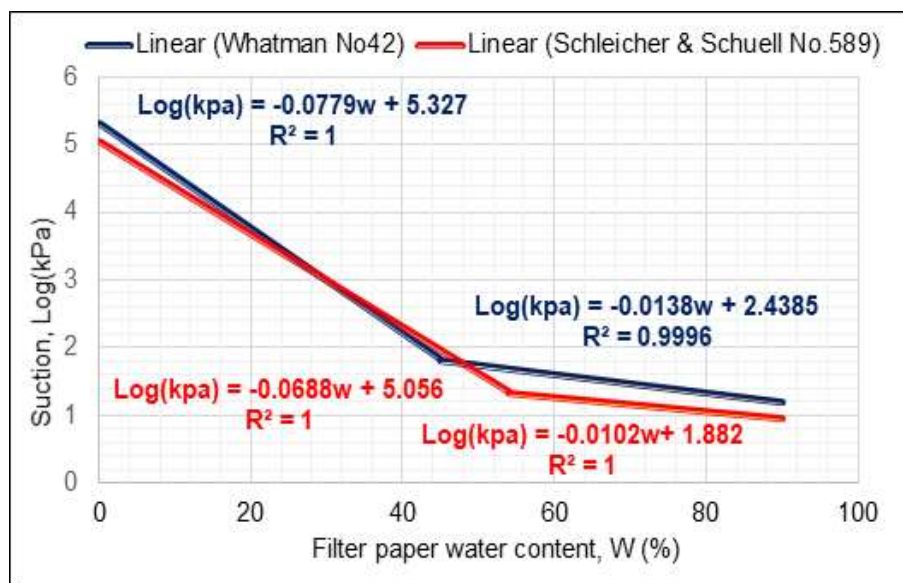


**Figure 4.21:** Filter papers calibration curves (ASTM D5298)



### Filter paper calibration in the laboratory

A glass jar with airtight lid, a top filter paper, and a bottom filter paper were used as shown in Figure 4.22. The glass jar was filled with known molality salt solution for filter paper calibration process as shown in Figure 4.22. Cylindrical plastic support, which acts as a bearer of the filter paper was plunged inside the salt solution as shown in Figure 4.23, and the glass jar air-tightened lid as shown in Figure 4.23. After the equilibrium is achieved, the moisture content of the filter papers was measured in the order of 0.0001g. The calibration curve was built up using the filter paper moisture contents and the suction values.

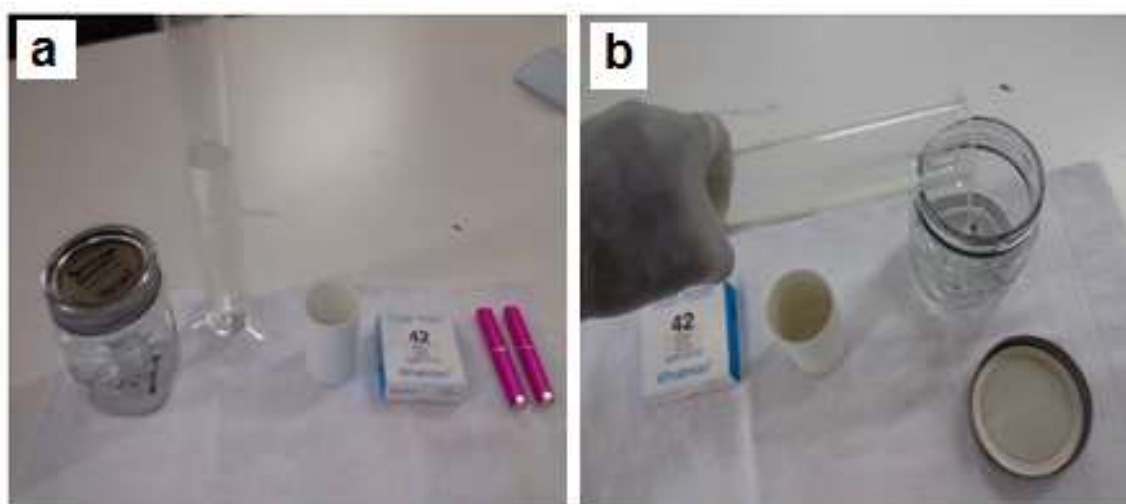


**Figure 4.22:** (a) Glass jar, salt solution, plastic support, filter paper, and tweezers. (b) A glass jar filled with salt solution.

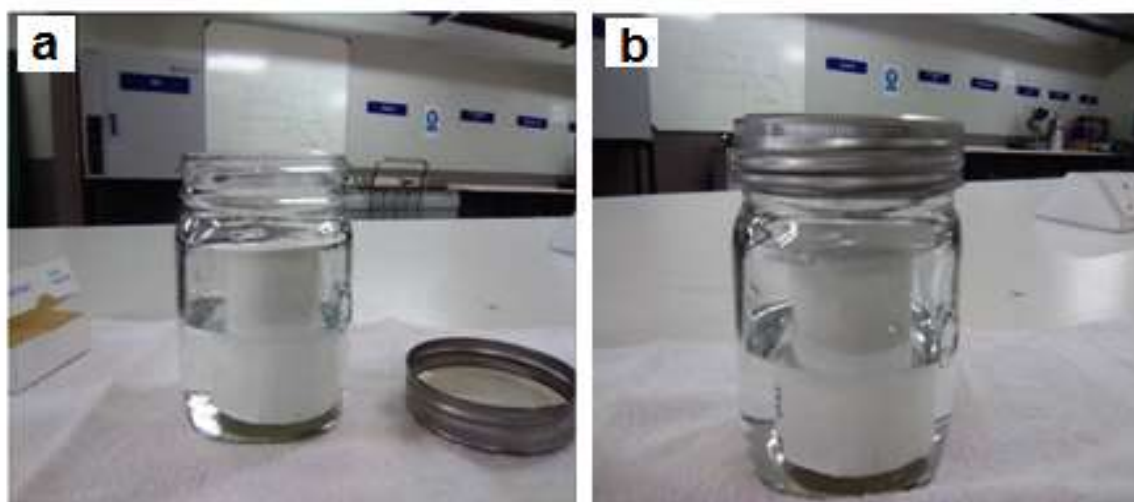


**Figure 4.23:** (a) Plastic support hold filter papers; (b) glass jar closes tightly.

#### 4.7.2 Indirect measurement of suction using filter paper

Apparatus for calibration procedure and for suction estimation:

- a) Whatman No 42 type filter paper was used to perform the test. The results of the test conducted by Sibley and Williams (1990) suggested that Whatman No.42 filter paper was the most suitable for use over a full range of suction assessed (Leong et al., 2002).
- b) Sealed containers; 250 ml glass jars with lids.
- c) Moisture tins with lids used to carry filter paper during moisture content determination.
- d) Salt solution; sodium chloride (NaCl) solutions in a range within 0 (i.e; distilled water) to about 2.7 molality.
- e) Oven for determining the moisture content of the filter papers by leaving them in for 24 hours at  $105 \pm 5^{\circ}\text{C}$  temperature in the aluminum moisture tins (as in the standard test method for water content determination of soil).
- f) A balance with accuracy to the nearest 0.0001 g is used for moisture content evaluation.
- g) A metal block is used as a heat sink to cool aluminum moisture tins for about 20 seconds after removing them from the oven.
- h) A temperature room in which the temperature fluctuations are kept below  $\pm 1^{\circ}\text{C}$  is used for the equilibrium period.

Moreover, latex gloves, tweezers, plastic tapes, plastic bags, scissors, and a knife are used to set up the test.

#### Total suction evaluation

- a) About 75 percent volume of a glass jar is filled up with the soil specimen; more the remaining empty space is smaller, the time required for the filter paper to reach equilibrium is significantly reduced.
- b) Ring support (1.5 to 2.5 cm depth) is put on top of the soil to make a non-contact system between the filter paper and the soil sample.
- c) Two filter papers are put on the plastic ring support using tweezers. The filter papers must not be in contact with the soil, the lid, and the inside wall of the glass jar in any case.

- d) After, the glass jar is sealed with an airtight lid. In the case whereby the lid is not airtight type, used a plastic tape to seal the lid.
- e) The steps a; b; c and d are repeated for each soil specimen.
- f) Then the glass jar is put into temperature regulatory apparatus for equilibrium.

A typical setup for both total suction and matric suction evaluation is sketched in Figures 4.24 and 4.25.

The minimum equilibrium period is at least one week. Once the equilibrium time is terminated, the process for filter paper moisture content estimation is as follows:

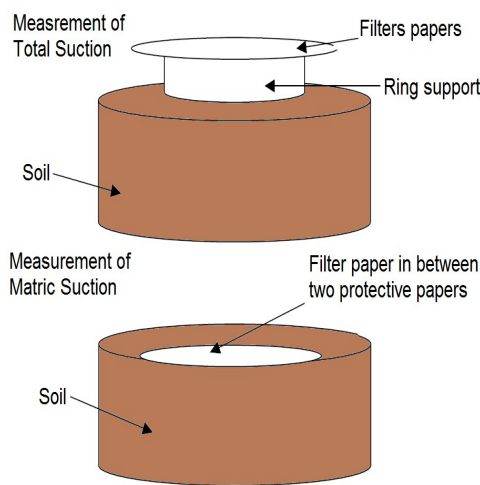


**Figure 4.24:** Non-contact and contact filter paper technique for measuring the total and matric suction (1<sup>st</sup> Step)

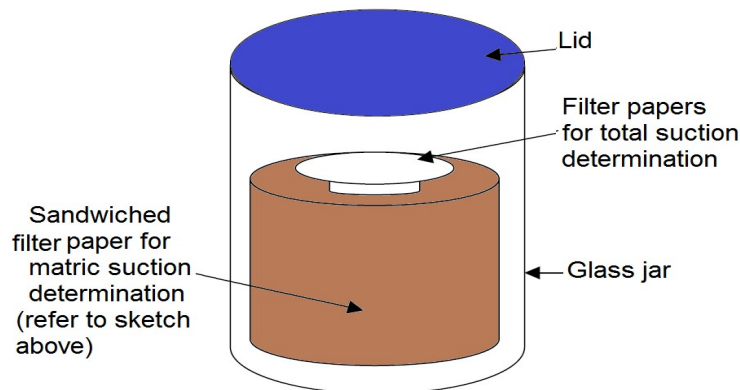


**Figure 4.25:** Non-contact and contact filter paper technique for measuring the total and matric suction (2<sup>nd</sup> Step)

- a) All the items used for soil suction estimation process must be cleaned, before taking measurements and latex gloves are used during the procedure. All the moisture tins used for water content measurement are



- weighed to the nearest 0.0001 g precision and recorded on a data sheet, prior to remove the glass jar from temperature regulatory apparatus.
- b) Then, all estimations are performed by two technicians. For example, while one technician is opening the sealed glass jar, the other technician is putting the filter paper into the moisture tin rapidly (i.e. few second, usually less than 5 seconds) by mean of tweezers.
  - c) After that, the mass of each moisture tins with filters paper inside is taken rapidly. The mass of moisture tins and wet filter papers are recorded with the corresponding moisture tin label (numbers and whether the top or bottom filter paper is inside)
  - d) Step (c) is followed for every glass jar. After that, all moisture tins are put into the oven with the lids half - close to allow evaporation. All filter papers are kept in the oven at  $105 \pm 5^{\circ}\text{C}$  temperature for 24 hours.
  - e) Moisture tins are closed with their lids to permit equilibrium for 5 minutes in the oven prior to undertake the measurements on the dried filter papers. After moisture tin is removed from the oven and put on a metal block for about 20 seconds to cool down. Then, the moisture tin with dry filter paper inside is weighed again quickly. The dry filter paper is taken from the can, and the cold can be weighed within a few seconds. Lastly, all the masses are booked on the data sheet.
  - f) Step (e) is repeated for every moisture tin.

### **Matric suction evaluation**

- a) The filter paper is inserted between two bigger sizes of protective filter papers. The filter papers used in suction estimation are 70 mm diameter, so either the filter paper is cut to a smaller diameter and inserted between two 70 mm papers or bigger diameter ( bigger than 70 mm) filter paper are used a protective filter paper.
- b) After that, these filter papers are inserted into the soil sample, which can fill the glass jar, in a proper contact manner. Adequate contact between the soil specimen and the filter paper is very relevant.

- c) Then, the soil specimen with the embedded filter papers is inserted into the glass jar container.
- d) The glass jar is sealed with an airtight lid, in case the lid is not airtight one, electrical tape can be used to seal up the lid.
- e) Step a; b; c; and d. are repeated for every soil specimen.
- f) The prepared glass jars are put in a temperature regulatory apparatus for equilibrium.

Once the equilibrium period is achieved, the process of the filter paper moisture content is conducted as follows:

- a) Before starting taking measurements, all the items used for suction measurement process are carefully cleaned and gloves are used throughout the procedure. All moisture tins that are used for water content determination are weighed to nearest 0.0001g accuracy before the moisture tins are taken to the temperature regulatory apparatus, and recorded on the measurement data sheet.
- b) Then, two technicians carry out all measurements. For example, while one technician is opening the sealed glass jar, the other technician places the filter paper into the aluminum can be using tweezers very quickly.
- c) After that, the mass of each can with the filter paper inside is taken rapidly. The masses of wet filter paper and moisture tins are recorded with the corresponding moisture tin number.
- d) Step (c) is followed for every glass jar. All moisture tins are put inside the oven with lids half - close to permit evaporation. All are kept at a  $105 \pm 5^{\circ}\text{C}$  temperature for 24 hours inside the oven.
- e) Moisture tins are closed with their lids and permitted to equilibrate for 5 minutes in the oven, prior for undertaking the measurements on the dried filter papers. After that, the moisture tin is removed from the oven and put on a metal block for about 20 seconds to cool down. Then, the moisture can with dry filter paper inside is weighed again very quickly. The dry filter paper

is removed from the moisture can, and the cold moisture is weighed in a few seconds. Lastly, all the masses are booked on a data sheet.

f) Step (e) is repeated for every moisture tin.

After obtaining moisture content from all filter paper a suitable calibration curve is used to determine the matric suction values in Log (kPa) or pF of the soil specimens.

Filter paper technique is a reliable method that can be used with suctions from 80 kPa to in excess of 6000 kPa a much larger than any other single technique (Chandler and Guitierrez, 1986)

### Equilibration period for filter paper approach

Equilibration period for filter paper approach from (Leong et al., 2002) is shown in Table 4.6

**Table 4.6:** Equilibration time for filter paper method (Leong et al., 2002)

References	Equilibration Time	Filter Paper Method
Fawcett and Collis-Georges (1967)	6-7 days	Contact
McQueen and Miller(1968b)	7 days	Contact
Al-Khafaf and Hanks(1974)	2 days	Contact and uncertain contact
Hamblin (1981)	Minutes-36 days	Contact
Chandler and Gutierrez (1986)	5 days	Contact
Duran (1986)	7 days	Noncontact
Greacen et al. (1987)	7 days	Contact
Sibley and Williams (1990)	3 days	Contact
	10 days	Noncontact
Lee and wray (1992)	14 days	Contact and noncontact
Houston et al. (1994)	7 days	Contact and noncontact
Harrison and Blight (1998)	7-10 days	Wetting and noncontact
	21 days	Drying and noncontact
	10 days	Wetting and contact
	25-30 days	Drying and contact

Wet specimens take longer to attain equilibrium, about 7 days. Sample usually achieved equilibrium in 4 days to a 1 % error (Swarbrick, 1995). Nonetheless, several researchers have used different time periods for the equilibrium of the filter paper with the suction of the soil specimen. Usually, 7 days are allowed but at list

5 days are required (Chandler and Guitierrez, 1986). Furthermore, ASTM D5298 suggested an equilibrium period of one week. In addition, several filter paper measurements were conducted by Ling and Toll (2000) shows that within one week the equilibrium is completed to approximately 97%.

### **Total suction & Matric suction measurement on compacted specimens**

Soil suction measurements were performed in the glass jars, which were placed in a temperature regulatory apparatus to keep the temperature fluctuations as low as possible, preferably around  $25 \pm 1$  °C.

Compacted soil specimens were removed from the constant temperature bath as shown in Figure 4.18, and prepared as shown in Figure 4.26 for soil suction measurement. The compacted soil specimens were divided into two cylindrical parts with a diameter of 75 mm and a depth of 35 mm so that the specimen can be placed and removed from the glass jar easily. For each soil specimen, the suctions were measure at several moisture contents on the dry side, on the optimum moisture content, and on the wet side.

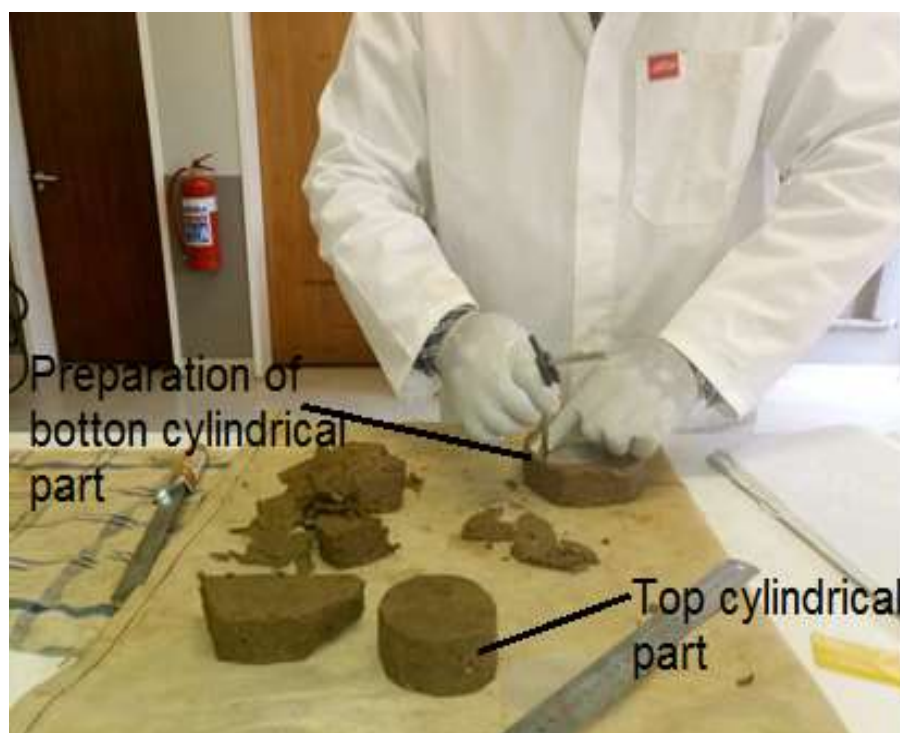


**Figure 4.26:** Preparation of compacted soil specimen for suction measurement.

Three filter papers (two protective and one for measurement with 70 mm radius) placed between these two surfaces by means of tweezers for matric suction measurement Figure 4.27.



**Figure 4.27:** Three filter papers placed for matric suction measurement.

To avoid hysteresis problems, filter papers were oven dried to remove moisture and ensure that the same wetting path is followed in each case to avoid hysteresis phenomenon (Swarbrick, 1995).

After the filter paper has been sandwich between the two surfaces, to protect the filter paper from vapour transfer edges of the compacted soil specimen, an electrical plastic tape was used to protect the filter papers by wrapping tightly as shown in Figure 4.28.

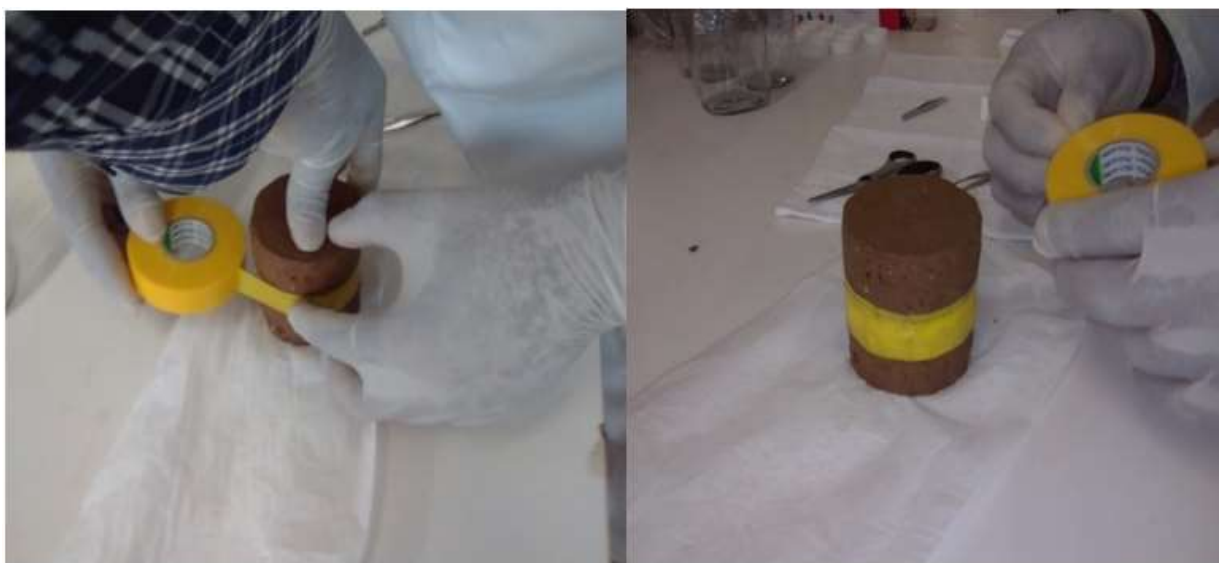


**Figure 4.28:** Edges of the sample sealed with electrical tape.

The wrapped specimen was placed into a glass jar and plastic ring support put on the top of the soil specimen. The filter papers are placed on the ring support for total suction determination, and the glass jar is sealed as shown in Figure 4.29.

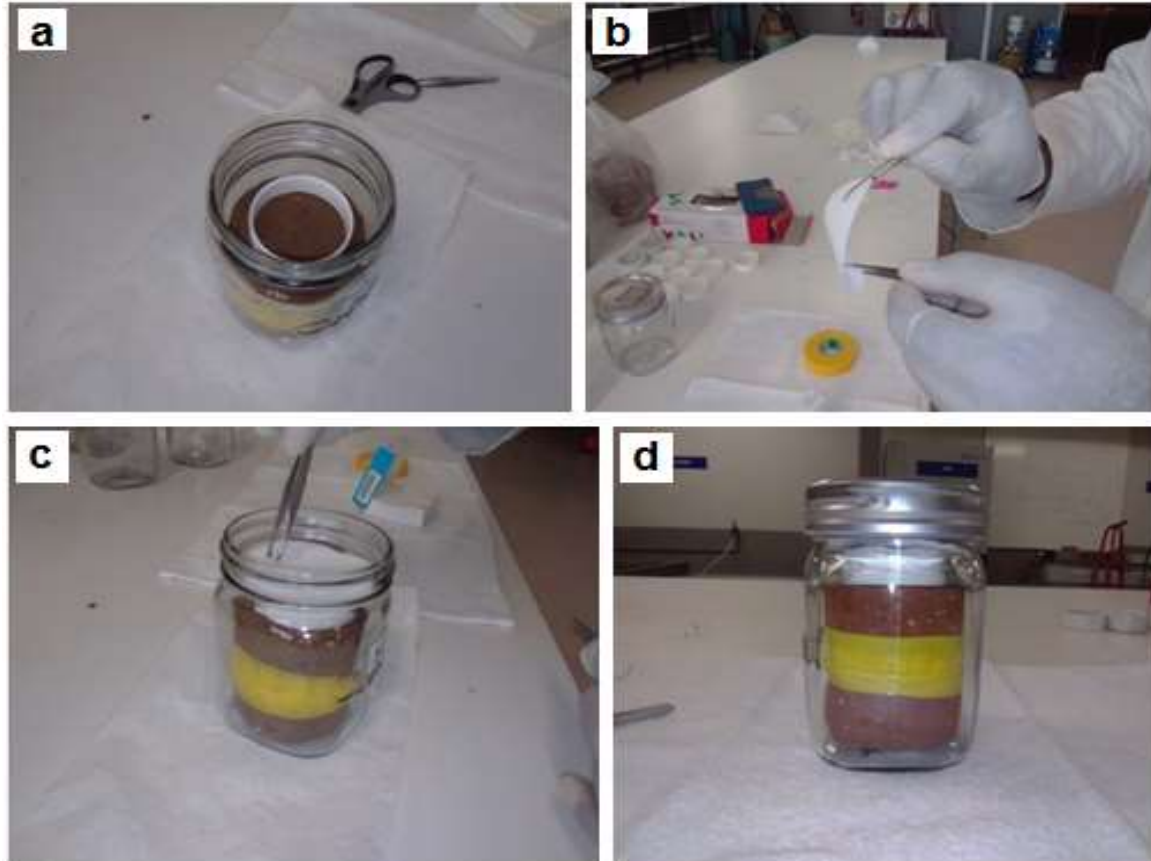


**Figure 4.29:** (a) Plastic ring put on soil sample (b) Filter paper carried using tweezers (c) Filter paper placed over the plastic ring support for total suction measurements (d) Sealed glass jar.



Labeled jars are placed into a temperature regulatory apparatus for an equilibrium period of 4 weeks as shown in Figure 4.30.



**Figure 4.30:** Temperature regulatory apparatus

Once the equilibrium was achieved after 4 weeks, the glass jars were taken out from the temperature regulatory apparatus. Prior to open the glass jar, a moisture tin, which would be used for moisture content, was weighed using a 0.0001g readable balance, and the cold tare mass ( $T_c$ ) recorded as presented in Figure 4.31.



**Figure 4.31:** Moisture tin is weighed before filter papers were taken out from the jar.

Then the glass jar was opened, top and bottom filter papers were taken one after another and placed in a labeled moisture tin quickly by mean of tweezers, the moisture tins were enclosed tightly rapidly to avoid moisture lost as shown in Figure 4.32. Afterward, the mass of the cold tare and the mass of the wet filter paper were recorded as  $M_1$ . The middle filter paper was taken out quickly and put into another labeled moisture tin, and the moisture tins were put into the oven.



**Figure 4.32:** Filter paper put into labeled moisture tine for suction measurement.

After an overnight oven dried of moisture tins, covers were closed and waited in the oven for 5 minutes to allow moisture tins to reach temperature equilibrium as shown in Figure 4.33a. Then, the moisture tins were taken one after another and prior to determine the mass of the moisture tins, they were put over the metal block to cool them rapidly as presented in Figure 4.33b. Cooled moisture tins were weighed in 20 seconds after taking them from the oven and the mass of the dry filter paper, and hot tare mass was recorded as  $M_2$ . In addition, the mass of the hot tare was recorded as  $T_h$ .



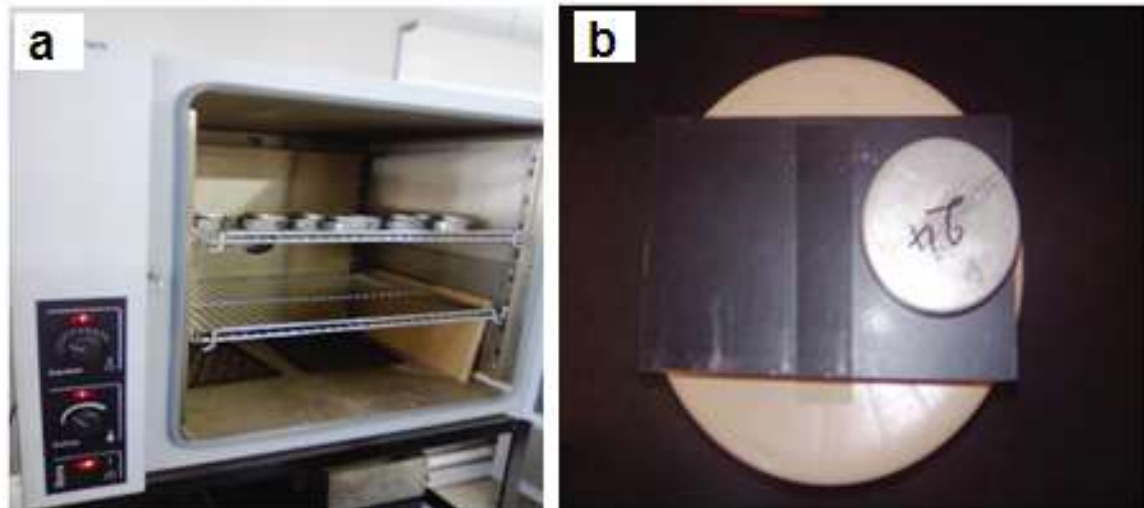


**Figure 4.33:** (a) the oven dried moisture tin (b) moisture tin put on the metal block to cool it down quickly.

The moisture content within the filter paper,  $W_f$ , is used to determine the total suction and the matric suction is computed using Equation 4.14.

$$W_f = \frac{M_w}{M_f} = \frac{m_1 - m_2 - T_c + T_h}{m_2 - T_h} \times 100 \quad (4.14)$$

Where:

$W_f$  = water content of filter paper, (%) ,

$m_1$  = Mass of wet filter paper + cold tare mass, (g),

$m_2$  = Mass of dry filter paper + hot tare mass, (g),

$T_c$  = Cold tare mass, (g),

$T_h$  = Hot tare mass, (g),

$M_w$  = Mass of water in filter paper, (g), and

$M_f$  = Mass of dry filter paper, (g).

After the determination of the water content within the filter paper Whatman No.42 type, the calibrated curve in Equation 5.6 is used to get the suction values. The soil suction measurement using a filter paper test data sheet is shown in Table 5.31 found in Appendix P.

## **4.8 Multiple regression analyses**

### **4.8.1 Introduction**

Regression analysis is one of the most extensively used methods for analyzing multifactor data. It is an efficient tool because it gives an easy method for assessing functional relationships between dependent variables and an independent variables, formulate equations or models that link the dependent variables and one or more independent variables. Nowadays, almost all analysis pertaining to regression analysis is performed using a software. NCSS11 software package is intensively used in this study.

### **4.8.2 Regression analysis process**

The regression analysis process in this study is conducted according to the following steps:

- Formulation of the problem
- Selection of the potentially relevant variables
- Collection of the data
- Model specification
- Choice of the fitting method
- Model fitting
- Model validation

### **4.8.3 Statement of the problem**

The question to be addressed by the multi-regression analysis is to build up models used to predict the swelling stress of compacted expansive soils using data collected from laboratory works. This first step is important because a poorly formulated question can lead to the selection of an irrelevant set of variables, a wrong choice of a model or incorrect method of analysis.

### **4.8.4 Selection of relevant variables**

The investigation carried out in Chapter 3 section 3.4 has revealed that several soil parameters have been used as independent variables to predict the swelling stress. These parameters can be classified into four groups as follows:

- unsaturated soil characteristics (matric suction, SWCC, AEV)
- geotechnical soil index properties (Atterberg limits, shrinkage limit, clay activity, dry density, Initial water content, etc.),
- expansive soil indexes (free swell index, free swell ratio),
- mineralogy characteristic (free swell ratio).

In this research work, the swelling stress is the dependent variable, and the independent variables are as follows: Matric suction, geotechnical index properties, expansive soil indexes.

#### 4.8.5 Data collection

Laboratory experiments were conducted to determine the hydromechanical and physical properties of the soil samples. The collected data consist of the observation of  $n$  specimens; each of the  $n$  observations deals with the measurement of the potentially relevant independent variables. Data are recorded in Table 4.7. A column table represents a variable, whereas a row represents the observations. All the independent variables used in this study are classified as quantitative.

**Table 4.7** Regression analysis data

Observations Number	Dependent variables	Independent variables ( $X_{ij}$ )						
	Swelling Stress $P_{sij}$ log(kPa)	Matric Suction $\Psi_{mij}$ log(kPa)	Initial Dry Density $\gamma_{dij}$ ( $\text{kN} \cdot \text{m}^3$ )	Plasticity Index $I_{Pij}$ (%)	Initial Water Content $W_{ij}$ (%)	Free Swell ratio (FSR) <sub>ij</sub>	Clay activity (Ac) <sub>ij</sub>	... (X) <sub>ij</sub>
1/specimen	$P_{S_{11}}$	$\Psi_{m_{12}}$	$\gamma_{d_{13}}$	$I_{P_{14}}$	$W_{15}$	(FSR) <sub>16</sub>	Ac <sub>17</sub>	... X <sub>1m</sub>
2/specimen	$P_{S_{21}}$	$\Psi_{m_{22}}$	$\gamma_{d_{23}}$	$I_{P_{24}}$	$W_{25}$	(FSR) <sub>26</sub>	Ac <sub>27</sub>	... X <sub>2m</sub>
3/specimen	$P_{S_{31}}$	$\Psi_{m_{32}}$	$\gamma_{d_{33}}$	$I_{P_{34}}$	$W_{35}$	(FSR) <sub>36</sub>	Ac <sub>37</sub>	... X <sub>3m</sub>
4/specimen	$P_{S_{41}}$	$\Psi_{m_{42}}$	$\gamma_{d_{43}}$	$I_{P_{44}}$	$W_{45}$	(FSR) <sub>46</sub>	Ac <sub>47</sub>	... X <sub>4m</sub>
.	.	.	.	.	.	.	.	... .
n/specimen	$P_{S_{n1}}$	$\Psi_{m_{n2}}$	$\gamma_{d_{n3}}$	$I_{P_{n4}}$	$W_{n5}$	(FSR) <sub>n6</sub>	Ac <sub>n7</sub>	... X <sub>nm</sub>

$i = 1, 2, 3, \dots, n$  &  $j = 1, 2, 3, \dots, m$

#### 4.8.6 Model specification

NCSS11 software proposed many models that can be used to build up a relationship between dependent variable and independent variables based on the type of regressions and the conditions.

The hypothesized model is either refuted or validated by the analysis of the data collected from laboratory tests. The model selected is specified only in the form. However, it could also depend on unknown parameters to be determined. The form of the selected function can be linear or non-linear. The terms linear and non-linear in this study does not describe the relationship between the dependent variable and independent variables. It is related to the fact that the regression parameters enter the model linearly or non-linearly.

A multivariate statistical method allows the use of more than one independent variable in order to consider the combined effects of more than one independent variable. Johnson (2005) stated that the prediction model takes the form of Equation 4.15.

$$Y = \beta_0 + \sum_i^m \beta_i \cdot X_i + \varepsilon \dots \dots \dots (4.15)$$

Where:

$\beta_0$  = the intercept,

$\beta_i$  = regression coefficients representing the contribution of the, independent variables  $X_i$ ,

$m$  = the number of the relevant soil parameters, and

$\varepsilon$  = the random error representing the discrepancy in the approximation.

For the curve estimation procedure, regression statistics were performed for different regression models, including linear, logarithmic, inverse, quadratic, cubic, power, compound, growth and exponential models shown in Table 4.8. The correlation coefficient  $R^2$ , the mean square error, MSR, the relative standard deviator, RSD, were investigated to select the best predictive model for swelling stress estimation. The  $R^2$  is computed from the sum of the square of the vertical offsets (the residuals) of the points from the best-fit regression curve. It was found that linear function exhibited the strongest and most relevant choice.

**Table 4.8:** List of variable statistical models and their regression equation

Keyword	Equation	Linear transformation
Linear	$Y = \beta_0 + \beta_1 X$	
Multiple linear	$Y = \beta_0 + \beta_1 X_1 + \beta_2 X_2 + \dots + \beta_n X_n$	
Logarithmic	$Y = \beta_0 + \beta_1 \ln(X)$	
Inverse	$Y = \beta_0 + \beta_1 / X$	
Quadratic	$Y = \beta_0 + \beta_1 X + \beta_2 X^2$	
Cubic	$Y = \beta_0 + \beta_1 X + \beta_2 X^2 + \beta_3 X^3$	
Compound	$Y = \beta_0 \beta_1^X$	$\ln(Y) = \ln(\beta_0) + X \ln(\beta_1)$
Power	$Y = \beta_0 X^{\beta_1}$	$\ln(Y) = \ln(\beta_0) + \beta_1 \ln(X)$
Exponential	$Y = \beta_0 e^{\beta_1 X}$	$\ln(Y) = \ln(\beta_0) + \beta_1 X$
Growth	$Y = e^{\beta_0 + \beta_1 X}$	$\ln(Y) = \beta_0 + \beta_1 X$
Where $\beta_0 = a$ constant, $\beta_n =$ regression coefficient, $X_n =$ independent variable, and $\ln =$ natural logarithm.		

#### 4.8.7 Model fitting

The following step in this analysis is to calculate the parameters of the multi-regression analysis, or using the method of estimation to fit the model to data obtained from the experiment. The prediction of the dependent variables conducted in the manner that the set of the independent variables values are not far outside the range of our data collected from several laboratory tests.

#### 4.8.8 Model validation

The validity of this multiple regression analysis depends on the assumptions about the data and the model because the accuracy of the analysis and the conclusion derived from our analysis depends crucially on the validity of the assumption. As mentioned before, a relevant and comprehensive literature investigation has been conducted to identify the soil parameters that influence the swelling stress of compacted unsaturated expansive soils. Concerning the model, since we are dealing with several independent variables, several models are analyzed using NCSS11. Then after, a suitable and efficient model was selected according to the coefficient of correlation  $R^2 \geq 0.8$ , relative standard deviator  $RSD \leq 3 \%$ , and mean square error  $MSR = 0$ . The validation of the proposed models is done by comparing the value obtained from the experiments to the predicted values given by the proposed models. Furthermore, by comparing the results obtained from the proposed models and the values obtained from other models.

In this research work, multiple regression analyses are used to diagnose, validate, and even modify the inputs. The process is repeated until a satisfactory result is obtained. A satisfactory output is an estimated model that satisfies the assumptions and fits the data reasonably well.

---

## CHAPTER 5: ADVANCED TESTING AND ANALYSIS

### 5.1 Introduction

In this study, several laboratory tests which include particle size distribution, Atterberg limits, linear shrinkage, X-ray diffraction (XRD), specific gravity, free swell index, free swell ratio, modified Proctor compaction test, soil suction measurement using filter paper technique, zero swelling test (ZST), and the soil water characteristic curve (SWCC) were performed. In order to characterize the swelling stress of compacted expansive soils, correlations between the swelling stress and other soil parameters were established. Moreover, models to predict the swelling stress of compacted expansive soils were developed. The laboratory tests procedures were described in Chapter 4. In order to reduce discrepancies and obtain reliable results, all experiments were replicated three times. As the results were close, the average values are submitted as a final result.

In this chapter, laboratory tests results are analyzed, discussed, presented in a form of graphs, figures, and summarized in tables.

Secondly, the analysis and discussion of correlations between swelling stress and other soil properties such as unsaturated soil characteristics (matric suction, SWCC), geotechnical index properties (plasticity index, liquid limit, initial water content, initial dry density, linear shrinkage, activity of clay, clay fraction), expansive soil characteristics (free swell index, free swell ratio).

Thirdly, predictive models to estimate the swelling stress of compacted expansive soils were obtained from laboratory data. Models were developed by multi-regression analysis using software NCSS11.

The validation of the proposed models is achieved by comparing the predicted values to values obtained from experimental works. Furthermore, predicted values are compared to results obtained from other models.

### 5.2 Soil characteristic properties

Standard laboratory experiments were conducted in this research to obtain the physical and hydromechanical properties of soils.

#### 5.2.1 Grain size classification analysis

Particle size analysis test was performed on soils WKS, WBS, BLS, PTS, and BTS in accordance with ASTM D6913 for sieve analysis, and ATSM D7928 for



hydrometer analysis. Particle size analysis of the fine fraction (< 0.075 mm) of the soils was estimated by sedimentation technique. The results of grain size distribution are given in Figures 5.1, 5.2a, and 5.2b. Furthermore, the results of grain size distribution are summarized in Table 5.1 found in appendix A.

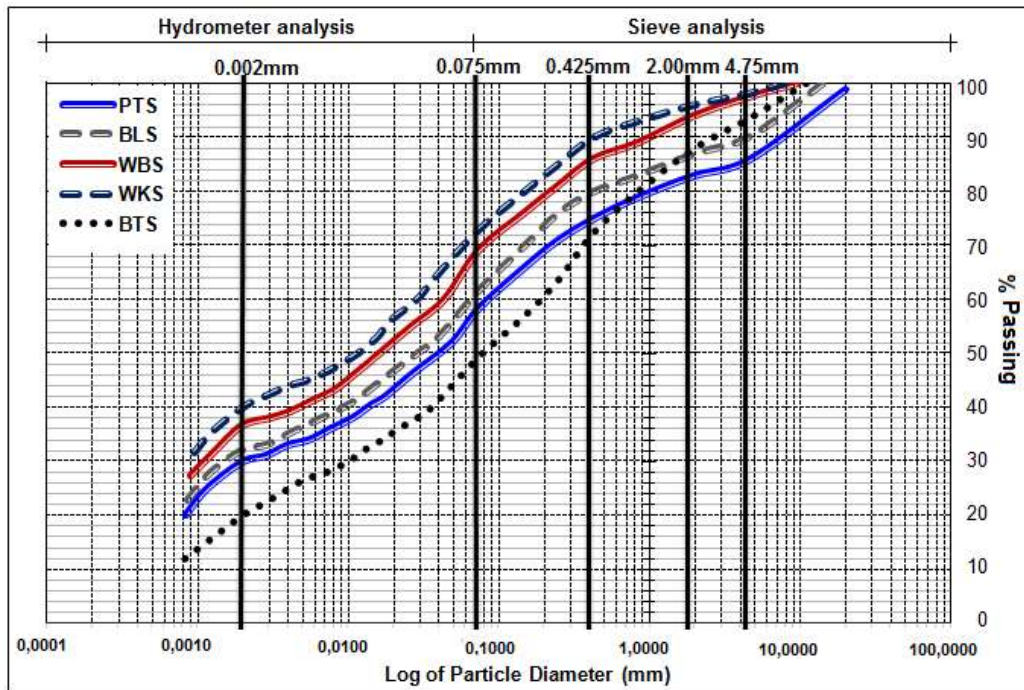


**Figure 5.1:** Grain size distribution curve

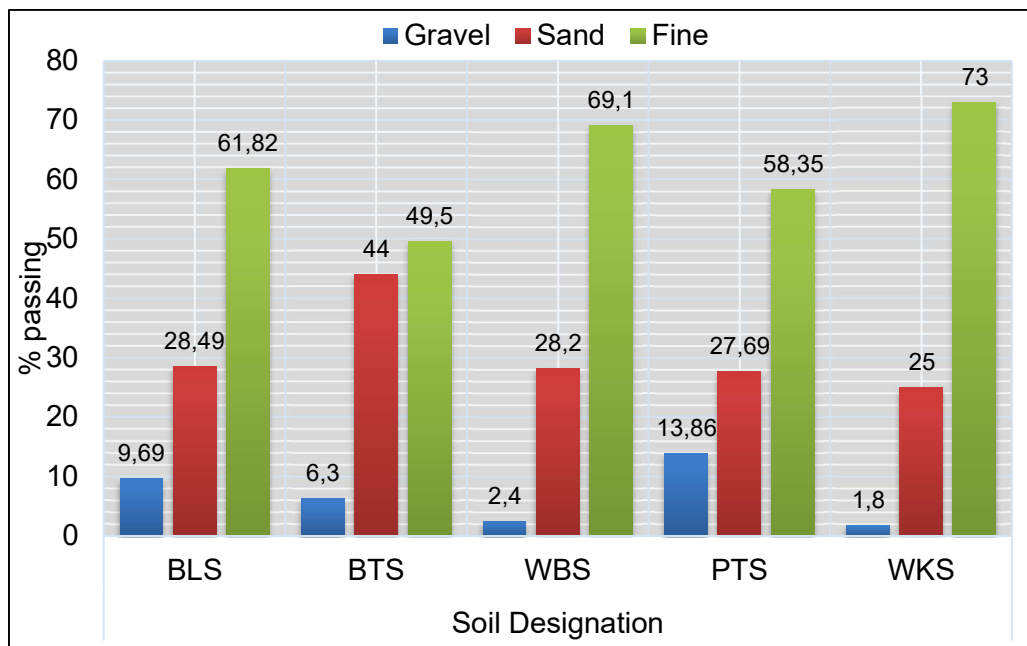


**Figure 5.2a:** Chart-grain size distribution



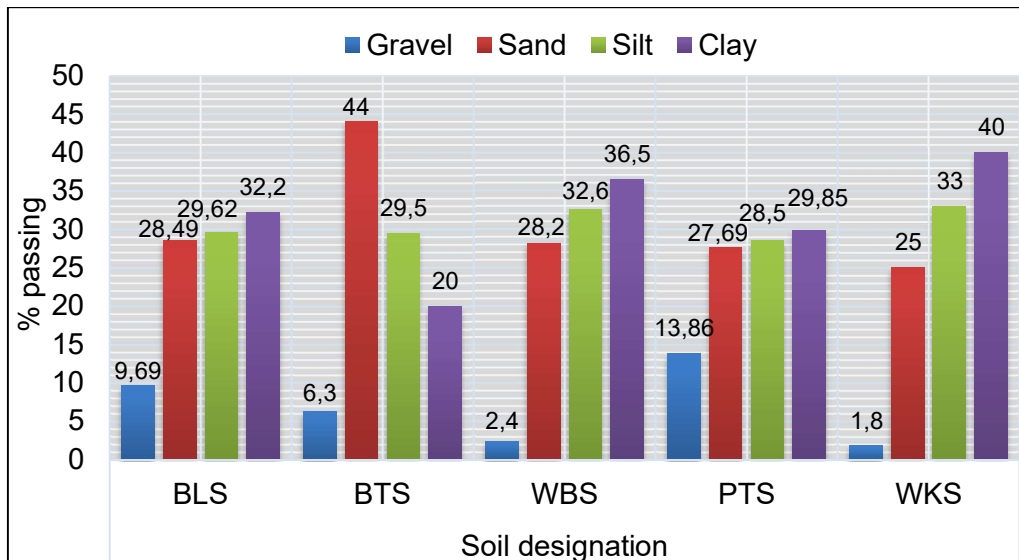


**Figure 5.2b:** Chart-grain size distribution

### 5.2.2 Unified soil classification system

In accordance with ASTM D2487, coarse-grained are classified base on their grain size distribution, and fine-grained soils are classified base on their plasticity. Atterberg limits were determined according to ASTM D4318. Atterberg limits results are presented in Table 5.2 found in Appendix A. WKS displays higher plasticity index, and BTS smaller plasticity index. This can be explained by the amount of fine in the soil. WKS contained a higher amount of fine estimated at 73%, and BTS the smaller amount of fine 49.5 %. Casagrande liquid limit test charts are presented on Figures 5.5 to 5.9 found in Appendix A, B, C respectively for soils BLS, BTS, WBS, PTS, and WKS. The results of Casagrande’s plasticity chart are shown in Figures 5.3; 5.4, and 5.10.

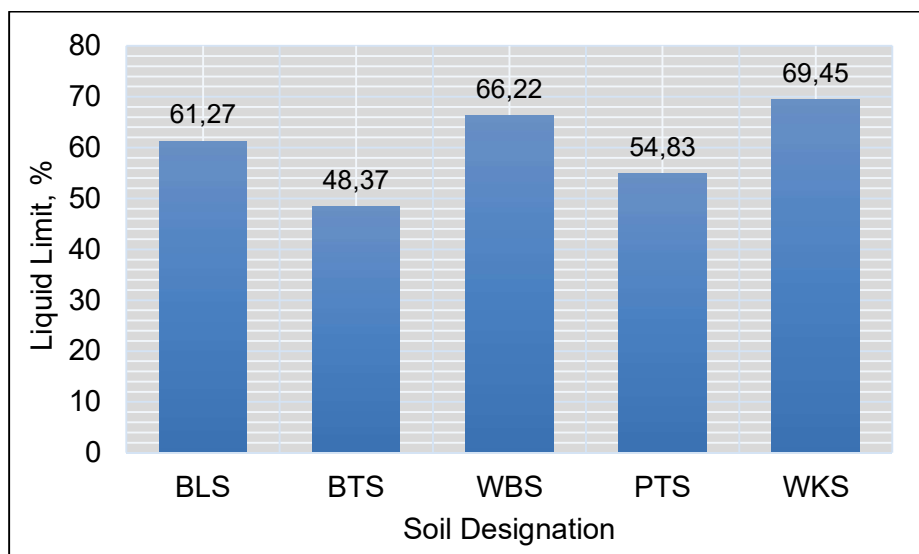


**Figure 5.3:** Liquid limit versus soil designation.

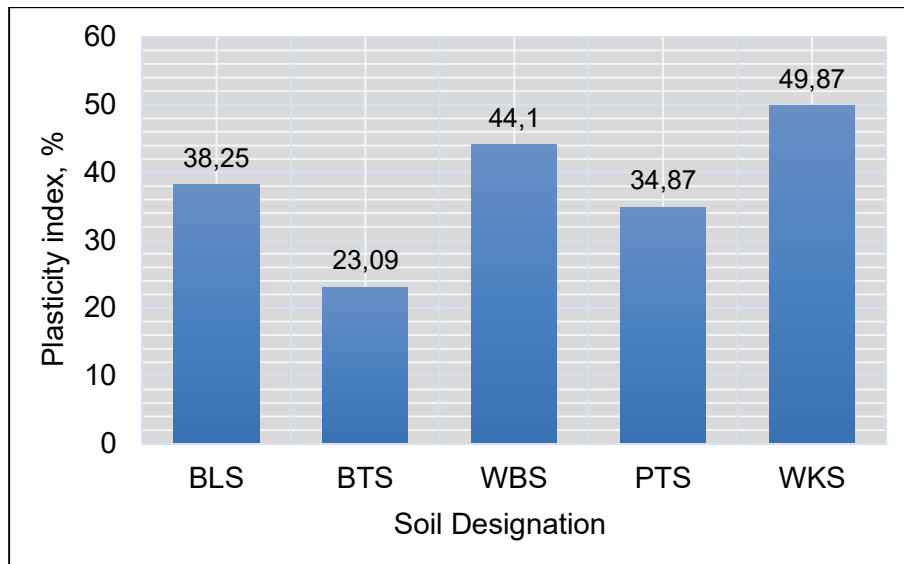


**Figure 5.4:** Plasticity index versus soil designation

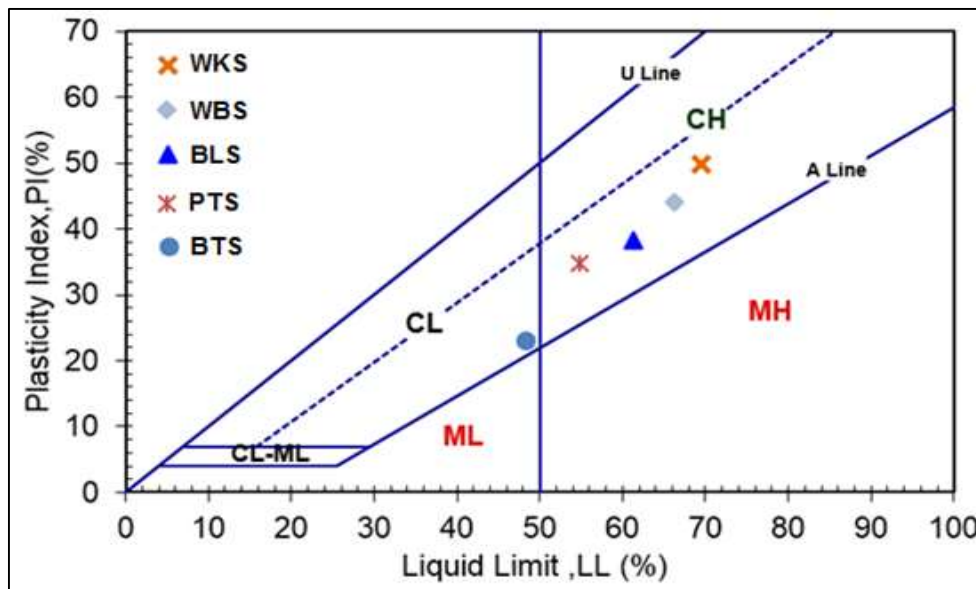


**Figure 5.10:** Casagrande's plasticity chart

### 5.2.3 Linear shrinkage

The linear shrinkage was determined in accordance with TMH1-Method A4 standard. The final results of linear shrinkage test are given in Table 5.3 found in Appendix C. According to the results, BTS soil displays a higher linear shrinkage value estimated at 13.89 % and a lower swell potential. The linear shrinkage of soils WKS and WBS are respectively 6.12 % and 7.14 %, with high swell potential. Soils PTS and BLS, have respectively a linear shrinkage of 12.06 % and 8.96 %, with moderated swell potential. In the other hand, we observed that BTS which exhibits a higher linear shrinkage contained a smallest quantity of clay estimated

at 20 %, while WKS exhibits a smaller linear shrinkage, and displays a clay content estimated at 40 %. In consequence, the clay content within expansive soil influences the linear shrinkage value of the soil, as the quantity of clay within the soil reduces, the linear shrinkage value increases and vice versa. The result of linear shrinkage test is presented in Figure 5.11.

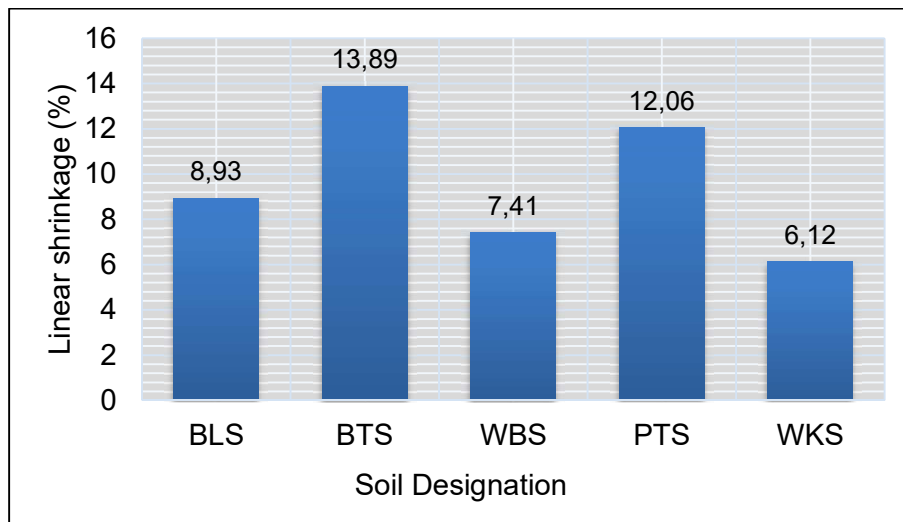


**Figure 5.11:** Linear shrinkage of soil designation.

#### 5.2.4 Specific Gravity

The specific gravity ( $G_s$ ) of a soil is the ratio of density or specific weight of the soil particles to the density or unit weight of water. The specific gravity was determined using density bottle (pycnometer) according to ASTM D854. Three different tests were conducted on each specimen and the mean value submitted as a final result. The specific gravity data sheet is given in Table 5.4 found in Appendix C. The specific gravity values were found to be 2.68, 2.63, 2.76, 2.66, and 2.70 respectively for BLS, BTS, WBS, PTS, and WKS. The results are shown in Figure 5.12.

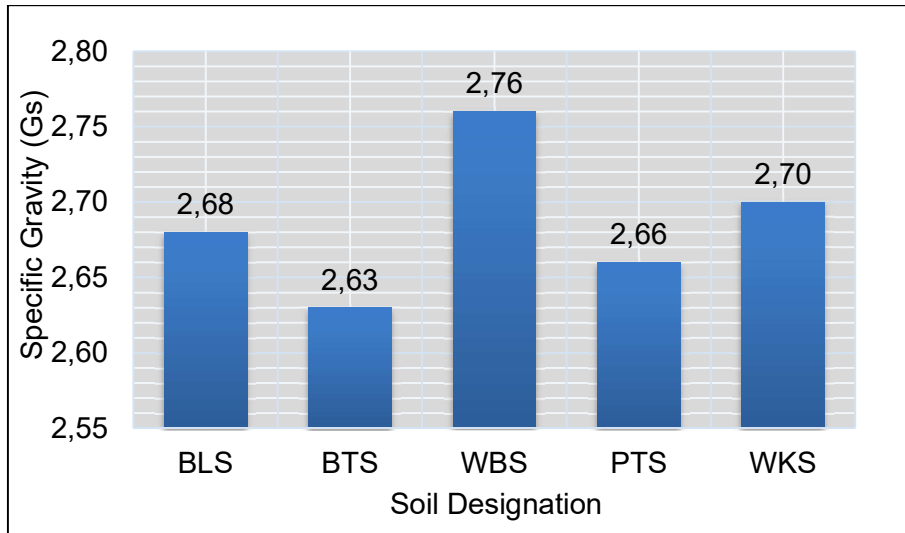


**Figure 5.12:** Specific gravity of soil designation.

### 5.2.5 Activity of clay

The activity of clay is a ratio of plasticity index to the percentage of clay sample within the soil. The soil activity test results are shown in Figure 5.13.

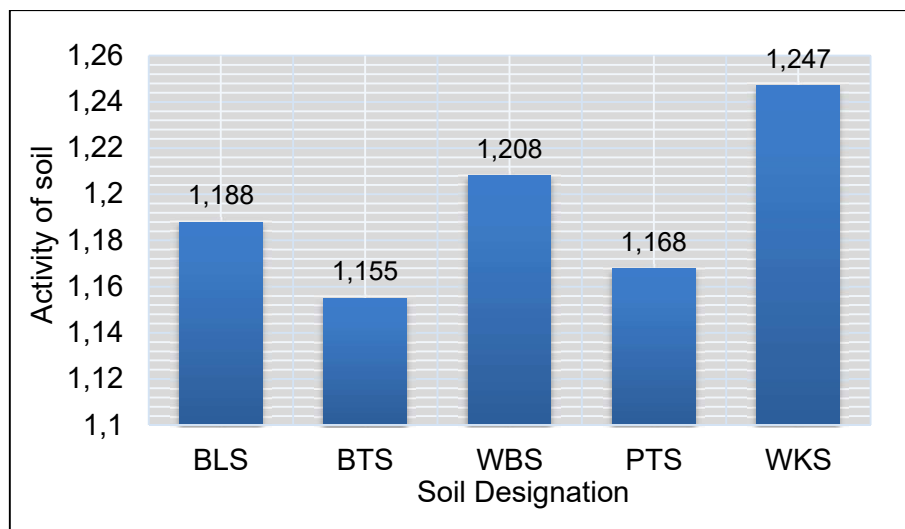


**Figure 5.13:** Activity of soil designation.

### 5.2.6 Free swell index results analysis

The free swell index test was performed in accordance with BIS, 1.1977. The reading after 24 hours of the two volumes  $V_k$  (kerosene), and  $V_d$  (distilled water) on a glass cylinder as shown in Figure 4.10 in Chapter 4 was recorded in Table 5.5 found in Appendix D, the results are shown in Figure 5.14. According to the results, WKS exhibits a high potential of expansiveness with a free swell index estimated at 116 %, whereas BTS exhibits a low potential of expansiveness with a free swell index estimated at 42.85 %. The other soil samples PTS, BLS, WBS

displays a moderate swelling potential with a free swell index estimated respectively at 57.14 %, 66.66 %, and 84.66 %. According to the results, Free State province soils are potentially expansive over the areas of study. Nonetheless, the potential of expansiveness changes significantly from one location to another due to the variability of the soil material. The soil classification based on the free swell index is given in Table 5.6 found in Appendix D.

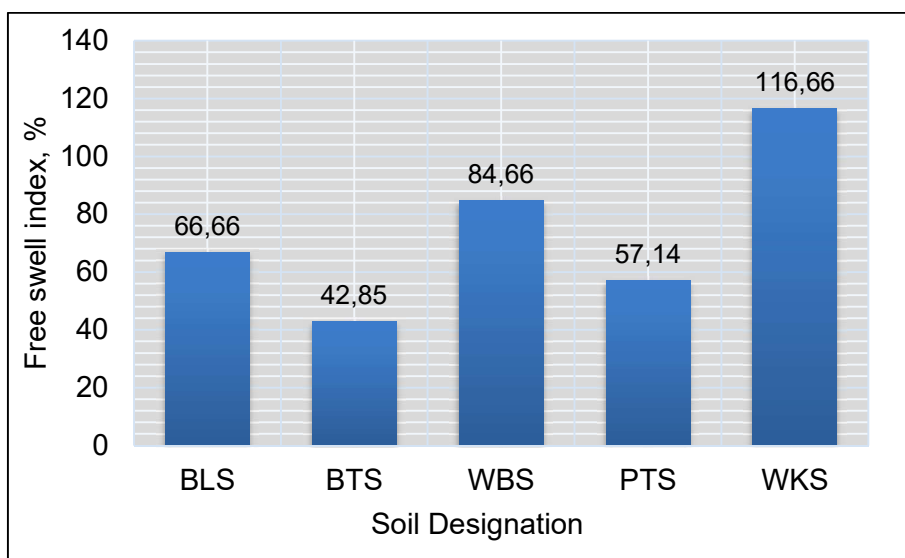


**Figure 5.14:** Free swell index test results

### 5.2.7 Free swell ratio result and analysis

The free swell ratio test was conducted in accordance with the technique proposed by Sridharan & Prakash (2000). The reading after 24 hours of the two volumes  $V_k$  (kerosene), and  $V_d$  (distilled water) on a glass cylinder is recorded in Table 5.7 found in Appendix D, and the Free swell ratio test results presented in Figure 5.15. WKS exhibits a high potential of expansiveness with a free swell ratio estimated at 2.2, whereas BTS displays the lower potential of expansiveness with a free swell index estimated at 1.4. Other soils PTS, BLS; WBS displays a moderate swelling potential with a free swell ratio estimated respectively at 1.6, 1.7, and 1.8. Furthermore, the free swell ratio results are used to identify the dominant clay mineral within the soil. The results of the free swell ratio revealed that WKS, WBS, BLS, and PTS are formed with smectite (montmorillonite) as dominant clay mineral, while the BTS sample is formed with a mixture of smectite (montmorillonite) with another mineral. The classification of soils based on the free swell ratio is given in Table 5.8 found in Appendix D.

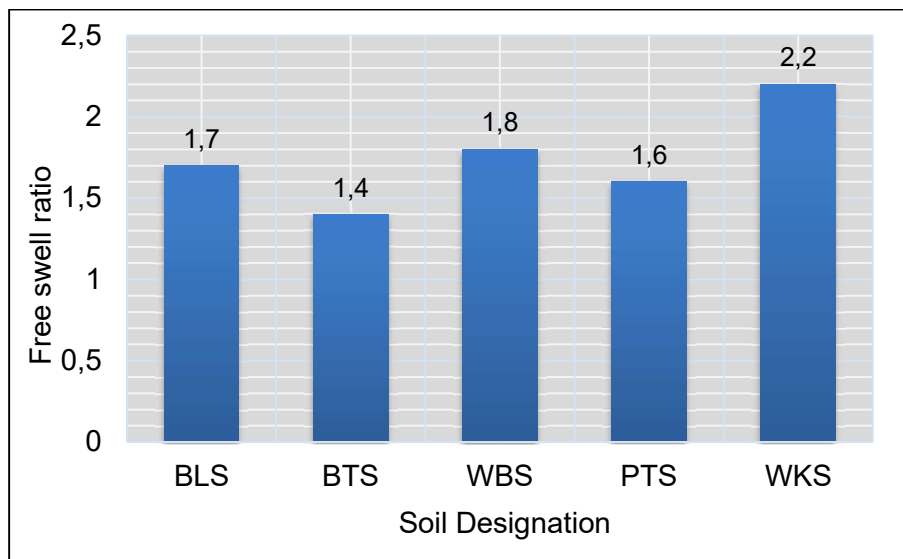


**Figure 5.15:** Free swell ratio test results

### 5.2.8 Comparison free swell ratio and free swell index test results.

The expansive potential results obtained from the free swell index test and the free swell ratio test are very similar. However, the free swell ratio test method overcomes the limitation of free swell index method according to BIS, I (1977) which gives a negative free swell index for soil rich in kaolinite (Sridharan et al.,1985). In addition, the free swell ratio test can be used to assess the dominant clay mineral in the soil.

### 5.3 X-Ray diffraction results analyses.

The type of mineral in soil was investigated for a good understanding of soil properties and behaviour. Soil behaviour is also influenced by the type of minerals in the soil. Certain clay minerals have a tremendous impact on the reactivity of the soil than others. A Philips automated powder diffractometer shown in Figure 4.13, in chapter 4 was used for XRD analysis. The X-ray diffraction pattern of soils WKS, BLS, PTS, WBS, and BTS are presented respectively in Figures 5.16 to 5.20. The diffraction patterns confirmed the presence of major clay minerals (smectite/montmorillonite) and major non - clay minerals (Quartz, syn; Feldspar, syn) in these soils. The smectite is the main clay mineral present in these soils. The smectite clay mineral belongs to the group of phyllosilicates species where the most important are: montmorillonite, nontronite, saponite, etc. The summary of XRD results is found in Table 5.9 in Appendix E.

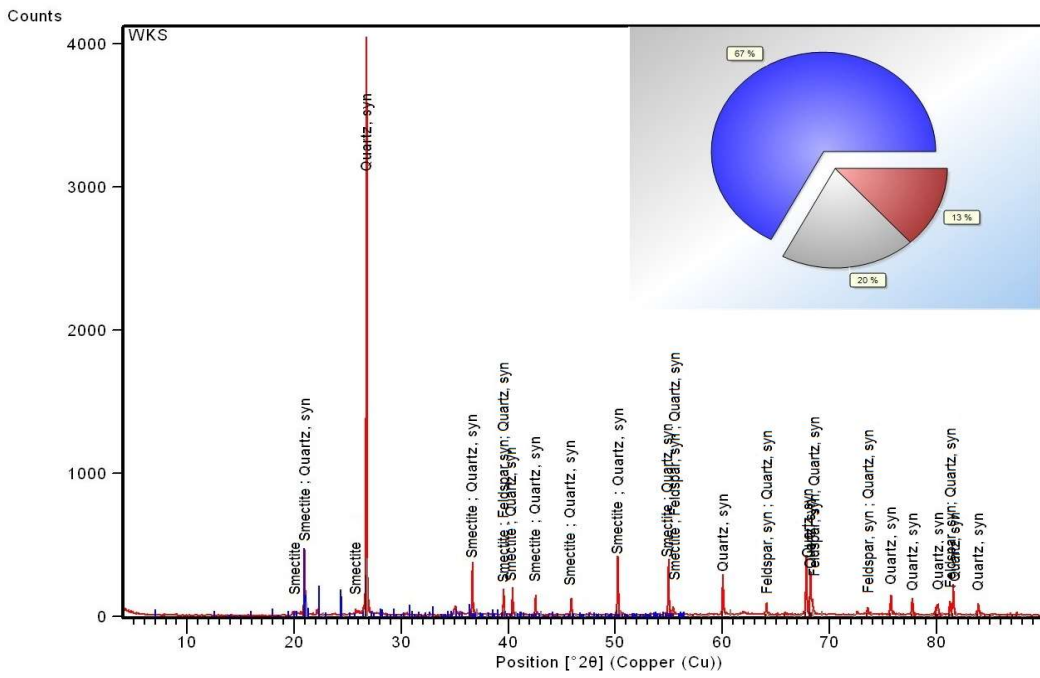


Figure 5.16: X-ray diffraction pattern (WKS)

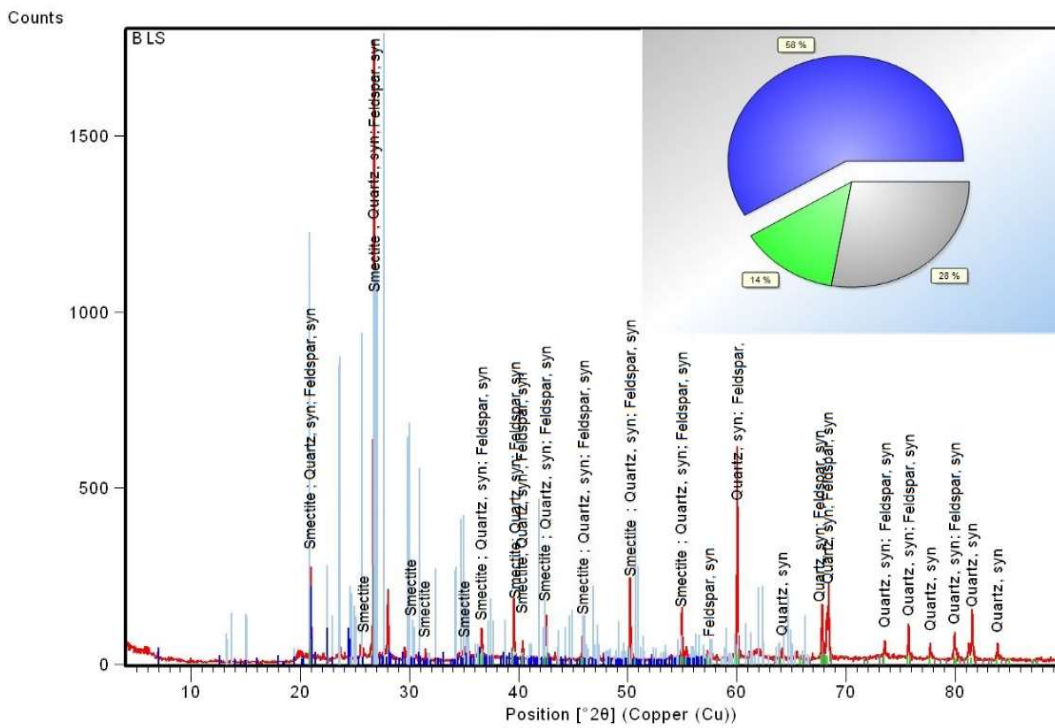


Figure 5.17: X-ray diffraction pattern (BLS)



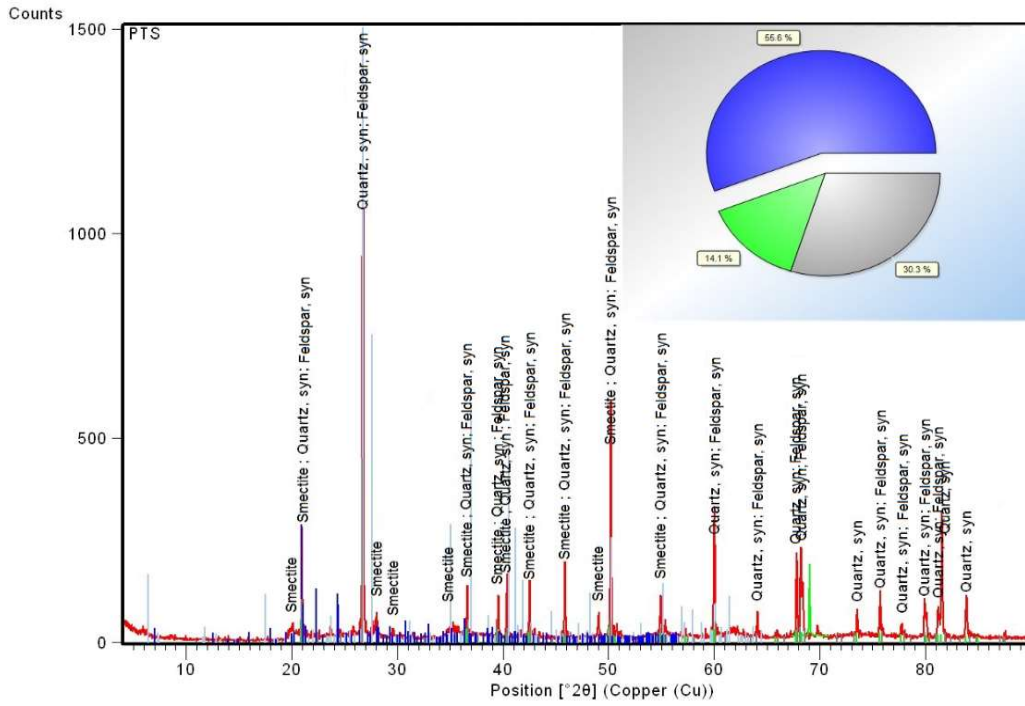


Figure 5.18: X-ray diffraction pattern (PTS)

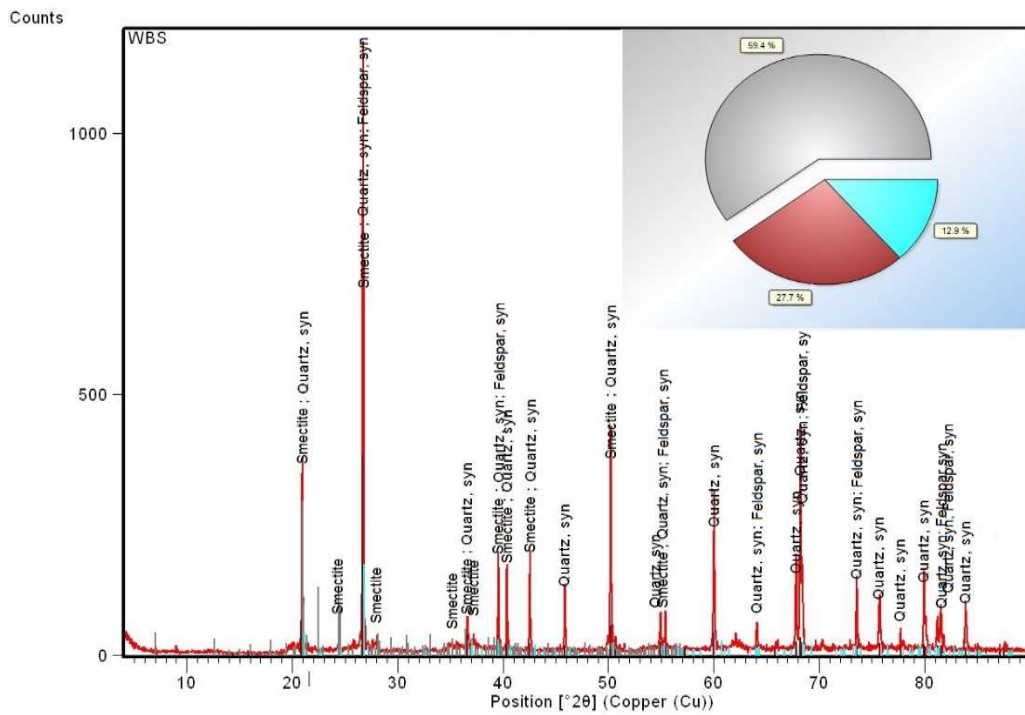
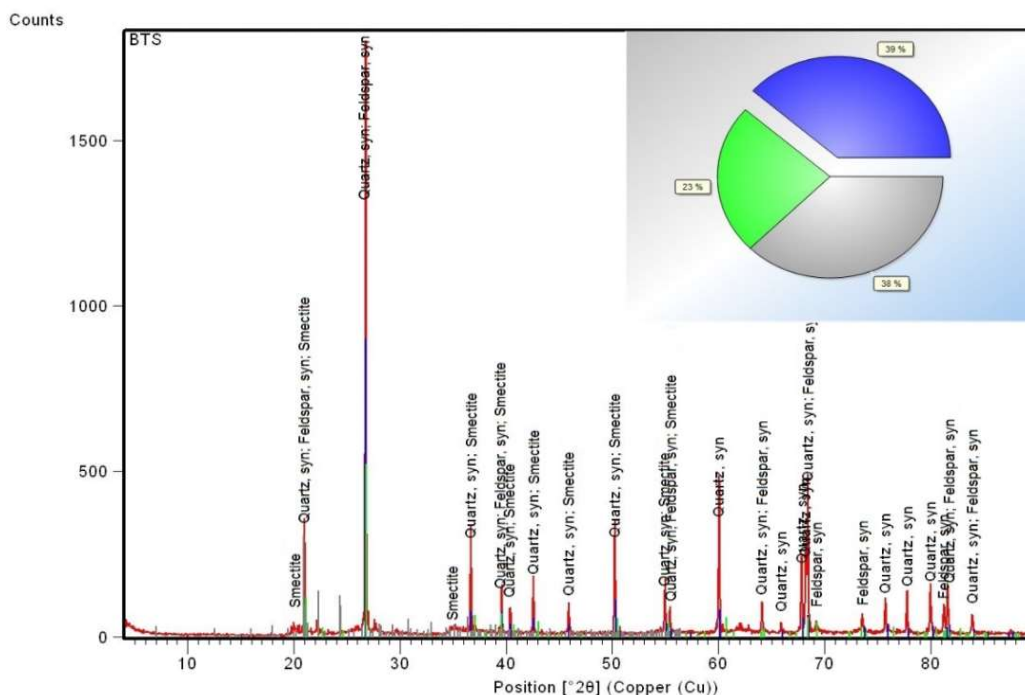


Figure 5.19: X-ray diffraction pattern (WBS)





**Figure 5.20:** X-ray diffraction pattern (BTS)

### 5.3.1 Comparison of results obtained from X-ray diffraction and free swell ratio.

The comparison of X-ray diffraction results and free swelling ratio results confirmed the reliability of the mineral composition of the soils investigated. Nonetheless, even though the free swell ratio method gives information about the dominant clay mineral in the soil, it cannot be used to identify a non-clay minerals and the quantity of clay mineral in the soil. The free swell ratio is limited and can be used for the primary investigation of the soil mineralogy. X-ray diffraction method is an efficient technique that required sophisticated equipment to assess the mineral composition of the soil. The mineralogical investigation shows that smectite / montmorillonite formed the major clay mineral in samples tested.

## 5.4 Proctor compaction test results

### 5.4.1 Compaction curves

The aim of compacting a soil is to enhance some desirable properties such as the reduction of water adsorption, compressibility, permeability. Additionally, increase the shear stress, bearing limit, etc. Nonetheless, the effect of compaction on soil properties depends generally on the structure attained by the soil during compaction.

The proctor compaction test was conducted according to TMH1-Method A7. The compaction curves were plotted by preparing the soil samples at different moisture content on the dry side at the optimum moisture content, and on the wet side. The dry density of each soil type was obtained on the dry side, optimum moisture content and on the wet side. The compaction curves for soils BTS, PTS, BLS, WBS, and WKS are shown in Figure 5.21. The compaction curves and zero air void line curves are plotted for each soil designation as shown in Figures 5.22 to 5.26. The determination of the maximum dry density and the optimum moisture content for each soil sample were done mathematically. The interpretation of the compaction curves revealed that BTS exhibits a higher maximum dry density  $18.76 \text{ kN/m}^3$ , and WKS displays the smaller maximum dry density of  $16.29 \text{ kN/m}^3$ . The maximum dry density for soil samples PTS, BLS, and WBS are respectively  $17.99 \text{ kN/m}^3$ ,  $17.16 \text{ kN/m}^3$  and  $16.29 \text{ kN/m}^3$ . Soil BTS which exhibits the highest maximum dry density, contained the smallest fine fraction 49.5%, whereas WKS which displays the smallest dry density, contained the highest fine fraction 73%. As the fine fraction material in the soil increases, the maximum dry density reduces upon the same compacting energy. Hence, the fine fraction materials in expansive soil influence significantly the maximum dry density.

WKS exhibits the highest optimum water content estimated at 26.34 %, while BTS displays the smallest optimum water content at 18.24 %. The optimum water content for soils WBS, BLS, and PTS are respectively 24.58 %, 22.61 %, and 20.38 %. WKS which exhibits the highest optimum water content, contained the highest fine fraction 73 %, whereas BTS, which displays the smallest optimum moisture content, contained the smallest fine fraction 49.5 %. As the fine fraction material in the soil increases, the optimum moisture content increases upon the same compacting energy. Therefore, the fine fraction materials in an expansive soils influence the optimum moisture content. The proctor compaction test results are given in Table 5.10 found in Appendix E.

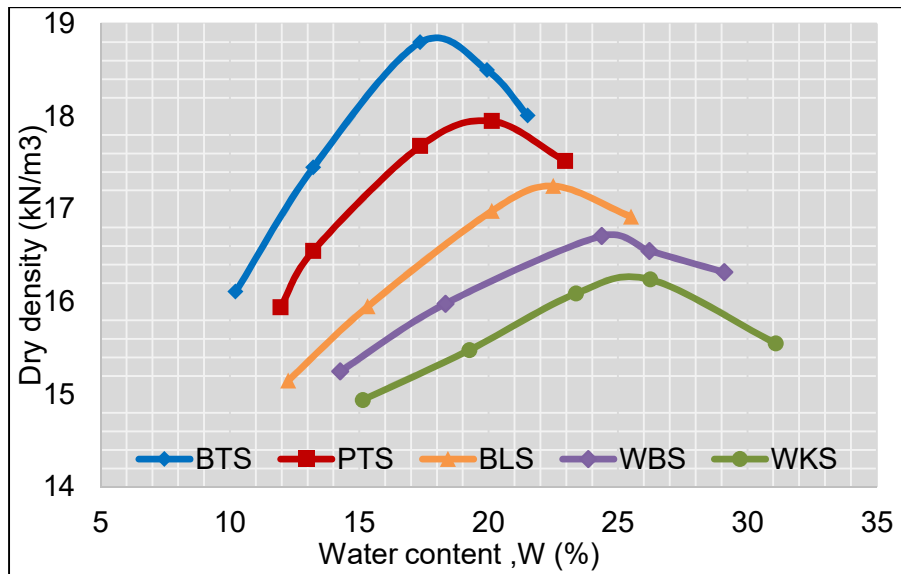


**Figure 5.21:** Compactive curves graph

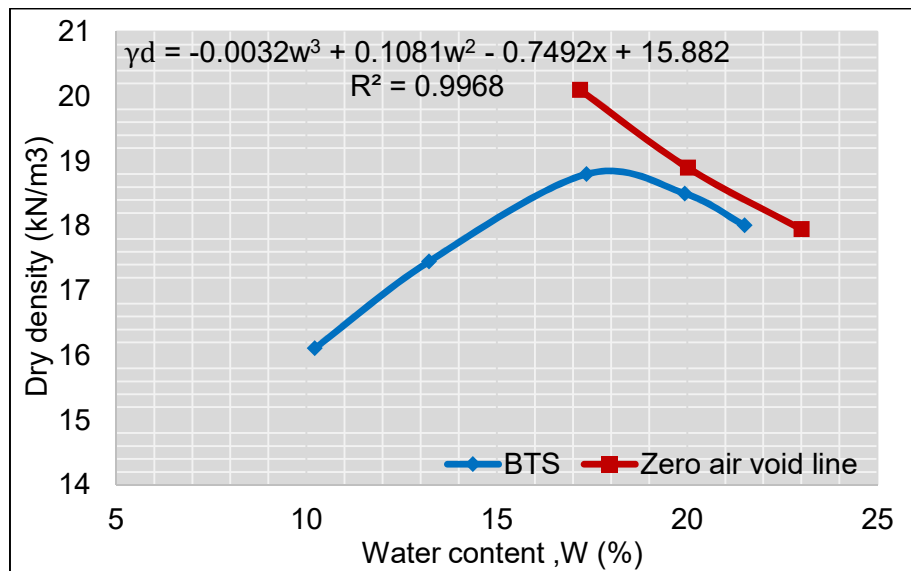


**Figure 5.22:** Compactive curve graph (BTS)

$$\gamma_d(w) = -0.0032w^3 + 0.1081w^2 - 0.7492w + 15.882 \quad (5.1)$$

$$\frac{\delta(\gamma_d)}{\delta w} = -0.0096w^2 + 0.2162w - 0.7492$$

$$\frac{\delta(\gamma_d)}{\delta w} = 0$$

$$-0.0096w_{opt}^2 + 0.2162w_{opt} - 0.7492 = 0$$

$$w_{opt} = 18.24 \%$$

$$\gamma_{dmax} = \gamma_d(w_{opt}) = 18.76 \text{ kN/m}^3$$

$$\gamma_{dmax} = 18.76 \text{ kN/m}^3$$

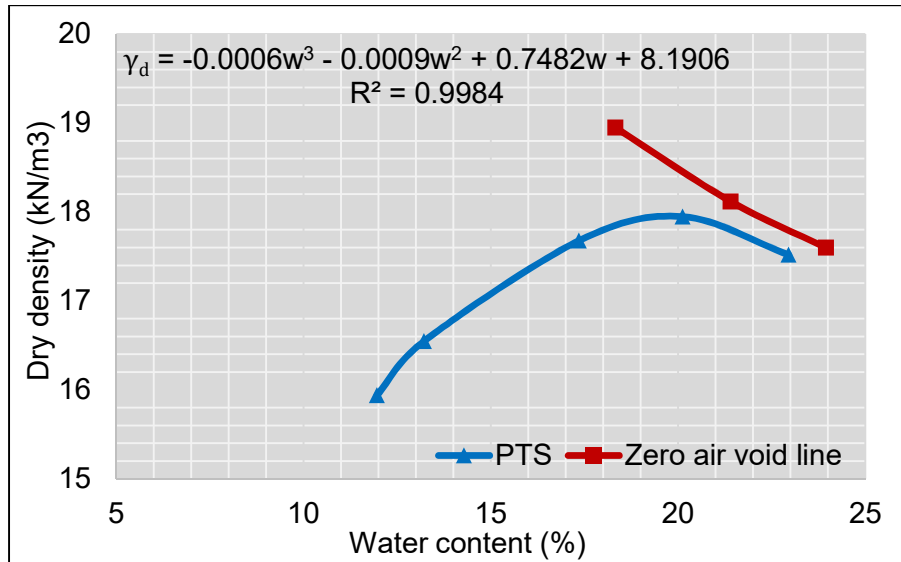


**Figure 5.23:** Compactive curve graph (PTS)

$$\gamma_d(w) = -0.0006w^3 - 0.0009w^2 + 0.7482w + 8.1906 \quad (5.2)$$

$$\frac{\delta(\gamma_d)}{\delta w} = -0.0018w^2 - 0.0018w + 0.7492$$

$$\frac{\delta(\gamma_d)}{\delta w} = 0,$$

$$-0.0018w_{opt}^2 - 0.0018w_{opt} + 0.7482 = 0$$

$$w_{opt} = 20.38 \%$$

$$\gamma_{dmax} = \gamma_d(w_{opt}) = 17.99 \text{ kN/m}^3$$

$$\gamma_{dmax} = 17.99 \text{ kN/m}^3$$

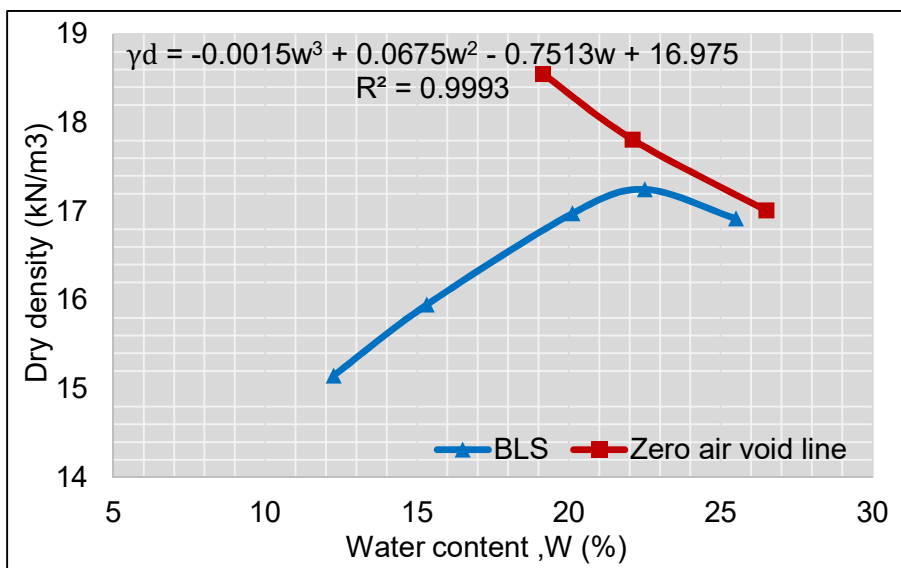


**Figure 5.24:** Compactive curve graph (BLS)

$$\gamma_d(w) = -0.0015w^3 + 0.0675w^2 - 0.7513w + 16.975 \quad (5.3)$$

$$\frac{\delta(\gamma_d)}{\delta w} = -0.0045w^2 + 0.135w - 0.7513$$

$$\frac{\delta(\gamma_d)}{\delta w} = 0,$$

$$-0.0045w_{opt}^2 + 0.135w_{opt} - 0.7513 = 0$$

$$w_{opt} = 22.61 \%$$

$$\gamma_{dmax} = \gamma_d(w_{opt}) = 17.16 \text{ kN/m}^3$$

$$\gamma_{dmax} = 17.16 \text{ kN/m}^3$$

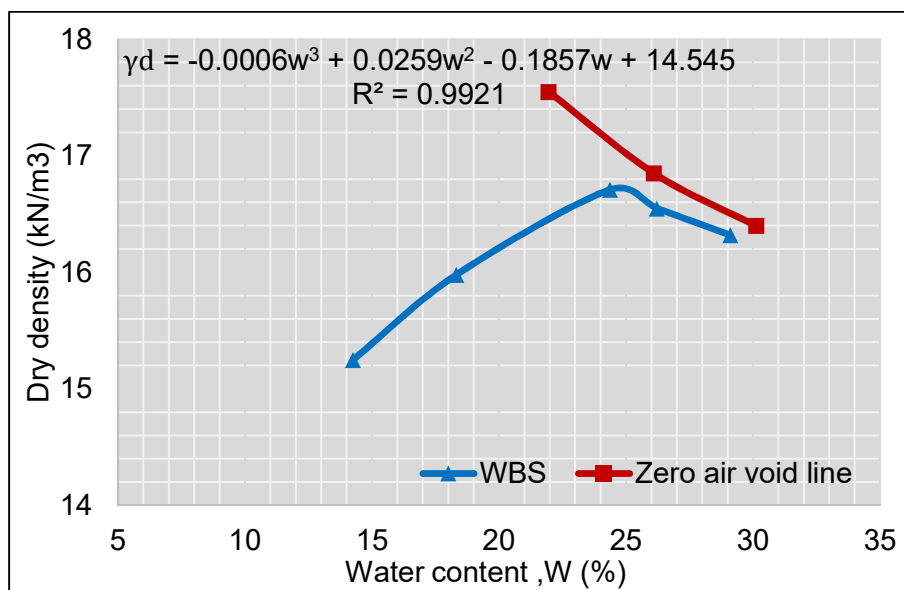


Figure 5.25: Compactive curve graph (WBS)

$$\gamma_d(w) = -0.0006w^3 + 0.0259w^2 - 0.1857w + 14.545 \quad (5.4)$$

$$\frac{\delta(\gamma_d)}{\delta w} = -0.0018w^2 + 0.0518w - 0.1857$$

$$\frac{\delta(\gamma_d)}{\delta w} = 0,$$

$$-0.0018w_{opt}^2 + 0.0518w_{opt} - 0.1857 = 0$$

$$w_{opt} = 24.58 \%$$

$$\gamma_{dmax} = \gamma_d(w_{opt}) = 16.52 \text{ kN/m}^3$$

$$\gamma_{dmax} = 16.71 \text{ kN/m}^3$$

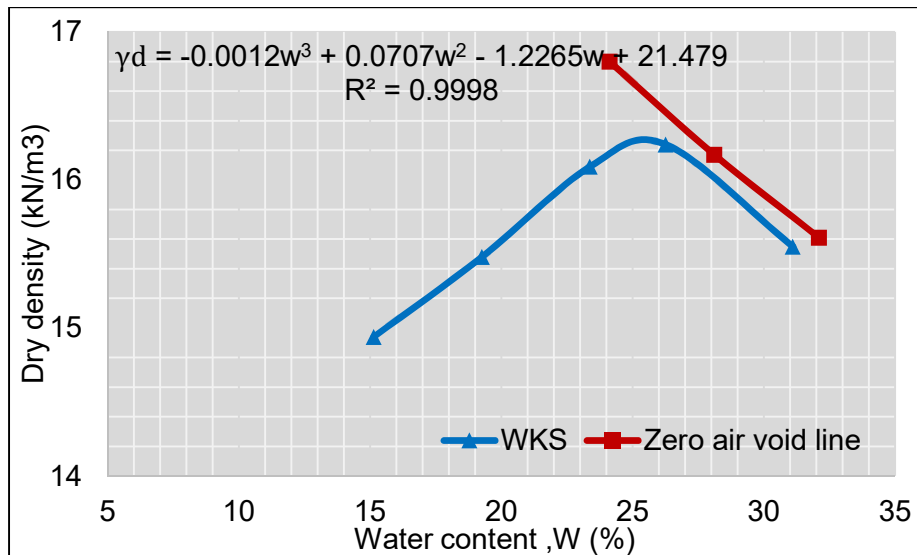


**Figure 5.26:** Compactive curve graph (WKS)

$$\gamma_d(w) = -0.0012w^3 + 0.0707w^2 - 1.2265w + 21.479 \quad (5.5)$$

$$\frac{\delta(\gamma_d)}{\delta w} = -0.0036w^2 + 0.1414w - 1.2265$$

$$\frac{\delta(\gamma_d)}{\delta w} = 0,$$

$$-0.0036w_{opt}^2 + 0.1414w_{opt} - 1.2265 = 0$$

$$w_{opt} = 26.34 \%$$

$$\gamma_{dmax} = \gamma_d(w_{opt}) = 16.29 \text{ kN/m}^3$$

$$\gamma_{dmax} = 16.29 \text{ kN/m}^3$$

### 5.5 Soil suction test results

The soil suction evaluation was conducted using filter paper technique according to ASTM D5298. Contact filter paper approach was used to determine the matric suction and the non-contact filter paper approach to evaluate the total suction. The filter paper technique is a non-expensive and simple laboratory test method used to evaluate the matric suction and the total suction for unsaturated soil. The filter paper suction measurement experiment was described in chapter 4. The results of soil suction test measurement are presented in Table 5.12 found in Appendix F.

### 5.5.1 Soil suction calibration curve

The soil suction measurement by filter paper approach is highly depended upon the calibration curve. The calibration procedure is presented in chapter 4. The obtained calibrated curve was compared to other curves such as Huseyin (2003), Schleicher & Schuell No. 589 White Ribbon, and Whatman No.42 type filter paper given by ASTM D 5298. The result of the calibration curve using salt solution is shown in Figure 5.27 as well as the calibrated curve Equation 5.6.

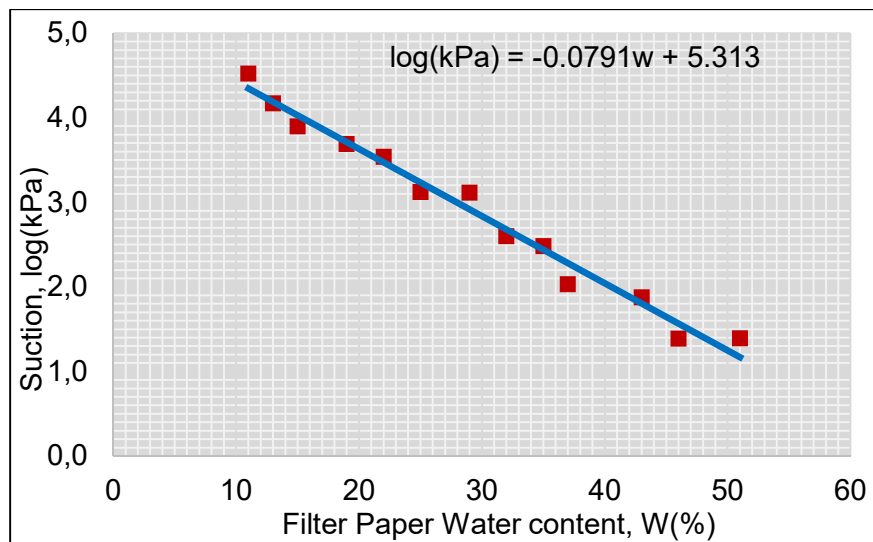


**Figure 5.27:** Calibrated curve using Whatman No 42 filter paper

$$\log(\text{kPa}) = -0.0791w + 5.313 \tag{5.6}$$

The calibrated curves and the equations proposed by other authors are presented in Table 5.11 found in Appendix E.

Figure 5.28 exhibits a comparison of calibrated curve equation 5.6 obtained from experiment, and the curves proposed by other authors. It was observed that, when the moisture content in the filter paper is within the range of within  $20 \% \leq W \leq 38 \%$ , the suction values given by four equations are very similar. However, when moisture content is within the range of  $0 \% \leq W < 20 \%$  and  $38 \% \leq W < 45 \%$ , the gaps between the calibrated curve and others curves proposed by ASTM D5298, and Huseyin (2003) still small. However, the curve proposed by Scheleicher & Schuell No.589 exhibits non-negligible discrepancies, this can be justified by the differences in features between Whatman No 42 filter paper and Scheleicher & Schuell No. 589 filter paper.



The validation of the calibrated curve was achieved by comparing experimental suction values and predicted suction values as shown in Figure 5.29. Furthermore, it was observed that the scatter of the data points plotted not only shows a good correlation with the experimental values but also, portrays very small discrepancies between themselves.

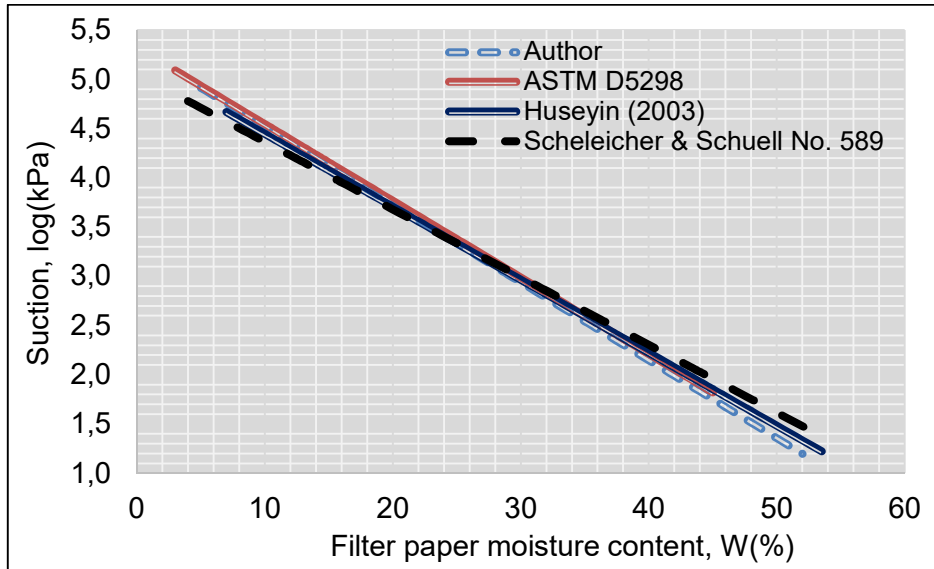


**Figure 5.28:** Calibrated curve and adopted curve graph

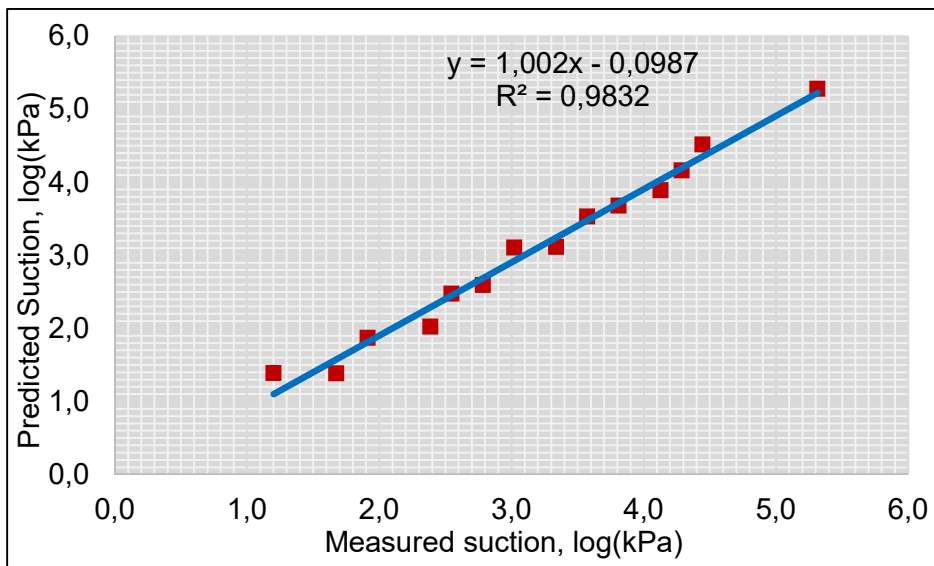


**Figure 5.29:** Measured versus predicted values of suction from the calibration curve.

### **5.5.2 Analysis and discussion of the relationship between soil suction and moisture content.**

In this study, soil suctions (total suction, matric suction, and osmotic suction) were determined using filter paper technique. The measurements were taken in a standard manner on compacted expansive soils, prepared at various moisture contents on the dry side, on the wet side, and at the optimum moisture content. Several properties of expansive unsaturated soil, such as the swelling stress, the volume variation, the hydraulic conductivity can be related to the water content in the soil voids at any soil potential. Thus, the relation between water content (gravimetric water content, volumetric water content) and soil potential is an essential feature of unsaturated soils.

The relation between soil suctions (total suction, matric suction, osmotic suction) and the gravimetric water content was investigated for each soil sample and presented in the form of a graph. Soil suction versus gravimetric water content graph for soils WKS, WBS, BLS, PTS, and BTS are shown respectively shown in Figures 5.33 to 5.37.

Figures 5.33 to 5.37 shows the variation of total suction, matric suction, and osmotic suction with respect to water content. Matric suction and total suction curves for all soil types are very similar one to another, especially in the higher moisture content range. A change in total suction is fundamentally equivalent to a variation in matric suction, and vice versa. In other words, the total suction curve is above the matric suction curve, but both are a very similar in shape. However, osmotic suction curve shape is very different from the total and the matric suction curves. Moreover, the matric suction contribution to the total suction is far greater than the osmotic suction contribution. Figures 5.30 to 5.32 shows the values of the total suction, matric suction, and osmotic suction at optimum moisture content (OMC). Figures 5.38 to 5.39 shows that WKS exhibits the highest total suction and matric suction values, while BTS displays the smallest total suction and matric suction values. It can be observed that the soil which contains the highest fine fraction WKS 73% displays the highest total and matric suction whereas the soil which contains the smallest fine fraction BTS 49.5 % exhibits the smallest total and matric suction. Therefore, for a compacted expansive soil, the matric suction and the total suction increases as the fine fraction within the soil increases.

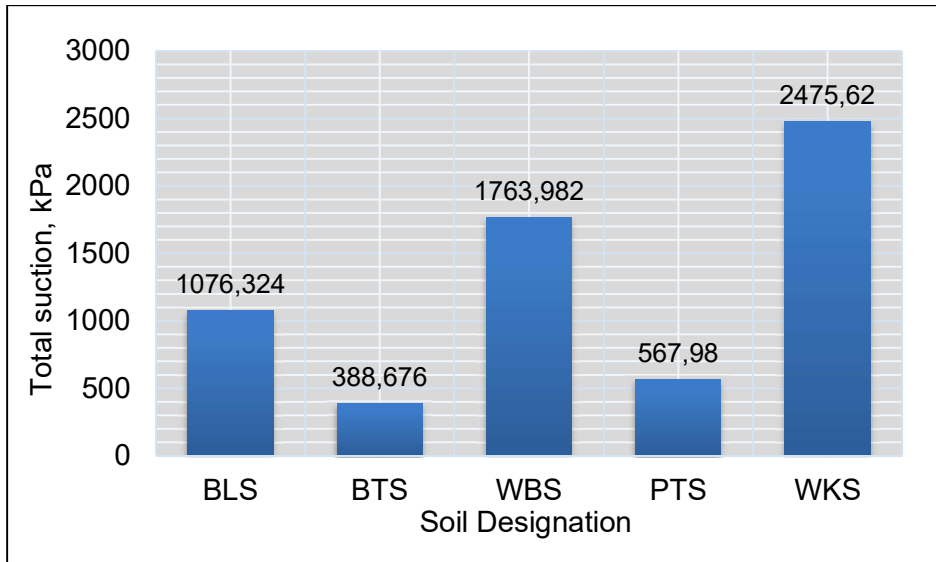


**Figure 5.30:** Total suction for soil designation @ OMC

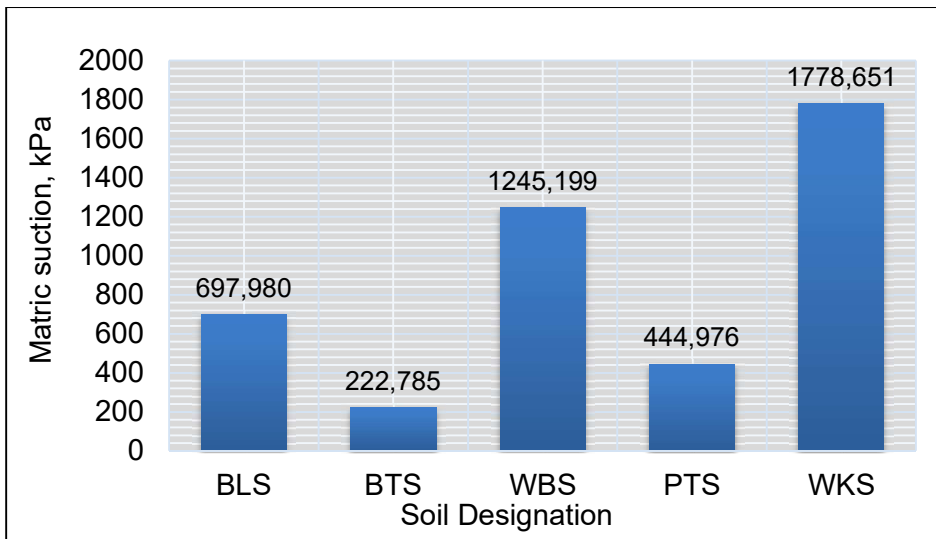


**Figure 5.31:** Matric suction versus soil designation at OMC

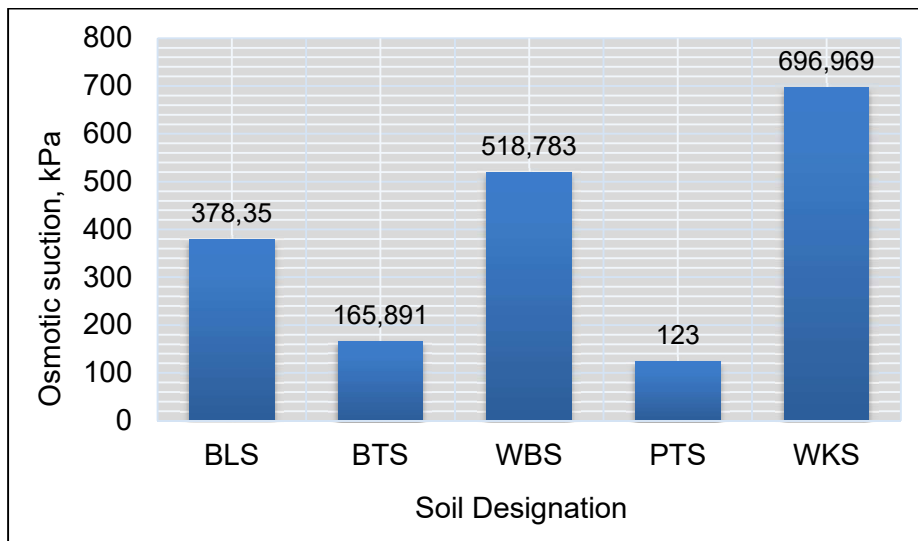


**Figure 5.32:** Osmotic suction for soil designation at OMC

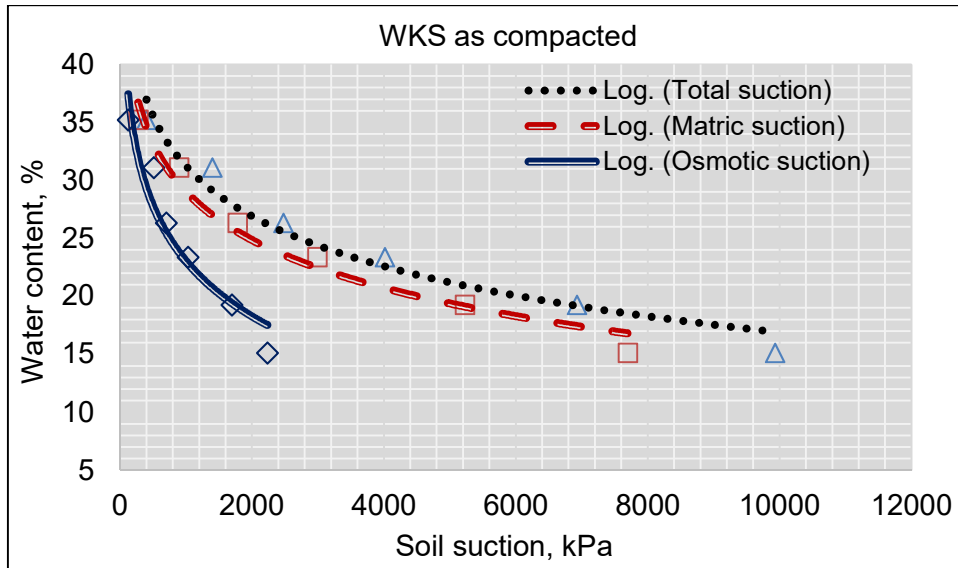


**Figure 5.33:** Suctions versus water content (WKS)

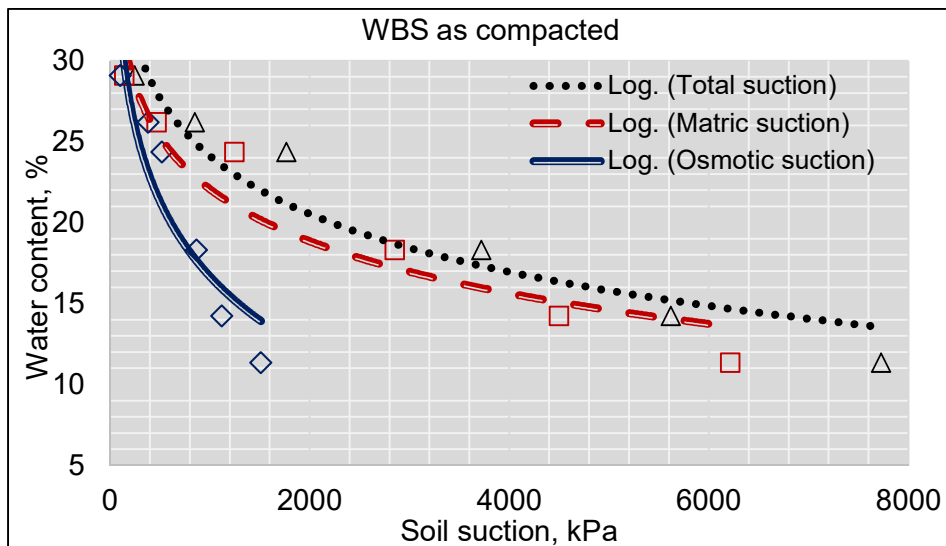


**Figure 5.34:** Suctions versus water content (WBS)

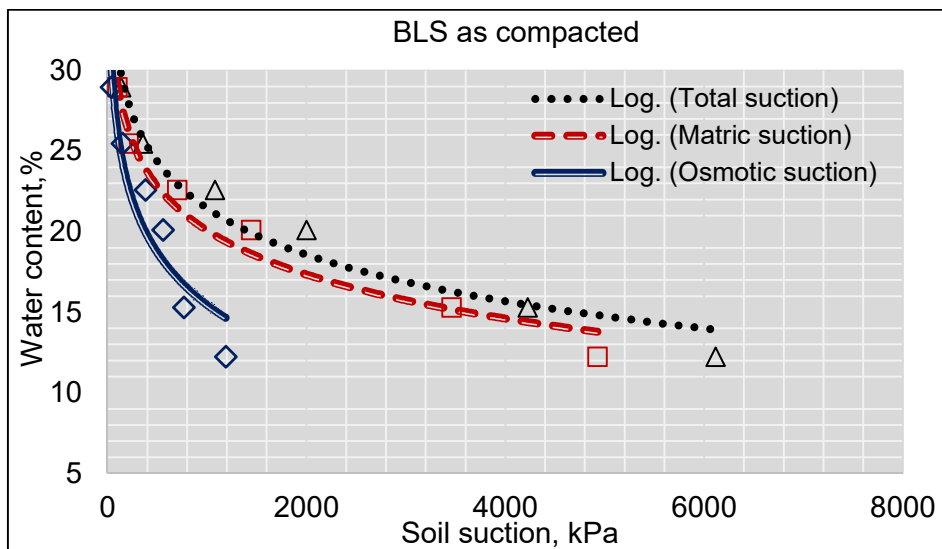


**Figure 5.35:** Suctions versus water content (BLS)

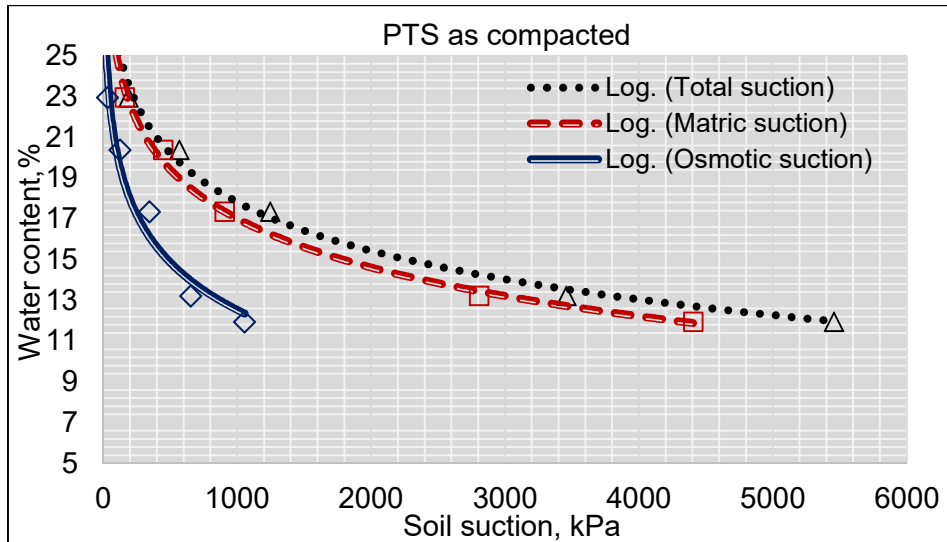


Figure 5.36: Suctions versus water content (PTS)

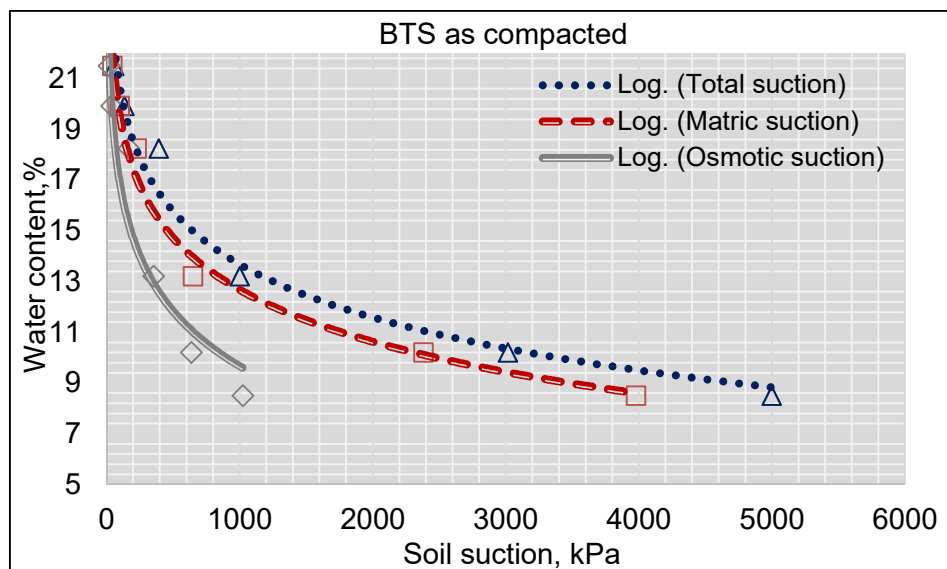


Figure 5.37: Suction versus water content (BTS)

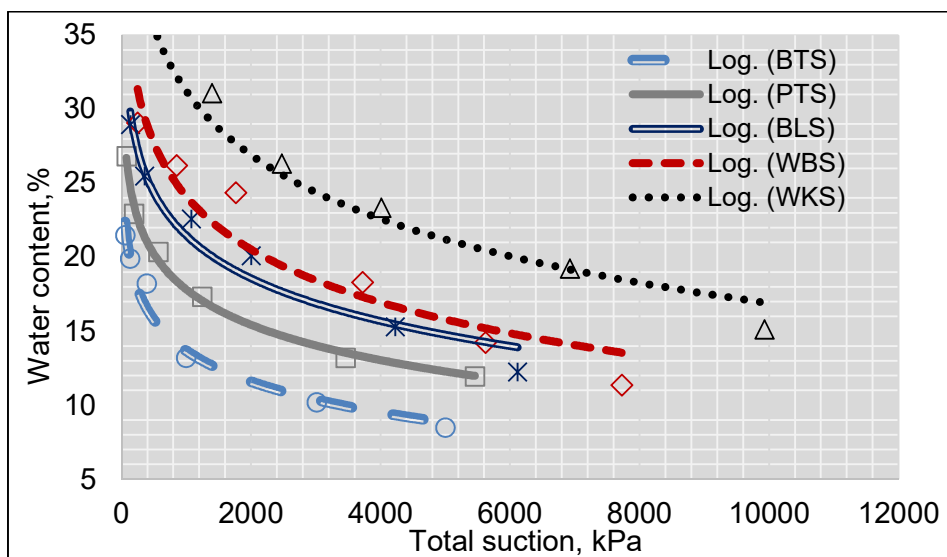
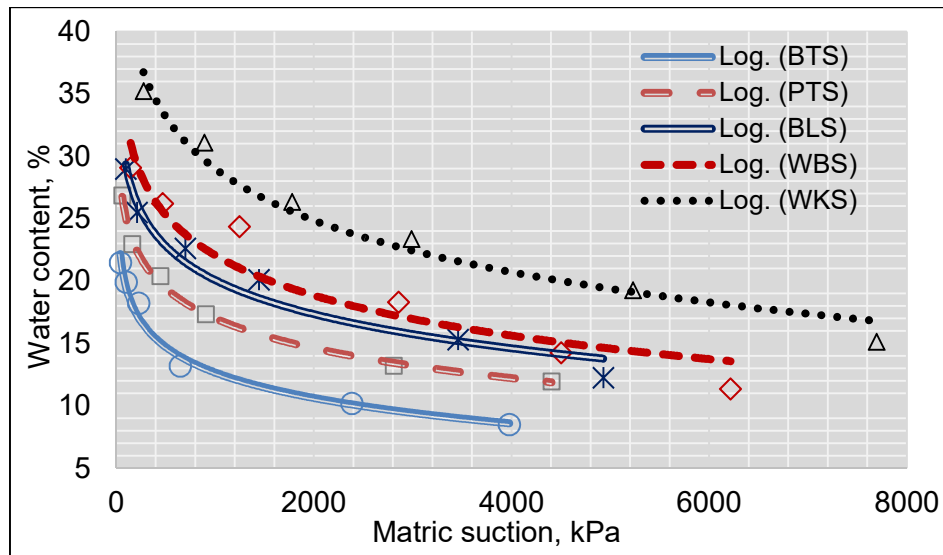


Figure 5.38: Total suction versus water content



**Figure 5.39:** Matric suction versus water content

## 5.6 Soil water characteristic curve

### 5.6.1 Introduction

Unsaturated soil behaviour is significantly dependent on the intensity of soil suction, which is affected by soil moisture content for a given soil. The SWCC represents the capacity of a soil to restrain water at over a range of suction (Fredlund, 2002). SWCC is an essential aspect of expansive unsaturated soil. SWCC is used to establish the relationship between the water content within the soil and the suction. The obtained curve gives good information about the distribution of voids within the unsaturated soils.

The SWCC was plotted using a logarithmic scale due to the great range of suction and the volumetric water content. The suction has been measured at different moisture content from compacted specimens using Whatman No 42 filter paper, other suction values were obtained by interpolating the measured values. The data used to plot the SWCC for soils WKS, WBS, BLS, PTS, and BTS are shown respectively in Tables 5.13 to 5.15 found in Appendix G, and in Tables 5.16 and 5.17 found in Appendix H

### 5.6.2 Modelling of SWCC

Several empirical, analytical and statistical models are proposed to fit the experimental data and to describe the SWCC. The most commonly used SWCC models are those proposed by van Genuchten (1980) and Fredlund & Xing (1994). In this study, the SWCC was determined using the matric suction versus the

volumetric water content. The measured volumetric water content obtained from the experiments were compared to the predicted volumetric water content based on the matric suction values given by the models proposed by Van Genuchten (1980), Fredlund and Xing (1994), and Seki (2007).

The SWCC for soils WKS, WBS, BLS, PTS, and BTS are shown respectively in Figures 5.42 to 5.46. As a result, the model proposed by Seki (2007) gives the best fitting compared to the model proposed by Fredlund and Xing (1994), and the model proposed by Van Genuchten (1980). This can be explained by the fact that the grain size distribution of soils WKS, WBS, BLS, PTS, and BTS are bimodal. Seki Model (2007) is developed for bimodal grain size distribution, whereas model by Van Genuchten (1980) and model by Fredlund and Xing (1994) are developed for unimodal grain size distribution.

### **5.6.3 Analysis and discussion of SWCC**

The SWCC results are summarized in Table 5.18 found in Appendix H. The SWCC shown in Figures 5.42 to 5.46 were used to determine the matric suction at air entry value (AEV), and the volumetric water content at air entry values. The AEV is the point at which the degree of saturation drops below 100 %. Figures 5.40 to 5.41 shows respectively the volumetric water content at AEV and the matric suction at AEV for the soils.

WKS yields a higher value of volumetric water content at AEV, whereas BTS yields the smaller volumetric water content value at AEV. The results can be explained by the influence of fine fractions. WKS displays a higher amount of fine 73 %, while BTS exhibits a smaller amount of fine 49.5 %. Vanapalli et al., (1999) pointed out that the soil with smaller particles such as silt and clay exhibits smaller pore and greater relative surface area, and present a tendency to desaturate at a slower rate.

BTS soil with a smaller percentage of fine fractions displays the smaller matric suction value at AEV than other soils WKS, WBS, BLS, and PTS. BLS soil yields higher values of matric suction at AEV. These results can be justified by the influence of initial water content and compaction energy. Soil compacted with an initial water content on the dry side, wet side, and at the optimum moisture content will give a sample that have differences in grain size distribution and soil structure (Gens et al., 1995; and Vanapalli et al., 1999). Moreover, an increase in



compaction effort implies an increase in dry density and decrease in void ratio. Therefore, some differences in the SWCC of the same compacted soil with different efforts are expected. The fine fraction, the compaction effort, and the initial water content influence significantly the SWCC.

#### 5.6.4 Soil water characteristic curve fit results

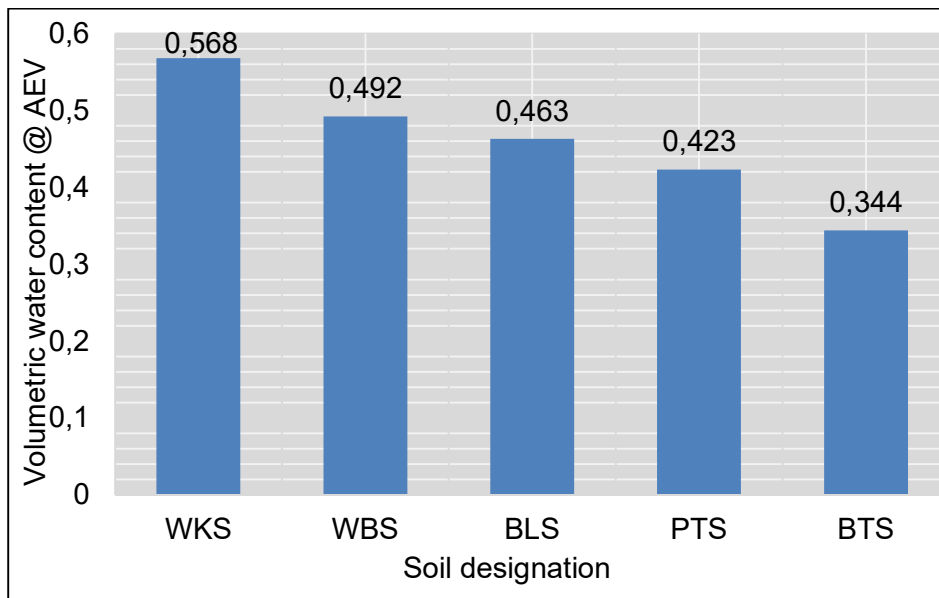


**Figure 5.40:** Volumetric water content at Air entry value (AEV)

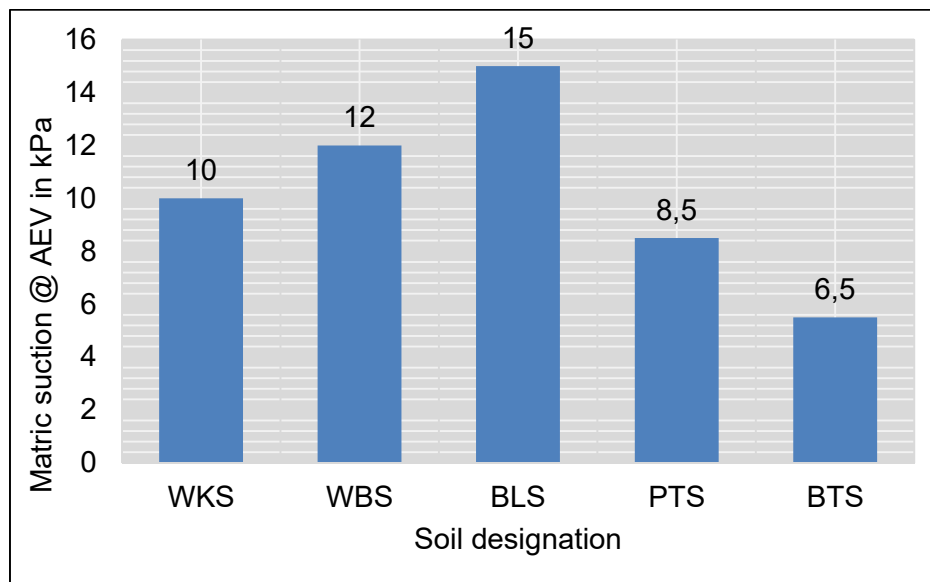


**Figure 5.41:** Matric suction at Air entry value (AEV)

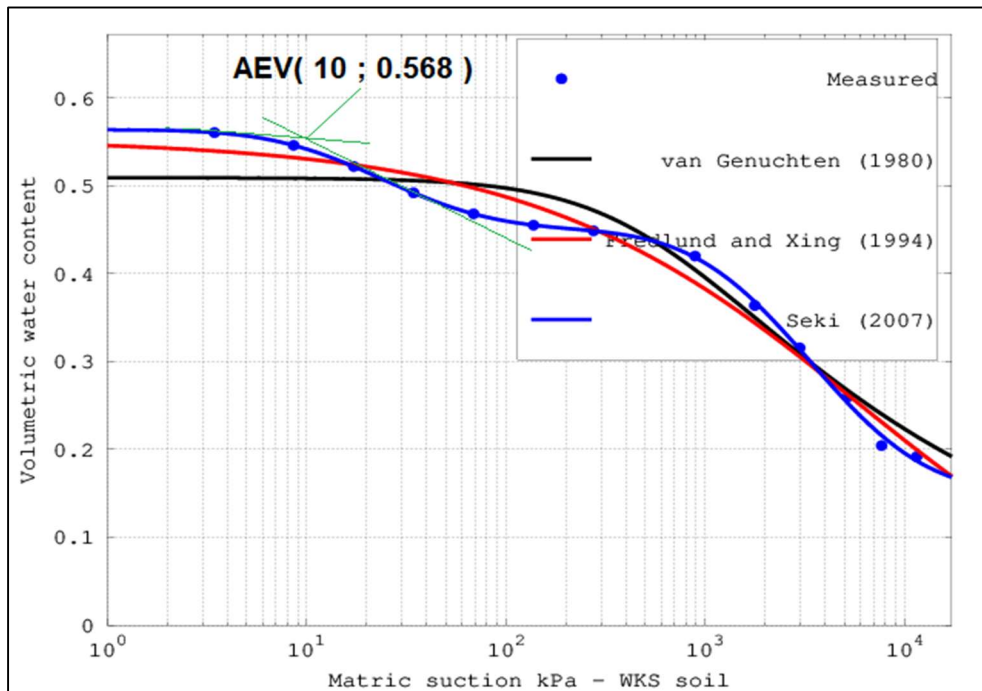


Figure 5.42: Soil water characteristic curve for WKS as compacted

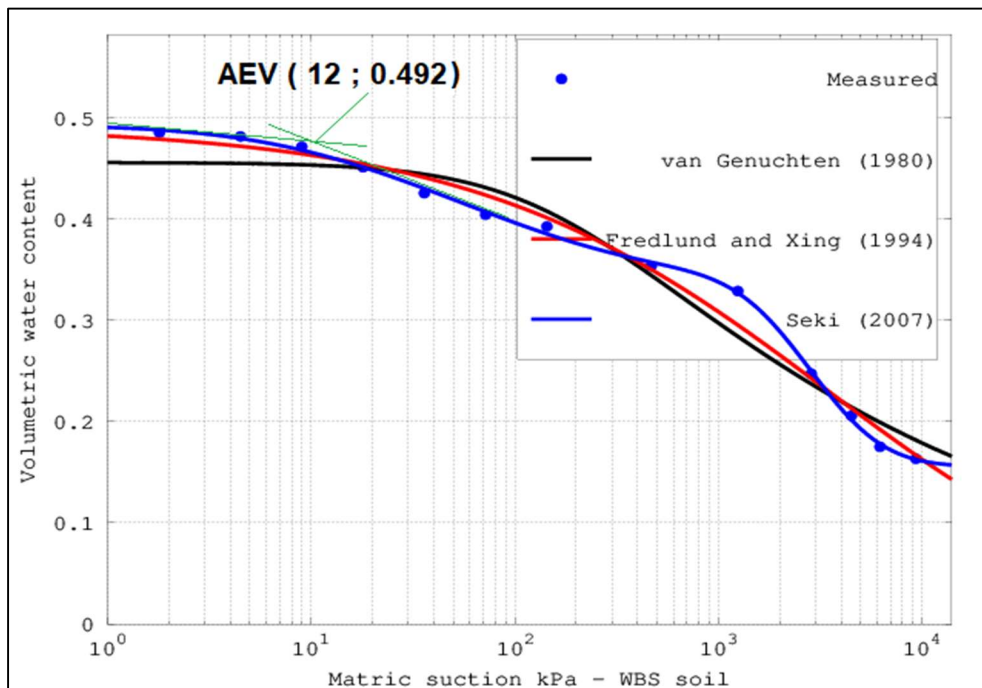
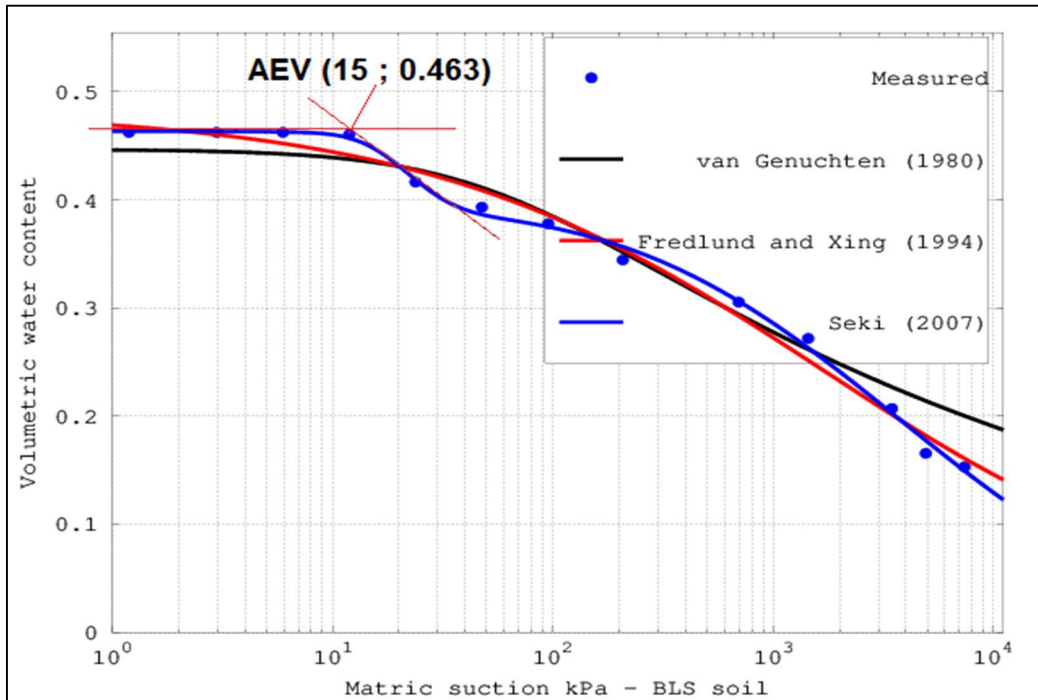
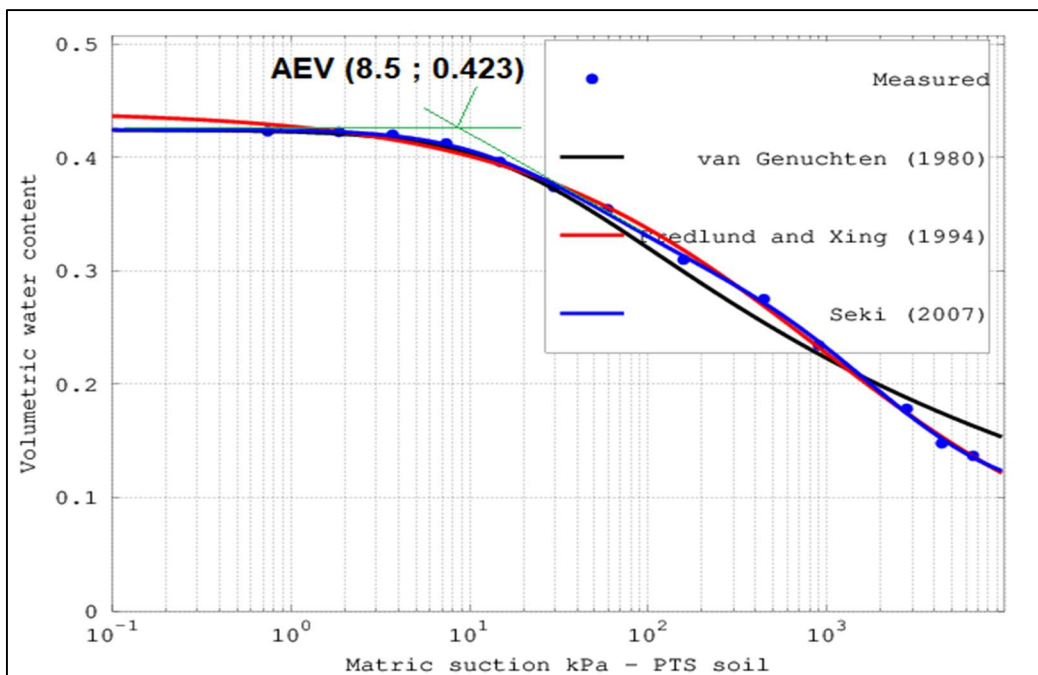


Figure 5.43: Soil water characteristic curve for WBS as compacted



**Figure 5.44:** Soil water characteristic curve for BLS as compacted



**Figure 5.45:** Soil water characteristic curve for PTS as compacted

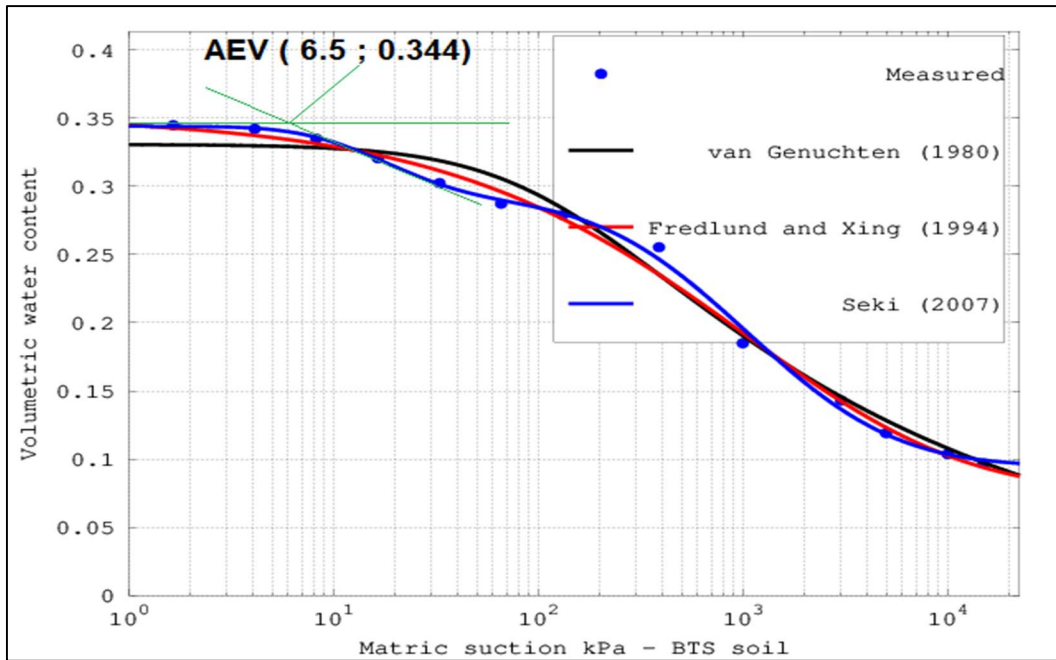


**Figure 5.46:** Soil water characteristic curve for BTS as compacted

### 5.6.5 Soil water characteristic curve fitting parameters and equations

The soil water characteristic curve fitting parameters and equations for soils WKS, WBS, BLS, PTS, and BTS are shown in Table 5.19 found in Appendix I, Table 5.20 found in Appendix J, and in Table 5.21 found in Appendix K. AIC (Akaike Information Criterion) =  $n \cdot \ln(RSS/n) + 2k$ , where  $n$  is sample size,  $RSS$  is residual sum of squares and  $k$  is the number of estimated parameters. The effective saturation,  $S_e = (\theta - \theta_r) / (\theta_s - \theta_r)$ . Therefore  $\theta = \theta_r + (\theta_s - \theta_r) S_e$ . For Seki model,  $Q(x)$  is the complementary cumulative normal distribution function, defined by  $Q(x) = 1 - \Phi(x)$ , in which  $\Phi(x)$  is a normalized form of the cumulative normal distribution function. In Fredlund and Xing model,  $e$  is the Napier constant. The model proposed by Seki (2007) was found to fit very well the experimental results compared to the SWCC curve fitting models as proposed by Van Genuchten (1980); and Fredlund and Xing (1994).

### 5.7 Swelling stress results analysis

The swelling stress experiment was performed by zero swell test technique according to ASTM D4546. The measurements were taken on compacted specimens on the dry side, optimum, and on the wet side. The technique used to measure the swelling stress was explained in detail in Chapter 4. The swelling stress results are given in table 5.22 found in Appendix L. The analysis of the

swelling stress results revealed that the swelling stress exhibits a tendency to decrease with the increment of initial water content for different specimens, even beyond the optimum moisture content. Nonetheless, at the optimum moisture content, the swelling stress shows a tendency to increase as the initial water content at the optimum moisture content increases for the different soils. Figure 5.47 shows different values of the swelling stress at the OMC for different soils. WKS soil displays the highest swelling stress value of 262.300 kPa, whereas BTS soil exhibits the smallest swelling stress value of 49.962 kPa. Figure 5.48 shows the maximum swelling stress for soil samples. WKS displays the highest swelling stress value estimated at 599.543 kPa, and BTS soil displays the smallest swelling stress value estimated at 112.414 kPa. As mentioned earlier, the relationship between the swelling stress and other soil parameters are investigated in section 5.9.

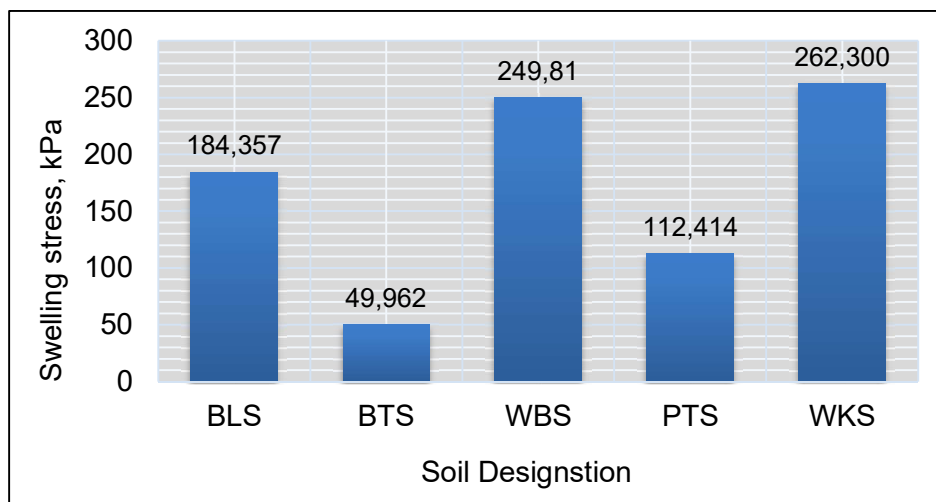


**Figure 5.47:** Swelling stress for soil designation at OMC

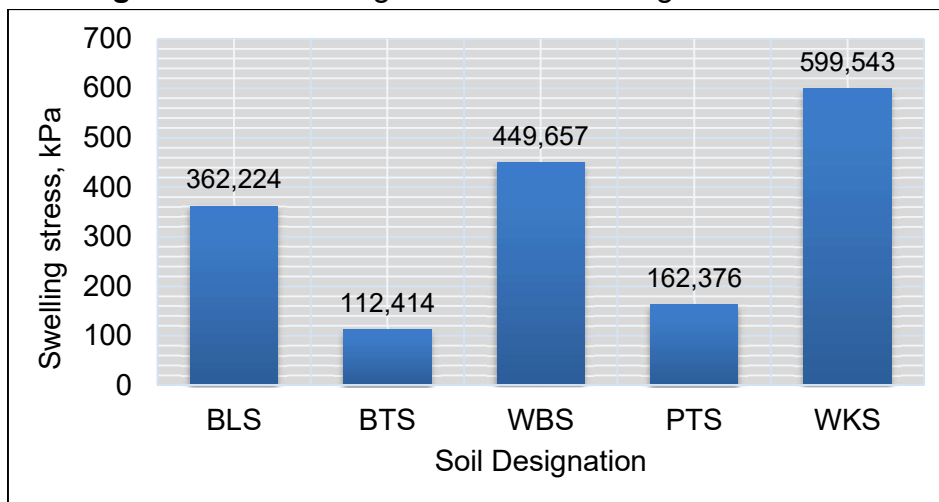


**Figure 5.48:** Maximum Swelling stress for soil designation

## **5.8 Summary of laboratory results**

The summary of laboratory test results is given in Table 5.23 to 5.25 found in Appendix M.

## **5.9 Analysis and discussions of the correlations between swelling stress and soil parameters.**

### **5.9.1 Analysis and discussion of the correlation between swelling stress and soil suction.**

The correlations between the swelling stress and the soil suctions (total suction, matric suction, osmotic suction) for compacted expansive soils were established by plotting the experimental values of the swelling stress versus the soil suctions (total suction, matric suction, osmotic suction) as presented in Figures 5.49 to 5.51. From these figures, it can be seen a tendency of the increment of the swelling stress as the soil suctions increases and manifested a linear relationship for soils WKS, WBS, BLS, PTS and BTS. Moreover, for a correlation to be considered as reliable, the correlation coefficient  $R^2$  of the trend line needs to exceed 0.8. It is apparent that there is a good correlation between the swelling stress and the soil suctions (total suction, matric suction, osmotic suction) since the strength of this correlation exceeds 0.8 for all soil. Furthermore, the scatters of the plotted data are in good coordination with small discrepancies. As expected, the soil suction is a fundamental property of unsaturated expansive soils and can be used to predict the swelling stress. Rao et al. (2004) attempted to establish a correlation between soil suction and swelling stress of heaving soils. As a result, it was found that the soil suction measurement can be used and an important parameter to predict the swelling stress of heaving soils.

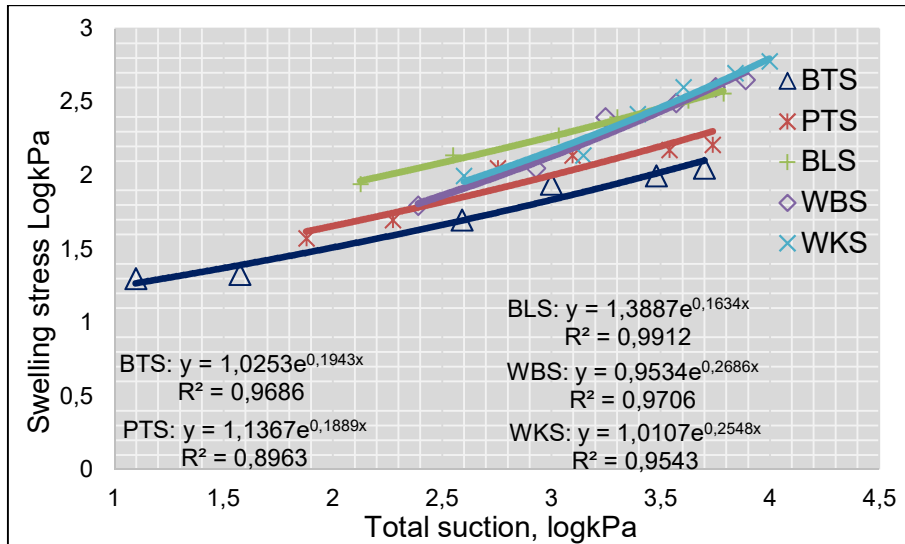


Figure 5.49: Swelling stress versus total suction

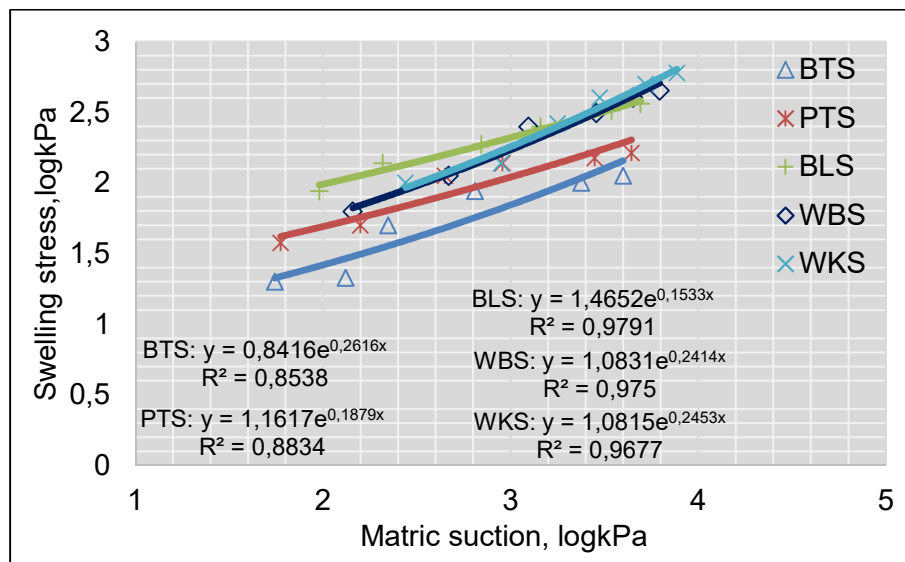


Figure 5.50: Swelling stress versus matric suction

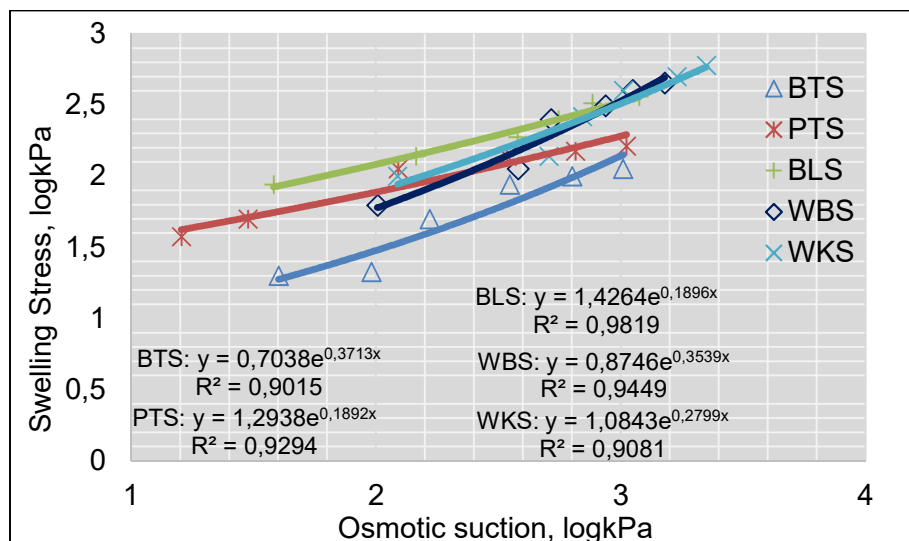


Figure 5.51: Swelling stress versus Osmotic suction



### 5.9.2 Analysis and discussion of the correlation between the swelling stress and initial dry density.

To investigate the relationship between the swelling stress and the initial dry density for compacted expansive soils, experimental values of the swelling stress versus the initial dry density were plotted as presented on Figures 5.52 to 5.53. In all cases, the swelling pressure shows a tendency to decrease with the increment of initial dry density and exhibits a linear relationship for soils WKS, WBS, BLS, PTS and BTS. Very small divergence was observed on the plotted data points with a correlation coefficient  $R^2$  greater than 0.8 for all soils. It can be observed that a valuable relationship among the swelling stress and the initial dry density. The initial dry density has an impact on the magnitude of the swelling stress for compacted expansive soils. Finally, the compaction at the OMC can reduce the swelling stress by 15 %. The results revealed that the swelling stress decreases as the initial dry density increases. This seems to be in contradiction with the common engineering facts. Nevertheless, this can be justified by the fact that the swelling stress obtained upon water addition from the specimens with a smaller initial water content is higher compare to the swelling stress obtained from the specimen with higher initial water content. Furthermore, the initial dry density increases as the initial water content increase up to the OMC. Therefore, the swelling stress will decrease as the initial dry density increase up to the OMC upon addition of water.

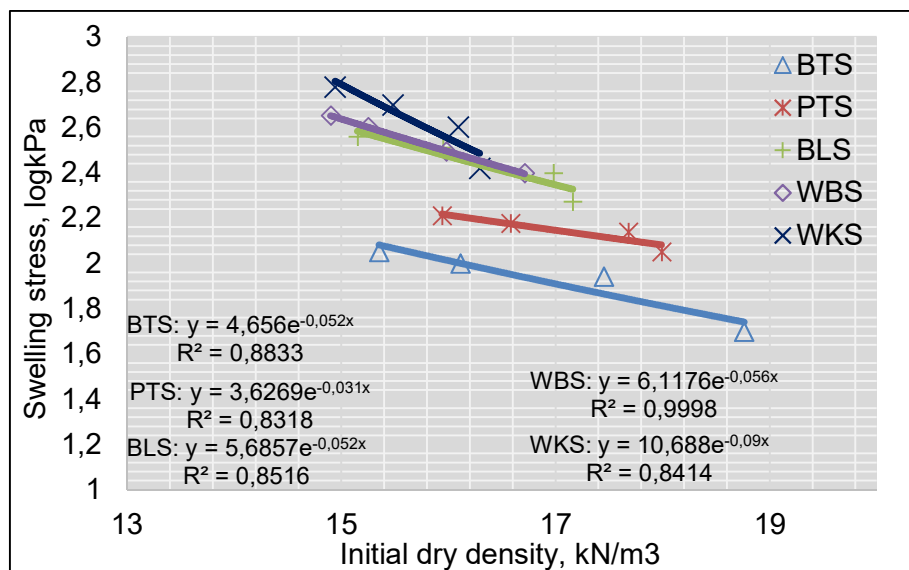
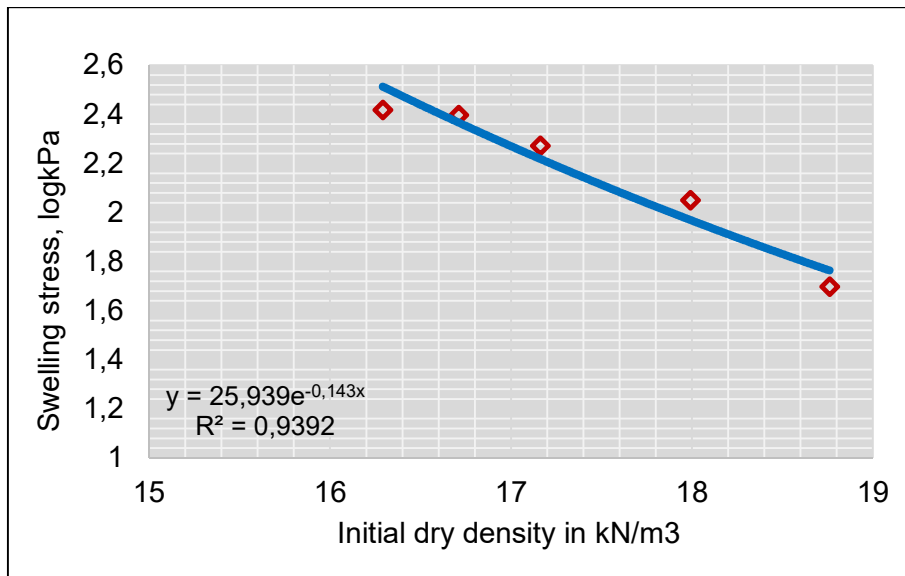


Figure 5.52: Swelling stress versus initial dry density



**Figure 5.53:** Swelling stress versus initial dry density at OMC

### 5.9.3 Analysis and discussion of the correlation between swelling stress and initial water content

To study the correlation among the swelling stress and the initial water content for natural compacted expansive soil, the values of the swelling stress were plotted against the initial water content as shown in Figure 5.54. It can be observed that there is a tendency of the decreasing of the swelling stress as the initial water content rises and shows a linear relationship for soils WKS, WBS, BLS, PTS and, BTS. Very small discrepancies between the scatter plotted data points were observed. The strength of this correlation is greater than 0.8 for all soils. There is a good correlation between the swelling stress and the initial moisture content. Nonetheless, at the optimum moisture content, the swelling stress shows a tendency to increase as the initial water content at the optimum increases for the different soils as shown in Figure 5.55. This can be explained by the fact that at the optimum moisture content the maximum air void has been reduced within the soil particles, and the dry density can no longer be enhanced by water addition. A variation of the initial water content of 8.1 % at the OMC can induce a change in swelling pressure around 212, 36 kPa. The results have revealed that the swelling stress decreases with the initial water content. This seems to be in contradiction with an established engineering fact. However, this can be justified by the fact that the swelling stress obtained upon water addition from the specimens with smaller initial water content is higher compared to the swelling stress obtained from the

specimen with higher initial water content. Therefore, the swelling stress will decrease upon an increase in initial water content. These results are in line with the results of the study conducted by Rank, Bhanderi, and Nagecha (2015) on the swelling potential of different expansive soils placed at the different dry density and initial water content. Moreover, the result is in line with the results of the study conducted by Cantillo, Mercado, and Pájaro (2017) on empirical Correlations for the swelling stress of expansive clays from the city of Barranquilla, Colombia. Nevertheless, at the OMC these results are in accordance with common engineering fact.

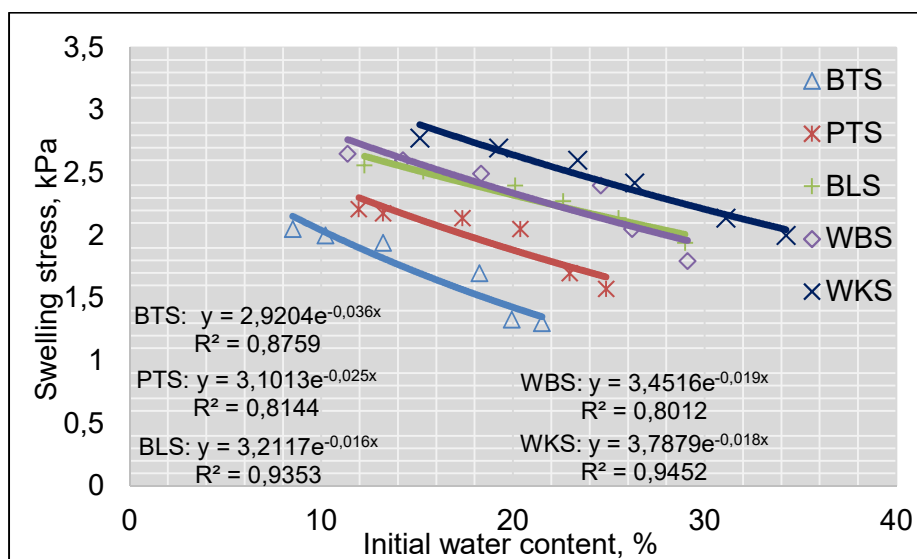


**Figure 5.54:** Swelling stress versus initial water content

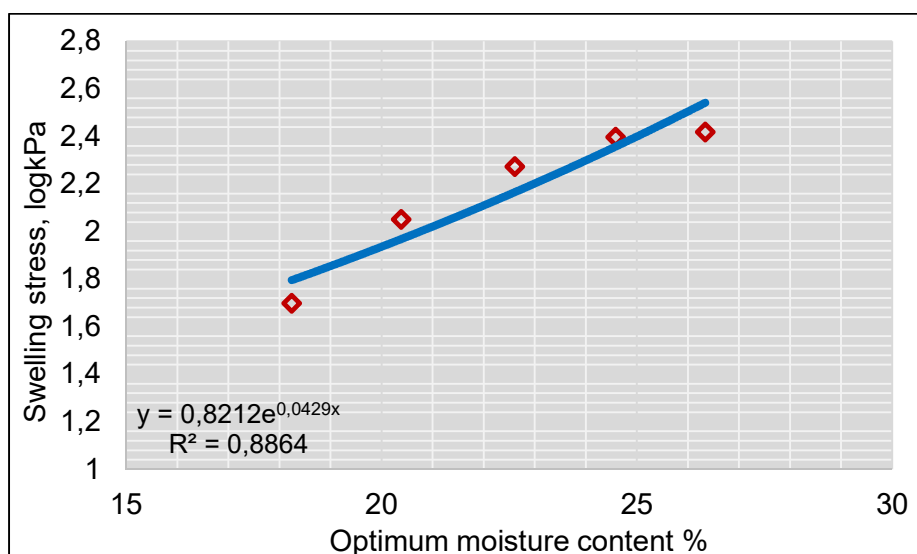


**Figure 5.55:** Swelling stress versus optimum water content

### 5.9.4 Analysis and discussion of the correlation between swelling stress and plasticity index

To evaluate the interrelation between the swelling stress and the plasticity index for compacted expansive soils at the optimum moisture content, experimental values of the swelling stress were plotted against the plasticity index as shown in Figures 5.56. It is observed a tendency of the increment of the swelling stress as the plasticity index increases and manifests a unique relationship for all soils. The increment of the plasticity index from 23.09 % to 49.87 % imparts significant increases in the values of the swelling stress from 49.88 kPa to 261.81 kPa. It is apparent that there is a good correlation between swelling stress and plasticity index since the correlation coefficient  $R^2=0.9269$  for all soil designation. The scatter of the plotted data is in good coordination with small discrepancies. Israr et al.,(2014) pointed out that the increment of plasticity limit increases significantly the swelling stress of expansive soils.

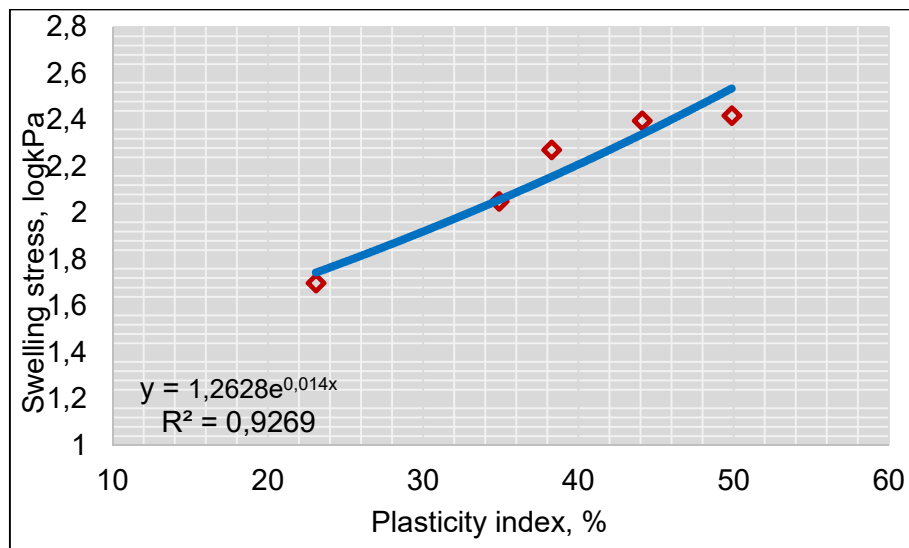


**Figure 5.56:** Swelling stress versus Plasticity index at OMC

### 5.9.5 Analysis and discussion of the correlation between swelling stress and liquid limit.

To assess the relationship between the swelling stress and the liquid limit of compacted expansive soil, the experimental values of the swelling stress were plotted against the liquid limit as shown in Figure 5.57. From the figure, we can observe a tendency of the increment of the swelling stress as the liquid limit increases and exhibited a linear relationship. The increment of the liquid limit from

48.37 % to 69.54 % reveals an important increment of the swelling stress values from 49.95 kPa to 262.29 kPa. It was observed very small discrepancies between the scatter plotted data points and a good correlation between the swelling stress and the initial dry density with a correlation coefficient  $R^2 = 0.9302$ .

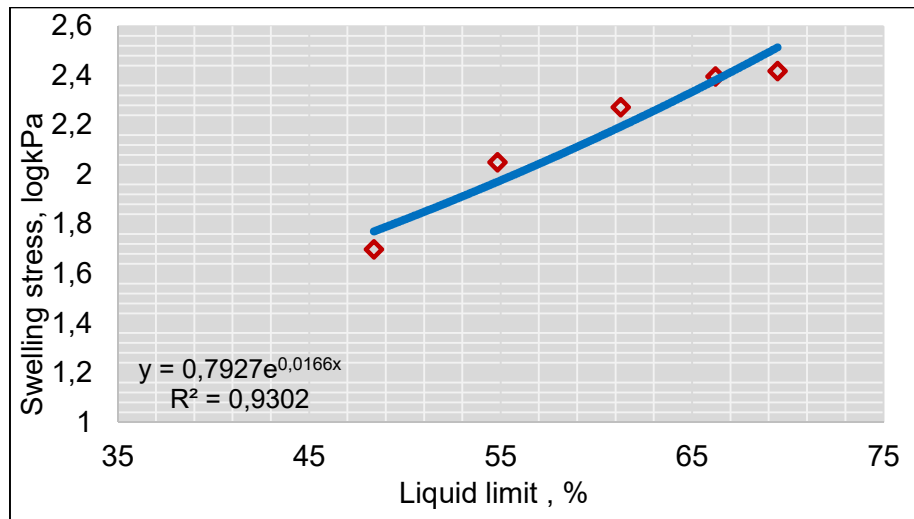


**Figure 5.57:** Swelling stress versus Liquid limit at OMC

### 5.9.6 Analysis and discussion of the correlation between swelling stress and linear shrinkage.

Plotted data shown in Figure 5.58 is used to determine the interrelation between the swelling stress and linear shrinkage of natural compacted expansive soils at the optimum moisture content. It can be observed that there is a tendency of decreasing of the swelling stress as the linear shrinkage increases. The resulting trend line is a linear function with a correlation coefficient  $R^2 = 0.908$ . The reduction of linear shrinkage from 13.89 % to 6.12 % imparts an important increment of the values of swelling stress from 49.95 kPa to 262.29 kPa. In addition, an increment of clay fraction from 20 % to 40 % leads to an important reduction of the linear shrinkage from 13.89 % to 6.12 % at the optimum moisture content. It can be concluded that as the linear shrinkage decreases, the swelling stress increases. The data set exhibits a linear relationship between the swelling stress and the linear shrinkage of high strength, and the clay fraction influence the linear shrinkage.

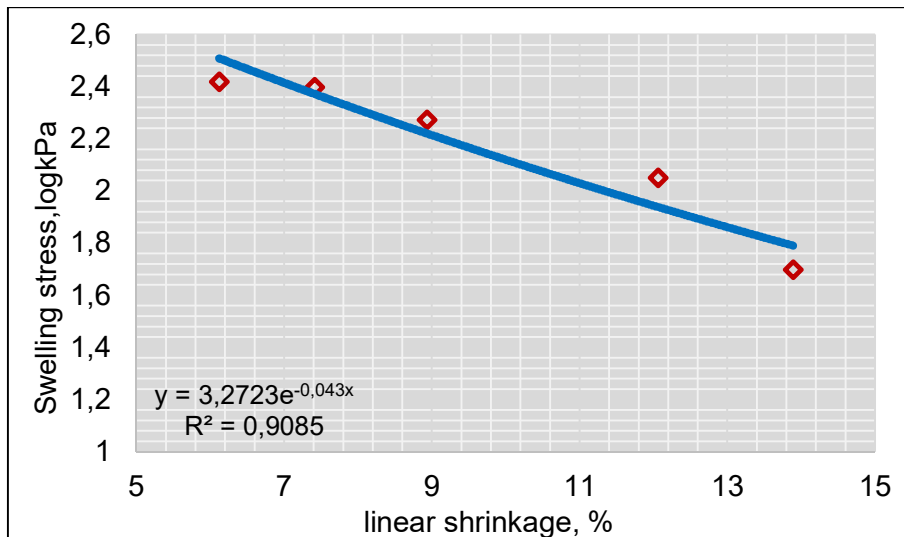


**Figure 5.58:** Swelling stress versus linear shrinkage at OMC

### 5.9.7 Analysis and discussion of the correlation between swelling stress and activity of clay.

To evaluate the interrelation between the swelling stress and the activity of clay of compacted expansive soils at the optimum moisture content, the experimental values of the swelling stress were plotted against the activity of clay as shown in Figure 5.59. It was observed a tendency of the increment of the swelling stress as the activity of clay increases and displays a unique relationship for all soils. The increment of activity of clay from 1.155 to 1.247 reveals significant increases in the values of the swelling stress from 49.88 kPa to 261.81 kPa at the optimum moisture content. The resulting trend line is a linear function with a correlation coefficient of  $R^2 = 0.8024$ .

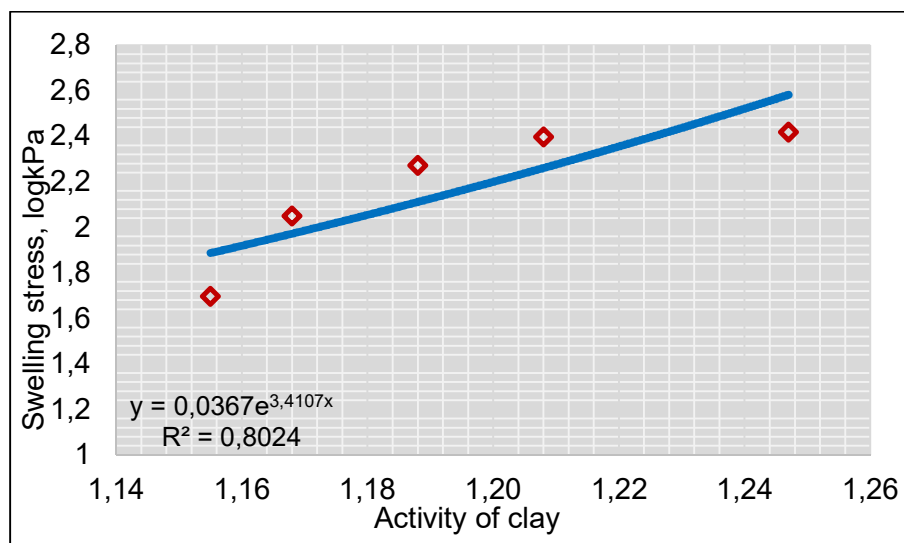


**Figure 5.59:** Swelling stress versus activity of clay at OMC

### 5.9.8 Analysis and discussion of the correlation between swelling stress and a free swell index

In order to observe how well the swelling stress and the swelling potential are related, these parameters are plotted and analyzed. The type of correlation is presented by a graph of the free swell index versus swelling stress using the experimental values as shown in Figure 5.60. The nature of the curve exhibits an increase in swelling stress with the increase of free swell index and exhibits a linear relation. The increasing of the free swell index from 48.85 % to 116.66 % reveals an increment of the values of swelling stress from 49.95 kPa to 262.29 kPa at the optimum moisture content. The result shows some discrepancies between the scatter plotted data with a correlation coefficient  $R^2 = 0.7051$ . Nonetheless, it clearly indicates the tendency of swelling stress to increase with the increment of free swell index values.

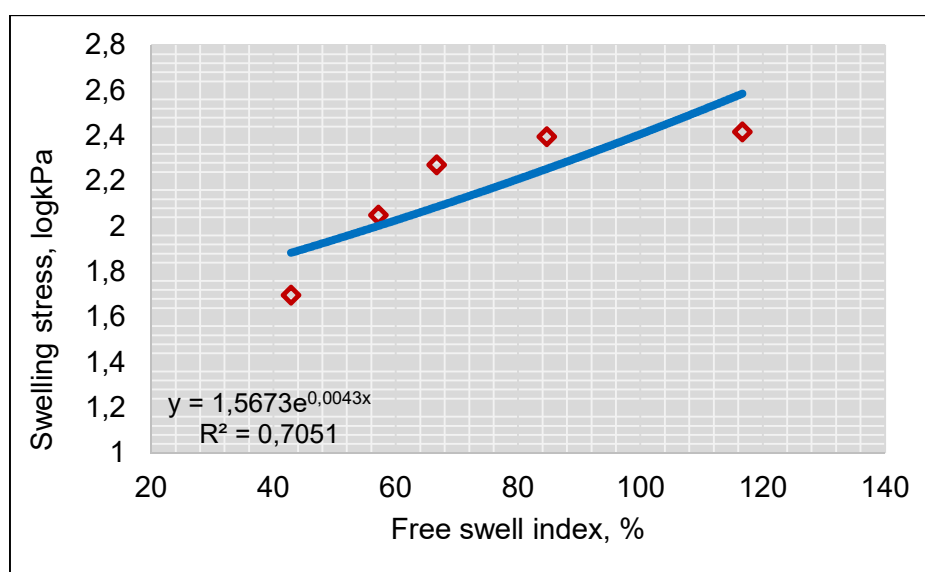


**Figure 5.60:** Swelling stress versus free swell index at OMC

### 5.9.9 Analysis and discussion of the correlation between swelling stress and free swell ratio

In order to determine the correlation between the swelling stress and the free swell ratio of compacted expansive soil, the values of the swelling stress versus free swell ratio were plotted as shown in Figure 5.61 at the optimum moisture content. The nature of the curve displays a tendency of the increment of the swelling stress as the free swell ratio increases and manifested a linear relationship. It is apparent that there is a good correlation between the swelling stress and the free swell ratio



with a correlation coefficient  $R^2 = 0.8603$ . The scatter of the plotted data is in good coordination with small discrepancies. Sridharan and Prakash (2000) pointed that the free swell ratio method is a very competitive method to assess the swelling behaviour of expansive soils and their mineralogy. The free swell ratio could be used as a parameter to predict the swelling stress of compacted expansive soil.

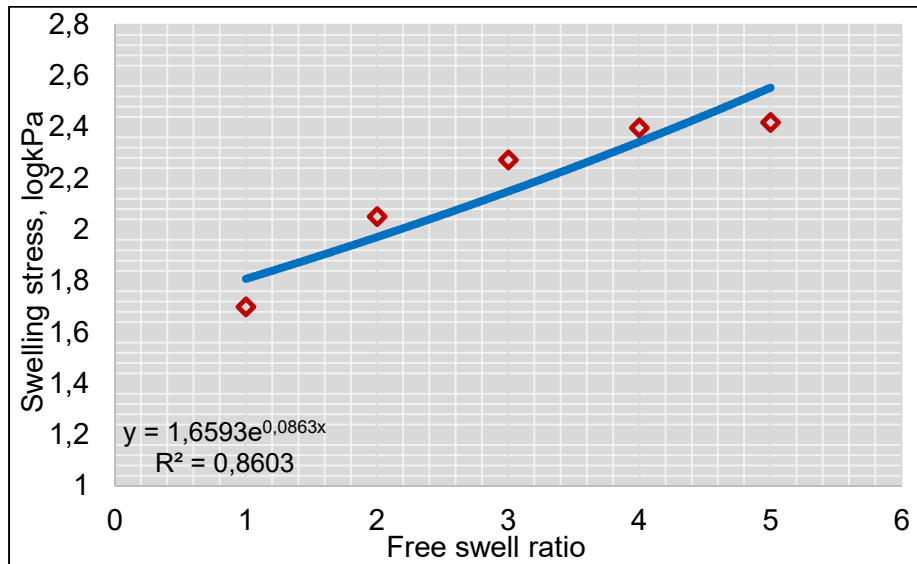


**Figure 5.61:** Swelling stress versus free swell ratio at OMC

#### 5.9.10 Analysis and discussion of the correlation between swelling stress and the clay fraction.

In order to observe how the swelling stress and the clay fraction in the soil are related, these parameters are plotted and analyzed. The type of correlation is presented by a graph of swelling pressure versus clay fraction using the experimental values as presented in Figure 5.62. As the clay percentage in the soil increases, it exhibits more swelling stress due to moisture change within the fine particles. The swelling stress is exhibited by the expansive clay mineral in the soil. As expected, the presence of the swelling clay minerals (smectite) has a great influence on the swelling stress of expansive soil. The increment of the clay content from 20 % to 40 % reveals an increment of swelling stress values from 49.95 kPa to 262.29 kPa at the optimum moisture content. The resulting trend line is a function with a correlation coefficient  $R^2 = 0.949$ , the scatter of the plotted data is in good coordination with small discrepancies.

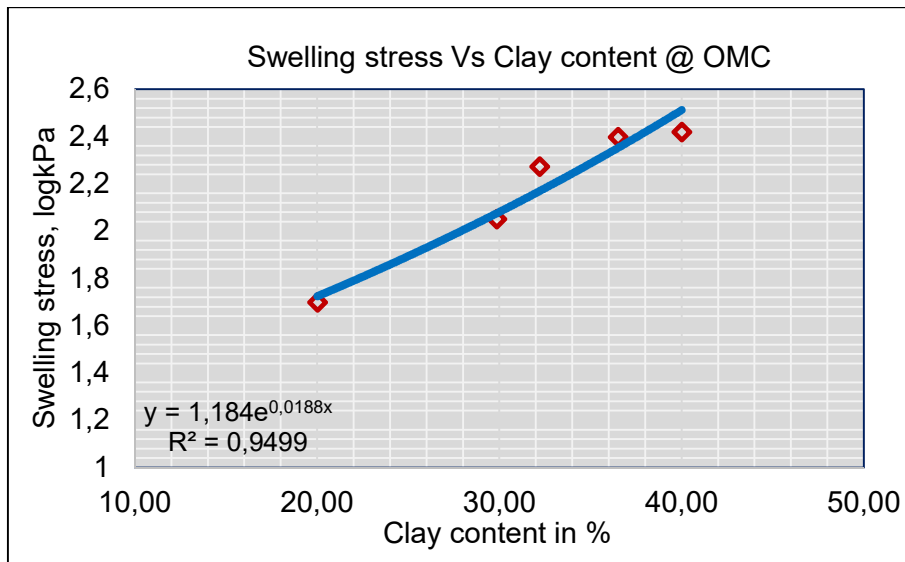


**Figure 5.62:** Swelling stress versus Clay fraction at OMC

### 5.9.11 Conclusion of the analysis and discussion of the correlation between swelling stress and soil properties.

The correlation between swelling stress, soil suction, and other soil parameters have been investigated in this section. As a result, the swelling stress of compacted expansive soils is influenced by the soil suctions, geotechnical index properties (Atterberg limits, linear shrinkage, initial water content, initial dry density, activity of clay, clay fraction), expansive soil properties (free swell index, free soil ratio), and the type of clay mineral. The resulting trend lines for all the correlations are a linear function with a correlation coefficient  $R^2 > 0.80$ . The scatter plotted data shows small discrepancies. The swelling stress of compacted expansive soils increases with the increment of matric suction, plasticity index, liquid limit, clay fraction, activity of clay, free swell index, and free swell ratio. Nonetheless, the values of the swelling stress reduce with the increments of the initial water content, initial dry density, and linear shrinkage. At the optimum moisture content, the swelling stress exhibits a stress within the range of 48.88 kPa to 261.81 kPa. Therefore, expansive soils from Free State province can produce an upward swelling stress beyond 48.88kPa, which is greater than bearing limit of the order of 40 kPa for lightweight footing hypothetically applied by most of the lightweight footing. The presence of the swelling clay mineral (smectite) has a considerable influence on the swelling stress of expansive soils.

## 5.10 Constitutive models to predict the swelling stress.

The characterization of the relation between swelling stress and soil properties was performed by investigating the nature of the correlation between the swelling stress, the suction matric, and other soil properties. Moreover, the characterization of the swelling stress and the soil properties relationship for compacted unsaturated expansive soils is achieved by developing models to predict the swelling stress with respect to the suction matric, and other soil properties such as initial water content, initial dry density, plasticity index, liquid limit, linear shrinkage, activity of clay, free swell index, and free swell ratio. A series of efficient combinations of suction matric and other soils properties are used as independent variables to develop the models as explained in chapter 4, section 4.8.

### 5.10.1 Determination of the models, multi-regression analysis coefficients, intercepts, and regression statistics.

The correlation Matrix A, and correlation Matrix B are shown respectively in Tables 5.26 found in Appendix N, and in Table 5.27 Found in Appendix O are used for multi-regression analysis.

Six models to predict the swelling stress of field compacted expansive soils were developed:

Model (1) is established with the following independent variables: matric suction ( $\psi_m$ ), liquid limit (LL), initial dry density ( $\gamma_d$ ), activity of clay ( $A_C$ ), with coefficients of correlation  $\lambda_1, \lambda_2, \lambda_3, \lambda_4$ , and the intercept  $\lambda_0$ .

Model (2) is built up with the following independent variables: matric suction ( $\psi_m$ ), initial water content ( $W_i$ ), liquid limit (LL), activity of clay ( $A_C$ ), with coefficients of correlation  $\eta_1, \eta_2, \eta_3, \eta_4$ , and the intercept  $\eta_0$ .

Model (3) is developed with the following independent variables: matric suction ( $\psi_m$ ), initial water content ( $W_i$ ), Plasticity (PI), liquid limit (LL), activity of clay ( $A_C$ ), with coefficients of correlation  $\xi_1, \xi_2, \xi_3, \xi_4, \xi_5$  and the intercept  $\xi_0$ .

Model (4) is formed with the following independent variables: matric suction ( $\psi_m$ ), plasticity index (PI), initial water content ( $W_i$ ), linear shrinkage (LS), free swell ratio (FSR), with coefficients of correlation  $\zeta_1, \zeta_2, \zeta_3, \zeta_4, \zeta_5$  and the intercept  $\zeta_0$ .

Model (5) is developed with the following independent variables: matric suction ( $\psi_m$ ), initial water content ( $W_i$ ), liquid limit (LL), plasticity index (PI), linear shrinkage (LS), activity of clay ( $A_C$ ), with coefficients of correlation  $\beta_1, \beta_2, \beta_3, \beta_4, \beta_5, \beta_6$ , and the intercept  $\beta_0$ .

Model (6) is established with the following independent variables: matric suction ( $\psi_m$ ), initial water content ( $W_i$ ), liquid limit (LL), linear shrinkage (LS), activity of clay ( $A_C$ ), initial dry density ( $\gamma_d$ ), and free swell index (FSI), with coefficients of correlation  $\mu_1, \mu_2, \mu_3, \mu_4, \mu_5, \mu_6, \mu_7$ , and the intercept  $\mu_0$ .

The values of regression analysis coefficients, intercepts, and regression statistics information are given in Tables 5.28 and 5.29 found in Appendix O

**Table 5.25:** Estimated models

Models	Estimated equations
Model 1	$\log(P_S) = \lambda_0 + \lambda_1 \log(\psi_m) + \lambda_2(LL) + \lambda_3(\gamma_d) + \lambda_4(A_C)$ (5.7)
Model 2	$\log(P_S) = \eta_0 + \eta_1 \log(\psi_m) + \eta_2(W_i) + \eta_3(LL) + \eta_4(A_C)$ (5.8)
Model 3	$\log(P_S) = \xi_0 + \xi_1 \log(\psi_m) + \xi_2(W_i) + \xi_3(PI) + \xi_4(LL) + \xi_5(A_C)$ (5.9)
Model 4	$\log(P_S) = \zeta_0 + \zeta_1 \log(\psi_m) + \zeta_2(PI) + \zeta_3(W_i) + \zeta_4(LS) + \zeta_5(FSR)$ (5.10)
Model 5	$\log(P_S) = \beta_0 + \beta_1 \log(\psi_m) + \beta_2(W_i) + \beta_3(LL) + \beta_4(PI) + \beta_5(LS) + \beta_6(A_C)$ (5.11)
Model 6	$\log(P_S) = \mu_0 + \mu_1 \log(\psi_m) + \mu_2(W_i) + \mu_3(LL) + \mu_4(LS) + \mu_5(A_C) + \mu_6(\gamma_d) + \mu_7(FSI)$ (5.12)

Where:

$P_S$  = swelling stress in , kPa,

$\psi_m$  = matric suction in , kPa,

PI = plasticity index in , %,

LL = liquid limit in , %,

LS = linear shrinkage in , %,

$W_i$  = Initial water content in , %,

$\gamma_d$  = Dry density in ,  $\text{kN/m}^3$ ,

$A_C$  = Activity of the clay,

FSR = Free swell ratio,

FSI = Free swell index in , %,

$\lambda_i, \eta_i, \xi_i, \zeta_i, \beta_i, \mu_i$ , are multi – regression coefficients,  $i = 1, \dots, n$ ., and

$\lambda_0, \eta_0, \xi_0, \zeta_0, \beta_0, \mu_0$ , are intercepts.

### 5.11 Validation of the models.

Considering the problematic behaviour of heaving soils, the parameters that influence it, the main objective would be to validate the models used to predict the swelling stress of compacted expansive soils proposed in this research work. The validation of the proposed models is done by comparing the results obtained from predictive models and the values obtained from experiments. Moreover, the validation of the developed models is done graphically by comparing the predicted values of the swelling stress obtained from the developed models, and predictive values obtained from other models developed by Tu and Vanapalli (2016), Yusuf and Orhan (2007), and Forouzan (2016).

#### 5.11.1 Model validation by comparing predicted swelling stress values to the values obtained from the experimental works

Several soil properties influence the swelling stress of compacted expansive soils as mentioned previously. The ultimate objective would be to validate the models proposed in this current study. The validation of the proposed models is conducted by comparing the experimental values of the swelling stress obtained from the zero - swell test (ZST) and the results obtained from predictive models. Graphical observation of Figures 5.63 to 5.68 shows that the scatter of results points generally follows the trend of 1:1 line for the six models. The scatter of the plotted data points not only shows a good correlation with respect to the experimental values, and exhibits very small disparities among themselves. Tables 5.26 and 5.27 shows that, for all the developed models, the correlation coefficient  $R^2$  exceeds 0.8, the relative standard deviator less than 3 %, and the mean square error equal to 0. It is apparent that there is a very good correlation between the experimental and predicted values. It is shown that the predicted values of the

swelling stress based on the proposed model agree closely with the experimental results of this study.

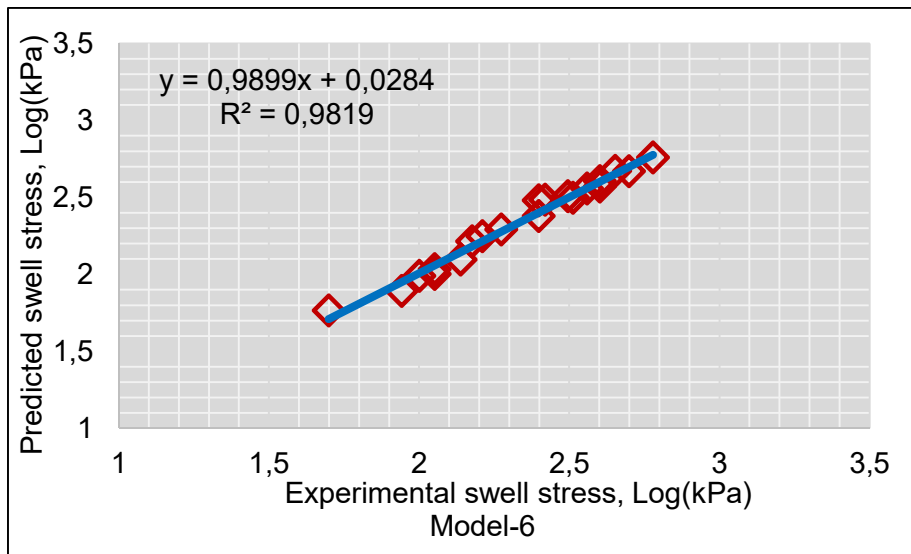


**Figure 5.63:** Comparison between experimental and predicted values of swelling Stress (model 6).

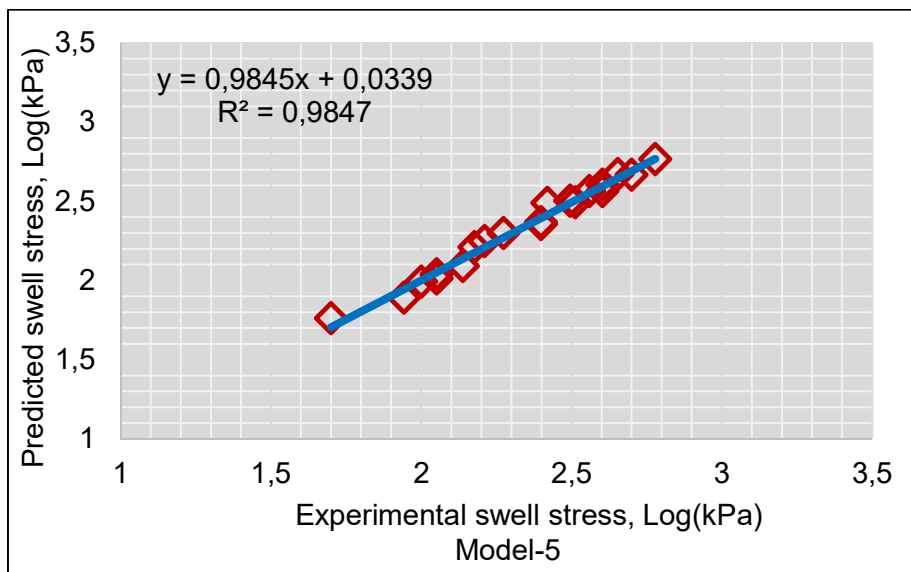


**Figure 5.64:** Comparison between experimental and predicted values of swelling Stress (model 5).

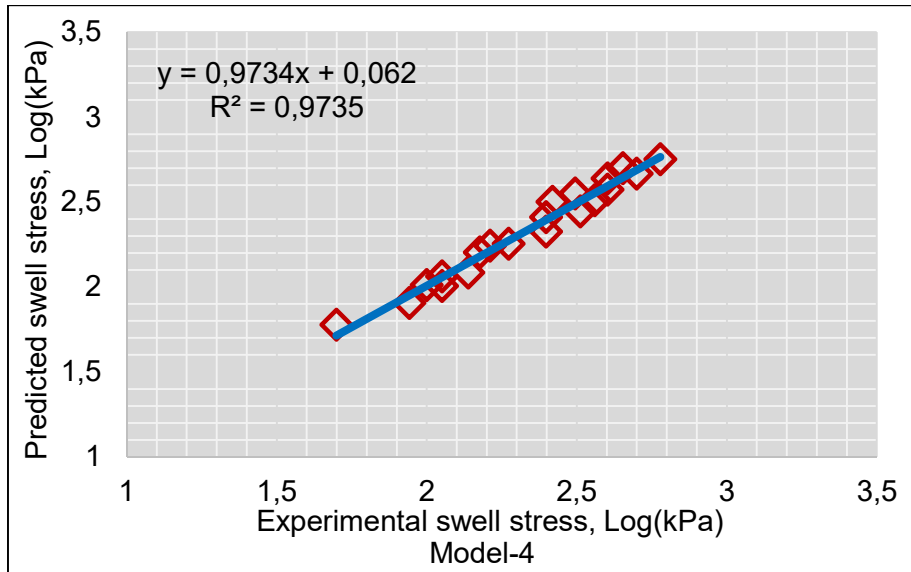


**Figure 5.65:** Comparison between experimental and predicted values of swelling Stress (model 4)

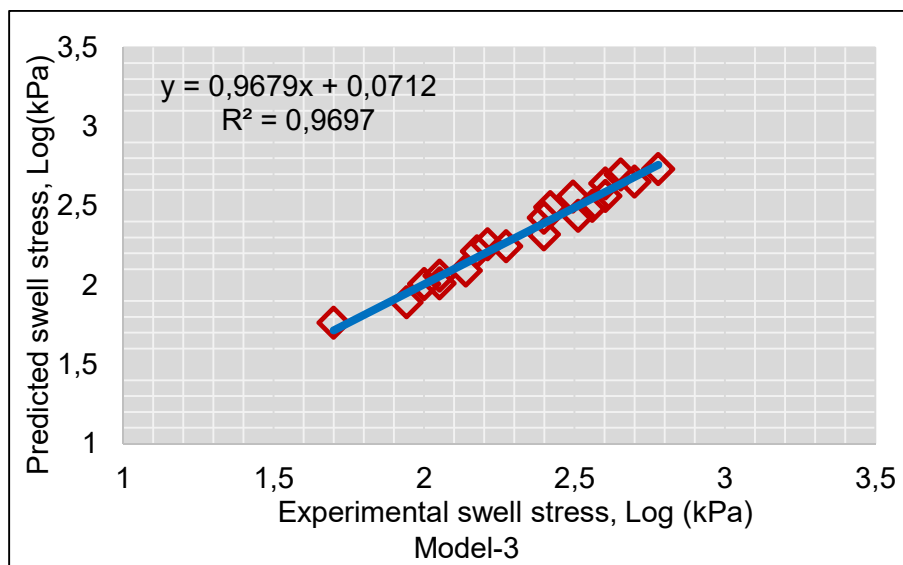


**Figure 5.66:** Comparison between experimental and predicted values of swell Stress (model 3)



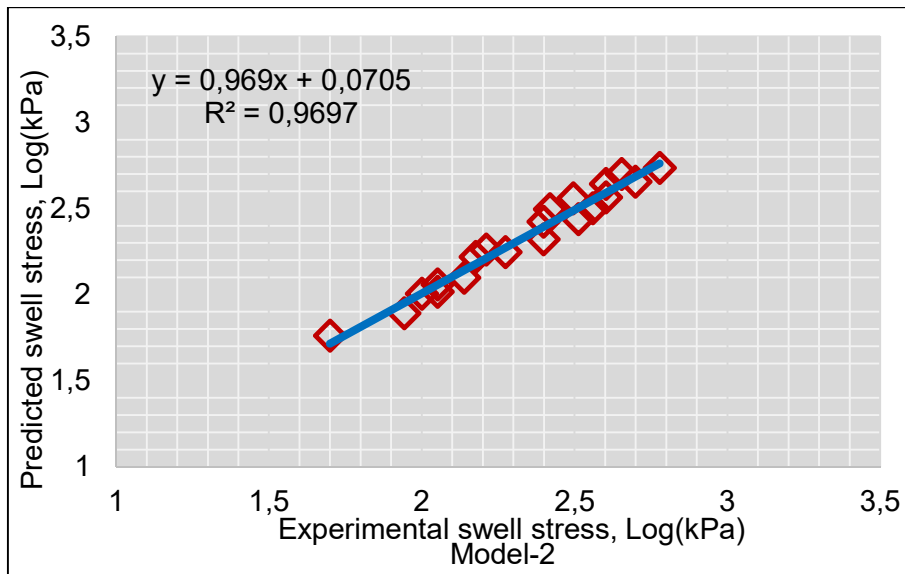


**Figure 5.67:** Comparison between experimental and predicted values of swelling Stress (model 2)

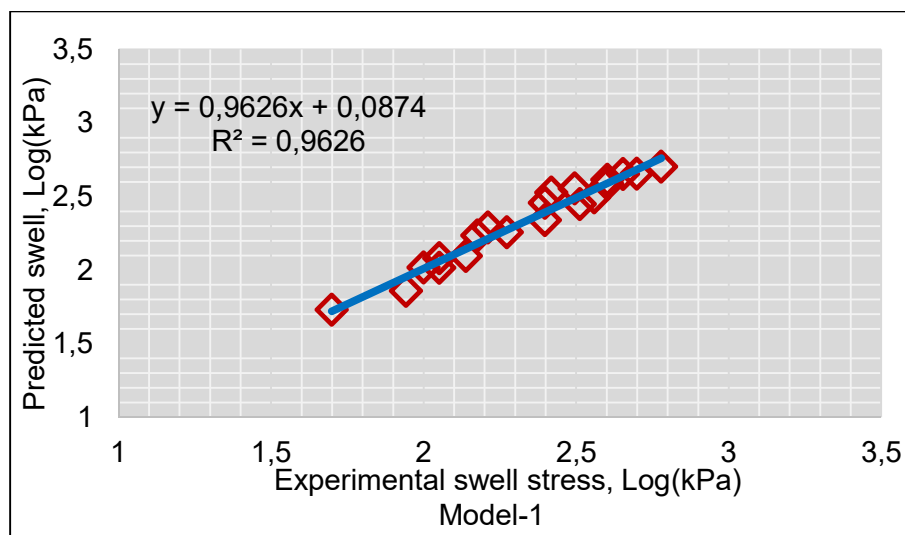


**Figure 5.68:** Comparison between experimental and predicted values of swelling stress (model 1)

### 5.11.2 Model validation by comparing predicted values of swelling stress to the results obtained from other models.

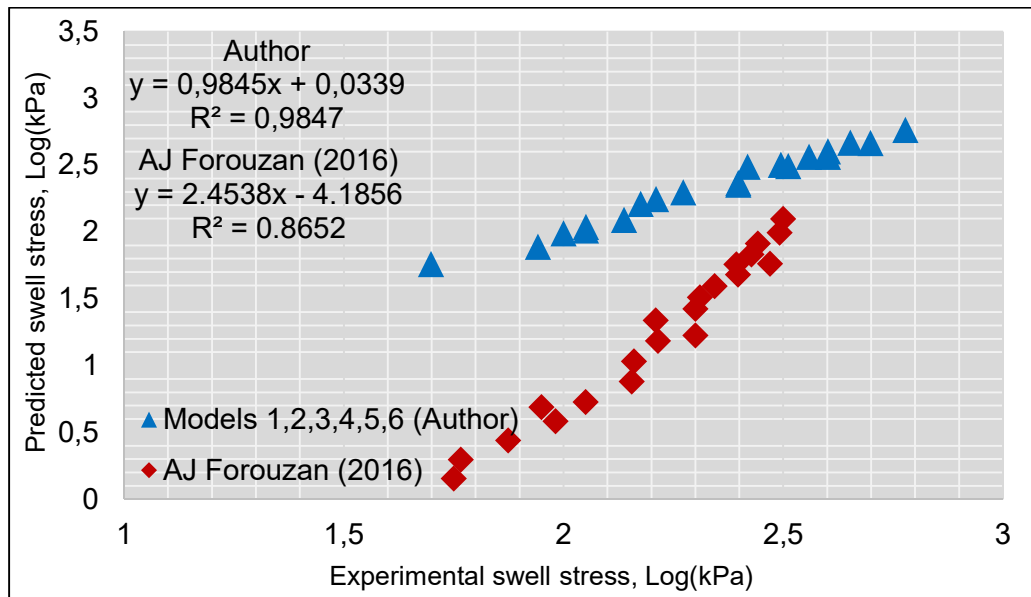
Figures 5.69 to 5.71 shows a graphical comparison between the predicted values of the swelling stress obtained from the models developed in this research work and models proposed by Tu and Vanapalli (2016), Yusuf and Orhan (2007), and Forouzan (2016).

Figure 5.69 shows a graphical comparison between the predicted values of the swelling stress from the models proposed in this study and the predictive model as proposed by Forouzan (2016). It can be observed that the models proposed in this study portrays a better correlation between the experimental and the predicted swelling stress values than the model previously proposed by Forouzan (2016). Furthermore, the proposed models displays data point close to 1:1 line. These discrepancies can be justified by the type of specimens used to develop the models. The models proposed in this study are developed using a field compacted expansive soils, whereas the model developed by Forouzan (2016) is built on artificial compacted expansive soils obtained by mixing kaolinite and bentonite. Moreover, the matric suction is not considered as a dependent variable in the model proposed by Forouzan (2016).

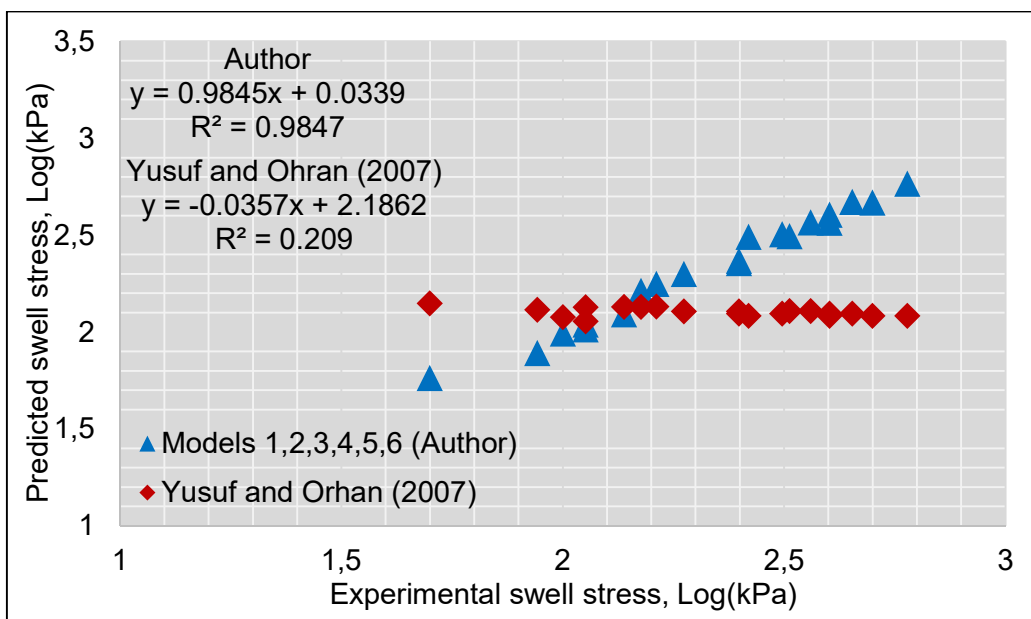
Figure 5.70 shows a graphical comparison between the predicted values of the swelling stress from the models designed in this research work and the predicted values obtained from models developed by Yusuf and Orhan (2007). The models proposed in this study illustrated a better relationship between experimental and predictive values of the swelling stress, unlike formerly model proposed by Yusuf and Orhan (2007) which exhibits a very small correlation coefficient. In addition, data plotted for the models proposed in this study are very close to 1:1 line. These disparities can be explained by the nature and the type of soil material used for the experiment. The model proposed by Yusuf and Orhan (2007) was developed using artificial soil obtained by mixing the sodium bentonite with kaolinite, while the models proposed in this current study are established using field compacted expansive soils.

Figure 5.71 shows a graphical comparison between the predicted values of swelling stress from the constitutive models developed in this study and the predictive models proposed by Tu and Vanapalli (2016). The models proposed in this research work portrays a better correlation between experimental and predicted values of swelling stress. The data plotted points are close to 1:1 line, like the model previously propose by Tu and Vanapalli (2016). These similarities can be explained by the type of specimen used to develop these models. The models proposed in this study are developed using field compacted expansive soils as the model previously proposed by Tu and Vanapalli (2016).

Conclusively, good correlation between predictive and experimental results acknowledges that the models proposed in this research work are capable to estimate the swelling stress with acceptable accuracy. The graphical comparison demonstrates a better correlation of the models developed in this research work than the models previously proposed by Forouzan (2016); Yusuf and Orhan (2007). Nevertheless, some similarities were observed with the results obtained from the model proposed by Tu and Vanapalli (2016).



**Figure 5.69:** Comparison of predicted values of swelling stress from proposed models, and predictive model by Forouzan (2016).



**Figure 5.70:** Comparison of predicted values of swelling stress from proposed models, and predictive model by Yusuf and Orhan (2007).

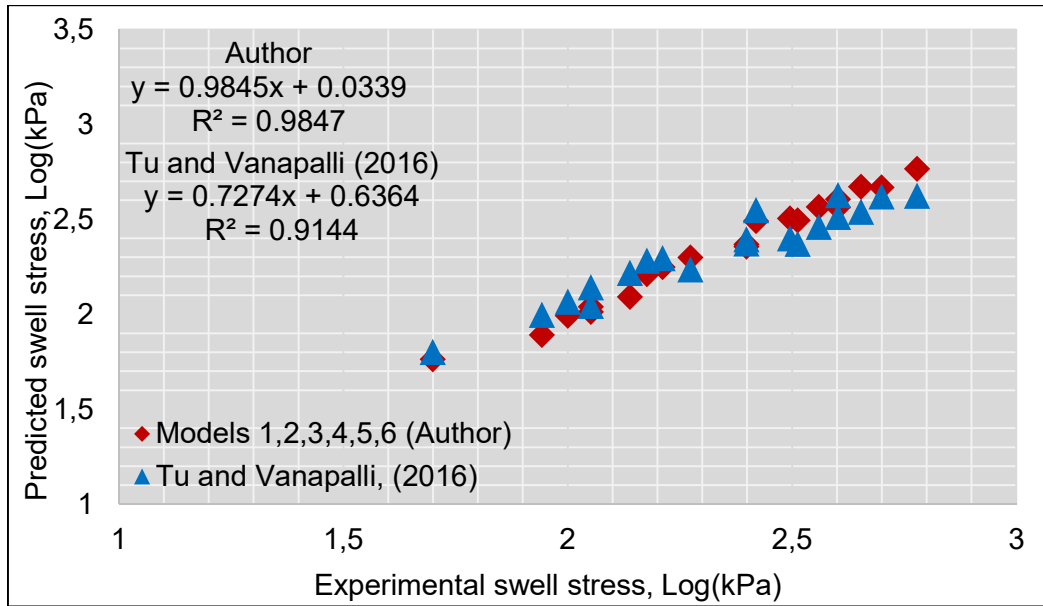


**Figure 5.71:** Comparison of predicted values of swelling stress from proposed models, and predictive model by Tu and Vanapalli (2016).

---

## CHAPTER 6: CONCLUSION AND PERSPECTIVES

### 6.1 Summary

The main objective of this study was to characterize the relationship between the swelling stress, the suction matric, and other soil parameters. Moreover, develop models to predict the swelling stress of compacted expansive soils. To achieve this aim, laboratory experiments such as particle size distribution, Atterberg limits, linear shrinkage, free swell index, free swell ratio, specific gravity, X-ray diffraction, modified Proctor compaction test, suction measurement, and zero-swell test (ZST) were conducted to assess the physical and hydromechanical properties of soil samples.

The data obtained from laboratory experiments were analyzed by multiple regression analysis using software NCSS11. Correlations were established between the swelling stress and the soil properties such as the matric suction, the geotechnical index properties, and the expansive soil parameters. Moreover, six mathematical models were proposed in this research work.

The validation of these models was conducted by comparing the predicted values obtained from the proposed models and the predicted values obtained from other existing models.

### 6.2 Conclusions

It was observed that, on the dry side of the OMC, there is an increase of the swelling stress of field compacted expansive soils as the matric suction increases. Nevertheless, the swelling stress reduces on the dry side of the OMC as the initial water content, the initial dry density, and the linear shrinkage increases upon water addition.

At the OMC, the swelling stress increases with the increment of plasticity index, liquid limit, activity of clay, free swell ratio and free swell index. Besides, at the OMC as the swelling stress values are within the range of 48.88 kPa to 261.81 kPa, and simultaneously, the matric suction values are within the range of 222.843 kPa to 1,778.27 kPa. The swelling stress values on the dry side of the OMC are higher than the values on the wet side.

The results obtained from this study revealed that the type of clay mineral have a key influence on the swelling stress. In addition, the soil suction, the geotechnical index properties, and the expansive parameters have a significant influence on the swelling stress of compacted expansive soils. However, it was observed that the compaction of expansive soil at the OMC can reduce the swelling stress of field compacted expansive soils by 15 %.

Free State field compacted expansive soils produce upward swelling stress within the range of 48.88 kPa to 261.81 kPa which is greater than the bearing limit of the order of 40 kPa applied for most lightweight footing. Moreover, the matric suction in these soils is within the range of 222.843 kPa to 1,778.27 kPa.

Lastly, good correlations were obtained from the proposed models. Data points are close to 1:1 line, the standard deviator < 3%, the mean squared error equal to 0, and the correlation coefficient  $R^2 > 0.8$ . Besides, the graphical comparison demonstrates a good correlation of the developed models. These models can be used as a reliable tool to predict the swelling stress with acceptable accuracy.

**6.3 Perspectives**

The experimental data obtained from this research work can be used to model the behaviour of compacted unsaturated expansive soils as continuum material using finite element analysis.

It would be interesting to study the influence of the swelling stress on the unsaturated shear strength of field compacted expansive soils.

As a final conclusion, six mathematical models are proposed in this study and can be used in engineering practice to address issues related to foundation design in expansive soils.

$$\log(P_s) = \lambda_0 + \lambda_1 \log(\psi_m) + \lambda_2(LL) + \lambda_3(\gamma_d) + \lambda_4(A_C) \dots \dots \dots \text{(Model 1)}$$

$$\log(P_s) = \eta_0 + \eta_1 \log(\psi_m) + \eta_2(W_i) + \eta_3(LL) + \eta_4(A_C) \dots \dots \dots \text{(Model 2)}$$

$$\log(P_s) = \xi_0 + \xi_1 \log(\psi_m) + \xi_2(W_i) + \xi_3(PI) + \xi_4(LL) + \xi_5(A_C) \dots \dots \dots \text{(Model 3)}$$

$$\log(P_s) = \zeta_0 + \zeta_1 \log(\psi_m) + \zeta_2(PI) + \zeta_3(W_i) + \zeta_4(LS) + \zeta_5(FSR) \dots \dots \dots \text{(Model 4)}$$

$$\log(P_s) = \beta_0 + \beta_1 \log(\psi_m) + \beta_2(W_i) + \beta_3(LL) + \beta_4(PI) + \beta_5(LS) + \beta_6(A_C) \dots \dots \dots \text{(Model 5)}$$

$$\log(P_s) = \mu_0 + \mu_1 \log(\psi_m) + \mu_2(W_i) + \mu_3(LL) + \mu_4(LS) + \mu_5(A_C) + \mu_6(\gamma_d) + \mu_7(FSI) \dots \dots \dots \text{(Model 6)}$$

**REFERENCES:**

- Abed, AA and Vermeer, PA. 2009. Numerical simulation of unsaturated soil behaviour. *International Journal of Computer Applications in Technology*, 34(1), pp 2-12.
- Al-Rawas, AA and Goosen, MFeds. 2006. *Expansive soils: recent advances in characterization and treatment*. Taylor & Francis.
- ASTM, D. 2014. Standard test methods for one-dimensional swell or collapse of soils. *D4546-14*.
- ASTM, A. 2009. D6913-04 Standard test methods for particle-size distribution (gradation) of soils using sieve analysis, ASTM Stand. Int.
- ASTM, 2016. Standard test method for particle-size distribution (gradation) of fine-grained soils using the sedimentation (hydrometer) analysis. *D7928-16*.
- ASTM, 2005. ASTM D4318, standard test method for liquid limit, plastic limit, and plasticity index of soils.
- ASTM, D2010. Standard test methods for specific gravity of soil solids by water pycnometer. *D854*.
- ASTM, 1991. Standard test method for measurement of soil potential (suction) using paper filter, ASTM D5298. *Annual Book of ASTM Standards*.
- Atterberg, AM. 1911. Über die physikalische Bodenuntersuchung und über die Plastizität der Tone. *Int. Mitt. Bodenkinde*, 1.
- Basma, AA., Al-Homoud, AS and Malkawi, AH. 1995. Laboratory assessment of swelling pressure of expansive soils. *Applied Clay Science*, Vol.9, pp 355-368.
- Basu, R and Arulanandan, K. 1974. A new approach for the identification of swell potential of soils. *Bulletin of the Association of Engineering Geologists*, 11: pp 315-330.
- BIS, I.1977. 2720 Methods of Test for Soils: Part 40 Determination of Free Swell Index of Soils.

- BRE. 1993. Low-rise buildings on shrinkable clay soils, *RE Digests*, pp 240-242.
- Brindley, GW and Brown, G. 1984. Crystal Structures of Clay Minerals and Their X-ray Diffraction Identification. *London: Mineralogical Society*. 495 p.
- BS, 5930 .1981. Code of practice for site investigations. British Standard Institution, London.
- Cameron, RE and Van Ee, JJ. 1992. *Guide to site and soil description for hazardous waste site characterization: Metals*. Environmental Monitoring Systems Laboratory, Office of Research and Development, US Environmental Protection Agency.
- Cantillo, V., Mercado, V and Pájaro, C. 2017. Empirical Correlations for the Swelling Pressure of Expansive Clays in the City of Barranquilla, Colombia. *Earth Sci. Res. J*, 21(1).
- Carter, M and Bentley, SP. 1991. Correlation of soil properties. Pentech Press, London. Casagrande, A. (1932).
- Chandler, RJ and Gutierrez, CI. 1986. The Filter Paper Method of Suction Measurement". *Géotechnique* 36 (2), pp 265-268.
- Chen, FH. 1973. The basic physical property of expansive soils. Proc. of the 3<sup>rd</sup> Int. Conf. on Expansive soils, Haifa, Israel, 1, pp 17-25.
- Chleborad, AF., Diehl, SF and Cannon, SH. 2005. *Geotechnical properties of selected materials from the Slumgullion landslide*.
- Crilly, MS and Driscoll, RMC. 2000. The behaviour of lightly loaded piles in swelling ground and implications for their design. *Proceedings of the Institution of Civil Engineers-Geotechnical Engineering*, 143(1), pp 3-16.
- Das, BM. 2002. Principles of geotechnical engineering, Thomson learning's California State University, Sacramento fifth edition. Ch2, pp 15-50.
- Das, BM. 2008. Advanced Soil Mechanics. 3rd Ed., *Taylor and Francis Group, New York, USA*.



- 
- Davies, JT and Rideal, EK. 1963. Interfacial Phenomena, 2<sup>nd</sup> ed., *Academic, New York, 584pp.*
- Deryagin, BV and Churaev, NV. 1987. Structure of water in thin layers. *Langmuir*, 3(5), pp 607-612.
- Department of Local Government, Housing and Works. 1990. Layman's Guide to Problem Soils, pp 37- 49.
- Diop, S., Stapelberg, F., Tegegn, K., Ngubelanga, S and Heath, L. 2011. A review on problem soils in south Africa. *Council for Geoscience*, 6, pp.1-48.
- Dregne, HE. 1976. Soils of arid regions. American Elsevier Publishing Company Inc, New York.
- Elisha, AT. 2012. Prediction of Swell Pressure of Black Cotton Soil of North-eastern Nigeria. *Electronic Journal of Geotechnical Engineering*, 17, pp1731-1739.
- Fattom, M and Barakat, S. 2000. Investigation of Three methods for Evaluating Swelling pressure of Soils, *Environmental & Engineering Geoscience* 5(3), pp 293-299.
- Forouzan, AJ. 2016. Prediction of Swelling Behavior of Expansive Soils Using Modified Free Swell Index, Methylene Bue and Swell Oedometer Test. *Middle East Technical University*.
- Fredlund, DG. 1979. Appropriate concepts and technology for unsaturated soils, Second Canadian Geotechnical Colloquium, *Canadian Geotechnical Journal* 16 (1), pp 121-139.
- Fredlund, DG and Hasan, J. 1979. One-dimensional Consolidation Theory: Unsaturated soils, *Can. Geotech* 16 (2), pp 521-531.
- Fredlund, DG. 1987. The stress state for expansive soils. In proc. 6<sup>th</sup> int. conf. Expansive soils, keynote Address, pp 1-9. December 1-3 New Delhi, India.
- Fredlund, DG and Rahardjo, H. 1987. Soil mechanics principles for highway engineering in Arid Regions. *Transportation Res. Records* 1137, pp 1-11.

- Fredlund, DG and Rahardjo, H. 1993. Soil mechanics for unsaturated soils. John Wiley & Sons, USA.
- Fredlund, DG and Xing, A. 1994. Equation for soil-water characteristic curve, *Canadian Geotechnical Journal*, 31 (3), pp 521-532.
- Fredlund, DG and Morgenstern, NR. 1977. Stress state variables for unsaturated soils. *Journal of Geotechnical and Geoenvironmental Engineering*, 103 (ASCE 12919).
- Fredlund, DG., Rahardjo, H and Fredlund.MD. 2012. Unsaturated Soil Mechanics in Engineering Practice. *John Willey & Sons, Inc.* ISBN: 978-1-118-13359-0 (Hardcopy). 926pp.
- Fredlund, MD. 1994. The role of unsaturated soil property functions in the practice of unsaturated soil mechanics. Ph.D. Dissertation, University of Saskatchewan, Saskatoon, SK, Canada.
- Fredlund, DG and Rahardjo, H. 1993. *Soil Mechanics for Unsaturated Soils*, John Wiley & Sons, Inc, pp 1 - 77, 247 -258.
- Fredlund, DG. 2000. The implementation of unsaturated soil mechanics into geotechnical engineering, The R.M. Hardy Address, *Canadian Geotechnical Journal*, 37(5), pp 963 - 986.
- Gens, A., Alonso, EE and Lloret, A. 1995. Effect of structure on the volumetric behaviour of a compacted soil. In *Proceedings Of the first International Conference on Unsaturated Soils / Unsat'95 / Paris / France / 6-8 September 1995. Volume 1.*
- Grim, RE. 1968. Clay Mineralogy McGraw-Hill. New York, p.206.
- Houston, SL, Houston, WN and Wagner, A. 1994. Laboratory filter paper suction measurements, *Geotechnical Testing Journal*, 17(2), pp185-194.
- Holtz, WG, 1954. Engineering properties of expansive clays. *Transactions of the American Society of Civil Engineers* , 121 , pp 641-677.

- Holtz, RD., Kovacs, WD and Sheahan, TC. 1981. *An introduction to geotechnical engineering* (Vol. 733). Englewood Cliffs, NJ: Prentice-Hall.
- Israelachvili, JN. 1991. Intermolecular and Surface Forces, 2<sup>nd</sup> ed., *Academic press, New York*.
- Israr, J., Farooq, K and Mujtaba, HH. 2016. Modelling of swelling parameters and associated characteristics based on index properties of expansive soils. *Pakistan Journal of Engineering and Applied Sciences*.
- Jennings, JEB and Knight, K. 1957. The prediction of total heave from the double oedometer test, Proc. Symp. Expansive Clays. SAICE, Johannesburg, 7(9), pp 13-19.
- Jones, L.D. and Jefferson, I. 2012. Expansive soils.
- Johnson, LT and Snethen, DR. 1978. Prediction of potential heave of swelling soil. *Geotechnical Testing Journal*, 1(3), pp 117-124
- Johnson, LD. 1973. Review of literature on expansive clay soils, US. Army Eng, waterways Exp.sta. Vicksburg, Ms, Misc. Paper S, pp 73-17.
- Jones, LD and Jefferson, I. 2012. Expansive soils. ICE Manual of Geotechnical Engineering .Institution of civil Engineers, [www.icemanuals.com](http://www.icemanuals.com); Ch 33, pp 413- 438.
- Jones, LD. 1999. A Shrink/Swell classification for UK clay soils. Unpublished B.Eng. Thesis. Nottingham Trent University, UK.
- Johnson, RA. 2005. Miller and Freund's probability and statistics for engineers. Seventh edition, Prentice Hall, Englewood Cliffs, New Jersey.
- Kaye, GWC and Laby, TH. 1973. Tables of Physical. *Chemical Constants*.
- Kariuki, PC and Van Der Meer, F. 2004. A unified swelling potential index for expansive soils. *Engineering geology*, 72(1-2), pp1-8.
- Kassif, G and Baker, R. 1971. Aging effects on swell potential of compacted clay. J.Soil Mechanics and Foundation Div., ASCE, SM 3: pp 529-540.

- Katti, RK., Kulkarni, SK and Fotedar, SK. 1969. Shear strength and swelling pressure characteristics of expansive soils. *Proceeding of the second International Research and Engineering Conference on expansive soils*, pp 334-347. Texas.
- Komornik, A and David, D. 1969. Prediction of swelling pressure of clays. *J. Soil Mech. Found. Div., Am. Soc. Civ. Eng.:(United States)*, 95.
- Kyklema, J. 2000. Fundamentals of Interface and Colloid Science, Volume III, Liquid-Fluid Interface, *Academic, New York*.
- Lambe, TW and Whitman, RV. 1969. Soil mechanics. John Willey & Sons. Inc., New York, 553.
- Lambe, TW and Whitman, RV. 1979. *Soil Mechanics*, Wiley, New York.
- Lang, ARG. 1967. Osmotic coefficients and water potentials of sodium chloride solutions from 0 to 40 C. *Australian Journal of Chemistry*, 20(9), pp 2017-2023.
- Leong, EC., He, L and Rahardjo, H. 2002. Factors affecting the filter paper method for total and matric suction measurements. *Geotechnical Testing Journal*, 25(3), pp 322-333.
- Ling, NL and Toll, DG. 2000. Suction and Strength Behaviour of Unsaturated Calcrete, Unsaturated Soils for Asia, Rahardjo, Toll & Leong (Eds), pp 533-538.
- Meigs, P. 1953. World distributions of arid and semi-arid homoclimates, in Review of research on arid zone hydrology. *Arid zone program*, 1,, pp 203-209.
- Mitchell, JK. 1976. Fundamentals of soil behaviour, John Willy, New York.
- Mitchell, JK. 1979. In situ techniques for site characterization, Proc. of ASCE Specially Workshop Site Charact. Exp., Evanston, pp 107-129.
- Mitchell, J.K. 1993. *Fundamentals of soil behavior* (No. Ed. 2). John Wiley and Sons, Inc.

- Murray, HH. 2007. Occurrences, processing and application of kaolins, bentonites, palygorskite-sepiolite, and common clays. *Applied Clay Mineralogy*. Elsevier, Amsterdam.
- Murthy, VNS. 2002. *Geotechnical engineering: principles and practices of soil mechanics and foundation engineering*. CRC press.
- Nelson, JD and Miller, DJ. 1992. *Expansive Soils: Problems and Practice in Foundation and Pavement Engineering*. John Wiley & Sons, Inc., New York.
- Nelson, JD., Overton, DD and Durkee, DB. 2001. Depth of wetting and the active zone. *Expansive clay soils and vegetative influence on shallow foundations*, ASCE Geotechnical special publications No.116,p 95-109.
- Odom, IE. 1984. Smectite clay minerals: properties and uses. *Philosophical Transactions of the Royal Society of London. Series A, Mathematical and Physical Sciences*, 311(1517), pp.391-409.
- Oloo, S., Schreiner, HD and Burland, JB., 1987. Identification and classification of expansive soils. In *6th International Conference on Expansive Soils*, pp. 23-29.
- Oweis, I and Khera. 1998. "Geotechnology of Waste Management".
- Patel, AD., Stamatakis, E., Davis, E and Friedheim, J. 2007. *High Performance Water Based Drilling Fluids and Method of Used*, Houston.
- Rank, K, Bhanderi, J and Nagecha, K .2015. Swelling potential of different expansive soil placed at different dry density and initial water content, IJAERD 2 (3).
- Rao, AS., Phanikumar, BR and Sharma, RS. 2004. Prediction of swelling characteristics of remoulded and compacted expansive soils using free swell index. *Quarterly Journal of Engineering Geology and Hydrogeology*, 37(3), pp 217-226.

- Reeve, MJ., Hall, DGM and Bullock, P.1980. The effect of soil composition and environmental factors on the shrinkage of some clayey British soils. *Journal of Soil Science*, 31(3), pp 429-442.
- Sachan, A and Penumadu, D. 2007. Effect of microfabric on shear behavior of kaolin clay. *Journal of geotechnical and geoenvironmental engineering*, 133(3), pp 306-318.
- Seki, K. 2007. SWRC fit—a nonlinear fitting program with a water retention curve for soils having unimodal and bimodal pore structure. *Hydrology and Earth System Sciences Discussions*, 4(1), pp 407-437.
- Seed, HB., Mitchell, JK and Chan, CK. 1960. *The strength of compacted cohesive soils*. Proceedings, ASCE Research Conference on Cohesive soils, Boulder, American Society of Civil Engineers, New York, pp 877-964.
- Sillers, WS and Fredlund, DG. 2001. Statistical assessment of soil-water characteristic curve models for geotechnical engineering. *Canadian Geotechnical Journal*, 38(6),pp 1297-1313.
- Sibley, JW., Smyth, GK and Williams, DJ. 1990. Suction-moisture content calibration of filter papers from different boxes. *Geotechnical Testing Journal*, 13(3), pp 257-262.
- Skempton, AW. 1953. The colloidal activity of clays. *Selected papers on soil mechanics*, pp 106-118.
- Sorochan, EA. 1991. Construction of buildings on expansile soils, A.A. Balkema/Rotterdam/Brookfield, pp 5-6.
- Sridharan, A and Prakash, K. 1998. Characteristic water contents of a fine-grained soil-water system. *Geotechnique*, 48(3), pp 337-346.
- Sridharan, A., Prakash K .1998b. Mechanism controlling the shrinkage limit of soils. *Geotech Test J ASTM* 21(3), pp 240-250.

- Sridharan, A and Prakash, K. 2000. Classification procedures for expansive soils. *Geotech.Eng*, 143, pp 235-240.
- Sridharan, A, Rao, SM and Murthy, NS. 1985. Free Swell Index of Soils: A Need for Redefinition. *Indian Geotechnical Journal*, 15(2), pp 94-99.
- Swarbrick, GE. 1995. Measurement of Soil Suction Using the Filter Paper Method. 1st Int. Conf. on Unsaturated Soils, Paris paper No: 246.
- Thakur, VKS and Singh, DN. 2005. Swelling and suction in clay minerals. *Advanced Experimental Unsaturated Soil Mechanics*, pp 27–31.
- TMH1 A7. 1986. Standard Methods of Testing Road Construction Materials. Technical Methods for Highways. The determination of the maximum dry density and optimum moisture content of gravel, soil and sand. Committee of State Road Authorities. Pretoria.
- Tu, H and Vanapalli, SK. 2016. Prediction of the variation of swelling pressure and one-dimensional heave of expansive soils with respect to suction using the soil-water retention curve as a tool. *Canadian Geotechnical Journal*, 53(8), pp1213-1234.
- Vanapalli, SK., Fredlund, DG and Pufahl, DE. 1999. The influence of soil structure and stress history on the soil-water characteristics of a compacted till. *Géotechnique* 49(2): pp 143–159.
- Van Genuchten, MT.1980. A closed-form equation for predicting the hydraulic conductivity of unsaturated soils 1. *Soil science society of America journal*, 44(5), pp.892-898.
- Van der Merwe, DH. 1964. The prediction of heave from the plasticity index and percentage clay fraction of soils. *Civil Engineering=Siviele Ingenieurswese*, 1964(v6i6), pp 103-107.
- Wang, YH and Fredlund, DG. 2003. Towards a better understanding of the role of the contractile skin, Proceedings of the Second Asian Conference on Unsaturated Soils, UNSAT-ASIA, Osaka, pp 419-424.

- Williams, AAB. 1958. Discussion of the prediction of total heave from double oedometer test. *Transactions, South African Institution of Civil Engineers*, 5(6), pp 49-51.
- Williams, AAB., Pidgeon, JT and Day, PW. 1985. Expansive soils. *Civil Engineering= Siviele Ingenieurswese*, 27(7), pp 367-377.
- Wu, FT. 1978. Mineralogy and physical nature of clay gouge. *pure and applied geophysics*, 116 (4-5), pp 655-689.
- YA, Tan .2016. Swelling Pressure and Retaining Wall Design in Expansive Soils. MScThesis, RMIT University, Melbourne.Australia.
- Yusuf, E and Orhan, E. 2007. Swell pressure prediction by suction methods. *Engineering Geology* 92, pp 133-145.
- Zha, FS., Liu, SY and Du, YJ. 2006. Evaluation of swell-shrinkage properties of compacted expansive soils using electrical resistivity method. In *Proceedings of the Sessions of GeoShanghai: Advances in Unsaturated Soil, Seepage, and Environmental Geotechnics*, pp 143-151.



**APPENDIX A**

**Table 5.1:** Grain size classification

Soil designation	Grain size distribution				
	clay, %	Silt, %	Fine, %	sand, %	Gravel, %
BTS	20	29.5	49.5	44.00	6.3
PTS	29.85	28.6	58.45	27.69	13.86
BLS	32.2	29.62	61.82	28.49	9.69
WBS	36.5	32.6	69.1	28.20	2.4
WKS	40	33	73	25.00	1.8

**Table 5.2:** Unified soil classification system (USCS)

Soil designation	Liquid limit,	Plasticity index,	Activity of clay	Soil classification
	LL (%)	PI (%)	A <sub>c</sub>	USCS
BTS	48.37	23.09	1.155	CL
PTS	54.83	34.87	1.168	CH
BLS	61.27	38.25	1.188	CH
WBS	66.22	44.10	1.208	CH
WKS	69.45	49.87	1.247	CH

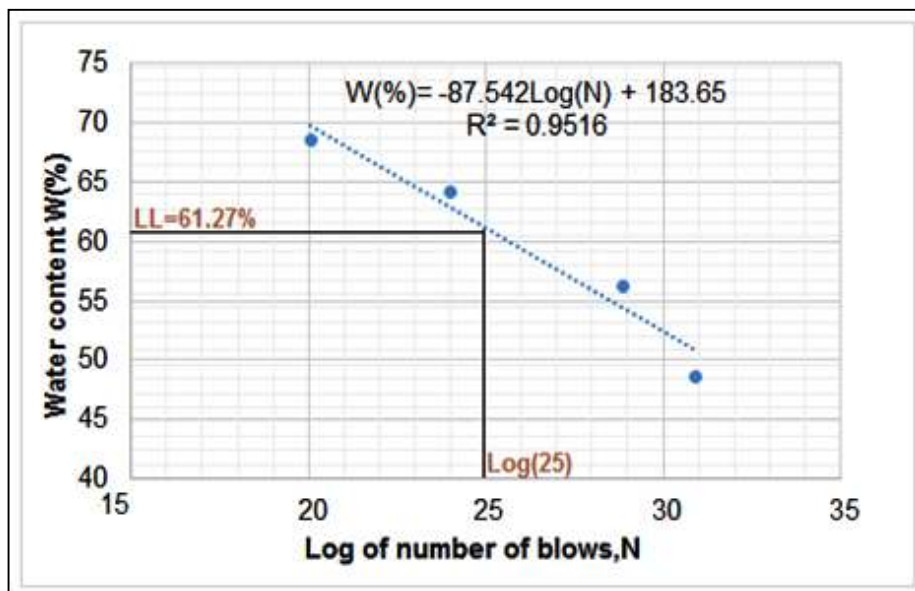


**Figure 5.5:** Casagrande liquid limit test (BLS)

APPENDIX B

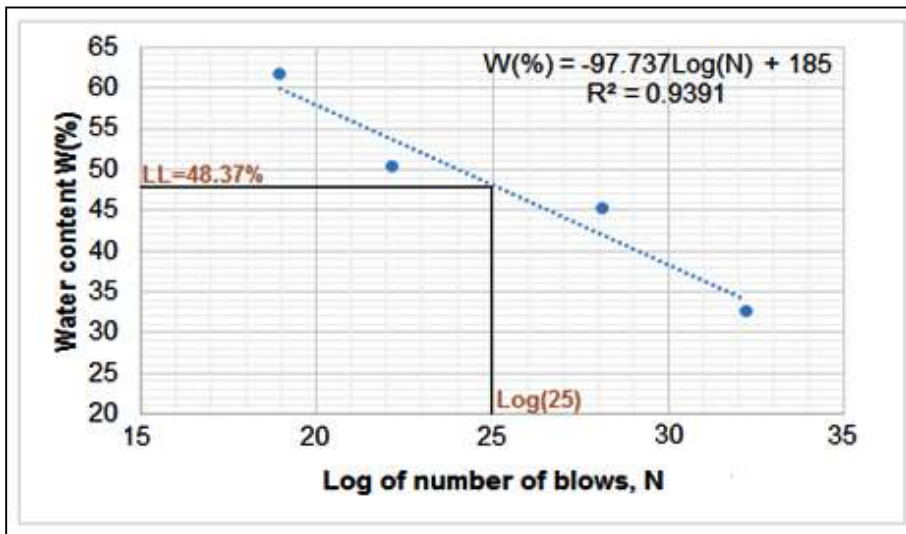


Figure 5.6: Casagrande liquid limit test (BTS)

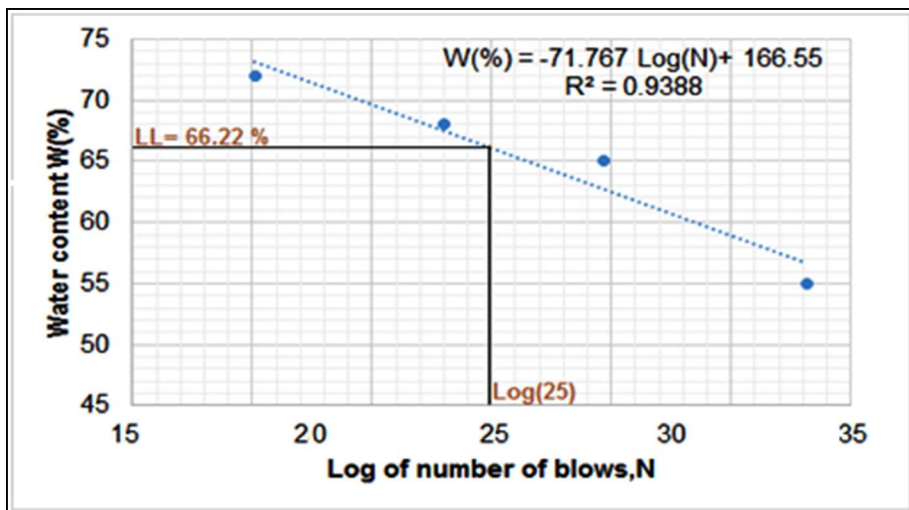


Figure 5.7: Casagrande liquid limit test (WBS)

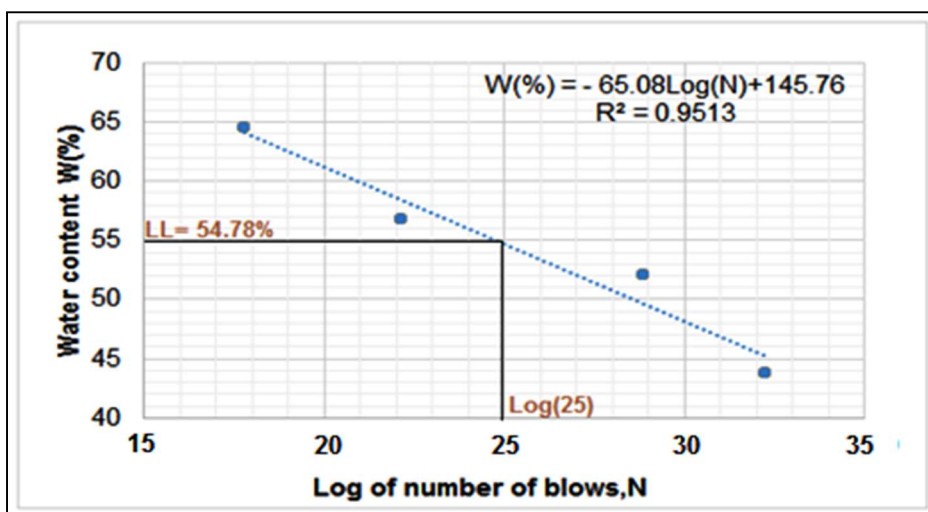


Figure 5.8: Casagrande liquid limit test (PTS)

APPENDIX C

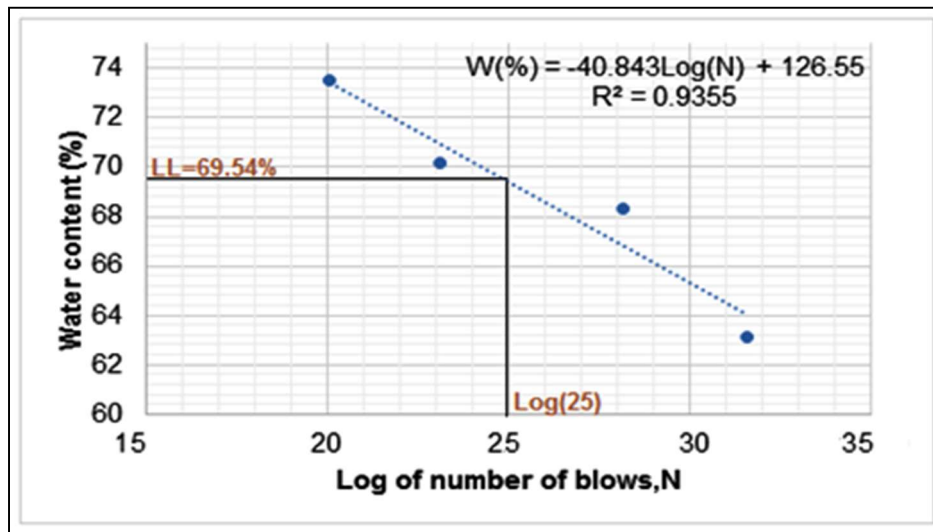


Figure 5.9: Casagrande liquid limit test (WKS)

Table 5.3: Linear shrinkage test results

Soil Designation	Trough No	Last number of blows, N	Shrinkage in mm	Factor (f*)	Linear shrinkage, LS (%)	Swell potential
PTS	105	31	17	0.71	12.06	medium
BLS	44	28	13	0.69	8.93	medium
WKS	10	27	9	0.68	6.12	high
BTS	23	29	20	0.69	13.89	low
WBS	52	26	11	0.67	7.41	high

Table 5.4: Specific gravity test results

Soil designation	WKS	BTS	PTS	BLS	WBS
M1 (Bot empty mass in grs)	455.42	442.88	455.42	442.88	455.42
M2 (Bot + dry soil mass in grs)	900.19	900.62	914.52	931.11	946.43
M3 (Bot + Soil + water mass in grs)	1779.86	1789.33	1786.32	1811.43	1813.32
M4 (Bot + water mass in grs)	1499.9	1505.4	1499.9	1505.4	1499.9
M2-M1 (grs)	444.77	457.74	459.1	488.23	491.01
M4-M1 (grs)	1044.48	1062.52	1044.48	1062.52	1044.48
M3-M2 (grs)	879.67	888.71	871.8	880.32	866.89
(M4-M1)-(M3-M2)	164.81	173.81	172.68	182.2	177.59
Specific gravity Gs= (M2-M1)/(M4-M1)-(M3-M2)	2.70	2.63	2.66	2.68	2.76

**APPENDIX D**

**Table 5.5:** Free swell index test results

Soil designation	Reading after 24 hours		Free Swell Index (%)
	Kerosene V <sub>k</sub> (ml)	Distilled water V <sub>d</sub> (ml)	
PTS	7	11	57.14
BLS	6	10	66.66
WBS	6.5	12	84.61
WKS	6	13	116.67
BTS	7	10	42.85

**Table 5.6:** Classification of soils based on FSI

Soil designation	Free swell index (%)	Potential of expansiveness	Clay type
PTS	57.14	Moderate	Swelling
BLS	66.66	Moderate	Swelling
WBS	84.66	Moderate	Swelling
WKS	116.66	High	high swelling
BTS	42.85	Low	mixture of swelling

**Table 5.7:** Free swell ratio test results

Soil designation	Reading after 24 hours		Free swell ratio
	Kerosene V <sub>k</sub> (ml)	Distilled water V <sub>d</sub> (ml)	
PTS	7	11	1.6
BLS	6	10	1.7
WBS	6.5	12	1.8
WKS	6	13	2.2
BTS	7	10	1.4

**Table 5.8:** Classification of Soils based on FSR

Soil designation	Free swell ratio	Clay type	Soil expansivity	Dominant clay mineral type
PTS	1.6	Swelling	Moderate	Montmorillonitic
BLS	1.7	Swelling	Moderate	Montmorillonitic
WBS	1.8	Swelling	Moderate	Montmorillonitic
WKS	2.2	Swelling	High	Montmorillonitic
BTS	1.4	Mixture of swelling and non-swelling	Low	Mixture of Montmorillonitic other clayey mineral

**APPENDIX E**

**Table 5.9:** Summary of X-Ray diffraction Results

Phase Name	Soil Designation									
	PTS		BLS		WBS		BTS		WKS	
	%	Colours Assignment	%	Colours Assignment	%	Colours Assignment	%	Colours Assignment	%	Colours Assignment
Smectite/ Montmorillonite	55.6	Blue	58	Blue	59.4	Grey	38	Grey	67	Blue
Quartz, syn	14.1	Green	14	Green	27.7	Brown	39	Blue	20	Grey
Feldspar, syn	30.3	Grey	28	Grey	12.9	Light-blue	23	Green	13	Brown

**Table 5.10:** Compaction test results

Soil designation	Optimum water content, %	Maximum dry density kN/m <sup>3</sup>
PTS	20.38	17.99
BLS	22.61	17.16
WBS	24.58	16.71
WKS	26.34	16.29
BTS	18.24	18.76

**Table 5.11:** Calibrated curves

Equation	Range of filter paper water content, W (%)	Reference
$\text{Log (kPa)} = 5.327 - 0.0779W$	$0 \leq W \leq 45$	ASTM D5298
$\text{Log (kPa)} = 5.056 - 0.0688W$	$0 \leq W \leq 54$	Scheleicher & Schuell No.589
$\text{Log (kPa)} = 5.1887 - 0.0741W$	$0 \leq W \leq 53$	Huseyin (2003)
$\text{Log (kPa)} = 5.313 - 0.0791W$	$0 \leq W \leq 52$	Author

**APPENDIX F**

**Table 5.12: Suction test results**

Soil Designation	Specimen	Water content of the samples, ( $W_i$ )	Total suction, ( $\Psi_t$ )	Matric suction, ( $\Psi_m$ )	Osmotic suction, ( $\Psi_o$ )
			kPa	kPa	kPa
WKS	WKS-1	15.13	9926.183	7693.66	2232.517
	WKS-2	19.25	6922.321	5227.777	1694.544
	WKS-3	23.37	4011.482	2986.456	1025.026
	WKS-4	26.34	2475.62	1778.651	696.969
	WKS-5	31.10	1397.745	890.47	507.275
	WKS-6	35.23	397.35	275.117	122.233
BLS	BLS-1	12.25	6112.321	4925.68	1186.64
	BLS-2	15.32	4221.982	3456.34	765.34
	BLS-3	20.12	1997.745	1442.11	555.64
	BLS-4	22.61	1076.324	697.98	378.35
	BLS-5	25.5	353.234	207.79	145.45
	BLS-6	28.98	133.456	95.35	38.11
BTS	BTS-1	8.5	4997.235	3975.678	1021.557
	BTS-2	10.21	3012.787	2379.348	633.439
	BTS-3	13.21	997.354	645.888	351.466
	BTS-4	18.24	388.676	222.785	165.891
	BTS-5	19.93	131.631	95.666	35.965
	BTS-6	21.5	55.233	39.987	15.246
WBS	WBS-1	11.37	7723.408	6213.234	1510.174
	WBS-2	14.25	5617.411	4498.234	1119.177
	WBS-3	18.32	3717.727	2853.32	864.407
	WBS-4	24.37	1763.982	1245.199	518.783
	WBS-5	26.21	847.98	467.431	380.598
	WBS-6	29.1	245.117	143.765	101.352
PTS	PTS-1	11.95	5455.68	4402.68	1053
	PTS-2	13.21	3456.34	2805.02	651.32
	PTS-3	17.35	1245.11	902.99	342.12
	PTS-4*	20.38	567.98	444.976	123
	PTS-5	22.95	187.79	157.789	30
	PTS-6	26.85	75.350	59.35	16

**APPENDIX G Table 5.13.: Soil water characteristic curve data (WKS)**

Matric suction kPa	Predicted volumetric water content	Measured volumetric water content
3.4397	0.499818886	0.56041988
8.5993	0.486845162	0.545873145
17.1985	0.465366044	0.521789772
34.3971	0.438746828	0.491943085
68.7942	0.417366118	0.467970052
137.5885	0.40585772	0.455066307
275.177	0.400095106	0.448605
890.47	0.383225544	0.41985
1778.6511	0.359500322	0.36369
2986.4562	0.333992486	0.315495
5227.7712	0.302178699	0.259875
7693.6666	0.280387913	0.204255
11540.4999	0.26314621	0.191694886

**Table 5.14: Soil water characteristic curve data (WBS)**

Matric suction kPa	Predicted volumetric water content	Measured volumetric water content
1.7970625	0.502576372	0.480595543
4.49265625	0.500636149	0.478740178
8.9853125	0.493991605	0.472386242
17.970625	0.477922861	0.457020285
35.94125	0.452832347	0.433027137
71.8825	0.427504311	0.408806856
143.765	0.410817642	0.392850000
467.431	0.402198812	0.353835000
1245.199	0.388685318	0.328995000
2853.32	0.368030322	0.247320000
4498.234	0.32592826	0.205875000
6213.234	0.305620846	0.175095000
9319.851	0.282594918	0.161903083

**Table 5.15: Soil water characteristic curve data (BLS)**

Matric suction kPa	Predicted volumetric water content	Measured volumetric water content
1.191875	0.502576372	0.462258039
2.9796875	0.500636149	0.462258039
5.959375	0.493991605	0.462257935
11.91875	0.477922861	0.460314439
23.8375	0.452832347	0.416360801
47.675	0.427504311	0.393072709
95.35	0.410817642	0.37773
207.79	0.402198812	0.34425
697.98	0.388685318	0.305235
1442.11	0.368030322	0.27162
3456.34	0.32592826	0.20682
4925.68	0.305620846	0.165375
7388.52	0.282594918	0.152915402

**APPENDIX H**

**Table 5.16:** Soil water characteristic curve data (PTS)

Matric suction kPa	Predicted volumetric water content	Measured volumetric water content
0.741875	0.502714243	0.423062626
1.8546875	0.502115261	0.422558549
3.709375	0.499293209	0.420183632
7.41875	0.490084177	0.412433707
14.8375	0.470690618	0.396112925
29.675	0.444313728	0.373915271
59.35	0.421094535	0.354375000
157.789	0.40448617	0.309825000
444.976	0.395622439	0.275130000
902.99	0.382869996	0.234225000
2805.02	0.337358137	0.178335000
4402.68	0.312114725	0.147825000
6604.02	0.288828912	0.136796282

**Table.5.17:** Soil water characteristic curve data (BTS)

Matric suction kPa	Predicted volumetric water content	Measured volumetric water content
1.6453875	0.502295617	0.344902832
4.11346875	0.498449637	0.342261978
8.2269375	0.487868601	0.334996477
16.453875	0.466993729	0.320662682
32.90775	0.440392285	0.302396718
65.8155	0.418432575	0.287318016
131.631	0.406347847	0.27902
388.676	0.39709737	0.25536
997.354	0.380197978	0.18494
3012.787	0.333516234	0.14294
4997.235	0.304786254	0.119
9994.47	0.266786759	0.1036
14991.705	0.248659934	0.096560899

**Table 5.18 :** Summary of SWCC results

Soil designation	WKS	BTS	WBS	BLS	PTS
Matric suction (kPa) @ AEV	10	6.5	12	15	8.5
Volumetric water content (%) @ AEV	0.568	0.344	0.492	0.463	0.423
Fine Fraction %	73	49.5	69.1	61.82	58.45



## APPENDIX I

**Table 5.19: SWCC fitting parameters and equations for soils WKS & WBS**

Soil type	Model	Equation	Parameter	R <sup>2</sup>	AIC
WKS	Van Genuchten	$S_e = \left[ \frac{1}{1 + (\alpha h)^n} \right]^m$ ( $m = 1 - 1/n$ )	$\theta_s = 0.50894$ $\theta_r = 1.59e - 05$ $\alpha = 0.0018093$ $n = 1.2824$	0.948	-85.438
	Fredlund and Xing	$S_e = \left[ \frac{1}{\ln[e + (\alpha/h)^n]} \right]^m$	$\theta_s = 0.55308$ $\theta_r = 1.77e - 06$ $a = 1.37e + 04$ $m = 3.9888$ $n = 0.49103$	0.976	-93.270
	Seki	$S_e = w_1 Q \left[ \frac{\ln(h/h_{m1})}{\sigma_1} \right] + (1 - w_1) Q \left[ \frac{\ln(h/h_{m2})}{\sigma_2} \right]$	$\theta_s = 0.56368$ $\theta_r = 0.14911$ $w_1 = 0.27315$ $h_{m1} = 24.204$ $\sigma_1 = 1.0285$ $h_{m2} = 3380.7$ $\sigma_2 = 1.0714$	0.998	-127.89
WBS	Van Genuchten	$S_e = \left[ \frac{1}{1 + (\alpha h)^n} \right]^m$ ( $m = 1 - 1/n$ )	$\theta_s = 0.45612$ $\theta_r = 1.82e - 06$ $\alpha = 0.0059306$ $n = 1.2290$	0.962	-91.003
	Fredlund and Xing	$S_e = \left[ \frac{1}{\ln[e + (\alpha/h)^n]} \right]^m$	$\theta_s = 0.49251$ $\theta_r = 5.64e - 06$ $a = 6406.1$ $m = 3.4899$ $n = 0.46824$	0.986	-101.74
	Seki	$S_e = w_1 Q \left[ \frac{\ln(h/h_{m1})}{\sigma_1} \right] + (1 - w_1) Q \left[ \frac{\ln(h/h_{m2})}{\sigma_2} \right]$	$\theta_s = 0.49297$ $\theta_r = 0.15564$ $w_1 = 0.45529$ $h_{m1} = 55.136$ $\sigma_1 = 1.8304$ $h_{m2} = 2854.6$ $\sigma_2 = 0.65587$	0.999	-133.35

## APPENDIX J

**Table 5.20:** SWCC fitting parameters and equations for soils BLS & PTS

Soil type	Model	Equation	Parameter	R <sup>2</sup>	AIC
BLS	Van Genuchten	$S_e = \left[ \frac{1}{1 + (\alpha h)^n} \right]^m$ $(m = 1 - 1/n)$	$\theta_s = 0.44658$ $\theta_r = 5.86e - 06$ $\alpha = 0.017062$ $n = 1.1659$	0.954	-89.313
	Fredlund and Xing	$S_e = \left[ \frac{1}{\ln[e + (\alpha/h)^n]} \right]^m$	$\theta_s = 0.48296$ $\theta_r = 2.79e - 08$ $a = 15522.2$ $m = 2.4423$ $n = 0.46550$	0.988	-104.48
	Seki	$S_e = w_1 Q \left[ \frac{\ln(h/h_{m1})}{\sigma_1} \right]$ $+ (1 - w_1) Q \left[ \frac{\ln(h/h_{m2})}{\sigma_2} \right]$	$\theta_s = 0.46340$ $\theta_r = 1.82e - 06$ $w_1 = 0.15047$ $h_{m1} = 21.917$ $\sigma_1 = 0.40629$ $h_{m2} = 3746.0$ $\sigma_2 = 2.2014$	0.997	-118.82
PTS	Van Genuchten	$S_e = \left[ \frac{1}{1 + (\alpha h)^n} \right]^m$ $(m = 1 - 1/n)$	$\theta_s = 0.42432$ $\theta_r = 4.52e - 07$ $\alpha = 0.048081$ $n = 1.1658$	0.984	-104.58
	Fredlund and Xing	$S_e = \left[ \frac{1}{\ln[e + (\alpha/h)^n]} \right]^m$	$\theta_s = 0.44102$ $\theta_r = 3.89e - 05$ $a = 575.31$ $m = 1.9971$ $n = 0.49403$	0.998	-129.98
	Seki	$S_e = w_1 Q \left[ \frac{\ln(h/h_{m1})}{\sigma_1} \right]$ $+ (1 - w_1) Q \left[ \frac{\ln(h/h_{m2})}{\sigma_2} \right]$	$\theta_s = 0.42419$ $\theta_r = 0.10084$ $w_1 = 0.41287$ $h_{m1} = 50.634$ $\sigma_1 = 1.4703$ $h_{m2} = 1875.6$ $\sigma_2 = 1.3830$	0.999	-140.38

APPENDIX K

**Table 5.21: SWCC fitting parameters and equations for soil BTS**

Soil type	Model	Equation	Parameter	R <sup>2</sup>	AIC
BTS	Van Genuchten	$S_e = \left[ \frac{1}{1 + (\alpha h)^n} \right]^m$ $(m = 1 - 1/n)$	$\theta_s = 0.33083$ $\theta_r = 3.68e - 07$ $\alpha = 0.0084159$ $n = 1.2528$	0.986	-108.96
	Fredlund and Xing	$S_e = \left[ \frac{1}{\ln[e + (\alpha/h)^n]} \right]^m$	$\theta_s = 0.35179$ $\theta_r = 0.073833$ $a = 6706.0$ $m = 7.11450$ $n = 0.52625$	0.994	-117.78
	Seki	$S_e = w_1 Q \left[ \frac{\ln(h/h_{m1})}{\sigma_1} \right]$ $+ (1 - w_1) Q \left[ \frac{\ln(h/h_{m2})}{\sigma_2} \right]$	$\theta_s = 0.34408$ $\theta_r = 0.094758$ $w_1 = 0.21145$ $h_{m1} = 17.921$ $\sigma_1 = 0.75790$ $h_{m2} = 1045.3$ $\sigma_2 = 1.3262$	0.997	-126.86

**APPENDIX L**

**Table 5.22: Zero swelling test results**

Soil designation	Specimen	Initial Water content, (W)	Total surcharge	Swelling stress, (P <sub>s</sub> )
		%	kg	kPa
BTS	BTS-1	8.50	2.250	112.414
	BTS-2	10.21	2.000	99.924
	BTS-3	13.21	1.750	87.433
	BTS-4	18.24	1.000	49.962
	BTS-5	19.93	0.750	37.471
	BTS-6	21.50	0.250	12.490
PTS	PTS-1	11.95	3.250	162.376
	PTS-2	13.21	3.000	149.886
	PTS-3	17.35	2.750	137.395
	PTS-4	20.38	2.250	112.414
	PTS-5	22.95	1.000	49.962
BLS	BLS-1	12.25	7.250	362.224
	BLS-2	15.32	6.500	324.752
	BLS-3	20.12	5.000	249.810
	BLS-4	22.61	3.750	187.357
	BLS-5	25.50	2.750	137.395
	BLS-6	28.98	1.750	87.433
WBS	WBS-1	11.37	9.000	449.657
	WBS-2	14.25	8.000	399.695
	WBS-3	18.32	6.250	312.262
	WBS-4	24.37	5.000	249.810
	WBS-5	26.21	2.250	112.414
	WBS-6	29.10	1.250	62.452
WKS	WKS-1	15.13	12.000	599.543
	WKS-2	19.25	10.000	499.619
	WKS-3	23.37	8.000	399.695
	WKS-4	26.34	5.250	262.300
	WKS-5	31.10	2.750	137.395
	WKS-6	35.24	2.000	99.924

**APPENDIX M**

**Table 5.23: Summary of laboratory results @ OMC**

Soil designation	Optimum Water content, (W)	Swelling stress, (P <sub>s</sub> )	Total suction, (Ψ <sub>t</sub> )	Matric suction, (Ψ <sub>m</sub> )	Osmotic suction, (Ψ <sub>o</sub> )	Initial dry density, (γ <sub>d</sub> )
	%	logkPa	logkPa	logkPa	logkPa	kN/m <sup>3</sup>
BTS	18.24	1.699	2.590	2.348	1.699	18.76
PTS	20.38	2.051	2.754	2.649	2.090	17.99
BLS	22.61	2.273	3.032	2.844	2.273	17.16
WBS	24.58	2.398	3.246	3.095	2.715	16.29
WKS	26.34	2.419	3.394	3.250	2.843	16.71

**Table 5.24: Summary of laboratory results**

Soil designation	Grain size distribution					Soil classification
	clay, %	Silt, %	Fine, %	sand, %	Gravel, %	USCS
BTS	20	29.5	49.5	44.00	6.3	CL
PTS	29.85	28.6	58.45	27.69	13.86	CH
BLS	32.2	29.62	61.82	28.49	9.69	CH
WBS	36.5	32.6	69.1	28.20	2.4	CH
WKS	40	33	73	25.00	1.8	CH

**Table 5.25: Summary of laboratory results**

Soil designation	Liquid Limit, (LL)	Plasticity Index, (PI)	Linear shrinkage, (LS)	Activity, (Ac)	Free Swell Ratio, (FSR)	Free swell index, (FSI)
	%	%	%			%
BTS	48.37	23.09	13.89	1.155	1.4	42.85
PTS	54.83	34.87	12.06	1.168	1.6	57.14
BLS	61.27	38.25	8.93	1.188	1.7	66.66
WBS	66.22	44.1	7.41	1.208	1.8	84.66
WKS	69.45	49.87	6.12	1.247	2.2	116.66

**APPENDIX N**

**Table 5.26: Correlation Matrix A**

Soil designation	specimen	Initial Water content ( $W_i$ )	Swelling stress ( $P_s$ )	Total suction ( $\psi_t$ )	Matric suction ( $\psi_m$ )	Initial dry density ( $\gamma_d$ )
		%	Log(kPa)	Log(kPa)	Log(kPa)	kN/m <sup>3</sup>
BTS	BTS-1	8.5	2.051	3.699	3.599	15.35
	BTS-2	10.21	1.999	3.479	3.376	16.11
	BTS-3	13.21	1.942	2.999	2.810	17.45
	BTS-4	18.24	1.699	2.590	2.348	18.76
	BTS-5	19.93	1.574	2.119	1.981	18.56
PTS	PTS-1	11.95	2.211	3.737	3.644	15.94
	PTS-2	13.21	2.176	3.539	3.448	16.58
	PTS-3	17.35	2.138	3.095	2.956	17.68
	PTS-4	20.38	2.051	2.754	2.649	17.99
	PTS-5	22.950	1.699	2.274	2.198	17.63
BLS	BLS-1	12.25	2.559	3.786	3.692	15.15
	BLS-2	15.32	2.512	3.626	3.539	15.95
	BLS-3	20.12	2.398	3.301	3.159	16.98
	BLS-4	22.61	2.273	3.032	2.844	17.16
	BLS-5	25.5	2.138	2.548	2.318	16.84
WBS	WBS-1	11.37	2.653	3.888	3.793	14.90
	WBS-2	14.25	2.602	3.749	3.653	15.25
	WBS-3	18.32	2.494	3.570	3.455	15.98
	WBS-4	24.58	2.398	3.246	3.095	16.71
	WBS-5	26.21	2.051	2.928	2.669	16.67
WKS	WKS-1	15.13	2.778	3.997	3.886	14.94
	WKS-2	19.25	2.699	3.840	3.718	15.48
	WKS-3	23.37	2.602	3.603	3.475	16.09
	WKS-4	26.34	2.419	3.394	3.250	16.29
	WKS-5	31.10	2.138	3.145	2.950	15.18

**APPENDIX O**                      **Table 5.27: Correlation Matrix B**

Soil designation	Liquid Limit, (LL)	Plasticity Index, (PI)	Linear shrinkage, (LS)	Activity of clay, (Ac)	Free swell ratio, (FSR)	Free swell index, (FSI)
	%	%	%			%
BTS	48.37	23.09	13.89	1.155	1.4	42.85
PTS	54.83	34.87	12.06	1.168	1.6	57.14
BLS	61.27	38.25	8.93	1.188	1.7	66.66
WBS	66.22	44.1	7.41	1.208	1.8	84.66
WKS	69.45	49.87	6.12	1.247	2.2	116.66

**Table 5.28: Intercepts, coefficients for regression analysis models**

Models		Model 1	Model 2	Model 3
Intercepts		$\lambda_0 = + 2.2355$	$\eta_0 = +1.4177$	$\xi_0 = +1.3544$
Regression coefficients		$\lambda_1 = + 0.2559$	$\eta_1 = + 0.1243$	$\xi_1 = +0.1287$
		$\lambda_2 = + 0.0359$	$\eta_2 = - 0.0143$	$\xi_2 = - 0.0139$
		$\lambda_3 = - 0.0086$	$\eta_3 = + 0.0413$	$\xi_3 = - 0.0015$
		$\lambda_4 = - 2.3206$	$\eta_4 = -1.4574$	$\xi_4 = + 0.0427$
				$\xi_5 = - 1.4465$
Multi-Regression summary report	R <sup>2</sup> *	0.9626	0.9696	0.9697
	RSD**	2.72%	2.45%	2.53%
	MSR***	0.0040	0.0033	0.0035

**Table 5.29: Intercepts, coefficients for regression analysis models**

Models		Model 4	Model 5	Model 6
Intercepts		$\zeta_0 = +2.9200$	$\beta_0 = +15.0003$	$\mu_0 = +13.890$
Regression coefficients		$\zeta_1 = +0.0951$	$\beta_1 = + 0.0574$	$\mu_1 = +0.1305$
		$\zeta_2 = +0.0100$	$\beta_2 = - 0.0203$	$\mu_2 = - 0.0203$
		$\zeta_3 = - 0.0168$	$\beta_3 = -0.1246$	$\mu_3 = - 0.0162$
		$\zeta_4 = - 0.0792$	$\beta_4 = + 0.0438$	$\mu_4 = - 0.1702$
		$\zeta_5 = - 0.1353$	$\beta_5 = - 0.3302$	$\mu_5 = - 9.2460$
			$\beta_6 = - 2.9440$	$\mu_6 = + 0.0284$
				$\mu_7 = +0.8825$
Multi-Regression summary report	R <sup>2</sup> *	0.9735	0.9846	0.9849
	RSD**	2.36%	1.87 %	1.93 %
	MSR***	0.0030	0.0019	0.0020

\*R<sup>2</sup>= Correlation coefficient, \*\*RSD= Relative standard deviator  
 \*\*\*MSR= Mean square error.

**APPENDIX P**

**Table 5.30: Compaction test data sheet**

Geotechnical Laboratory, Department of Civil Engineering , CUT					
COMPACTION TEST DATA SHEET: TMH-1 METHOD 7					
Sample No					
Date:					
Operator					
Mass taken (Kg)					
Description:					
I- APPROXIMATE VALUES					
a) Water added					
Basin number	1	2	3	4	5
Initial water content (W <sub>i</sub> ) %					
Added water in ( Millilitre)					
Added water in (kg)					
Mass of the soil, M <sub>soil</sub> (kg)					
Target moisture content % (W <sub>t</sub> )					
b) Dry density					
Mould No	1	2	3	4	5
Mould+ Base plate+ Glass lid in (kg)					
Mould+ Base plate+ Glass lid+ Water in (kg)					
Mass of water in (kg)					
Temperature t° Test					
Rd of water @ t° Test see chart					
Volume of mould in millilitre : V <sub>m</sub>					
Volume of mould (M <sup>3</sup> )					
Mass of mould + Wet soil (M <sub>1</sub> ), (kg)					
Mass of mould (M <sub>m</sub> ), (kg)					
Mass of wet soil :M <sub>1</sub> -M <sub>m</sub> , (kg)					
Total density, Y <sub>m</sub> = (M <sub>1</sub> -M <sub>m</sub> ) / V <sub>m</sub> ,in (kg /m <sup>3</sup> )					
Dry density ,(kg/m <sup>3</sup> )					
II- ACTUAL VALUES					
a) Moisture					
Container number	1	2	3	4	5
Mass of container + wet soil (M <sub>1</sub> ) in (Gramme)					
Mass of container + dry soil (M <sub>2</sub> ) in (Gramme)					
Mass of container (M <sub>c</sub> ) in (Gramme)					
Mass of water (M <sub>1</sub> -M <sub>2</sub> ) in (Gramme)					
Mass of dry soil(M <sub>2</sub> -M <sub>c</sub> ) in (Gramme)					
Moisture content (%) W = (M <sub>1</sub> -M <sub>2</sub> )/(M <sub>2</sub> -M <sub>c</sub> )*100					
Dry density , ( kg /m <sup>3</sup> )					
III- SUMMARY					
Maximum dry density, (Kg/m <sup>3</sup> )					
Optimum moisture content, W <sub>opt</sub> (%)					



**APPENDIX Q**

**Table 5.31:** Measurement of soil suction using filter paper- Data sheet

**ASTM D 5298 (1994)**

Geotechnical Laboratory, Department of Civil Engineering ,  
CUT

Soil designation .....

Date tested: .....

Tested by: .....

Sample		1-1		1-2		1-3		1-4		1-5	
Gravimetric water content of soil sample,W, ( %)											
Tin No											
Top filter paper / Bottom filter paper		<u>Top</u>	<u>Bot</u>	<u>Top</u>	<u>Bot</u>	<u>Top</u>	<u>Bot</u>	<u>Top</u>	<u>Bot</u>	<u>Top</u>	<u>Bot</u>
Cold Tare Mass, g	Tc										
Mass of wet Filter paper + Cold Tare Mass, g	m1										
Mass of Dry Filter paper + Hot Tare Mass, g	m2										
Hot Tare Mass, g	Th										
Mass of water in Filter Paper, g M2-Th	Mf										
Mass of water in Filter Paper, g M1-M2-Tc+Th	Mw										
Water content of filter Paper,g (Mw/Mf) %	Wf										
Suction , kPa	$\Psi$										
Suction , logkPa	$\Psi$										
Suction, PF = logkPa+1	$\Psi$										

